1

NASA CR-159400

DO NOT DESTROY

NASA-CR-159400

STRESS ANALYSES FOR STRUCTURES WITH SURFACE CRACKS

Final Report

by J. C. Bell

BATTELLE
Columbus Laboratories

10 JAN 1979
MCDONNELL DOUGLAS
RESEARCH & ENGINEERING LIBRARY
ST. LOUIS

prepared for

NATIONAL AERONAUTICS AND SPACE ADMINISTRATION

NASA Lewis Research Center
Contract NAS3-21020
Project Manager, G. T. Smith

M79-10258

ERRATA FOR NASA CR-159400

Page 14, last line: For "Discussion", read "Comments Concerning Results and Procedure".

Page A1, Figure A2: In the notes, the symbol for non-fitted check points should be "o", not "•".

Page B2, add this footnote: "Note: Superscripts on coordinates identify local system coordinates. See NASA CR 159401."

Page C27, figure for $\tau_{\theta z}/\sigma_o$: The blurred label on a curve should be "8".

ERRATA FOR NASA CR 159401

Page 36, line 14: For "Page 51", read "Page 53".

Page 57, line 1: For "562", read "552".

Page B2, line 15: For "on", read "uses".

Page B2, line 27: For "they derived", read "they are derived".

1. Report No.	2. Government Accession No.	3. Recipient's Catalog No.
NASA CR-159400		

4. Title and Subtitle	5. Report Date
STRESS ANALYSIS FOR STRUCTURES WITH SURFACE CRACKS	August 1978
	6. Performing Organization Code
7. Author(s) J. C. Bell	8. Performing Organization Report No
	10. Work Unit No
9. Performing Organization Name and Address Battelle Columbus Laboratories 505 King Avenue Columbus, Ohio 43201	11. Contract or Grant No NAS3-21020
	13. Type of Report and Period Covered Contractor Report
12. Sponsoring Agency Name and Address National Aeronautics and Space Administration Washington, D. C. 20546	14. Sponsoring Agency Code

15. Supplementary Notes

Project Manager, G. T. Smith, Materials and Structures Division, NASA Lewis Research Center, Cleveland, Ohio 44135

16. Abstract

Two original, basic forms of analysis, one treating stresses around arbitrarily loaded circular cracks, the other treating stresses due to loads arbitrarily distributed on the surface of a half space, are united by a boundary-point least squares method to obtain analyses for stresses from surface cracks in plates or bars. Calculations have been made for enough cases to show how effects from the crack vary with the depth-to-length ratio, the fractional penetration ratio, the obliquity of the load, and to some extent the fractional span ratio. The results include many plots showing stress intensity factors, stress component distributions near the crack, and crack opening displacement patterns. Favorable comparisons are shown with two kinds of independent experiments, but the main method for confirming the results is by wide checking of overall satisfaction of boundary conditions, so that external confirmation is not essential. Principles involved in designing analyses which promote dependability of the results are proposed and illustrated.

17. Key Words (Suggested by Author(s))	18. Distribution Statement
surface cracks, fracture analysis, numerical analysis, circular cracks, surface loads, coordinated stress analyses, stress intensity factors, crack stresses, crack opening, back effects, width effects, oblique loads, verification of analyses	Unclassified - unlimited

19. Security Classif. (of this report)	20. Security Classif. (of this page)	21. No. of Pages	22. Price*
Unclassified	Unclassified	150	$5.75

*For sale by the National Technical Information Service, Springfield, Virginia 22161

NASA-C-168 (Rev. 10-75)

TABLE OF CONTENTS

	Page
LIST OF SYMBOLS	vii
SUMMARY	1
INTRODUCTION	2
SURFACE CRACKS UNDER NORMAL LOADS	9
Cases with A/2C = 0.50	9
Some Principles for Design of Analysis	9
Case with A/T = 0.0	14
Cases with A/T > 0	19
Cases with A/2C = 0.25	21
Cases with A/2C = 0.10	26
Case with A/2C = 0.05	32
Patterns of Stresses and Crack Opening Displacements	33
SURFACE CRACKS UNDER OBLIQUE LOADS	38
Cases with A/2C = 0.50	39
Cases with A/2C = 0.25	43
Cases with A/2C = 0.10	45
SURFACE CRACKS IN BARS	47
COMMENTS CONCERNING RESULTS AND PROCEDURE	55
Observations Concerning Computed Results	55
Observations About Design of Analyses	57
Effectiveness of the Checking Process	59
CONCLUSIONS	61
REFERENCES	62

TABLE OF CONTENTS
(Continued)

APPENDIX A

BOUNDARY CONDITION AND CHECK POINTS SELECTED FOR CRACKS. A1

APPENDIX B

SURFACE LATTICES USED IN ANALYSES. B1

APPENDIX C

STRESS COMPONENTS NEAR SURFACE CRACKS UNDER NORMAL LOAD. C1

APPENDIX D

CRACK OPENING DISPLACEMENTS FOR CRACKS UNDER NORMAL AND OBLIQUE LOADS. . D1

APPENDIX E

STRESS INTENSITY FACTORS FOR SURFACE CRACKS UNDER OBLIQUE LOADS. E1

APPENDIX F

REMARKS ON FORMULAS FOR STRESSES AROUND AN EMBEDDED CRACK F1

LIST OF TABLES

Page

Table 1. Surface Cracks and Loads Chosen for Analysis 8

Table 2. Theoretical and Experimental Plate Width Effects on COD. 53

LIST OF FIGURES

		Page
Figure 1.	Surface Load Elements of Pyramidal Form.	4
Figure 2.	Notation Used in Analysis, as it Appears for Cracks Perpendicular to the Surface.	4
Figure 3.	Influence Factor for $\alpha'_{0,0}$ Affecting σ_z on Surface Cut by a Semicircular Crack.	12
Figure 4.	Stress Intensity Factors Along Semicircular Surface Cracks (A/2C = 0.5) Under Normal Loads	15
Figure 5.	Checks of σ_z at Non-Fitted Surface Points Around Semicircular Crack (A/2C = 0.5, A/T = 0.0) Under Normal Load.	17
Figure 6.	Checks of σ_ϑ at Non-Fitted Points of a Semicircular Surface Crack (A/2C = 0.5, A/T = 0.0) Under Normal Load.	18
Figure 7.	Comparisons Among Stress Intensity Factors for Semicircular Surface Cracks as Calculated by Several Investigators.	22
Figure 8.	Stress Intensity Factors Along Part-Circular Surface Cracks (A/2C = 0.25) Under Normal Load	24
Figure 9.	Calculated and Measured Stress Intensity Factors Along Part-Circular Surface Cracks with A/2C = 0.25, A/T = 0.7 Under Normal Load.	25
Figure 10.	Checks of σ_z at Non-Fitted Surface Points Near a Part-Circular Crack with A/2C = 0.25, A/T = 0.7, ν = 0.3 Under Normal Load	27
Figure 11.	Checks of σ_ϑ at Non-Fitted Points of a Part-Circular Crack with A/2C = 0.25, A/T = 0.7, ν = 0.3 Under Normal Load.	27
Figure 12.	Stress Intensity Factor Along Slender Circular Surface Cracks (A/2C = 0.10) Under Normal Load	31
Figure 13.	Stress Intensity Factor Along a Very Slender Circular Surface Crack (A/2C = 0.5, A/T - 0.05) Under Normal Load.	34
Figure 14.	Notation for Stress Positions and Crack Opening Displacements Along a Surface Crack.	35

LIST OF FIGURES
(Continued)

Page

Figure 15. Stress Intensity Factors Along Semicircular Cracks (A/2C = 0.5) Under a Lateral Shearing Load 41

Figure 16. Stress Intensity Factors Along Part-Circular Surface Cracks (A/2C = 0.25) Under Lateral Shearing Load 44

Figure 17. Stress Intensity Factors Along Slender Surface Cracks (A/2C = 0.10) Under Lateral Shearing Load. 46

Figure 18. Stress Intensity Factors Along Part-Circular Surface Cracks (A/2C = 0.25) Under Normal Load With and Without Effects from Back or From Sides. 49

Figure 19. Effect of Bar Width on Stress Intensity Factors Along Surface Cracks With A/2C = 0.25 and A/T = 0.7. 50

Figure 20. Theoretical and Experimental Plate Width Effects on Crack Opening Displacements. 54

LIST OF SYMBOLS

a = radius of crack circle

A = depth of penetration of surface crack

C = half length of surface crack

COD_I = crack opening displacement, first mode (See Figure 14; also = COD)

COD_{II}, COD_{III} = crack opening displacements, sliding modes (See Figure 14.)

E = Young's modulus

k = index related to radial variations in crack function series

k_1, k_2, k_3 = stress intensity factors (without factor $\sqrt{\pi}$. See Appendix F.)

$k_{I\infty}$ = $2\sigma_o\sqrt{a}/\pi = k_I$ for deeply embedded crack under uniform normal load σ_o

k_s = $2S\sqrt{a}/\pi$

K_I, K_{II}, K_{III} = stress intensity factors (being $\sqrt{\pi}$ times k_1, k_2 or k_3)

K_{IV} = unified stress intensity factor (See p 42.)

$K_{I\infty}$ = $2\sigma_o\sqrt{a/\pi} = K_I$ for deeply embedded crack under uniform normal load σ_o

K_s = $2S\sqrt{a/\pi}$ = reference stress intensity factor under uniform shear S

K_{ref} = $2\sigma_o\sqrt{a/\pi}$ = reference stress intensity factor presuming oblique load σ_o

m = index related to angular variations in crack function series

p, s, t = constants for pyramidal surface loads ($\sim -\sigma_z, \tau_{zx}, \tau_{yz}$ respectively)

P, S = uniform normal load (P) or shear load parallel to lip of crack (S)

r, θ, z = cylindrical coordinates associated with crack (See Figure 2.)

r' = distance from crack front, in plane perpendicular to crack front

T = thickness of plate or bar (also called z_t)

u, v, w = dimensional components of displacement in x,y,z directions

u', v', w' = dimensionless components of displacement ($= \frac{\mu u}{Pa}, \frac{\mu v}{Sa}, \frac{\mu w}{Sa}$ respectively)

W = width of bar

x, y, z = rectangular coordinates associated with front face (See Figure 2.)

y_m = half width of bar

z_t = thickness of bar or plate (also called T)

$\alpha'_{m,k}$ = constants for normal crack loads symmetric around $\theta = 0$ (See App.F)

$\beta'_{m,k}, \gamma'_{m,k}$ = constants for tangential crack loads symmetric around $\theta = 0$

$\hat{\alpha}'_{m,k}$ = constants for normal crack loads antisymmetric around $\theta = 0$

$\hat{\beta}'_{m,k}, \hat{\gamma}'_{m,k}$ = constants for tangential crack loads antisymmetric around $\theta = 0$

β = obliquity of load from remote tension

ζ = z/a

θ = cylindrical coordinate polar angle, $\theta = 0$ at crack root (Figure 2)

θ_{tip} = angular distance from crack root to crack tip

μ = shear modulus = $E/[2(1+\nu)]$

ν = Poisson's ratio

ρ = r/a

ρ' = r'/a

$\sigma_x, \sigma_y, \sigma_z$ = normal stress components in rectangular system

$\sigma_r, \sigma_\theta, \sigma_z$ = normal stress components in cylindrical system

σ_o = crack load produced by remote tension

$\tau_{yz}, \tau_{zx}, \tau_{xy}$ = shearing stress components in rectangular system

$\tau_{\theta z}, \tau_{zr}, \tau_{r\theta}$ = shearing stress components in cylindrical system

τ_{oc} = octahedral shear stress

φ = inclination of line segment r' to crack plane (See Figure 13.)

STRESS ANALYSIS FOR STRUCTURES WITH SURFACE CRACKS

by J. C. Bell

SUMMARY

Two original, basic forms of analysis, one treating stresses around arbitrarily loaded circular cracks, the other treating stresses due to loads arbitrarily distributed on the surface of a half space, are united by a boundary-point least squares method to obtain analyses for stresses from surface cracks in plates or bars. Calculations have been made for enough cases to show how effects from the crack vary with the depth-to-length ratio, the fractional penetration ratio, the obliquity of the load, and to some extent the fractional span ratio. The results include many plots showing stress intensity factors, stress component distributions near the crack, and crack opening displacement patterns. Favorable comparisons are shown with two kinds of independent experiments, but the main method for confirming the results is by wide checking of overall satisfaction of boundary conditions, so that external confirmation is not essential. Principles involved in designing analyses which promote dependability of the results are proposed and illustrated.

INTRODUCTION

The purpose of this investigation has been to provide stress analysis which can aid designers of structures such as space vehicles or aircraft in judging the significance of surface cracks. Presuming specific crack geometries and loads, linear elastic fracture analysis has been used to evaluate stress intensity factors of kinds commonly used to predict crack growth and also to find many stress and displacement patterns around cracks. The significance of this research lies not only in the specific results and what may be inferred from them, but also in the considerable light cast on the extent to which it is now possible to analyse stresses due to the presence of surface cracks.

The methods used for this analysis proceed from two basic forms of theory, one describing stresses due to arbitrarily distributed normal and tangential loads on a deeply embedded circular crack, the second describing stresses due to arbitrarily distributed normal and tangential loads on the surface of a half space. A description of both these theories has been provided elsewhere in much the form in which they were first developed [1]*. In addition, a more organized derivation of the basic analysis for the circular crack is being published [2], and illustrative results from it for several simple cases have been published already [3]. This theory is a broad generalization of an earlier one by Sneddon [4].

The use of the cited basic crack theory limits consideration to planar cracks which have circular or part-circular fronts, but this limitation is repaid by the great flexibility allowable in the load patterns. That flexibility is very helpful in analysing cracks for which nearby or intersecting body surfaces distort the effective crack loads substantially. The usability of the theory depends on special methods that have been devised for evaluating integrals of a seemingly formidable class that arise profusely in the expressions for stresses and displacements. Those methods are successful enough to change those integrals from a burden into an asset. A paper describing these methods has been prepared for publication and should be available soon.**

---

* Numbers in brackets refer to entries in the References.

** J. C. Bell, "Evaluation of Integrals Involving Products of Bessel Functions Having Application to Crack Stress Analysis".

In the crack stress theory, all the expressions for stresses and displacements are double series with terms that are functions of the position coordinates multiplied by coefficients (load constants) that are the same for all the series. For the boundary stresses on the crack, the expressions become Fourier series in the angular position, with each term multiplied by a series of Jacobi polynomials with the argument $(1-2\rho^2)$, where ρ is a dimensionless radial coordinate. Knowledge of the boundary stresses on the entire circular crack would allow determination of all the crack load constants and hence of all stresses and displacements throughout the body if it were infinite, but such knowledge is obscured when there are nearby body surfaces. Thus analysis of surface cracks is concerned mainly with the interplay of effects from crack loads and surface effects.

The surface load theory used here is built on effects from elemental loads acting on rectangular areas on the surface of a half space, but unlike previous theories its elemental loads are essentially pyramidal in form, varying linearly in two directions from an interior peak to an unloaded boundary, as shown in Figure 1. Use of arrays of overlapping elements with arbitrary peak loads (surface load constants) permits representation of continuous load distributions which are arbitrary except that they vary linearly in both directions over each rectangle on the surface. Such representations for surface loads avoid the load discontinuities and artificially high local stresses that would be implied by use of load elements with uniform profiles. This avoidance of gross local distortion of stresses also allows performance of a vital checking process as explained later.

The crack and body geometry considered in much of the research to be described is illustrated in Figure 2. The body is a plate partly penetrated by a crack perpendicular to the faces of the plate. A rectangular coordinate system (x, y, z) is fixed by the front surface and the crack, and a cylindrical coordinate system $(r, \theta, \mathfrak{z})$ is fixed by the crack circle. (Note that the letters z and $\mathfrak{z}$ are to be distinguished, and that further local rectangular systems may be associated with any plane face.) The crack radius a is used as the reference length, so with $\rho = r/a$ and $\zeta = \mathfrak{z}/a$, the cylindrical coordinates are often written as (ρ,θ,ζ). The crack shape is defined by its depth-to-length ratio A/2C and by its fractional penetration ratio A/T. The loads

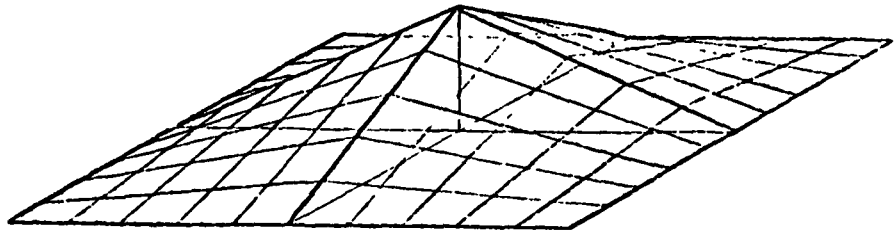

a. A typical pyramidal element

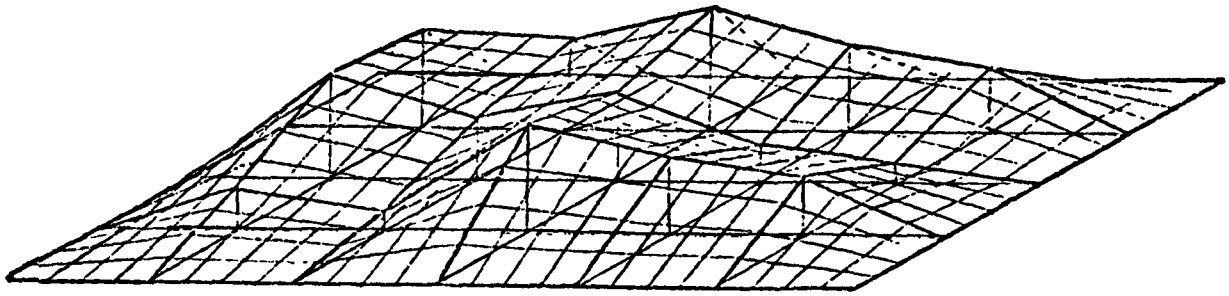

b. A typical composite load represented by pyramidal elements

FIGURE 1. SURFACE LOAD ELEMENTS OF PYRAMIDAL FORM

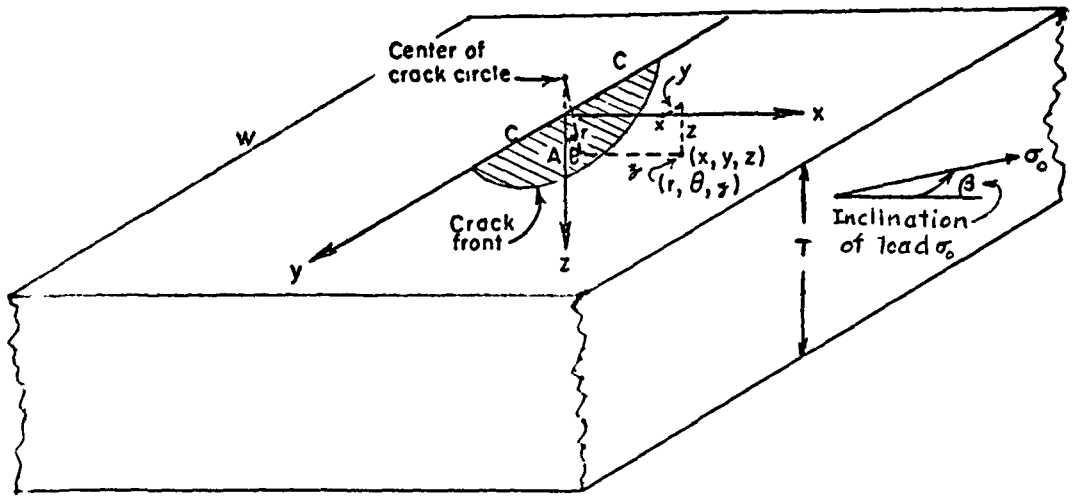

FIGURE 2. NOTATION USED IN ANALYSIS, AS IT APPEARS FOR CRACKS PERPENDICULAR TO THE SURFACE

considered here are related to a remote tension σ_o, but they may be applied obliquely at some angle β as shown. In the present work, the length of the plate in the x-direction is always large, but for some of the cases the plate has a finite width W, and then the parameter W/2C is also important.

The surface crack analysis takes as its assigned loads the stresses which would exist at the location of the crack if no crack were there but which cannot be transmitted with the crack present. It does not suffice merely to fit such crack loads as one would if the crack were deeply embedded, for loads on the crack induce spurious stresses on the surface or surfaces of the enclosing body. To eliminate those surface stresses, freeing stresses are applied to the body surfaces, but these induce spurious stresses on the crack, and so on. In the present work, this chain of interactions is resolved in one calculation for selecting crack and surface load constants simultaneously by least squares fitting of the desired resultant boundary conditions at selected points scattered over the crack and body surfaces, and this fitting determines the load constants for both the crack and the body surfaces. In principle this process is straightforward, but in practice it requires resolution of both numerical and logical problems.

Treatments for the numerical problems of evaluating the influences of crack and surface load constants and of finding a boundary-point least-squares fit of selected boundary conditions have been assembled in a computer program called FRAC3D and companion programs called LATTICE and MATSOL. FRAC3D incorporates an array of special methods for evaluating the integrals used by the crack functions together with formulas for the influence each crack load constant has on the stresses and displacements at any given point. Using input generated by LATTICE to define the bases of pyramidal surface loads, FRAC3D also calculates the influence each surface load constant has, including considerable bookkeeping to avoid much otherwise repetitious arithmetic, attributable for example to symmetries. It performs the necessary transformations of coordinates and stress components to make the many contributions compatible in summing. It does this for load constants for as many as six body faces (for a rectangular block shape) as well as for the crack, and the crack can be arbitrarily deep and even tilted. In its "SOLVE" mode, FRAC3D constructs a system of boundary condition equations to be solved for the many

load constants, but the actual solving for them is performed by the program MATSOL which also computes stress intensity factors at many points along the crack front. Then if stress or displacement calculations are desired also for points anywhere in the body, they can be found from the load constants by returning to the program FRAC3D, using it in its "RESULT" mode. The formal processes for doing these operations are described in a User's Manual issued as a supplementary report (NASA CR159401), but practical considerations in doing that work are better understood if one considers the treatments given to the various cases discussed in the present report.

The performance of surface crack analyses by the present computer program involves many choices to be made by the analyst. He must design rectangular latticework to define load bases for the surface-load theory, and he must select the series terms to be used actively in the crack theory. These choices are not trivial, and the results of the calculations often depend signficantly on what choices are made. Pursuit of accuracy by great subdivision of surface latticework or by enlargement of crack function series often proves to be self defeating, for reasons to be discussed in connection with specific cases later. Thus the analyst requires insight concerning choices that promote good design of a surface crack analysis; and since the propriety of a chosen design can not yet always be known in advance, he must also have a way to decide whether the results that follow from it are proper for the case it was chosen to treat.

The reason why a given calculation may not apply properly to the case for which it was performed arises from the use of pointwise satisfaction of boundary conditions. (It cannot arise from inconsistent treatment of internal stress relationships in the body, since the functions arising from both of the present basic theories satisfy all the conditions for elastic behavior exactly.) Since only pointwise satisfaction of boundary conditions is enforced, it is entirely possible for the satisfaction of proper conditions at non-fitted points on the boundaries to be missed, often badly. Therefore, a policy has been applied in performing the stress analyses here to check how well the proper boundary conditions would be satisfied by a computed solution at many boundary points not used in finding that solution. A computed solution is deemed

acceptable only when overall satisfaction of boundary conditions is achieved, as judged from the results of this checking and the light of Saint-Venant's principle.

It should not be thought that the need for caution in accepting calculated stress analyses for surface cracks is a difficulty peculiar to the current methodology, since analogous weaknesses due to pointwise fitting of boundary conditions or approximation of field equations are common to all the methods that have been used for this class of problems. Indeed, the present method is probably the most advantageous of all, since it offers such a transparent means for checking the overall satisfaction of the necessary conditions.

The analyses here have been divided into three tasks. In the first task, cracks with various geometries (that is various A/2C and A/T but with $W/2C = \infty$ only) are treated with uniform normal loads. In the second task, most of these cracks are treated for loads applied obliquely. In the third task the plate may have various finite widths, but the load is only normal. The specifications for the cases in these three tasks are shown in Table 1.

The following discussion of analyses groups the cases first according to the tasks and next according to the depth-to-length ratio A/2C, since the requirements for design of the analysis are governed largely by those factors. Requirements for the design which are common to all the cases are discussed mainly in connection with the first case.

The fourth task was to make the computer programs operational on an NASA computer. This has been done, using an early form of the User's Manual provided as a separate report (NASA CR159401). Some discussion of this part of the work is included later.

Many results will be persented here in graphical form, though they were obtained in numerical form from the computer, which was usually either a CDC Cyber 73 or a CDC 6500.

TABLE 1. SURFACE CRACKS AND LOADS CHOSEN FOR ANALYSIS

Task	Load	A/2C	A/T	W/2C
I	Uniform normal	0.50	0.0, 0.5, 0.7. 0.9	∞
		0.25	0.0, 0.5, 0.7, 0.9	∞
		0.10	0.0, 0.5, 0.7, 0.9	∞
		0.05	0.0	∞
II	Variously oblique	0.5	0.0, 0.5, 0.7, 0.9	∞
	(β = 24°, 45°, 60°)	0.25	0.0, 0.5, 0.7, 0.9	∞
		0.10	0.0. 0.5, 0.7	∞
III	Uniform normal	0.25	0.0, 0.5, 0.7	2.0
		0.25	0.7	1.5
		0.25	0.7	3.0

SURFACE CRACKS UNDER NORMAL LOADS

The surface cracks chosen for analysis presuming a uniform normal load σ_o (which corresponds to having remote tension perpendicular to the crack) included cases for four depth-to-length ratios A/2C with several fractional penetration ratios A/T, as shown in Table I. Since cases with the same A/2C form a natural group, such groups will be discussed separately, but several matters affecting all groups will be treated in connection with the first group (with A/2C = 0.50) and especially with the first case (with A/T = 0.0).

Cases with A/2C = 0.50

If A/2C = 0.50, the crack is semicircular. It might be expected that such cracks would be simplest to analyze, and indeed stress intensity patterns for such cracks in semi-infinite bodies (so that A/T = 0.0) were published quite early [5,6]. The apparent simplicity vanishes, however, if the plate has a back surface (so that A/T > 0.0), and some previous investigators seem to have avoided such cases. Thus the semicircular crack is interesting and not trivial.

Some Principles for Design of Analysis

Since the crack load here is implicitly normal to the crack and symmetric around $\theta = 0$, regardless of the presence of the body surfaces, the crack function series should use as load constants only those related to normal loads symmetric around $\theta = 0$. In the notation of Appendix F or Reference 1, these are the $\alpha'_{m,k}$. The constants related to shear loads (there called $\beta'_{m,k}$, $\gamma'_{m,k}$, $\hat{\beta}'_{m,k}$ and $\hat{\gamma}'_{m,k}$) should vanish*, as should those for antisymmetric normal loads (the $\hat{\alpha}'_{m,k}$). In the expressions for normal loads on the crack, each constant

* In the notation of References 2 and 3, these shear load constants are $a_{m,k,2}$, $a_{m,k,3}$, $\hat{a}_{m,k,2}$ and $\hat{a}_{m,k,3}$, respectively. The $\alpha'_{m,k}$ and $\hat{\alpha}'_{m,k}$ are there called $a_{m,k,1}$ and $\hat{a}_{m,k,1}$. The way in which the crack load constants enter the analysis is explained further in Appendix F.

$\alpha'_{m,k}$ is multiplied by a term including a factor cos $m\theta$. Since a series of such terms is even in θ and complete as a Fourier series over the range $-\frac{\pi}{2} < \theta < \frac{\pi}{2}$ even if only even values are used for m, it is sufficient to use only those terms for which m is even. Beyond this, it has been found that the rapidity at which many crack functions become large as their evaluation points are shifted on the crack plane toward the crack front depends largely on the sum m + 2k*, and that increase of this sum increases numerical difficulties with the integrals used in the crack functions. For these reasons, it was decided that for normally loaded semicircular cracks the crack load constants to be used would be only the $\alpha'_{m,k}$ with m even and with m + 2k only up to some fixed value, normally 16. Since m and k begin with 0 and range upward, this allowed all the crack function series to have 45 terms.

Use of the boundary point least squares fitting process requires selection of points where the fitting is to be done. Since there were usually 45 crack load constants to be fitted for semicircular cracks, and since least-squares fitting typically benefits from using about twice as many points as there are constants, 99 points were selected for the fitting of boundary conditions. These points, together with 89 selected for checking purposes, are shown in Figure A1 in Appendix A. It can be seen that the pattern for these points was chosen partly by a polar design near the crack front and partly by a linear design near the crack lip, with extra concentration of points near each of those potentially troublesome boundaries. An effort was made also to get points at enough circumferential and radial spacings to exceed the counts of angularly and radially distinct functions to be fitted. The motivation behind these choices also governed point selection for cracks with other ratios A/2C as shown in Appendix A.

---

* It may be noted that as the evaluation point approaches the crack front many crack functions become infinite if the point is off the crack but not if it is on the crack. In particular, the radial variation of the boundary stresses on the crack is expressible in terms of polynomials of r if r < a, and the polynomials remain finite as $r \to a$. For r > a the polynomial representations of the same stress components are not relevant, even on the crack plane, and indeed the relevant functions become large in proportion to $1/\sqrt{r-a}$. The ability of the present crack functions to represent such behavior analytically illustrates the power and adaptability of the theory being used here.

The choice of surface load functions to be used is set by the rectangular latticework used on each surface of the body. Since doubly linear interpolation of the freeing loads is implied within each rectangle, the rectangles should be small enough so that kind of interpolation will suffice. To get a crude estimate of the freeing loads which may be needed, one may consider the patterns of stresses that would arise on the front or back surface if there were no surface effects, that is as if the body were infinite. Such a pattern for stresses σ_z, proportional to that from a uniform normal crack load, is shown in Figure 3 for part of the plane cut by a semicircular crack (along $x = 0$ over $-1 < y < 1$), presuming Poisson ratio 0.3. For a unit load, these factors would be multiplied by $\alpha'_{0,0} = \sqrt{2/\pi} \approx 0.80$. Also shown is part of the latticework actually chosen for the fitting process. Only one quadrant of the lattice is shown, since it is symmetric around both the x and y axes, as are all lattices to be used here. Since the shear stresses τ_{yz} and τ_{zx} implied by crack loads defined by constants $\alpha'_{m,k}$ with m even vanish on the front surface for a semicircular crack, as the formulas of Appendix F show, the stress σ_z is the only one needing to be freed on that surface when the crack is semicircular and the body is a half space (A/T = 0.0). Thus the detail of the lattice of Figure 3 seems reaonable for this case, though it must be admitted that unexpected contingencies may arise in the fitting process to make the freeing load patterns quite different from this estimate. The entire lattice for this case is shown as Figure B1 in Appendix B, where lattices for all the cases are collected.

The surface load elements to be used can be visualized readily by noting that their peaks occur wherever two lattice lines cross, with both extending in both directions beyond the crossing. Such points are called pyramid points, and it should be noted that many of them occur on the axes of symmetry when the symmetric extensions of the pattern are recognized. The base for each pyramidal load element includes the four smallest rectangles adjoining the pyramid point which can together form a single larger rectangle. Over each such base three pyramidal loads may act, defined by peak loads p ($\sim -\sigma_z$), s ($\sim \tau_{zx}$) and t ($\sim \tau_{yz}$). Symmetry, of course, demands here that s should vanish for pyramid points on the y-axis while t should on the x-axis.

It is also necessary to choose points where boundary conditions are to be fitted on the body faces. In earlier work it had been tempting to choose

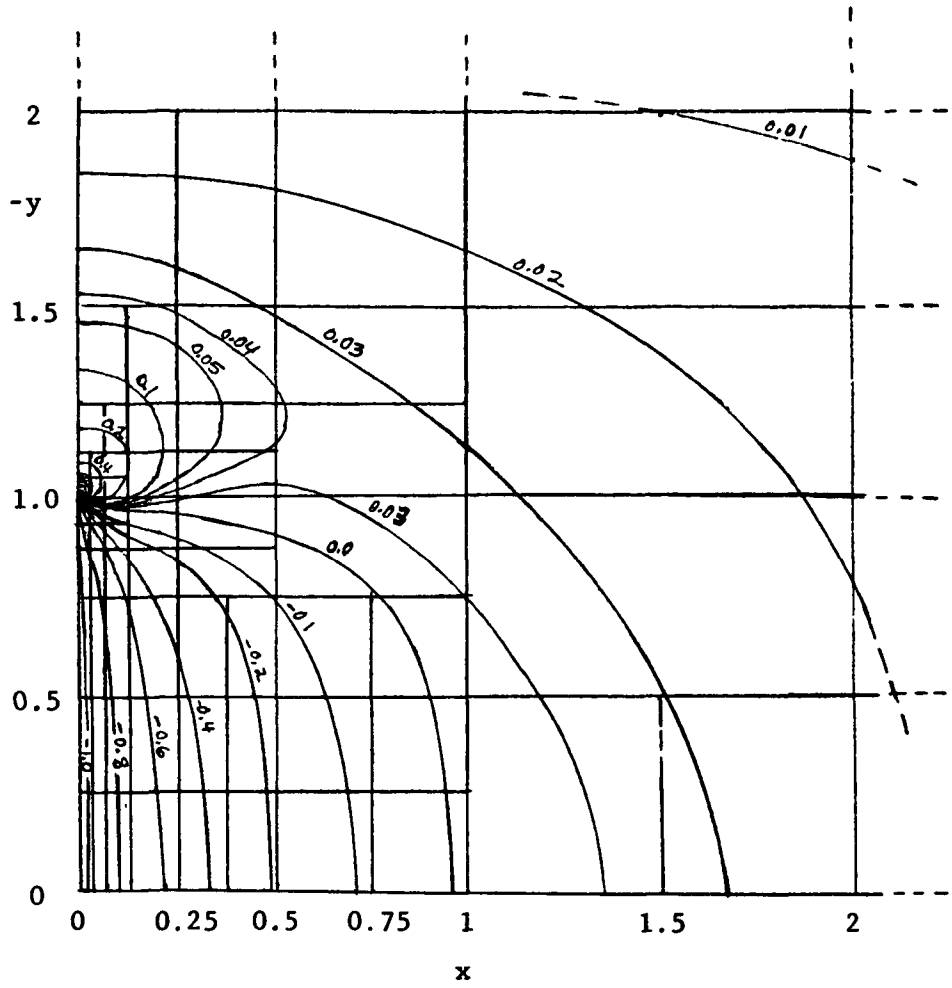

FIGURE 3. INFLUENCE FACTOR FOR $\alpha'_{0,0}$ AFFECTING σ_z ON SURFACE CUT BY A SEMICIRCULAR CRACK

many such points, perhaps twice as many as the number of pyramid points, but it was found that then the calculated load constants, stress intensity factors, and so on were extremely dependent on where the points were placed. An eventual interpretation of this phenomenon was that when more boundary conditions are assigned on a surface than the number of load constants available on that surface, then the crack load constants become engaged in the fitting of surface load conditions, and they are badly adapted to that function. A general rule seemed evident: crack constants should be used only to fit crack conditions and necessary interactions with the surfaces, while surface constants should be used only to fit surface conditions and necessary interactions with the crack. Happily a convenient way was found to effect this division of roles among the two classes of load constants, namely to assign surface boundary conditions only at pyramid points. This assured that each boundary condition assigned on a body surface would have an associated surface load constant with the primary function of satisfying that condition. Moreover, the surface loads at most pyramid points are strongly dominated by a single surface load constant, so there is little confusion of roles among surface load constants in fitting of surface boundary conditions. Thus a key choice made in the present work is simply that surface boundary conditions have been assigned only at pyramid points, except when the pyramid point happens to be the crack tip. At the tip the complex variations of crack stresses would make the pyramid point poorly representative of the possible choices, as Figure 3 suggests. (There $\sigma_z \to \infty$ along most rays approaching the crack, but not on the crack.) This plan for surface boundary-condition points has been used in all the analyses in this report, but some variation has been allowed for the point near the crack tip.

The boundary conditions assigned at each selected point on the crack or on a body face are that the three stress components that could be transmitted across the face there must have the proper overall values when contributions from all load constants are taken together. (FRAC3D arranges this automatically after being given the boundary condition point.) On the body faces those proper values are zero, and if the crack is subjected to a uniform normal load the conditions there are $\sigma_z = -\sigma_o$ and $\tau_{\theta z} = \tau_{zr} = 0$. In the calculation, a factor σ_o has been removed from all the stresses, so all the calculated stresses and surface constants should be multiplied by σ_o if dimensional values are desired. Also in the calculations the crack radius a was treated as the unit length, so

that linear coordinates shown are multiples of a. Moreover, the calculated crack opening displacements effectively include a factor $\mu/(\sigma_o a)$ where μ is the shear modulus.

Another condition applied to all the analyses is that considering all the crack loads and freeing loads the body must still be in equilibrium. For the cases of normally loaded surface cracks in plates, this means that the sum of the loads p applied at all pyramid points, weighted according to their pyramidal bases and their directions of action (whether +z or -z), must vanish.

Case with A/T = 0.0

With the above principles and choices, the analysis was undertaken, beginning with the case having A/2C = 0.50 and A/T = 0.0, presuming a unit normal crack load, so that $\frac{\sigma_z}{\sigma_o} = -1$ on the crack. Poisson's ratio was taken to be 0.3, the value to be used for all calculations reported here unless otherwise stated. After a special computer program called LATTICE was used to obtain many indices associated with bases for pyramidal surface loads, its output was used as input for FRAC3D in producing the system of boundary condition equations. Then MATSOL was used to solve the system for the load constants, essentially by a method of successive elimination which has been found to yield high accuracy. From the crack constants, using formulas on Page A-9 of Reference 14, the first-mode stress intensity factor k_1 was found at many points along the crack from root to tip. (Most commonly, 41 points have been used from root to tip, though only 21 were used here. Changing this count is trivial.) This factor k_1 was normalized by dividing it by the value the load would have implied around a deeply embedded crack, that is by $k_{1\infty} \equiv 2\sigma_o \sqrt{a}/\pi$, so that the printed output was $k_1/k_{1\infty}$. Since the commonly used factor K_I is simply $k_1\sqrt{\pi}$, the output can also be read to be $K_I/K_{I\infty}$. These results for the stress intensity factor are shown in Figure 4. Actually several slightly different sets of results were found by using various placements of the boundary condition point near the crack tip. The results shown used a point midway from the tip to the next lattice point beyond the tip on the crack plane. Results found with other placements will be described later in the Discussion.

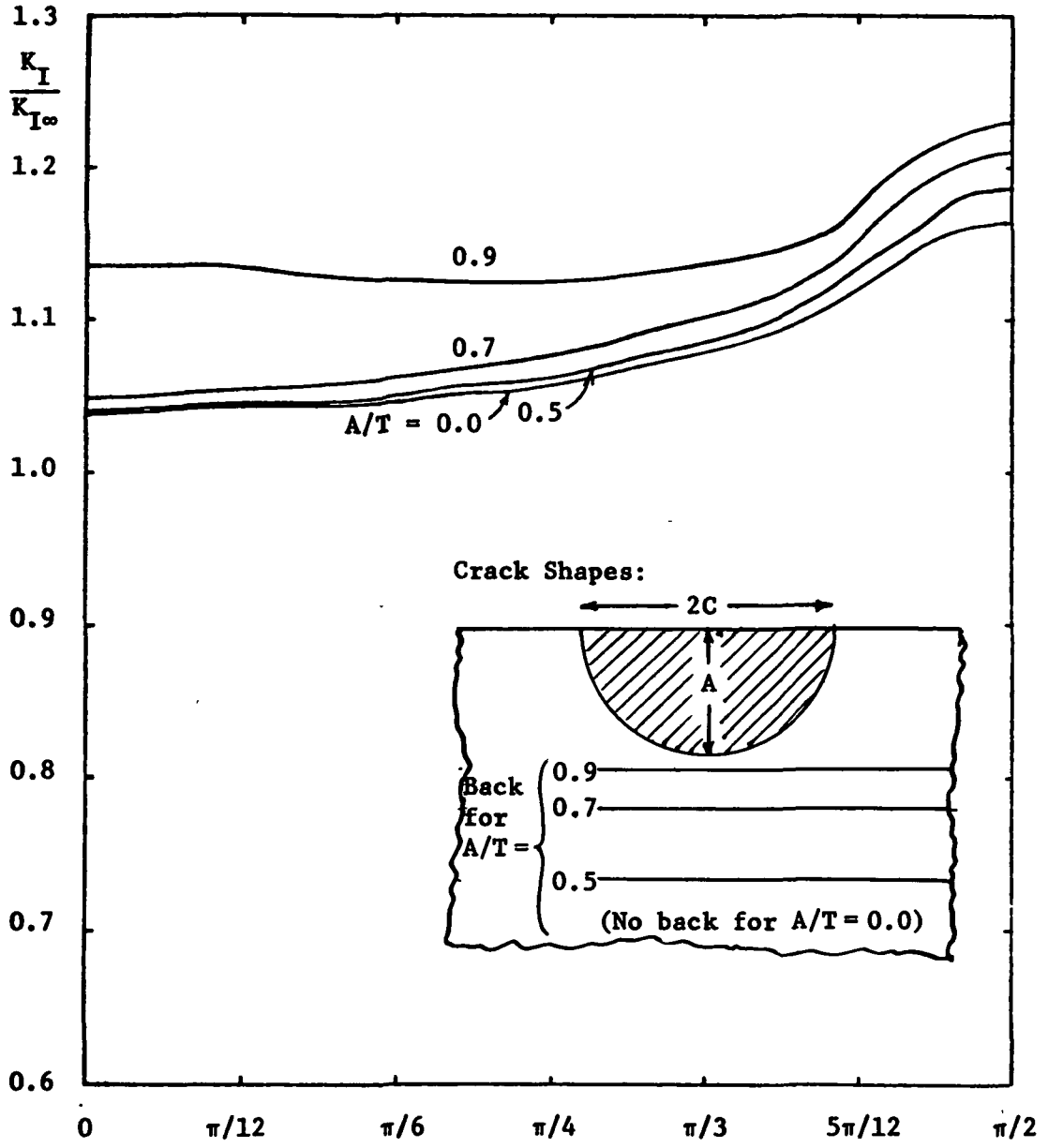

FIGURE 4. STRESS INTENSITY FACTORS ALONG SEMICIRCULAR SURFACE CRACKS (A/2C = 0.5) UNDER NORMAL LOADS

This stress-intensity factor distribution for A/T = 0 is like factors that have been reported by Smith and others [5,6] except that theirs rise more rapidly near the crack tip. Their results were found by fitting two basic analyses at discreet points, somewhat as was done here, but with basic analyses that were less developed. In view of the adaptability of the basic theories and the fineness of detail used here (which is greater than in a previous analysis which used the same methods and gave nearly the same stress intensity pattern), the present results should be afforded a high degree of credibility, but details near the crack tip are not entirely certain.

The method used here for justification of results, however, is not comparison with other authors' results, but is instead the checking of overall satisfaction of boundary conditions. To this end, values for the stress σ_z were found at the midpoints of all the surface rectangles and for σ_z at all the checkpoints shown in Figure A1, using the load constants found by solving the assigned boundary conditions. The misfits obtained at this array of non-fitted points, as percents of the applied load, are shown in Figures 5 and 6. Being calculated for points well removed from the points where fitting was done, these misfits should be among the poorest that could be found, yet except in small regions near the crack tip and lip these misfits are small. Differences between the calculated stress system and the ideally desired stress system must be traceable to the overall pattern of boundary stress misfits, so Saint-Venant's principle implies here that the differences between the calculated and the ideal systems are small, except very near the crack lip and tip. This reasoning provides confidence in the calculated results. The difficulty near the lip probably is traceable to the discontinuity required in Fourier series to fit some implied discontinuous stress or movement. In anticipation of such problems, considerable refinement had been built into the front lattice near the crack lip.

One other check, more necessary for cases involving back surfaces, is that σ_x and τ_{zx} should become small near the upper x-limit of the lattice, while σ_y and τ_{yz} should be small near the upper y-limit. For the present case, all such stresses were found to be less than 0.02. Thus again the calculated stress system seems good.

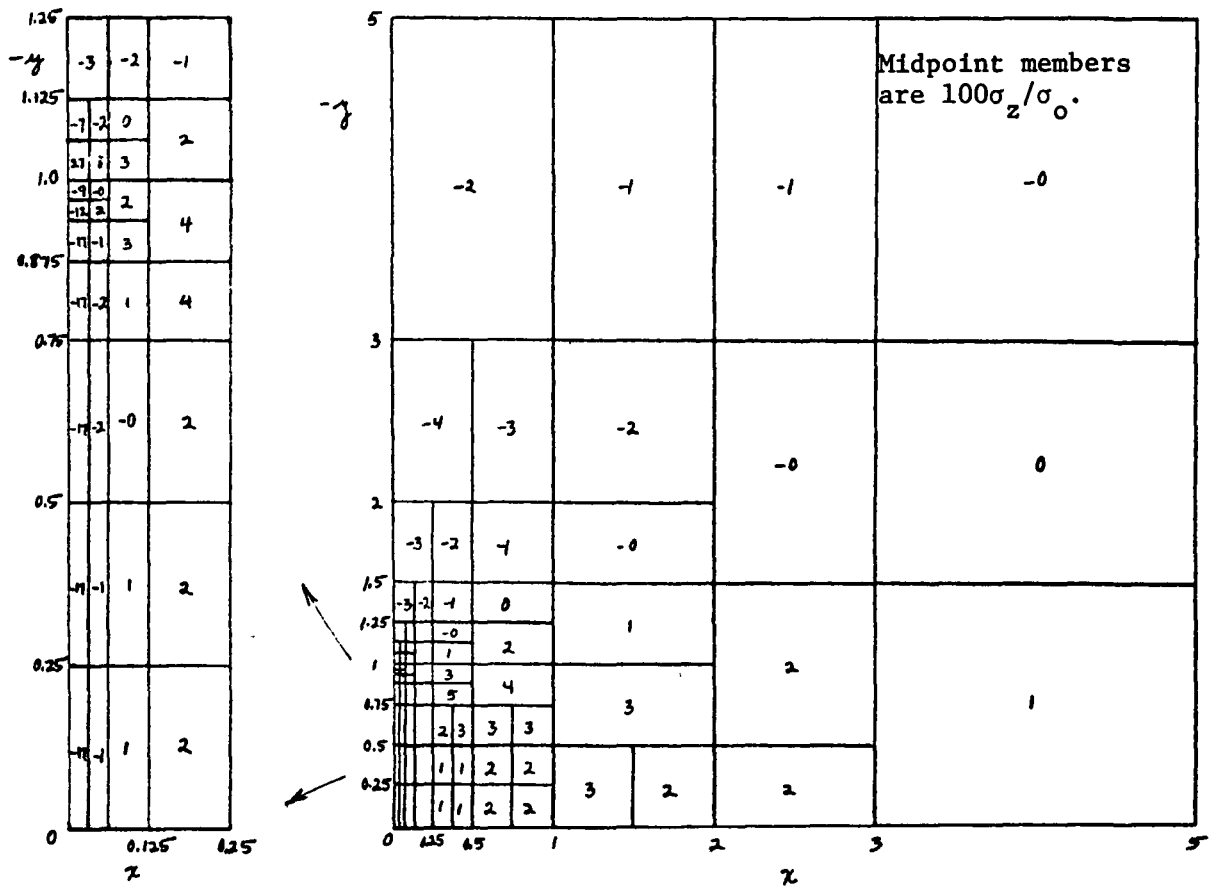

FIGURE 5. CHECKS OF σ_z AT NON-FITTED SURFACE POINTS AROUND SEMICIRCULAR CRACK (A/2C = 0.5, A/T = 0.0) UNDER NORMAL LOAD

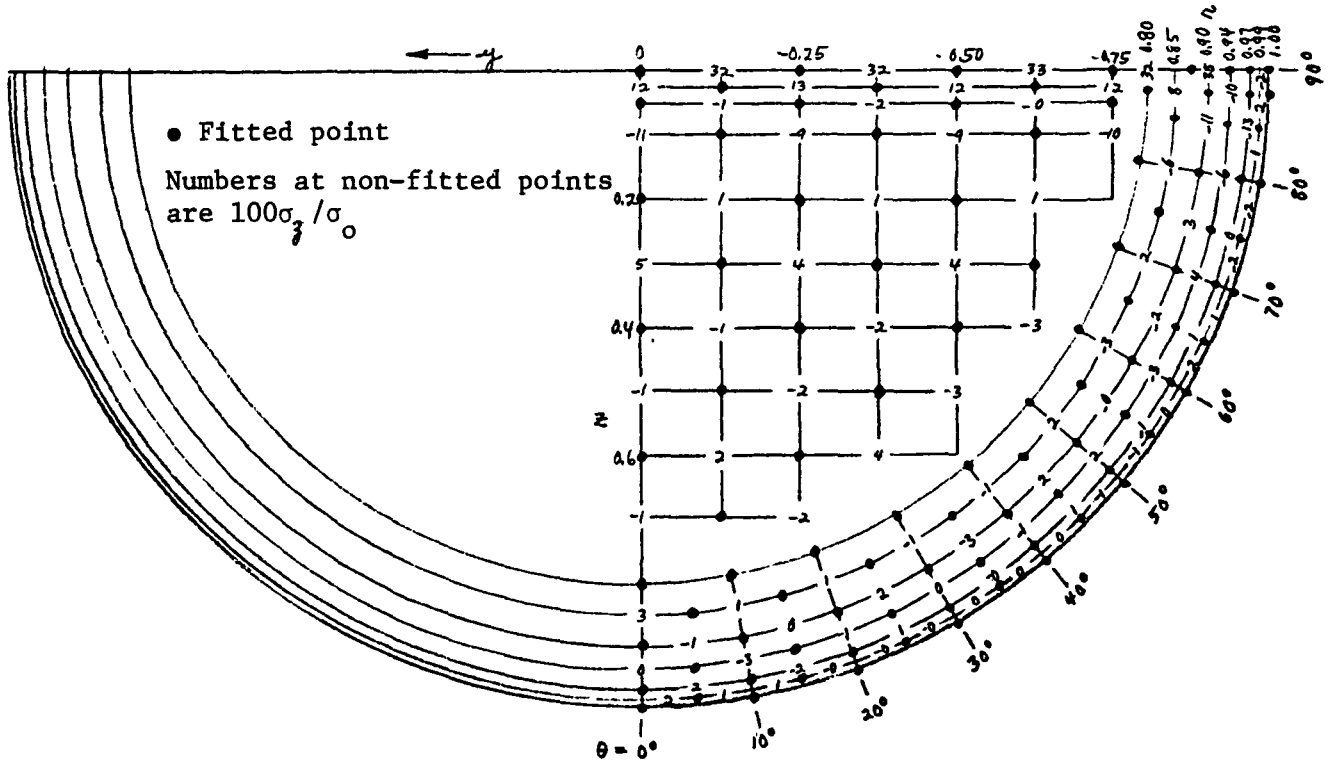

FIGURE 6. CHECKS OF σ_z AT NON-FITTED POINTS ON A SEMICIRCULAR SURFACE CRACK (A/2C = 0.5, A/T = 0.0) UNDER NORMAL LOAD

Cases with A/T > 0

Turning to cases with a semicircular crack in a finite plate so that A/T > 0, it was apparent that some new features would need to be added. One new requirement was suitable back lattices, so some promising ones were chosen depending on A/T, as shown in Figure B2. In choosing, it was recognized that disturbances of stresses from a crack radiate toward the back quite strongly in directions tilted about 45° from the crack plane. This, together with the distance from the back to the crack, influenced the spacing and breadth of the refined latticework nearest the root of the crack.

A second new consideration was that freeing forces on the back would need to include shearing as well as normal stresses, and the presence of shearing stresses applied to the back would imply a need for shearing components among the freeing loads applied to the front. Thus a full complement of freeing loads was admitted on both the front and back surfaces. The same patterns were applied for series structure and boundary condition positions as had been applied when A/T = 0, yet when new calculations were made presuming A/T = 0.5, the results were very poor. Not only was the level of the stress intensity factor greatly reduced where intuition said it should increase, it was also found that the non-fitted boundary conditions far from the crack were poorly satisfied, and even the satisfaction of fitted conditions at distant points was bad. A change was needed.

An attempt was made to emulate the treatment of the case with A/T = 0.0 by dropping the shear freeing loads and the shear boundary conditions from the front face, but this proved to be inadequate. Since boundary conditions at distant points were proving difficult of satisfaction, an attempt for improvement was sought by doubling the range of the latticework in both directions. This only made the solution worse.

It was clear that some new principle was at work. After reflection, it was realized that whereas the constants $\alpha'_{m,k}$ describing normal loads on the crack were not allowed by the formulas to produce any shearing loads on the front surface (See Appendix F, putting m even and $\theta = \pm \frac{\pi}{2}$ in the formulas for $\tau_{\theta z}$ and $\tau_{r\theta}$.), the shearing loads on the front surface could exercise great influence on the normal stress on the crack. Thus a non-reciprocal relationship existed between the constants $\alpha'_{m,k}$ for the crack and the constants s and t

for the front surface, with those constants s and t assuming the role of unrestrained tyrants. That relationship could not be tolerated, especially since the only reason for admitting those front constants s and t had been to compensate for some minor shearing stresses emanating from freeing loads on the back surface.

With this interpretation in view, it was decided to return to the boundary condition equations obtained using the original lattices but while solving them to delete all influence that front-surface loads s and t might have on the normal stress on the crack. This performed wonders in improving the solution for the case with A/T = 0.5, most noticeably in the more distant parts. The influence of those front-surface loads s and t was restored, however, in checking the fitted boundary conditions, and those conditions were found to be satisfied nearly as well as they were by the original, distorted solution. Even with this new method of solution, however, some small difficulty remained in fitting boundary conditions far from the crack, so recourse was taken to weighting those conditions more heavily in the least-squares fitting process. In particular, weights were assigned to conditions at the more distant points in approximate proportions to the area each point sampled. With this additional change, the solution for the case with A/T = 0.5 achieved approximately the same apparent quality as had been attained with A/T = 0. The calculated stress intensity factor for the case with A/T = 0.5 using this method has been added to Figure 4. Further solutions for the cases with A/T = 0.7 and 0.9 obtained by the same methods were found without difficulty and are also shown in Figure 4.

It is reasonable to inquire what may be learned more broadly from this experience. One thing is that unreciprocated relationships between two sets of load constants can be very poisonous to a solution. The lack of influence of the $\alpha'_{m,k}$ on front-surface shears produced a particularly dangerous situation here, but that may not have been the only trouble. It appears likely that the diminishing ability of the crack constants to influence any conditions at great distances from the crack also admitted errors in the parts of the solution for the more distant parts, especially when moments generated jointly by freeing forces on the front and back surfaces could influence normal stress on the crack significantly. This consideration may explain why the

insistence on better satisfaction of conditions at more distant parts helped. It also argues against extending analyses for the effects of surface loads to distances beyond those where the effects of the crack should be felt.

It seems probable that efforts by previous investigators to merge two forms of whole-body analysis by applying discreet boundary conditions (as is done here) have encountered problems similar to those found here. One may wonder whether this is partly why Thresher and Smith [6], in a study including back surface effects, omitted solutions for semicircular cracks in plates of finite thickness. For a very thick plate (A/T = 0), they found the $K_I/K_{I\infty}$ shown in Figure 7, together with earlier results from Smith, Emery and Kobayashi [5], in a comparison with results from the present study. It can be seen that results from these three studies generally agree, but as $\theta \to \pi/2$ the rise found by the present study is noticeably the gentlest.

Also included in Figure 7 are factors $K_I/K_{I\infty}$ found by finite element methods by Raju and Newman [7] and by Yagawa, Ichimiya and Ando [8]. Their cases with A/T = 0.2 should be nearly comparable to those found by the other methods, so the close agreement between the results of the present study (with A/T = 0) and those of Raju and Newman (with A/T = 0.2) is noteworthy. For higher values of A/T, the results from the finite element calculations diverge from each other and even more from the results from the present study as shown in Figure 4. The concensus regarding back-surface effects with semicircular cracks is therefore weak, especially for large A/T.

Cases with A/2C = 0.25

Analysis for cracks with length-to-depth ratio 0.25 proved to be much more straightforward. The relative ease of analysis here may have been partly attributable to considerable efforts that had been devoted to such cases at an earlier time, but it was also probably inherent in the analyses themselves. If A/2C = 0.25 the problem of unreciprocated relationships between crack and surface load constants is abated, yet the problems characteristic of small ratios A/2C do not seem to arise. Thus A/2C = 0.25 is a convenient ratio for the analysis of surface cracks having circular fronts.

If A/2C = 0.25, the surface lattices must be different from those

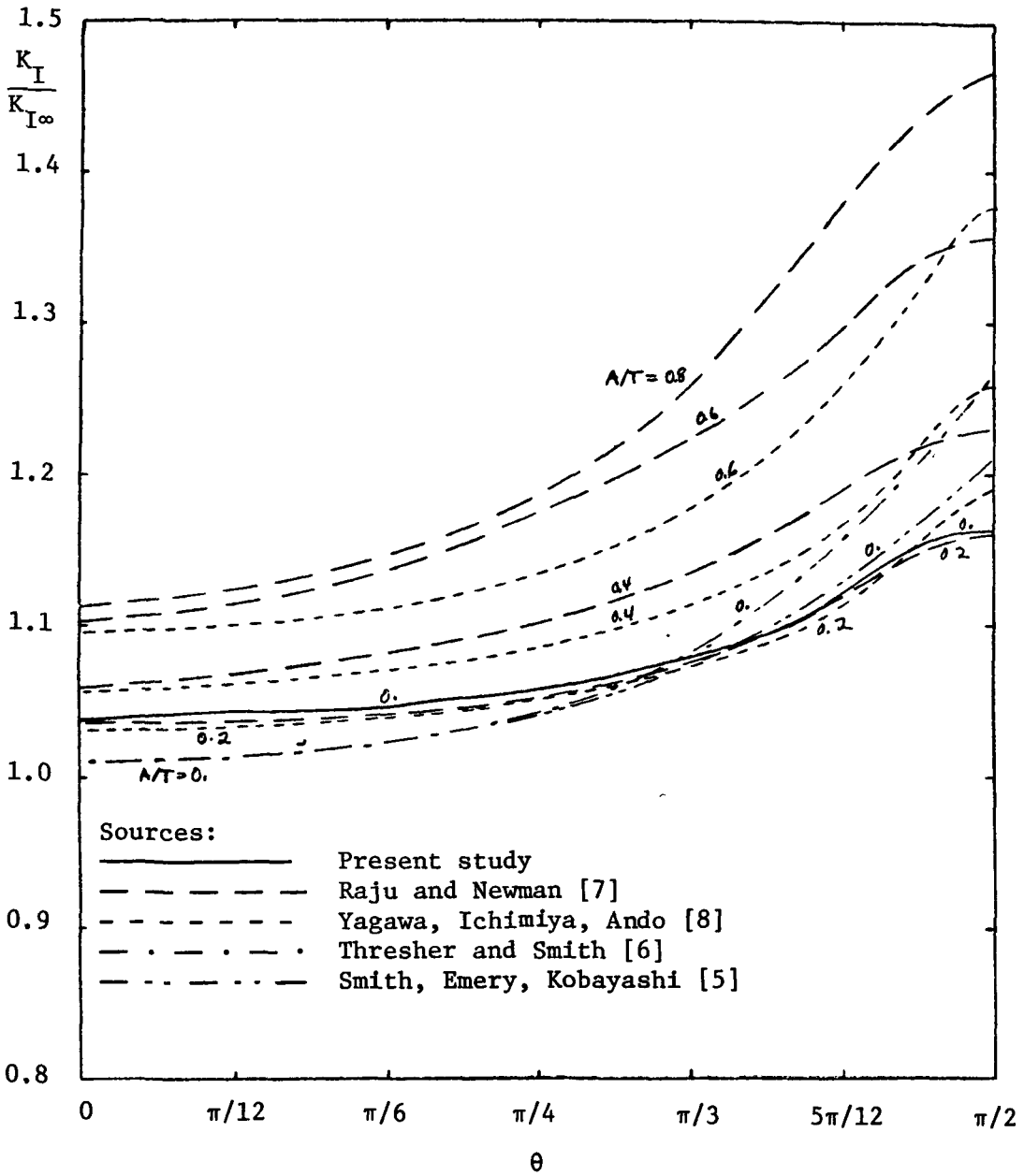

FIGURE 7. COMPARISONS AMONG STRESS INTENSITY FACTORS FOR SEMICIRCULAR SURFACE CRACKS AS CALCULATED BY SEVERAL INVESTIGATORS

used with semicircular cracks, but the earlier experience had furnished some good ones. A single front lattice was taken as suitable for the cases with A/T = 0.0, 0.5 and 0.7, and it is shown in Appendix B as Figure B3. A single back lattice was used for the cases with A/T = 0.5 and 0.7, as shown in Figure B4. With A/T = 0.9, some extension of the latticework laterally had been found desirable (presumably to account for plate bending), so for that case new front and back lattices were used, as shown in Figure B5 and B6. The boundary condition points used in conjunction with these lattices were again the pyramid points, except near the crack tip. Near the crack tip, because of an earlier search for representative boundary conditions, the s and t conditions were assigned as they were with the semicircular crack, but the p condition was set at a point one-fourth the way from the tip to the next lattice point along a line perpendicular to the crack. This somewhat unusual choice of tip boundary conditions should give good results if A/2C = 0.25, but they should differ only slightly from those found with the tip condition placement used with A/2C = 0.5. (Stress intensities found with either placement for the case with A/T = 0.7 agreed closely except very near the tip, where the off-plane boundary condition gave a result about 0.05 higher.)

The series structure used for cases with A/2C = 0.25 was the same as was used for semicircular cracks, that is an m-even series triangulated on k to keep 45 load constants. Eighty boundary condition points and 71 check points were selected on the crack, as shown in Figure A2.

The stress intensity factors $K_I/K_{I\infty}$ obtained by the analyses for these cases are shown in Figure 8. A striking feature of these results, as compared to results obtained by F. Smith and Thresher [6] is the maximum value located away from the crack root when A/T = 0.7 or 0.9. This shape is similar to that obtained by C. W. Smith experimentally [9], though his materials had Poisson's ratio ν near 0.5 whereas the present calculations used $\nu = 0.3$ to be nearer to that for common structural materials. The degree of agreement between his experiments and analyses of the present form is shown in Figure 9, including a solution for $\nu = 0.5$ found independently of the present project, and is very encouraging. These new results also agree with an observation occasionally mentioned by experimentalists, namely that part-circular cracks tend to ellipticize as they grow. Thus the results here promise to offer new insights into

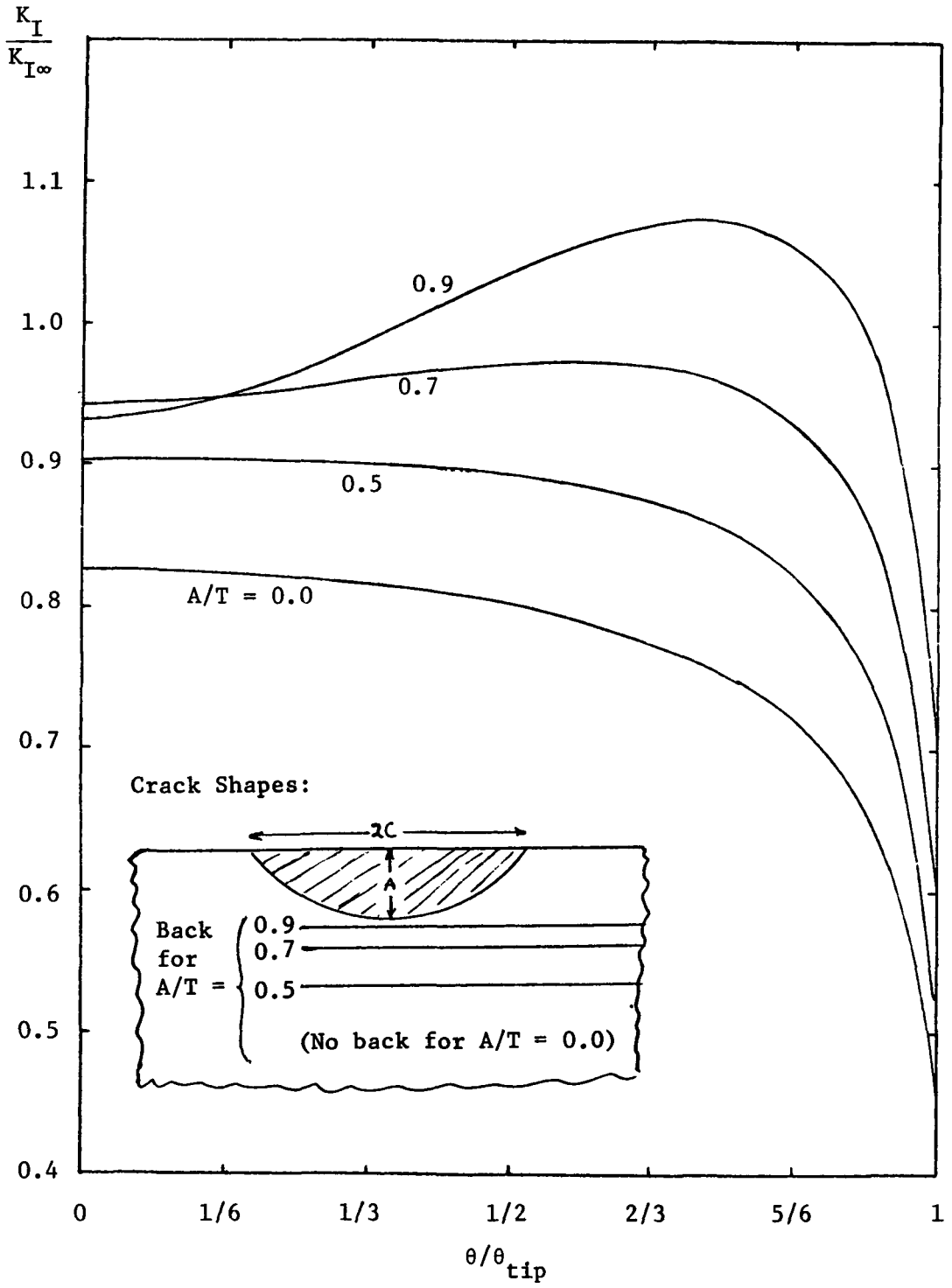

FIGURE 8. STRESS INTENSITY FACTORS ALONG PART-CIRCULAR SURFACE CRACKS (A/2C = 0.25) UNDER NORMAL LOAD

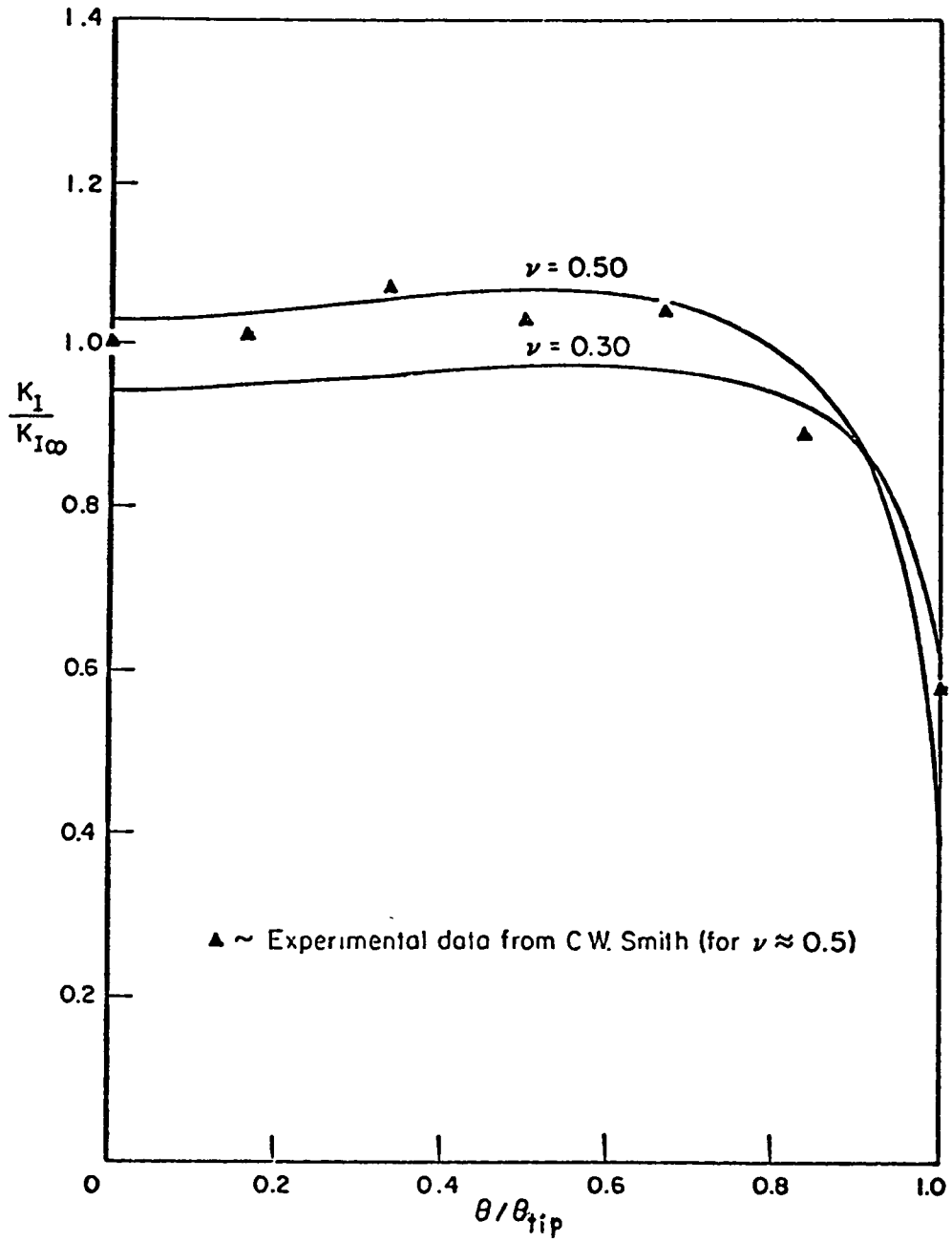

FIGURE 9. CALCULATED AND MEASURED STRESS INTENSITY FACTORS ALONG PART-CIRCULAR SURFACE CRACKS WITH A/2C = 0.25, A/T = 0.7 UNDER NORMAL LOAD

crack stability and growth.

The test for dependability derivable from the present theory itself was made, of course, by checking boundary conditions at non-fitted points on both the body surfaces and the crack. The misfits for σ_z on the front surface and for σ_y on the crack, as percentages of the crack load, are shown in Figures 10 and 11 for the case with A/2C = 0.25, A/T = 0.7 and ν = 0.3. (Checks for the case with ν = 0.5 showed misfits that are slightly larger). These checks suggest that the fitting of conditions is good, so that the solution is of high quality. Of course, a complete study of check points would include fittings of 3 stress components on each of the three faces. The full check is not shown here, but it indicated similar quality in all nine fitting patterns. Much more checking applied to analyses for other cases was also done but will not be elaborated here.

Cases with A/2C = 0.10

To begin treatment of the cases with A/2C = 0.10, which may be said to have slender cracks, new lattices were designed to accommodate freeing stresses from a crack on the xz plane with lip covering $\frac{-5}{13} \leq y \leq \frac{5}{13}$ and reaching down to where $z = \frac{1}{13}$. The crack series were taken with 36 terms, using only even values of m, with reductions in the number of k's as m increased, and for determining the crack constants 75 boundary condition points were chosen on the crack. The computations began as for the cases with larger A/2C, but trouble appeared very soon. In particular, it could be shown by inspection that the first solution for load constants for the case with A/T = 0 could not possibly furnish a least-square solution for the boundary condition equations that had been used to determine those constants. The solution could not possibly be right, and the stress-intensity factors computed from it reflected that by being negative. Thus began a long search for a usable design for analysis for a slender crack. To keep the work simple, the case with A/T = 0.0 was employed.

The first remedy tried for this analysis was to use double precision in redoing the least-squares fitting process. This was permissible since use of double precision in the fitting process did not need to be preceded by any consideration of accuracy in the coefficients of the equations to be fitted,

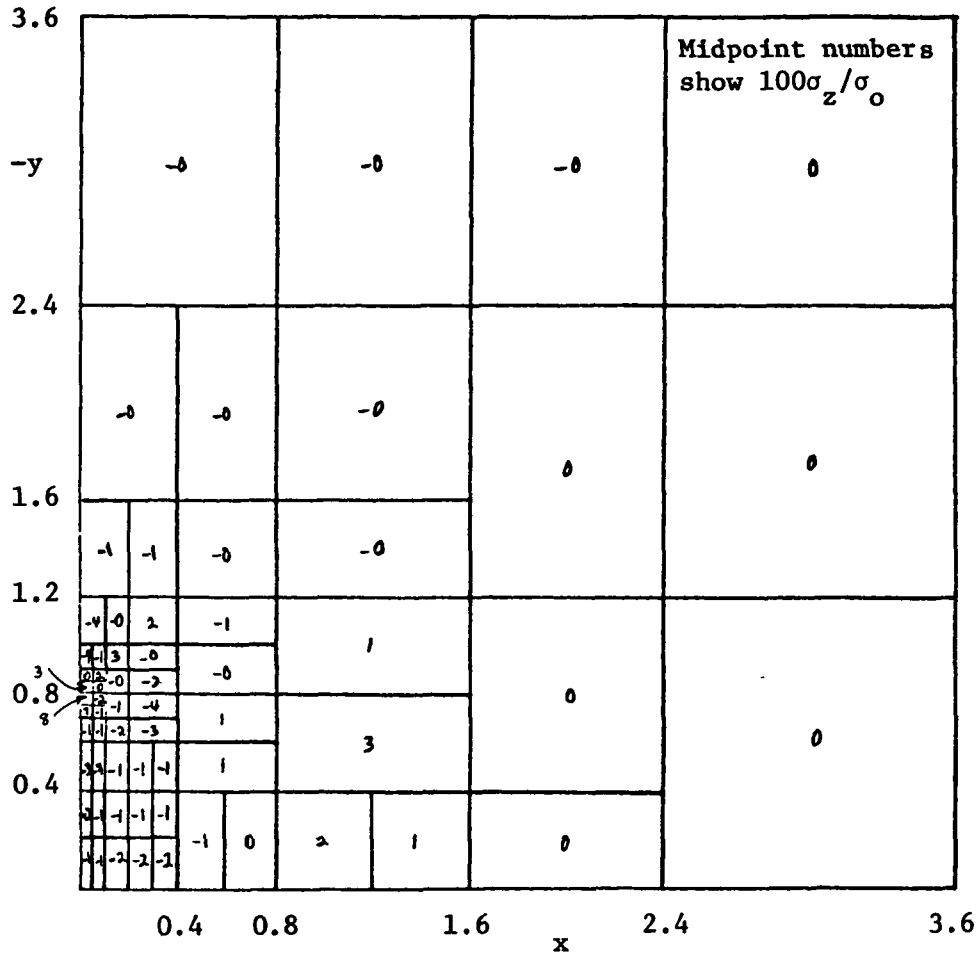

FIGURE 10. CHECKS OF σ_z AT NON-FITTED SURFACE POINTS NEAR A PART-CIRCULAR CRACK WITH A/2C = 0.25, A/T = 0.7, ν = 0.3 UNDER NORMAL LOAD

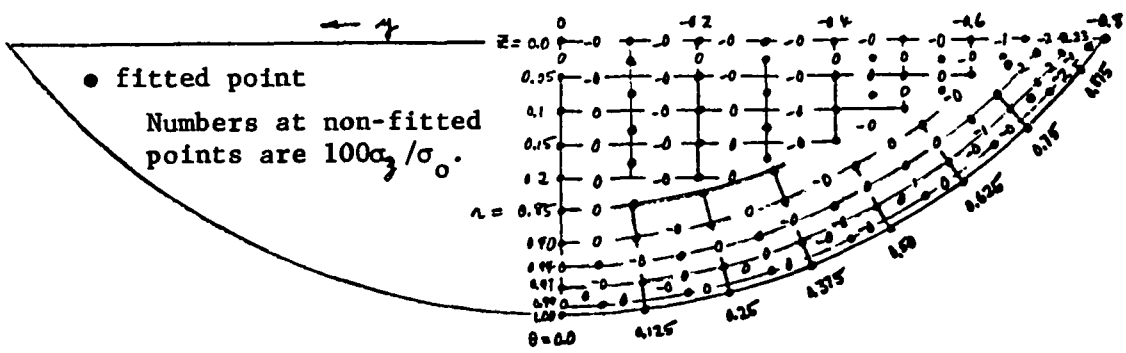

FIGURE 11. CHECKS OF σ_z AT NON-FITTED POINTS OF A PART-CIRCULAR CRACK WITH A/2C = 0.25, A/T = 0.7, ν = 0.3 UNDER NORMAL LOAD

since here only the accuracy of the fitting was at stake. The CDC Cyber 73 on which the work was done normally carries 15 significant digits, so with double precision it carried 30. Use of that precision did produce splendid fitting of the boundary conditions used, especially for points on the crack, but the following checks at non-fitted boundary points showed errors many times larger than the assigned crack load. Again the solution could not possibly be accepted.

Pursuit of a solution by assigning more latticework and continuing use of double precision was prohibitive - the 300,000 word high-speed memory on the largest computer at Battelle would have been much too small. Therefore, in view of indications that the crack was being overfitted at the expense of fitting on the plate surfaces, means were selected to produce a better balance in the fitting process. The original set of boundary condition equations was edited by reducing the number of crack constants used and by making roughly proportional reduction in the number of boundary condition points used on the crack. The first such reduction was cautious, but improvement was noticed, so further reductions were made until only 15 crack constants and 25 crack boundary points remained. With that reduction it was found that double precision was no longer needed, the fitting of boundary conditions all over the crack remained good, and troublesome misfits at non-fitted points on the front surface had been divided by factors of 10 to 100. Yet some uncomfortable misfits remained, so a further kind of revision was needed.

In order to obtain further improvement, a new set of boundary condition equations was computed including two basic changes: the front lattice was enlarged somewhat and further subdivided to reach the form shown in Figure B7 in Appendix B, and for the crack function series the terms for odd m as well as even m were retained. The purpose of retaining terms for odd m's was not to be able to use more terms—it was instead to make a broader selection of terms available. (Even hundreds of crack terms could be deleted during the editing effected by MATSOL.) In particular it was desired to find what could be done with series involving terms for m's that are multiples of 3, since it was suspected that such a choice might be particularly adapted to

cracks for which A/2C = 0.10.*

From solutions of variously edited versions of this new matrix it was soon found that use of m-triple series is beneficial, and indeed for the case with A/T = 0.0 there seemed to be fair latitude in further details of the structure of the crack series. Since series with 10 to 12 terms still seemed desirable, the assignment of boundary condition points on the crack eventually was accepted to be that shown in Figure A3 of Appendix A, using 25 points for fitting and 30 for checking.

With the case for A/T = 0.0 reasonably well solved, attention was given to cases with larger A/T. After a few attempts, an apparently reasonable solution was found for the case with A/T = 0.5, using the lattices shown in Figures B7 and B8 in Appendix B, and using a 12-term series. Included in the series were the first five k terms with m = 0, the first four with m = 3, the first two with m = 6, and the first one with m = 9.

Before the case for A/T = 0.7 was undertaken, it seemed apparent that even with m-triple series the solution might be very dependent on further details of term selection for the series. Since also it was recognized that the plate here is thin enough so that there might be significant bending of the plate over a fairly wide range, a pair of broader lattices was chosen, but arranged so that editing by MATSOL could trim their size. These lattices are shown as Figures B9 and B10. In addition crack function series with many terms were included to allow wide selection of series terms. Then an extended search for an acceptable solution began, using variously edited versions of a single set of boundary condition equations.

---

* The use of terms with m's which are multiples of three provides Fourier series which form complete sets over an angular spread $\frac{-\pi}{3} \leq \theta \leq \frac{\pi}{3}$. Such a spread of θ is large enough to span the part of the front surfaces needing fitting when A/2C = 0.10, but it excludes the extra part in $\frac{-\pi}{2} \leq \theta \leq \frac{\pi}{2}$ for which the m-even series provides. The exclusion of the extra part avoids ambiguities which would otherwise degrade the fitting of overall boundary conditions.

Repeated trials showed that the solution for the case with $A/2C = 0.10$ and $A/T = 0.7$ could depend heavily on the further details of even the m-triple series, so monitoring of misfits for non-fitted points on the front and back surfaces was vital. It was also found that moderate changes in weighting of subsets of the boundary conditions had significant effect. It was also found that lattices more extensive than those used for the earlier cases with $A/2C = 0.1$ simply promoted errors. After eleven trials, a solution was finally found which seemed reasonably dependable. Its series terms are not only triply spaced in m, they are also doubly spaced in k. There are three terms for $m = 0$, two for $m = 3$, two for $m = 6$, one for $m = 9$ and one for $m = 12$. Latticework for $\left|\frac{26}{25}x\right| > 2.4$ or $\left|\frac{26}{25}y\right| > 2.4$ was deleted, but the remaining boundary condition equations for $\left|\frac{26}{25}x\right| > 1.2$ were weighted doubly. The solution obtained for $K_I/K_{I\infty}$ is shown in Figure 12.

Since the case here with $A/T = 0.7$ had been found so unstable during the solving process, it seemed that any comparison between its solution and those for $A/T = 0$ or 0.5 should at least be based on crack series with the same structure. Therefore, new solutions for those earlier cases were computed, using the same kind of series as for $A/T = 0.7$. The changes thus produced in the earlier cases were minor, as was reasonable since their solutions had already seemed fairly stable. Thus the three stress intensity factor patterns shown in Figure 12 are based on uniform structure of the crack series, and appear to be dependable.

An analysis for the case with $A/T = 0.9$ was attempted, using the lattices shown in Figures B11 and B12, and using the same crack series design as had been used for the cases with smaller A/T. Unfortunately, this design was not very successful for this case, as was indicated by fairly widespread difficulty with non-fitted boundary conditions on the front face. The tabulated values of K_I did show a maximum value about midway between the root and tip of the crack (as the case with $A/2C = 0.25$ and $A/T = 0.9$ shows), but the overall level of the K_I was lower than that for any of the other cases with $A/2C = 0.1$, presumably because the boundary conditions were not enforced adequately in the overall sense. Further variations of design would have been needed to refine the analysis for this case to the point of acceptability.

The problems that were encountered in these cases with the slender

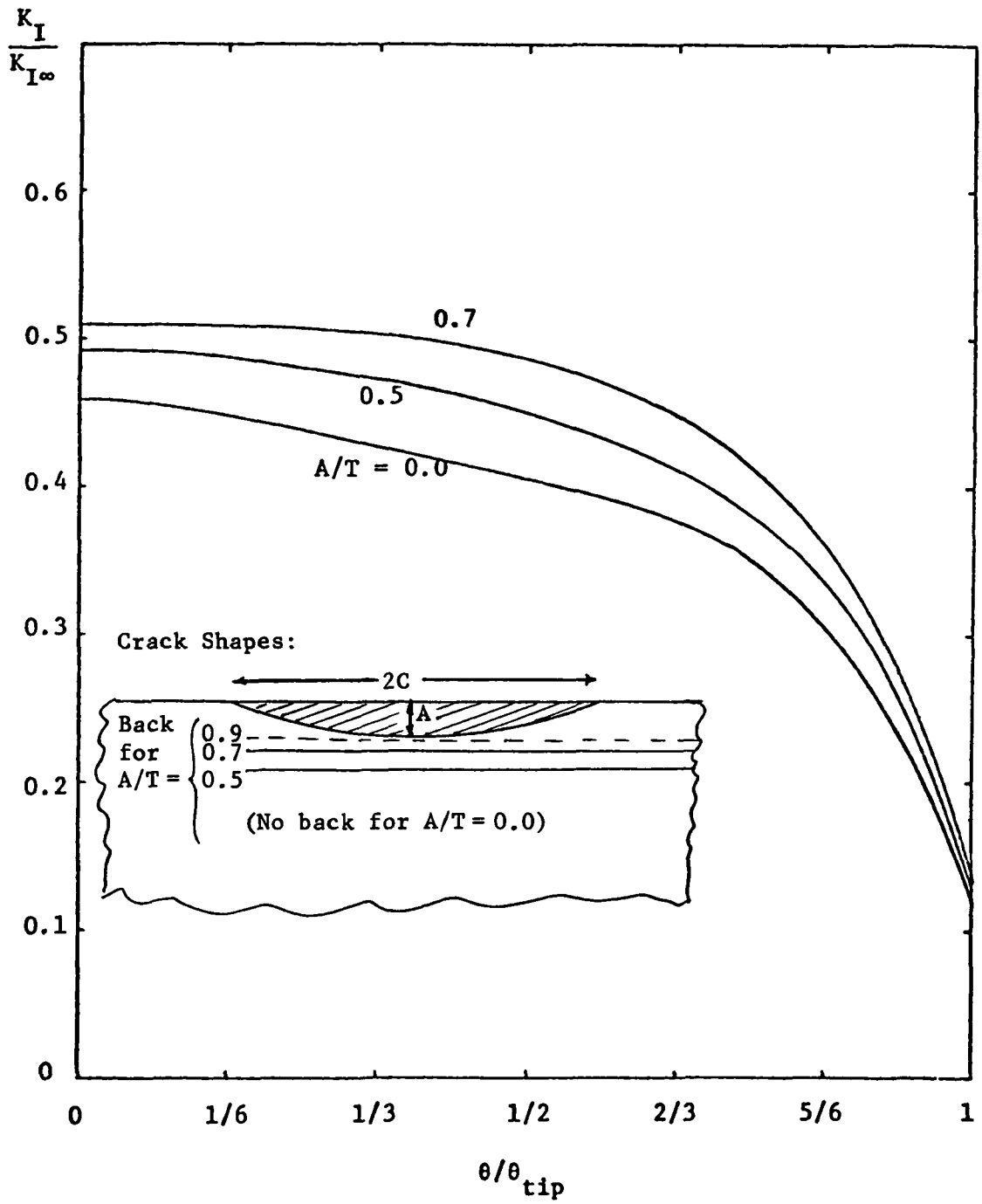

FIGURE 12. STRESS INTENSITY FACTOR ALONG SLENDER CIRCULAR SURFACE CRACKS (A/2C = 0.10) UNDER NORMAL LOAD

crack (with A/2C = 0.10) may be interpretable in various ways, but the following views appeal to the present author. First, when many terms were used in the crack series there was too little individuality among the contributions from those terms so the fitting became unworkably indeterminate. That seems to have been why double precision was needed with 36 crack terms, but not when less than 20 were used. Use of few terms helped also to reduce misfits at non-fitted points by permitting less variation among the effective boundary conditions over the entire surface of the body. Secondly, in the successful analyses, the triple spacing of m produced a series suited to an adequate but not excessive range of θ; and in a somewhat similar vein the double spacing of k introduced terms with enough individuality to fit the needs but not so much as to make great ambiguity in fitting. Thirdly, the deletion of excessively extended latticework avoided use of boundary conditions at points where the influence of crack loads is felt too weakly to be used dependably, and extra weighting of the remaining outer parts of the latticework restrained some specious role-switching of surface load constants. These interpretations may not be precisely correct, but they are plausible enough to show that there can be many kinds of pitfalls in long calculations which merge two basic kinds of analyses by pointwise fitting of boundary conditions, especially when one kind employs functions intricate enough to represent effects from cracks.

Case with A/2C = 0.05

A very slender crack, with A/2C = 0.05, was considered, but only for a thick body so that A/T = 0. Such a crack, as part of a crack with unit radius, cuts the surface over the range $-\frac{20}{101} < y < \frac{20}{101}$, and penetrates to the depth where $z = \frac{2}{101}$. A new lattice for the freeing load analysis was needed, and the one chosen is shown in Figure B13. The pattern for boundary conditions and check points is shown in Figure A4 of Appendix A. Since the crack and even the significant part of the body surface covered so short a span of the angle θ, it was decided to use crack series terms only with indices m divisible by 4, and since the crack is so shallow to use indices k divisible by 4. The series actually used had three k's for m = 0, two k's for m = 4 or 8, and one k for m = 12 or 16. Happily, this design was successful in

producing a solution which showed good quality when tested for satisfaction of non-fitted boundary conditions. The solution obtained for $K_I/K_{I\infty}$ is shown in Figure 13.

Patterns of Stresses and Crack Opening Displacements

An advantage of the present method for analyzing surface cracks is that after a suitable set of load constants has been found, only a straightforward calculation is required to evaluate stresses and displacements at any chosen set of points in the body. Thus for all the normally loaded surface cracks for which stress intensity factors have been presented, further calculations were made to get patterns of stresses and crack opening displacements. The results from these calculations are shown in Appendices C and D. The coordinates θ, ϕ and r' used to identify the stress positions are shown in Figure 14, as are the notations for the three crack opening displacements (shown for a lip point). Of course, COD_{II} and COD_{III} vanish if the crack load is purely normal.

To have enough stress evaluations so that stress distributions could be visualized somewhat, the evaluations for each crack were to employ three values of θ, four off-plane angles ϕ and five radii r'. To make the results orderly, it was decided to use values of r' and ϕ that were as uniform as possible for any one crack, though the varying length of the rays for varying θ and ϕ meant that uniform selections of r' were not always feasible. The values of θ used always included 0 and θ_{tip} plus some intermediate value, and if the stress intensity was maximum at an intermediate θ that became the third chosen θ. Since variations with ϕ were expected to be interesting over a wide range, the values chosen (except at crack tip) were 0, 45°, 90° and 135°, and since 180° would yield crack opening displacements that too was used. The selections of r' varied according to the plate thicknesses available for the individual crack. Note that the ρ' used in Appendix C is $\rho' = r'/a$, where a is crack radius.

A further choice made to promote orderliness was that the stresses would be expressed in terms of the cylindrical coordinates associated with the crack. This choice seems to have been a good one, since the patterns of the six stress components in that system were found to be remarkably consistent

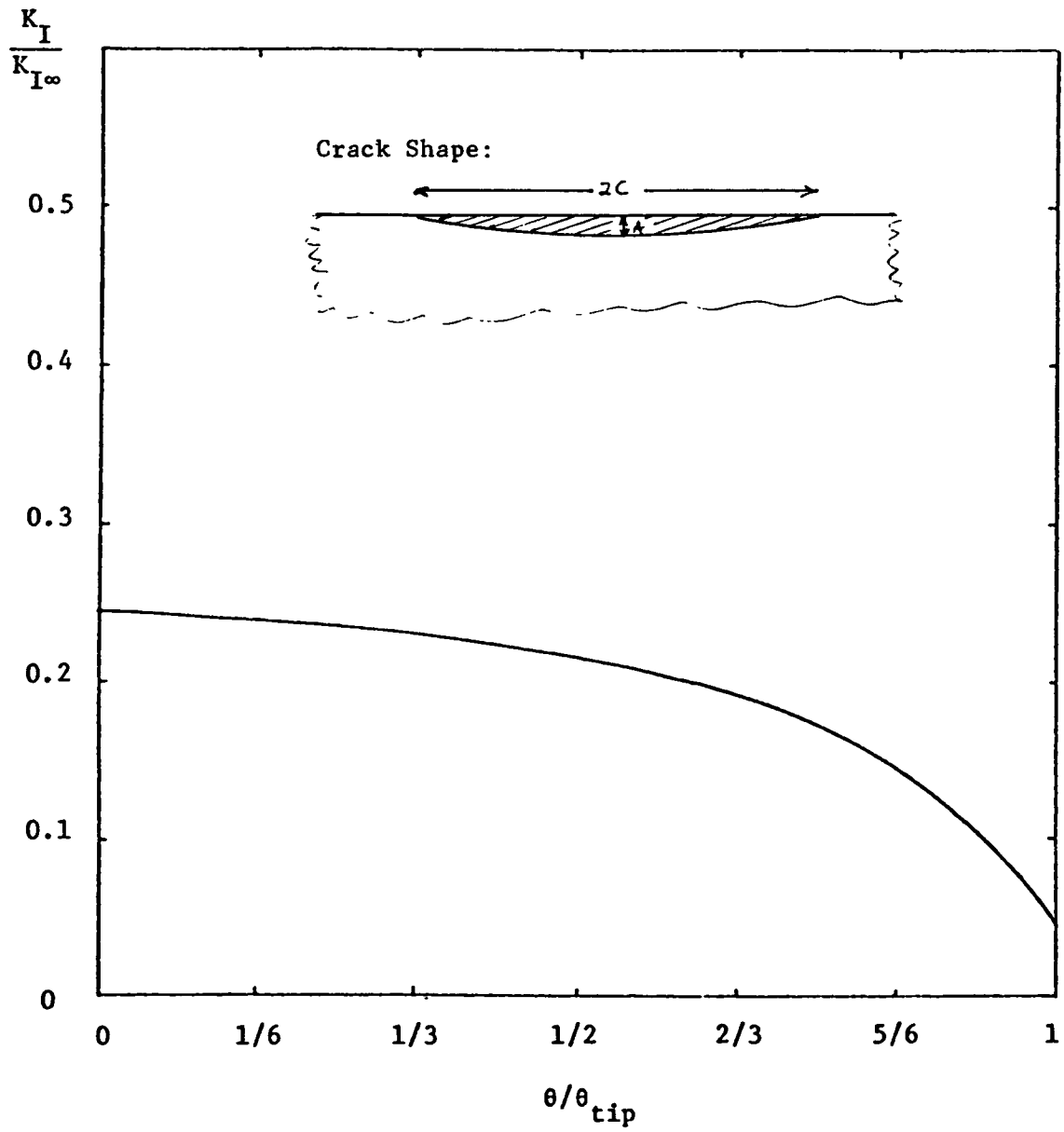

FIGURE 13. STRESS INTENSITY FACTOR ALONG A VERY SLENDER CIRCULAR SURFACE CRACK (A/2C = 0.05, A/T = 0.0) UNDER NORMAL LOAD

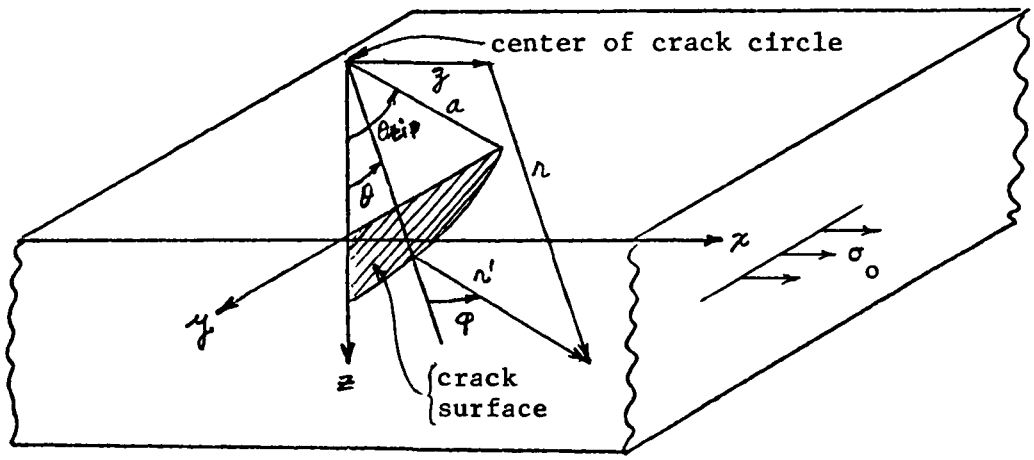

a. Coordinates (r', ϕ, θ) of positions for stresses

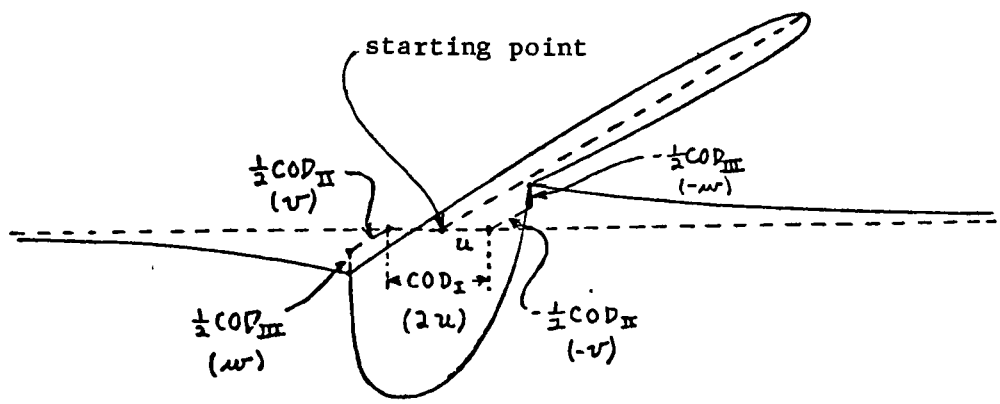

b. Components of crack opening displacement

FIGURE 14. NOTATION FOR STRESS POSITIONS AND CRACK OPENING DISPLACEMENTS ALONG A SURFACE CRACK

as θ varies and even among all the cracks. Thus, it is possible to scan the results shown in Appendix C and see a characteristic pattern for each stress component, maintained with fair constancy through all the cases. After the general pattern has been noted for each component, it becomes possible to make more intelligible comparisons between the results for the several cases. Of course the overall level for many sets of curves should be expected to vary in correspondence with the local value of the stress intensity factor. Thus it is possible to see, for example, that among the stress calculations at the position $\theta = 0$ for semicircular cracks the values for σ_z rise higher for $A/T = 0.9$ than for any other A/T. Interestingly, the highest σ_z is not on the crack plane where $\varphi = 0$, but instead is somewhere near $\varphi = 45^\circ$, and σ_r becomes large more rapidly than does σ_z as $r \to a$ with $\varphi = 0$.* Such comparisons can be continued by the reader according to his interest, perhaps at length. For example, one might seek to interpret directions of observed crack growth by considering angular variations of stresses, and later to predict such directions.

The values shown for the stresses in Appendix C of course refer to the crack load as a reference stress. To find dimensional stress levels, the entries should be multiplied by σ_o.

With semicircular cracks, σ_θ should vanish for $\theta = \frac{\pi}{2}$, since it is normal to the surface. Its failure to do so for $\rho' \leq 0.03$ is due, of course, to sparsity of detail in the freeing loads fitted there. Further subdivision of the front lattice near the crack tip would improve the accuracy at the expense of more computing, and it could be even better to use a freeing surface load element having a singularity approximating that from the crack loads, but that is not available now. Values of σ_r and σ_z also have minor defects if $\theta = \frac{\pi}{2}$ and φ is near π because of lack of fitting along the lip. The defective parts for these results are shown in Appendix C as dashed lines. Even for $\theta < \frac{\pi}{2}$

---

* Even near a deeply buried circular crack under uniform normal load, Reference 3 shows σ_z maximum for a similar $\varphi > 0$, and this agrees with brief tabular results in Reference 4. Reference 3 also shows σ_r for that case becoming large more rapidly than does σ_z as $r \to a$ with $\varphi = 0$, and Reference 4 would agree except for errors. (Cf.[3].) The relative magnitudes of these stresses comments strangely on the usual definition of the stress intensity factor K_I.

the inaccuracies near the lip affect some results for σ_r, σ_θ and σ_z for semicircular cracks at points where $\varphi \to \pi$. These defects, however, should concern only solutions in small regions near the crack tip and lip.

It was recognized that the multiplicity of results for individual stress components might be more burdensome than some reader might like, despite a desire to comprehend the stress patterns. Therefore, a combined form of stresses was included among the calculated results, namely the octahedral shear stress [10], which is

$$\tau_{oc} = \left[\frac{2}{3}\left\{\frac{1}{6}\left[(\sigma_r-\sigma_\theta)^2 + (\sigma_\theta-\sigma_z)^2 + (\sigma_z-\sigma_r)^2\right] + \tau_{\theta z}^2 + \tau_{zr}^2 + \tau_{r\theta}^2\right\}\right]^{1/2}.$$

This quantity has the advantage of being independent of the coordinate system being used. It is related to strain energy due to distortion, and it occurs frequently in the theory of plasticity. No drawings of this quantity are provided here, but tables of it could be assembled for the same cases and places used in preparing Appendix C by referring to data sheets accumulated during performance of this research.

For all the above cases of cracks with normal loads, crack opening displacements were evaluated at several positions along the crack lip and at several positions between the center of the lip and the root of the crack. These results are provided in Appendix D by plots of the quantity $u' = \mu u/(Pa)$, with u being the local x-displacement of one face and P being the normal load. Here $P = \sigma_o$. Thus

$$COD_I = 2u = 2u' \sigma_o a/\mu.$$

The three dimensional character of the crack opening is illustrated by showing variations of u' along both the y and the z axes.

Even with purely normal loads, points on the crack face can undergo displacements in up to three directions. Thus the overall length of the crack may change, and the lips of the crack may rise away from the original front plane. These latter forms of motion, however, are alike for both faces of the crack under uniform normal load, so they do not produce any form of crack opening. The other components of crack opening displacements shown in Appendix D were from shearing loads to be discussed later.

SURFACE CRACKS UNDER OBLIQUE LOADS

If a plate with a surface crack normal to the surface is subjected to remote tension σ_o applied obliquely at angle β as shown in Figure 2, then the implied stress from crack loads has the components (see Reference 10, p 19)

$$\sigma_x = -\sigma_o \cos^2 \beta, \quad \tau_{xy} = \sigma_o \sin \beta \cos \beta.$$

In the cylindrical coordinate system these implied stresses are

$$\sigma_z = \sigma_x = -\sigma_o \cos^2 \beta \quad ,$$

$$\tau_{\theta z} = -\tau_{xy} \cos \theta = -\sigma_o \sin \beta \cos \beta \cos \theta \quad ,$$

$$\tau_{zr} = -\tau_{xy} \sin \theta = -\sigma_o \sin \beta \cos \beta \sin \theta.$$

Thus the effective crack loads are $P \equiv \sigma_o \cos^2 \beta$ applied normally to the crack and $S \equiv \sigma_o \sin \beta \cos \beta$ applied as shear parallel to the crack lip. Loads of the first kind have already been treated for all the geometries for which oblique loads are specified in Table 1, so to treat the cases with oblique loads it is only necessary to add the effects from properly proportioned uniform shear loads parallel to the crack lip. The finding of these latter effects is the principal thrust of this second task.

With shearing crack loads of this kind, the selection of crack load constants to be used changes. The constants to be used here are those for shear loads applied in the antisymmetric fashion, namely $\hat{\beta}'_{m,k}$ and $\hat{\gamma}'_{m,k}$ (in the notation of Appendix F). Another change from previous cases is in the symmetries around the xz plane and yz plane, which are used in reducing the quantity of load constants, boundary conditions, and so forth. Happily, it can be be shown that this second kind of loading admits as many symmetries as the first kind does, but all symmetries for the first become antisymmetries for the second, and all antisymmetries for the first become symmetries for the second. Another change is that with the crack load being a uniform shear τ_{xy}, the equilibrium condition needed explicitly is that of rotational equilibrium around the z axis, instead of the translational equilibrium parallel to the z axis that was needed before.

A few changes were required to make the program FRAC3D fully applicable for cracks subjected to shear loads, but with those changes completed, the treatment of the new cases began. The methodology used was much as had been applied for the previous cases, though some extra problems did arise. The new problems here too varied mainly with changes in A/2C, so again cases with the same A/2C will be discussed together.

Cases with A/2C = 0.50

For the semicircular crack on the surface of a very thick body (so that A/2C = 0.5 and A/T = 0.) it was found satisfactory to use the same front lattice as was used for a normal load and also to use the same assignments of boundary condition points on the surface and generally on the crack, but a new structure was needed for the crack series. The need apparently arose from the fact that the crack loads, undisturbed by surface effects, would be representable by terms for which the index m would be unity so the use of terms with even m would be disadvantageous.* With this understanding, it was decided to use only terms for which m is odd, and to limit the values of k so that $m + 2k \leq 15$ (or occasionally $m + 2k \leq 17$). With the indices thus limited, the crack constants $\hat{\beta}'_{m,k}$ and $\hat{\gamma}'_{m,k}$ cannot influence any shearing loads on the surface of the body, and the normal loads possible there have a step across the crack lip. Thus for the case with A/T = 0, the freeing loads on the surface were limited to normal loads (shearing loads were forbidden), and along the crack even normal freeing loads were omitted since they could not match a step function. To accommodate the lack of surface loads along the crack lip, the normal boundary conditions there were also omitted, but this loss of analytic conditions was effectively compensated by the antisymmetry of the freeing σ_z across the crack plane. (The σ_z from the crack constants also vanished along the lip considering the constants being used.) Thus a reasonable set of load constants and boundary conditions was available, but it was to be expected that boundary

---

* Attempts to use series with both odd and even m's proved very unsatisfactory, apparently because of ambiguity in fitting due to such series' capacity to represent functions over the entire span $-\pi < \theta < \pi$.

conditions near the crack lip might be poorly satisfied because of the step behavior of some functions along that line. The fine detail already assigned along the lip promised to mitigate possible ill effects from that limitation.

With this design for the analyses and presuming a uniform shear load S ($\sim\tau_{xy}$) on the crack, calculations were made for the case with A/2C = 0.50 and A/T = 0. In these calculations a factor S was removed from all the stresses and load constants (as σ_o had been when the load was normal). The computed stress intensity factors k_2 ($\sim\tau_{\zeta r}$) and k_3($\sim\tau_{\theta\zeta}$) were normalized through division by $k_s = 2S\sqrt{a}/\pi$, so that the k_s is analogous to the former $k_{1\infty}$. Since the usual K_{II} and K_{III} are $K_{II} = k_2\sqrt{\pi}$ and $K_{III} = k_3\sqrt{\pi}$, the computed results could be read to be K_{II}/K_s and K_{III}/K_s, where $K_s = k_s\sqrt{\pi}$, and these factors are shown in Figure 15. The waviness of K_{III} for θ near $\pi/2$ is plausibly attributable to difficulty of fitting conditions near the crack tip, but the smallness of K_{III} in that range makes that waviness seem unimportant.

In view of the difficulties that had attended the analysis of normally loaded semicircular cracks in plates of finite thickness (that is with A/T = 0.5, 0.7, 0.9), it seemed evident that special treatment of the boundary condition equations would be needed also with the shear-loaded crack. Thus, freeing shear loads were admitted for both surfaces, but during the fitting of the load constants the front-surface shears were denied any influence on the shear stresses on the crack. Again the normal stress conditions on the crack lip were omitted, and area-based weighting was applied to ensure close fitting of surface boundary conditions at points relatively far from the crack. With these arrangements in the analytic design, the computation for the shear loaded semicircular cracks proceeded smoothly for the cases with A/T = 0.5, 0.7, and 0.9. The stress intensity factors K_{II} and K_{III} for these cases are included in Figure 15.

The stress intensity factors K_{II} and K_{III} shown here are plausible modifications of the factors that would arise around a circular crack in an infinite body loaded in uniform unidirectional shear [3]. They also provide plausible limiting cases to factors found by Smith and Sorenson [11] for surface cracks which are semielliptical but not semicircular.

Under a uniform normal load the only non-zero stress intensity factor is K_I, while under a uniform shear load τ_{xy} the only non-zero factors are K_{II} and K_{III}. Thus, under a load corresponding to a remote tension σ_o applied with

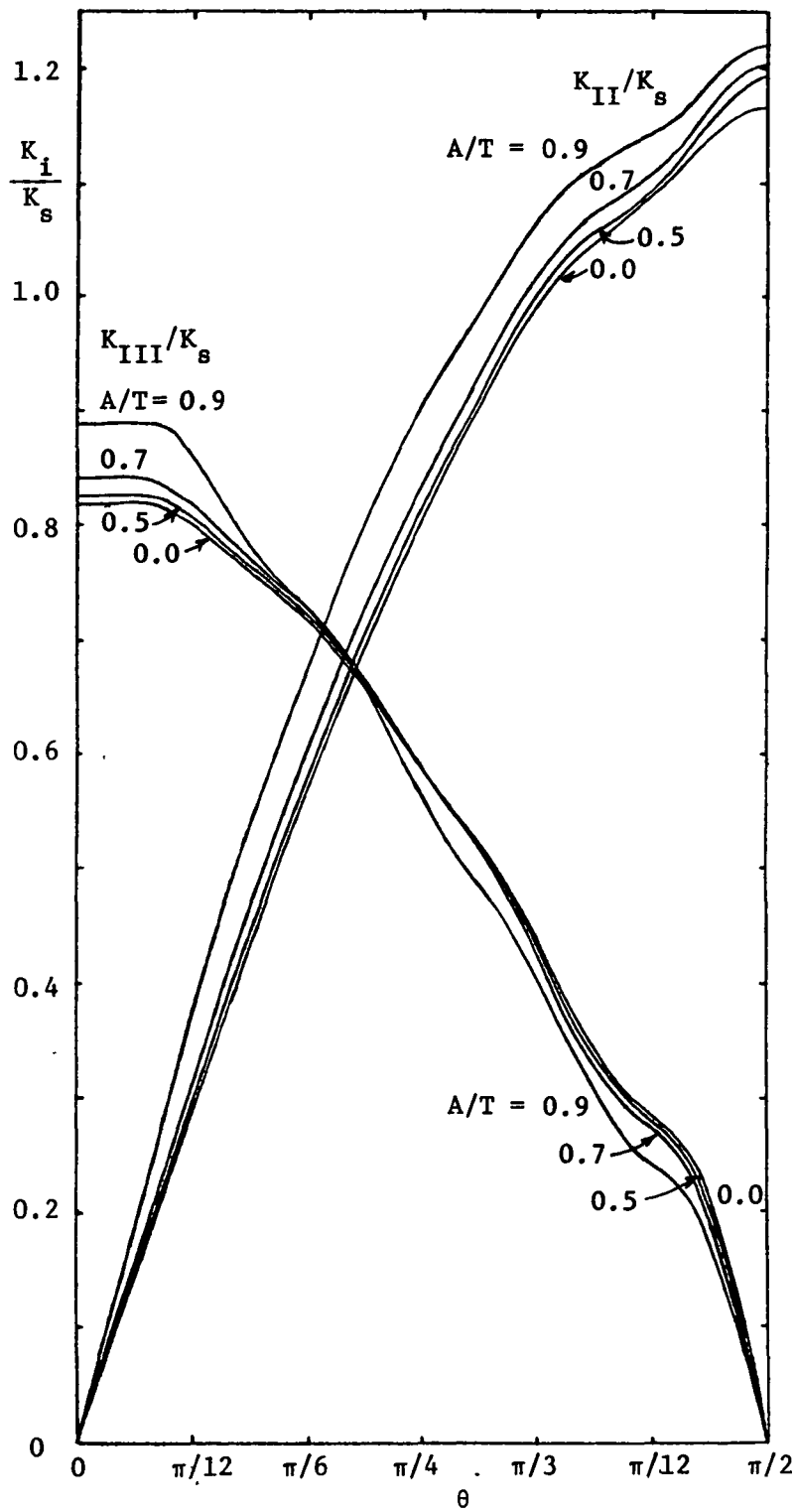

FIGURE 15. STRESS INTENSITY FACTORS ALONG SEMICIRCULAR SURFACE CRACKS (A/2C = 0.5) UNDER A LATERAL SHEARING LOAD

obliquity β, and letting $K_{ref} = 2\sigma_o\sqrt{a/\pi}$, the stress intensity factor K_I/K_{ref} for a semicircular crack becomes simply $\cos^2\beta$ times the quantity represented in Figure 4, and the factors K_{II}/K_{ref} and K_{III}/K_{ref} become $\sin\beta\cos\beta$ times the quantities represented in Figure 15. To put these results into dimensional form they need only be multiplied also by K_{ref}. Thus, Figures 4 and 15 together contain the stress intensity factors for obliquely loaded semicircular cracks. It is helpful, of course, to see how the introduction of the factors $\cos^2\beta$ and $\sin\beta\cos\beta$ modifies these results, so this is shown for all these semicircular cracks in drawings in Appendix E. After these factors have been applied so that all these factors are directly comparable, it is reasonable to seek some single stress intensity factor characterizing the overall tendency for further crack growth. It is not entirely clear what that single factor should be, but Sneddon [12] has proposed the factor

$$K_{IV} = \left[K_I^2 + (1-\nu)(K_{II}^2 + K_{III}^2)\right]^{1/2}.$$

In order to provide at least a temporary unified factor, the quantity K_{IV}/K_{ref} also has been drawn with the results for the other factors in Appendix E.

Under a uniform normal load the only non-zero crack opening displacement component is COD_I, but under a uniform shear load τ_{xy} the only non-zero crack opening components are COD_{II} and COD_{III} as identified in Figure 14. Since COD_I has already been supplied to within the factor $2P\,a/\mu$ if the crack has a normal load P, the components COD_{II} and COD_{III} for the cracks with uniform shear load S ($\sim\tau_{xy}$) are also recorded in similar fashion in Appendix D. More precisely, the drawings there show $v' \equiv \frac{\mu v}{Sa}$ and $w' \equiv \frac{\mu w}{Sa}$, so with a shear load S parallel to the lip of the crack one would have

$$COD_{II} = 2v = 2v'\ S\ a/\mu,\quad COD_{III} = 2w = 2w'\ S\ a/\mu.$$

Alternatively, if the load comes from remote tension σ_o applied obliquely at the angle β, the three components of crack opening displacements are

$$COD_I = 2u'\ \sigma_o a \cos^2\beta/\mu\ ,$$
$$COD_{II} = 2v'\ \sigma_o a \sin\beta\cos\beta/\mu\ ,$$
$$COD_{III} = 2w'\ \sigma_o a \sin\beta\cos\beta/\mu\ ,$$

and the local values of u', v', and w' can be read from graphs in Appendix D. There are, of course, other contributions to the crack face displacements which may shorten, lift, or warp the faces, but those displacements are shared alike by both faces.

For semicircular cracks, the vanishing of w' at $z = 0$, as shown in Appendix D, is somewhat misleading. The quantity w' actually should have a step as z passes through zero, but the series for w' varies continuously so it vanishes. Even approximation of this step height is awkward.

Cases with A/2C = 0.25

In contrast to the semicircular cracks, the cracks with A/2C = 0.25 being subjected to a uniform shear load τ_{xy} required no special treatment except (i) to use the constants $\hat{\beta}'_{m,k}$ and $\hat{\gamma}'_{m,k}$, (ii) to reverse the symmetries from those used with the normal crack load, and (iii) to apply only rotational equilibrium around the z axis. The same lattices were used as with the normal load, and the crack series were taken with indices m and k selected as they had been with the normal load. Thus m was taken to be even, and the limitation $m + 2k \leq 16$ was applied. This produced 45 constants $\beta'_{m,k}$ but only 36 constants $\hat{\gamma}'_{m,k}$ since $\hat{\gamma}'_{o,k} \equiv 0$ for all k. One other slight change was that the surface boundary conditions near the tip were here assigned halfway from the tip to the next lattice point beyond the tip but on the plane of the crack. Other boundary condition points were used as before, but those on the crack used the conditions $\sigma_z = 0$, $\tau_{\theta z} = -S \cos\theta$, $\tau_{zr} = -S \sin\theta$. Thus only simple changes were made. The computations proceeded without any special difficulty and led to load constants that checked well.

The stress intensity factors K_{II}/K_s and K_{III}/K_s computed for cracks with A/2C = 0.25 and A/T = 0.0, 0.5, 0.7 and 0.9 under uniform shear load S are shown in Figure 16. To convert these results to dimensional form they need only to be multiplied by $K_s = 2S\sqrt{a/\pi}$. To get the three stress intensity factors K_i/K_{ref} if a remote tension σ_o is applied obliquely at angle β one may use Figures 8 and 16, multiplying values in Figure 8 by $\cos^2\beta$ and those in Figure 16 by $\sin\beta \cos\beta$. Values of these kinds for the obliquities with $\beta = 0°$, 24°, 45° and 60° are given in Appendix E, together with the combined value K_{IV}/K_{ref}.

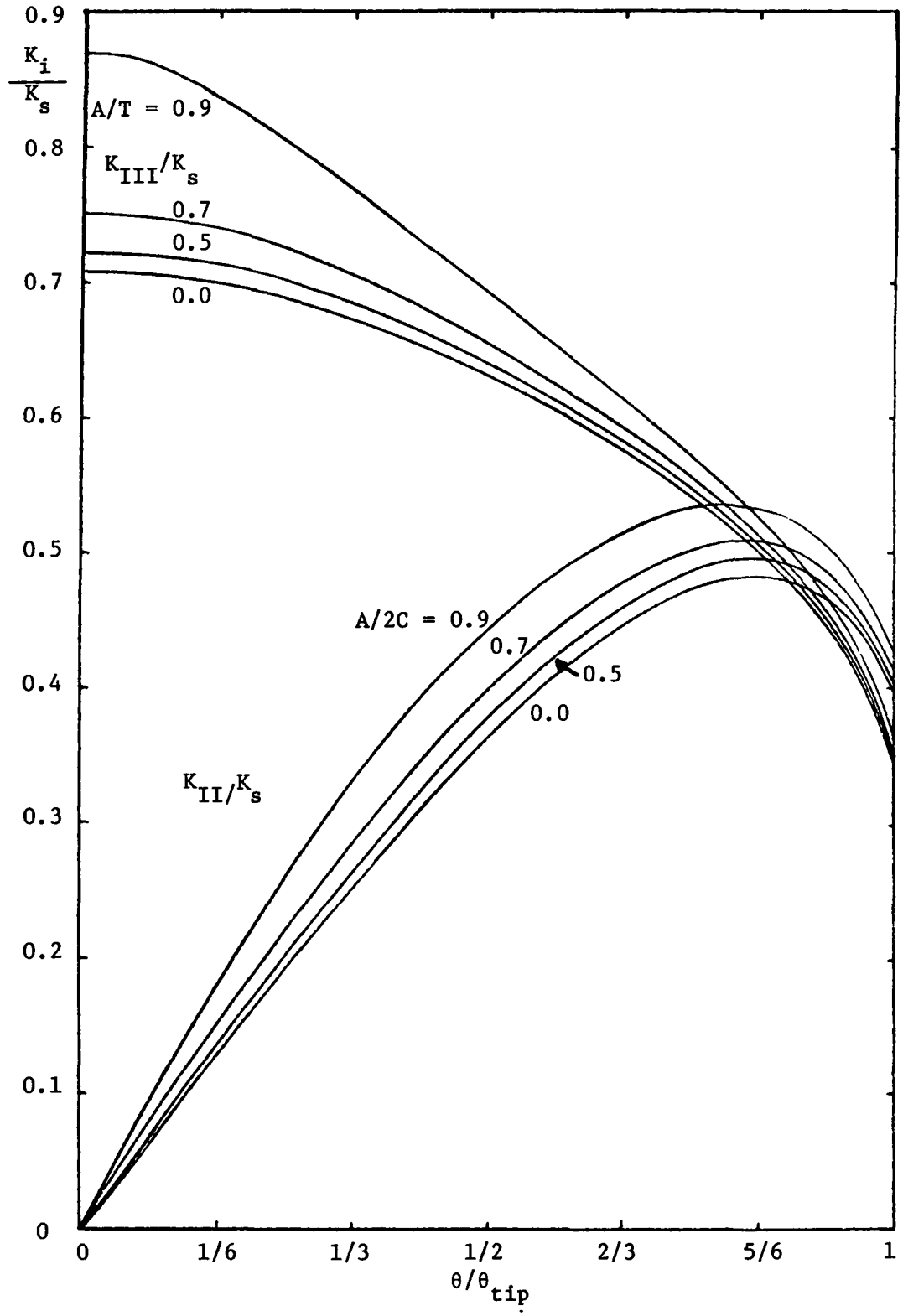

FIGURE 16. STRESS INTENSITY FACTORS ALONG PART-CIRCULAR SURFACE CRACKS (A/2C = 0.25) UNDER LATERAL SHEARING LOAD

To get crack opening displacements resulting from a uniform shear load S, one may use values shown in Appendix D for $v' \equiv \frac{\mu v}{Sa}$ and $w' = \frac{\mu w}{Sa}$, multiplying them by $2S\ a/\mu$ to get COD_{II} and COD_{III}. To get the crack opening displacements due to remote tension σ_o applied obliquely at angle β, one may apply the same conversion factors to the μ',v', and w' from Appendix D as were applied for values for the semicircular cracks.

Cases with A/2C = 0.10

For slender cracks with A/2C = 0.10 under uniform shear load τ_{xy}, the analyses again proceeded as modified forms of those for same cracks under a normal load, with changes comparable to those used for A/2C = 0.25. However, with A/2C = 0.10, the selection of indices for the crack constants $\hat{\beta}'_{m,k}$ and $\hat{\gamma}'_{m,k}$ included only m's divisible by 3 and k's divisible by 2. Three k's were used for m = 0, two k's were used for m = 3 and m = 6, and one k was used for m = 9 and m = 12. The count of crack constants thus was 9 of the form $\hat{\beta}'_{m,k}$ and 6 of the form $\hat{\gamma}'_{m,k}$ (there being none of form $\hat{\gamma}'_{0,k}$).

The stress intensity factors K_{II}/K_s and K_{III}/K_s computed for A/2C = 0.10, with A/T = 0.0, 0.5 and 0.7 under uniform shear load $S(\sim\tau_{xy})$ are shown in Figure 17. For conversion to dimensional form they require only multiplication by $K_s = 2S\sqrt{a/\pi}$. Using $K_{ref} = 2\sigma_o\sqrt{a/\pi}$, the three stress intensity factors K_i/K_{ref} from remote tension σ_o applied at obliquity β are obtainable from Figures 12 and 17 through multiplication by $\cos^2\beta$ (for i = I) or by $\sin\beta\cos\beta$ (for i = II or III). Values of these three factors are shown graphically in Appendix E for β = 0°, 24°, 45° and 60°, and again K_{IV}/K_{ref} is included.

The crack opening displacements COD_{II} and COD_{III} from a uniform shear load S $(\sim\tau_{xy})$ are again obtainable from plots of v' and w' given in Appendix D, through multiplication of those entries by $2S\ a/\mu$. Again to get the crack opening displacements due to remote tension σ_o applied with obliquity β one may apply the same conversion factors to the u', v', and w' from Appendix D as were applied for values for the semicircular cracks.

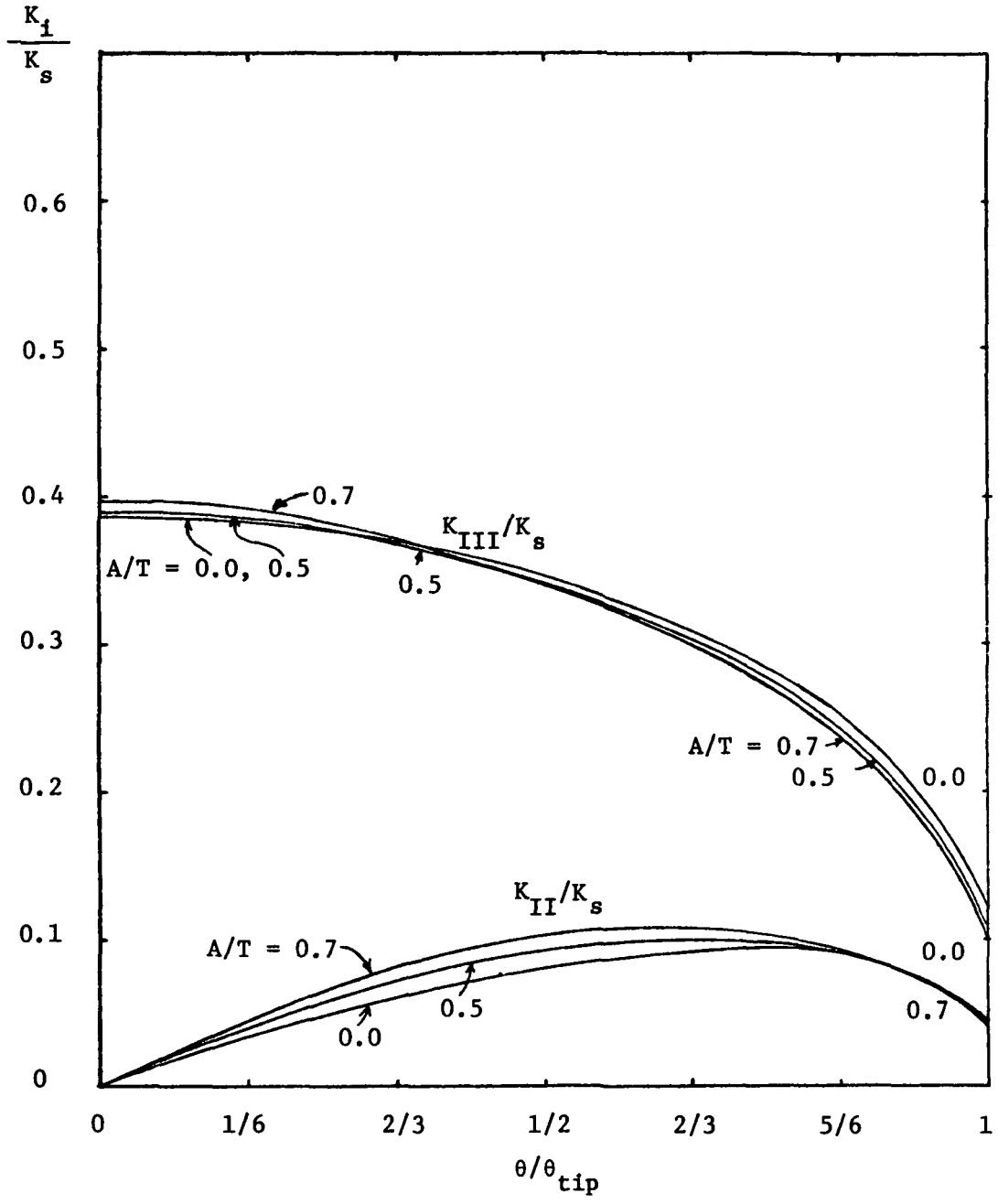

FIGURE 17. STRESS INTENSITY FACTORS ALONG SLENDER SURFACE CRACKS (A/2C = 0.10) UNDER LATERAL SHEARING LOAD

SURFACE CRACKS IN BARS

In order to investigate how the effects of surface cracks may be altered by finite width of the plate, several cases were investigated in which the plate, as shown in Figure 2 is presumed to have sides at the positions $y = \pm y_m$ so that the body is a bar. The program was already equipped to handle such cases, identifying the front surface ($z = 0$) as Face 1, the back surface ($z = z_t$) as Face 4, the surface at $y = -y_m$ as Face 3, and the surface at $y = y_m$ as Face 6. The only new features needed for the analytic design were lattices for the two new sides plus a strategy for treating boundary conditions along the edges of the bar.

During the construction of the program FRAC3D, it was conceived that it might be desirable to avoid sharp declines in surface freeing loads near the edges of the bar. To accomplish this, it was seen that pyramidal loads might have bases extending beyond the edges of the bar so that peak loads might be placed directly on an edge, provided only that proper continuity was assured between shear loads acting on the adjoining faces. To arrange for this continuity, restrictions on the independence of shearing loads along edges were built into the symmetry apparatus in FRAC3D. Thus the use of bordered lattices became possible with the last rows of rectangles situated beyond the edges of the bar.

The specifications for this task had provided an option of analyzing cracks either with $A/2C = 0.5$ with $A/2C = 0.25$. Since the latter value had proved to be much simpler in the previous analyses, it was chosen for use with the bar. Then, using the width $W/2C = 2$, the bar analysis was begun by treating the cases with $A/T = 0$ and $A/T = 0.5$. For both these cases, bordered lattices were designed as shown in Figures B14 and B15 of Appendix B. The portions of the lattices lying beyond the edges are shown as dashed lines. Using these lattices, boundary conditions were assigned at all the pyramid points, including those on the edges. Since the load was to be a uniform normal load σ_o, the crack series and boundary conditions were assigned as they had been for the infinitely wide plate having a normally loaded crack with $A/2C = 0.25$.

The analyses based on these designs produced plausible solutions

except for having high freeing loads along the edges and concomitant high misfits of boundary conditions at the centers of rectangles along the edges. The somewhat strange effects along the edges were particularly bad for the case with A/2C = 0.5. In searching for a way to avoid these large but relatively isolated misfits, the same sets of boundary condition equations were simply edited to remove effects of surface loads with peaks along the edges and to drop boundary conditions along the edges. The results of this change were that small misfits arose along each edge but the misfits of non-fitted points were drastically reduced, while other quantities such as the stress intensity factors were scarcely altered. Thus it was decided to drop the bordering, and along the edges to rely simply on fairly detailed subdivision of the rectangular bases for freeing loads. Lattices selected later illustrate this policy.

The solutions for $K_I/K_{I\infty}$ found for the cases with A/2C = 0.25, W/2C = 2, A/T = 0.0 or 0.5 without use of bordering are shown in Figure 18. Here again $K_{I\infty} = \sigma_o\sqrt{a/\pi}$ where σ_o is the normal load. Also shown in Figure 18 is $K_I/K_{I\infty}$ obtained for the case with the same A/2C and W/2C but with A/T = 0.7, as derived using the lattice shown in Figure B16 of Appendix B. In order to show how much change arose from finite width of the bar, results from previous calculations using an infinite W/2C are shown as dashed lines. It can be seen that the width effect on $K_I/K_{I\infty}$ is mainly an overall increase which is generally small but is greatest for A/T = 0.7, especially where the stress intensity is highest.

It was desired further to find how the stress intensity factor should rise as W/2C decreases, so cases were added with A/2C = 0.25, A/T = 0.7 and W/2C = 1.5 or 3, to compare with the related previous analyses using W/2C = 2 or ∞. The lattices used for these two additional cases are shown in Figures B17 and B18 of Appendix B. The stress intensity factors $K_I/K_{I\infty}$ obtained for these two new cases plus the two others sharing the same A/2C and A/T are shown in Figure 19. Again the main width effect is a general rising of the stress intensity factor as W/2C decreases. The effects seem very small for W/2C > 3, and are appreciable but not large even for W/2C down to 1.5. These calculations show little width effect near the end of the crack, but such might appear if W/2C were nearer unity. (A small discrepancy in location of boundary condition points near the crack tip made the spacing of these curves slightly irregular.)

Since the loads for the above cases are normal loads and there is

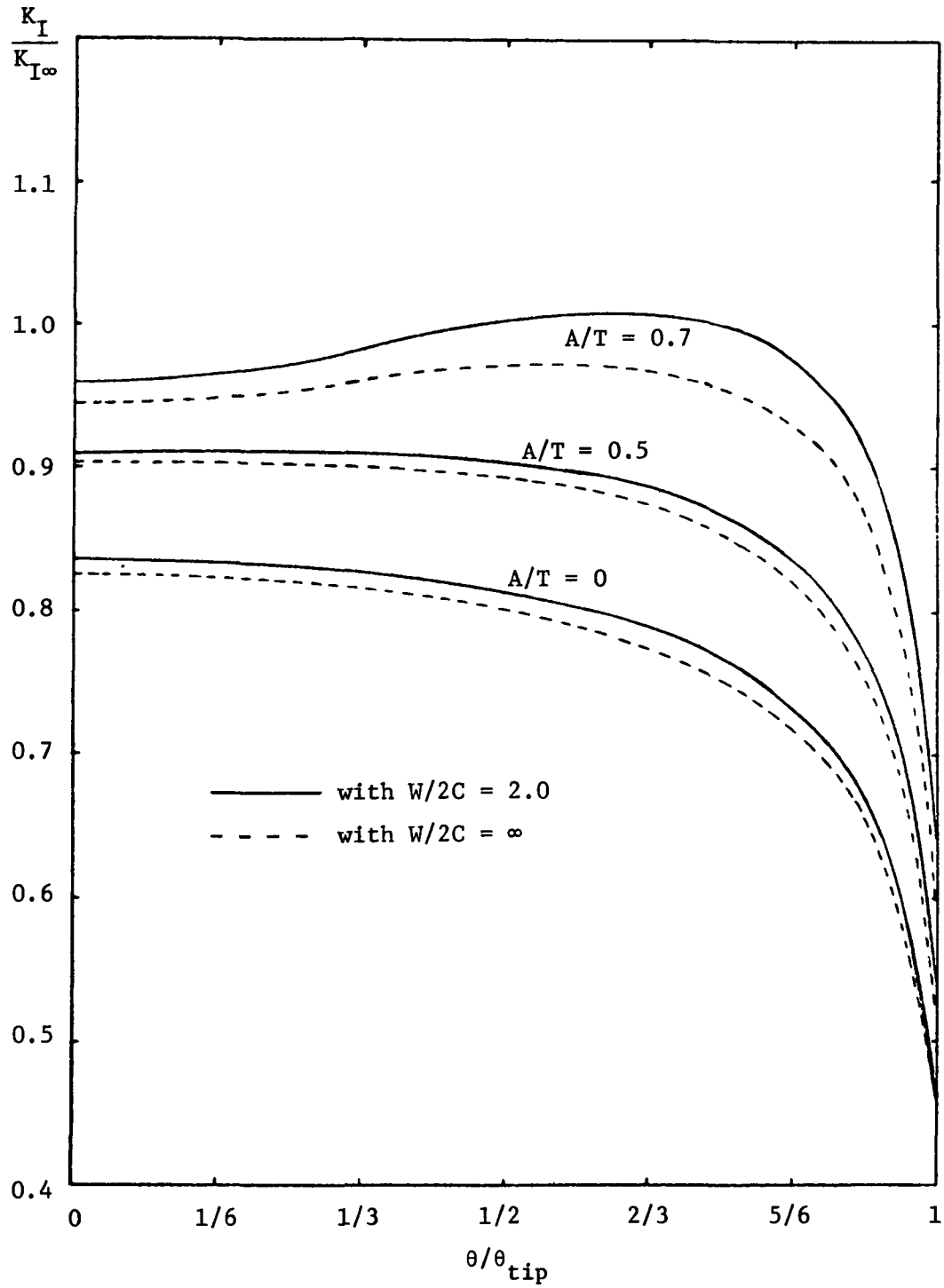

FIGURE 18. STRESS INTENSITY FACTORS ALONG PART-CIRCULAR SURFACE CRACKS (A/2C = 0.25) UNDER NORMAL LOAD WITH AND WITHOUT EFFECTS FROM BACK OR FROM SIDES

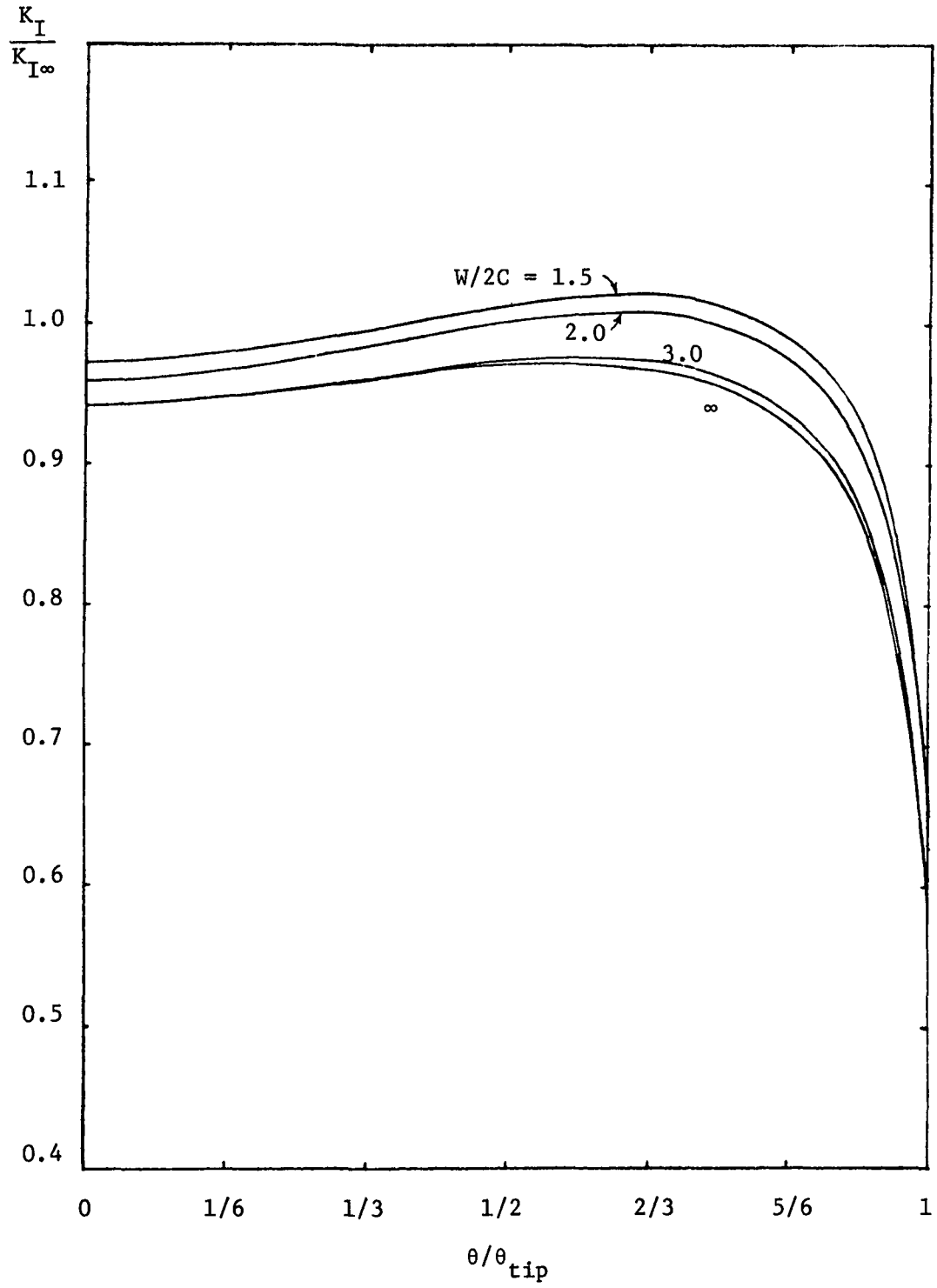

FIGURE 19. EFFECT OF BAR WIDTH ON STRESS INTENSITY FACTORS ALONG SURFACE CRACKS WITH A/2C = 0.25 AND A/T = 0.7

symmetry around both the xz and yz-planes the only crack opening displacements are of the form COD_I. Values for these displacements are displayed implicitly in Appendix D where the variations of $\mu' \equiv \frac{\mu u}{Pa}$ are shown in Figure D5 for the cases used for Figure 18 and again for those used for Figure 19. Since here $P = \sigma_o$, the values of COD_I can be found as $2u' \sigma_o a/\mu$.

A principal reason for choosing the cases represented in Figure 19 was to make comparison with measurements of crack opening displacements that had been made by Collipriest [13]. He used a 1/4-inch aluminum plate over a foot long and initially six inches wide. Across the longitudinal center line of the plate he grew a crack with depth 0.170 in. and length 0.720 in, so that its defining parameters could be approximated as $A/2C = 0.170/0.720 = 0.236 \approx 0.25$ and $A/T = 0.170/0.248 = 0.685 \approx 0.70$. The crack was not entirely circular or elliptical, but by assuming it to be circular with sagitta 0.170 in. and chord 0.720 in. it is implied that the crack radius was 0.466 in. This latter estimate is probably low, however, since assuming the crack to be elliptical would make its radius be 0.762 in. at its root. Thus his dimensions are not perfectly relatable to dimensions assumed for the cases of Figure 19, but they seem near enough to justify making rough comparisons.

Collipriest subjected his specimen to remote tension σ_o, measured the widest crack opening displacement COD, and recorded $(COD)E/\sigma_o$, where E is Young's modulus so that $E = 2\mu\ (1+\nu)$. He then several times trimmed the plate to narrower width and repeated the COD measurements. Assuming ν to be 0.3 as is typical for aluminum, it is possible now to compare his results with predictions based on the COD_I computed at the center of the crack lip for the cases shown in Figure 19, though there is some uncertainty in the value to use for the crack radius in the theory. To use the theory to predict what values he should have found, one may use the relationship

$$\frac{(COD)\ E}{\sigma_o} = 4\ (1+\nu)\ a \cdot u',$$

taking the u' at the center of the crack lip. The theory may seem to be applied most consistently by taking a = 0.466 in., but to find whether the theory and experiments show similar width effects it seems equally permissible to presume a = 0.627 in. so that the two methods will agree for very

wide plates. Using both these values, comparisons between the theory and experiment are shown in Table 2, with entries interspersed according to the values of W/2C. The comparison is also shown graphically in Figure 20.

Employing the values based on a = 0.627in., it can be seen that the predicted plate-width effects are indeed similar to the measured ones to within the accuracy that the measured values seem to have had. The discrepancy between the alternative theoretical values reflects that the theory and experiments are not perfectly matched, but the mismatch seems within that which could be related simply to the differing shapes of the crack fronts. Thus, on the whole, the two types of results agree to within any reasonable expectations.

TABLE 2. THEORETICAL AND EXPERIMENTAL PLATE WIDTH EFFECTS ON COD*

Width W/2C	u'	Theoretical (COD) E/σ_o a = 0.466 in	Theoretical (COD) E/σ_o a = 0.627 in	Measured (COD) E/σ_o
∞	0.4218	1.022	1.375	--
8.324	--	--	--	1.34
7.671	--	--	--	1.38
6.268	--	--	--	1.37
4.868	--	--	--	1.37
4.222	--	--	--	1.38
3.394	--	--	--	1.40
3.0	0.4252	1.030	1.386	--
2.558	--	--	--	1.44
2.0	0.4409	1.068	1.437	--
1.5	0.4451	1.079	1.451	--

*Dimensions include A = 0.170 in, 2C = 0.720 in., T = 0.248 in.
The crack radius a is doubtful, but the values used are plausible.

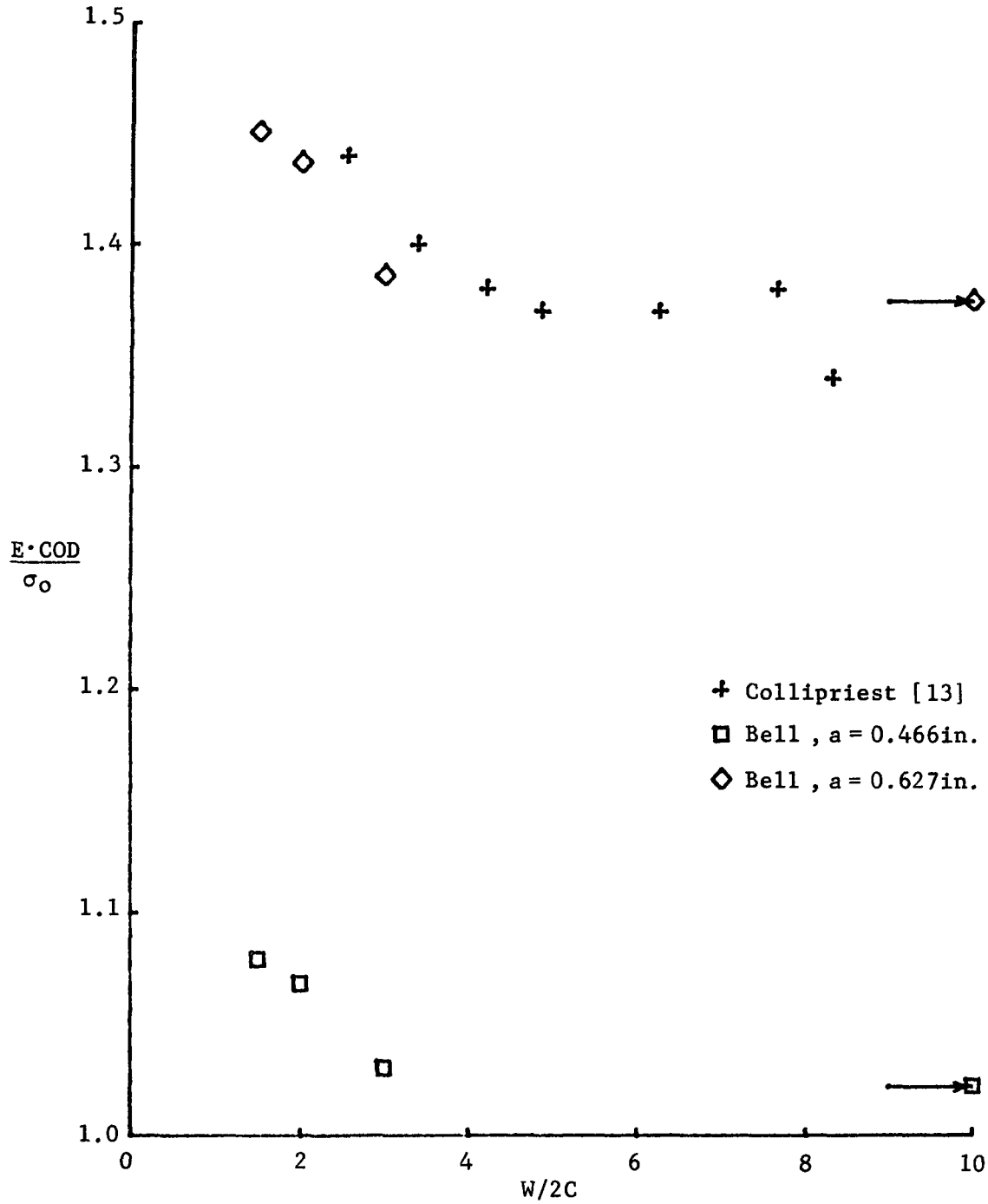

FIGURE 20. THEORETICAL AND EXPERIMENTAL PLATE WIDTH EFFECTS ON CRACK OPENING DISPLACEMENTS

COMMENTS CONCERNING RESULTS AND PROCEDURE

Observations Concerning Computed Results

The analyses which are reported here cover enough cases to show how effects from part-circular surface cracks vary with the depth-to-length ratio A/2C, the fractional penetration ratio A/T, the load obliquity angle β, and to some extent the fractional span ratio W/2C. In treating this range of cases, several previously unanalyzed ones have been covered, including the slender cracks ($A/2C \leq 0.10$), the obliquely loaded cracks ($\beta > 0$), and those with finite fractional span ($W/2C \leq 3$), though some partially comparable analyses have been performed for elliptical cracks by other investigators. Even the analyses for normally loaded semicircular cracks in plates of finite thickness seem new among analyses by methods other than finite elements. The variation of the stress intensity factors shown among all these cases should be helpful to a stress analyst or designer of structural parts in estimating how variations in crack geometry or loading may alter the danger that a crack may grow.

The attempt to attain accuracy in the solutions has led to finding qualitatively new effects in some cases which had been treated previously by other investigators. In particular, for the normally loaded cracks with $A/2C = 0.25$ and with $A/T = 0.7$ or 0.9, the peak stress intensity factors are here found to occur about midway between the root and tip of the crack instead of at the root. This result agrees with some measured stress intensity factors [9] and also with inferences some experimenters have made from crack growth. The analysis provides an explanation, by showing that there is outward bowing of the plate in the vicinity of the crack, and the bowing counteracts the load at the root of a crack which extends near enough to the back face. Thus, the additional information provided by this newer methodology can be significant.

Another example of a qualitatively new implication seems to appear in results for semicircular cracks, for which the stress intensity factor is minimum at the root of the crack except when $A/T = 0.9$. This suggests that if the crack is far enough through (probably more than 0.9 of the way) then in growing the crack may first break through the back, whereas if it were

not so far through the plate it would first tend to grow laterally. The relative insensitivity of the stress intensity factor to proximity of the back for the less penetrating semicircular cracks may suggest also why the stress intensity factor for the bar seems so little distorted near the end of the crack: the side of the bar is still too far away for such distortions even when $W/2C = 1.5$.

A perceptive interpreter may see many more inferences in the reported stress intensity factors, but there is also another potentially rich source of inferences in the computed stress patterns. The variations of the individual components of stress around the crack front are probable contributors to the direction of crack growth, so knowledge of those components as provided here for many cases should help first in correlating data on crack growth and later in predicting the growth more precisely. If the octahedral shear stress, as a stress invariant related to strain energy of distortion, is desired for assistance in crack growth studies, it too can be found from the data sheets accumulated during the computation of stresses for the cases covered in Appendix C. Moreover, if further detailed stresses are desired for these cases or for cases which were analyzed but not used for stress computations, it should be possible to find more stress patterns by computations beginning with the load constants which have been saved as computer input for the great majority of all the cases listed in Table 1.* Much potential help exists here for investigating the relations between stresses and surface cracks.

The crack opening displacements presented in Appendix D offer another avenue for correlation with experimental work. One such comparison has been provided in Table 2, but many more should be possible. Thus, by observing how the normal load factor P and the shear load factor S change with the obliquity β, one should be able to make comparisons with measurements of all three components of crack opening displacement as identified in Figure 14, if those measurements are made under oblique loads. The more

---

* Load constants were retained on magnetic tape for all cases analysed on computers at Battelle. This includes all but the last two cases of Task I, the next to last of Task II, and the last two of Task III. The other five cases were analysed using the CDC computer at Langley Research Center after FRAC3D and its companion programs had been made operational on that machine through joint effort by personnel of Battelle and of Lewis Research Center.

subtle displacements related to plate face bending, crack lengthening and crack warping also can be computed from load constants that have been retained (though FRAC3D first needs checking for consistency in dimensional factors implied for contributions from surface loads versus those from crack loads).

Observations About Design of Analyses

Ability to run the programs LATTICE, FRAC3D and MATSOL successfully in a computer does not of itself imply the ability to perform analyses of the kinds that are reported here. Casual reading of the sections of this report treating normally loaded cracks, obliquely loaded cracks and bars should make that clear. Study of those sections, however, being coupled with thought about how stresses can be transmitted throughout a body with a crack, can provide much useful guidance for the performance of further analyses.

Principles already stated concerning the design of lattices have included that there should be enough subdivision so that the two-dimensional linear interpolation can provide adequate representation of the needed freeing loads. A computer often can be used in making preliminary estimates of those loads. The lattices should be extensive enough to cover the regions which may be influenced by the crack load, but if there are both front and back surfaces then caution should be used in extending the lattices beyond the regions where the crack loads have significant influence. There is danger if surface load constants or interactions between them can influence crack stresses but crack loads cannot influence the surface stresses. The analyses for both the semicircular and the slender cracks under normal loads illustrate this hazard.

The choice of terms to be used in the crack series is often vital to the success of an analysis. None of the cracks treated in this report comprised more than a semicircle, and a consequence of this was that none of the analyses used more than half of the terms that could have been used for variations in the circumferential direction. As the angular length of the crack shortened, the spacing of the terms in the crack series was widened for the index related to angular variations (m). Thus for A/2C = 0.5 or 0.25 m was doubly spaced, for A/2C = 0.10 it was triply spaced, and for A/2C = 0.05 it was quadruply spaced. Such spacings may not always be absolutely necessary, but they proved to be quite beneficial.

The reason for care in the spacing of terms used in the crack series is probably that the terms must combine enough variations so that they can be fitted to the functions needed by the analysis but yet do this without the ambiguity that use of excessive terms would imply. One analysis (that for A/2C = 0.10 and A/T = 0.0 with normal load) was found to be numerically unmanageable until many terms were removed from the crack series. Such a requirement may seem repugnant to analysts who expect simply to add more terms when more accuracy is required, but it may be seen as being reasonable when one considers the quantity of arithmetic operations involved and the dangers of producing an indeterminate solution from the simultaneous equations. In more colloquial terms, too many cooks can spoil the broth, and here they can do it by near-indeterminacy plus accumulation of roundoff errors. Of course, enough terms must remain to fulfill the needs, so the wealth of crack functions available through the use of the program FRAC3D becomes important in supplying the breadth of term selection needed in analyzing slender cracks.

Lest it be thought that care in crack term selection is unimportant, it may be remarked that apparently minor changes in the series structure used for the case with A/2C = 0.1 and A/T = 0.7 under normal load made the computed stress intensity factor at the root of the crack shift from 0.29 to 0.72, and the variations with θ also shifted vigorously. Without the use of careful checking of individual solutions the scattering among them would have produced intolerable confusion. A consensus solution would not have sufficed.

Another principle already stated is that crack constants should be used only to fit crack conditions including necessary interactions with the surfaces, while surface constants should be used only for surface conditions including necessary interactions with the crack. This principle was embraced by analyses used here when surface boundary condition points were placed only at pyramid points except for the boundary condition point near the crack tip. Before that choice of the points was enforced, it had been found that by shifting the boundary condition points to various positions in the surface rectangles the stress intensity factor at the root of the crack for one sample case shifted from 0.79 to 1.36. The appearance of such ambiguity was a strong reason for the introduction of checking at non-fitted points.

The fitting of boundary conditions near the crack tip remains somewhat problematic. An early study of variations of crack stress functions near

the tip of a crack with A/2C = 0.25 led to placement of boundary conditions used here for the normally loaded cracks with A/2C = 0.25. That placement proved to be less desirable for cracks with A/2C = 0.5, however, since its use produced solutions that checked less satisfactorily near the crack tip than did those shown in Figure 4 and also had small-amplitude waves along the rest of the crack front. Moving that boundary condition point onto the crack plane as already described improved the solutions for the semicircular cracks and yielded Figure 4. In view of this improvement, the waviness which persists in the results shown in Figure 15 may be expected to be due to some minor defect in the design of the analysis which produces only minor changes in stress intensity factors.

This experience with fitting of conditions near the crack tip, plus the observation that boundary condition misfits at non-fitted points tend to be largest near the crack tip, implies that computed stress intensity factors and stresses tend to be poorest near the crack tip. Considerable refinement of the latticework has been used there, but more might be used if the results are to be regarded as being vital. Another more remote possibility is to produce a modified surface load theory in which triangular base areas could be used, in order to accommodate better the tendency crack stress variations have to reach peak values near the tip along lines oblique to the crack plane. Thus possibilities exist for further work here if it is desired.

Effectiveness of the Checking Process

Without the checking of boundary conditions at non-fitted boundary points and at points near the outer boundary of the lattices many analyses given here would have floundered in uncertainty. The only analyses which automatically gave dependable results were those for cracks with A/2C = 0.25. For cracks with other depth-to-length ratios the checking process was often used in order to find how an analysis had failed and what might be tried to improve it. It should be noted for the great majority of retrials to find solutions the original system of boundary condition equations was reused but was trimmed of load constants or boundary conditions in a new way.

While the checking process used here proved to be very useful,

it must be admitted that it is not absolute in its inferences about accuracy of the analyses. Small errors in fitting individual boundary conditions are bound to arise, and there can be uncertainty about what such defects may do to the stress intensity factors, stresses and displacements. It is helpful, of course, to gauge the influence of boundary-condition errors by appeal to Saint-Venant's principle which states that if two alternative systems of boundary forces on a body are alike in their resultant forces and moments and differ in detail only over a region of dimension δ, then the stresses produced by the two systems would agree except within distances of order δ from the region where the boundary forces differ. This principle can be quite reassuring, but further examination of the importance of boundary-condition errors could well be appropriate.

It may be restated that the present methodology lends itself well to accuracy studies since the only approximations made to the ideal conditions for analyzing elastic stresses come in the boundary conditions, and those conditions are applied in a straightforward manner. Analyses which use internal matching of conditions (as with finite elements), or discontinuous boundary conditions, or boundary conditions in which both stresses and displacements are approximated could well prove harder to validate conclusively. Problems regarding the accuracy of three dimensional fracture analysis seem to be widespread in view of the often encountered desire to validate a given solution from one investigator by comparing it to one from another, as if a consensus were the proper criterion for establishing truth in this field. That situation needs to be remedied, and it is hoped that the present work provides progress in the right direction.

It is tempting to wonder whether difficulties concerning the balancing of interactions between two sets of load constants might be discerned in a straightforward way by mathematical examination of the system of boundary conditions, and whether such difficulties could be mitigated by some well defined mathematical procedure. These are problems in the use of boundary point least-squares solutions which appear to need investigation but which promise to be difficult, especially unless the two sets of constants are associated with well defined basic analyses comparable to the ones being used here. These are good problems for future research.

CONCLUSIONS

In brief, the results of the research described here are:

(i) Analyses are provided for enough surface cracks to show how their effects vary with the depth to length ratio A/2C, with the fractional penetration ratio A/T, with the load obliquity angle β, and to some extent with the fractional span ratio W/2C. Several of these analyses cover cases either previously unresolved or formerly solved only with significantly less completeness.

(ii) The analyses provide results covering stress intensity factors, stress patterns and displacement patterns so that the information can be used in many ways. Progress was also made in making the information more accessible, both by inclusion of much detail here, by making preparations for further calculations which might be desired, and by making the computer programs operational on NASA as well as Battelle equipment.

(iii) Many observations have been provided concerning ways to make the design of the analyses promote the finding of valid analyses. The discussions of the many cases included in this report illustrate many useful techniques for improving the likelihood of success.

(iv) A useful method has been devised and employed to gauge the accuracy of a particular analysis without recourse to any external analysis. This capability for self checking goes far toward meeting a great need of three-dimensional fracture analyses.

REFERENCES

[1] Bell, J. C., "Analytical Methods for Improved Fracture Analysis", Technical Report AFFDL-TR-75-67, prepared for the Air Force Flight Dynamics Laboratory, WPAFB, by Battelle's Columbus Laboratories, August 30, 1975.

[2] Bell, J. C., "Stresses from Arbitrary Loads on A Circular Crack", International Journal of Fracture, Vol. 15, No. 1, February 1979.

[3] Bell, J. C., "Stresses from Variously Loaded Circular Cracks", Journal of the Structural Division of the ASCE, Vol. 103, No. St2, 1977, pp 355-376.

[4] Sneddon, I. N., "The Distribution of Stress in the Neighbourhood of a Crack in an Elastic Solid", Proceedings of the Royal Society, London, Series A, Vol. 187, 1946, pp 229-260.

[5] Smith, F. W., Emery, A. F., and Kobayashi, A. S., "Stress Intensity Factors for Semi-Circular Cracks, Part 2 - Semi-Infinite Solid", Trans. ASME, Journal of Applied Mechanics, Vol. 34, 1967, pp 953-959.

[6] Thresher, R. W. and Smith, F. W., "Stress Intensity Factors for a Surface Crack in a Finite Solid", Trans. ASME, Journal of Applied Mechanics, Vol. 39, 1972, pp 195-200.

[7] Raju , I. S. and Newman, J. C., Jr., "Improved Stress Intensity Factors for Semielliptical Surface Cracks in Finite-Thickness Plates", NASA-TMX-72825, Langley Research Center, May, 1977.

[8] Yagawa, G., Ichimiya, M., and Ando, Y., "Two- and Three-Dimensional Analyses of Stress Intensity Factors Based on Discretization Error in Finite Elements", Numerical Methods in Fracture Mechanics, Proceedings of First International Conference, held at University College Swansea, January 9-13, 1978. Published by University College Swansea, Swansea, U.K., 1978.

[9] Smith, C. W. and Jolles, M., "Stress Intensities in Deep Surface Flaws in Plates Under Mode I Loading", Proceedings of Eighth Southeastern Conference on Theoretical and Applied Mechanics, April 1976, Developments in Theoretical and Applied Mechanics, Vol. 8, pp 151-160, Virginia Polytechnic Institute, Blacksburg.

[10] Timoshenko, S. P. and Goodier, J. N., Theory of Elasticity, Third Ed., McGraw-Hill, New York, 1970, pp 224-226, 248.

[11] Smith, F. W. and Sorenson, D. R., "Mixed Mode Stress Intensity Factors for Semielliptical Surface Cracks", Technical Report No. 5, Final Report NASA Grant NGL-06-002-063, Dept. of Mech. Eng., Colorado State University, June 15, 1974.

REFERENCES
(Cont'd)

[12] Sneddon, I. N. and Lowengrub, M., Crack Problems in the Classical Theory of Elasticity, John Wiley and Sons, New York, 1969, pp 9, 10.

[13] Ehret, R. M., "Part Through Crack Elastic Compliance Calibration", SD 71-329, North American Rockwell, Space Division, October 1971.

[14] Bell, J.C., Hopper, A.T. and Hayes, P.A., "User's Manual for Program FRAC3D - Supplement to Report on Stress Analysis for Structures with Surface Cracks", NASA CR 159401, August 1978.

APPENDIX A

BOUNDARY CONDITION AND CHECK POINTS SELECTED FOR CRACKS

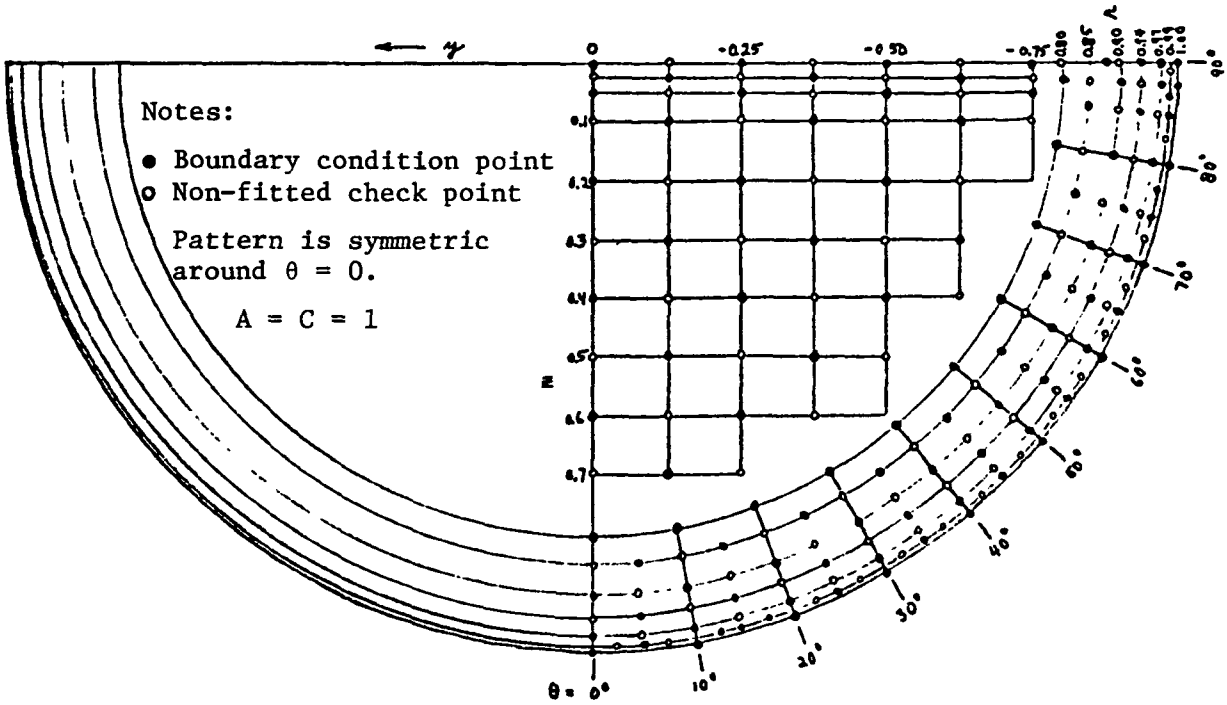

FIGURE A1. BOUNDARY CONDITION POINTS AND CHECK POINTS SELECTED ON CRACKS WITH A/2C = 0.50

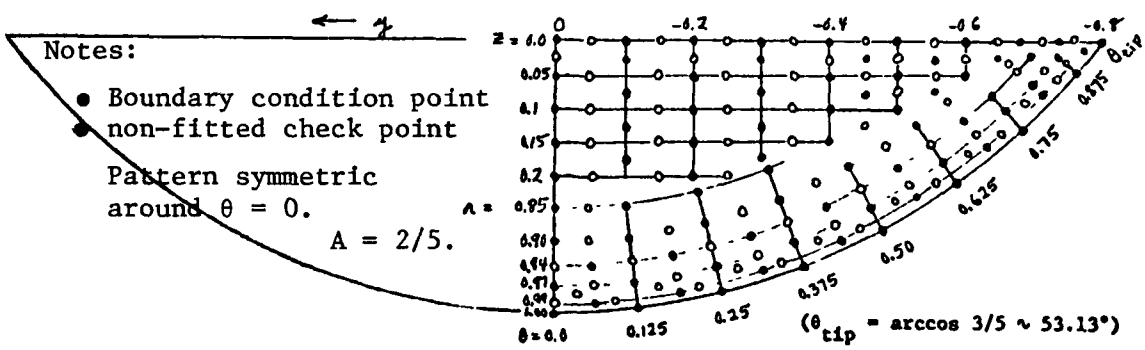

FIGURE A2. BOUNDARY CONDITION POINTS AND CHECK POINTS SELECTED ON CRACKS WITH A/2C = 0.25

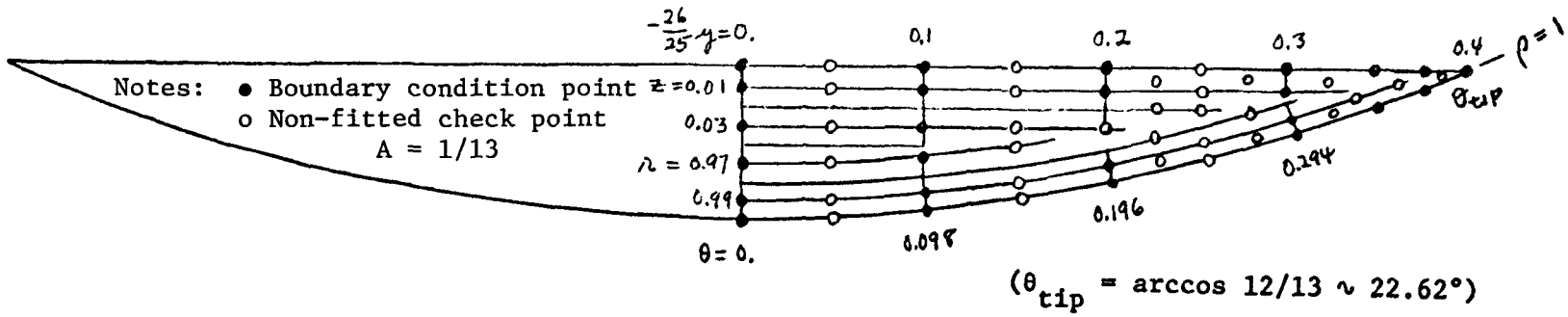

FIGURE A3. BOUNDARY CONDITION POINTS AND CHECK POINTS SELECTED ON CRACKS WITH A/2C = 0.10

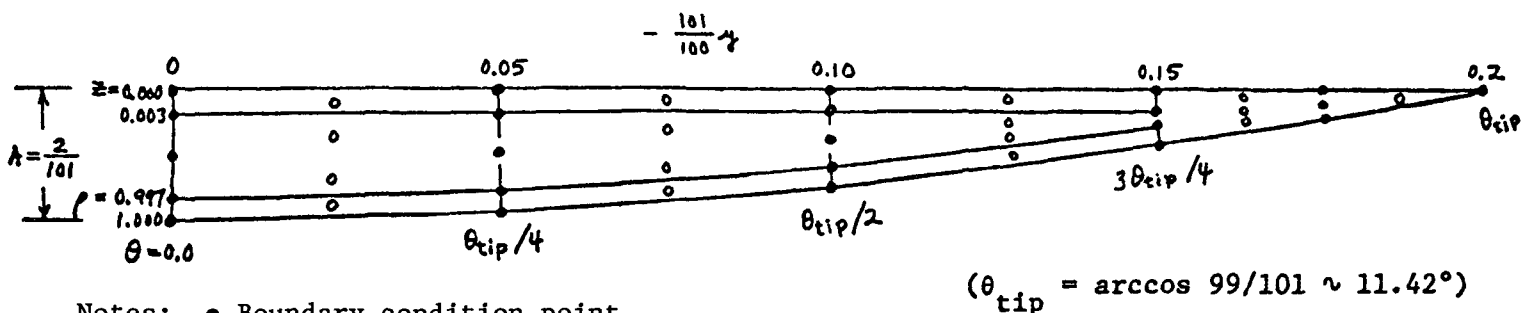

FIGURE A4. BOUNDARY CONDITION POINTS AND CHECK POINTS SELECTED ON CRACKS WITH A/2C = 0.05

APPENDIX B

SURFACE LATTICES USED IN ANALYSES

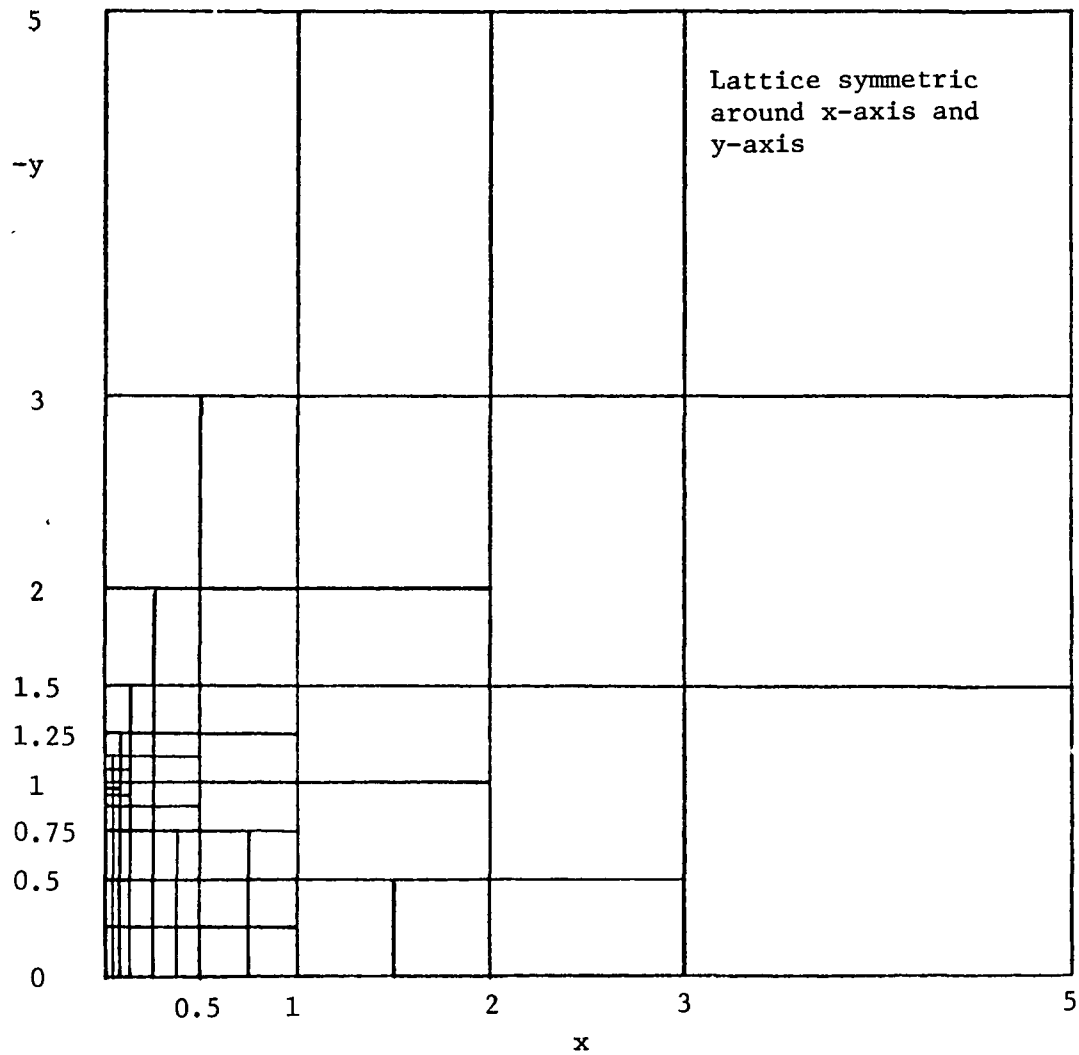

FIGURE B1. FRONT LATTICE FOR SURFACE CRACKS IN PLATE WITH A/2C = 0.50, A/T = 0.0 to 0.9

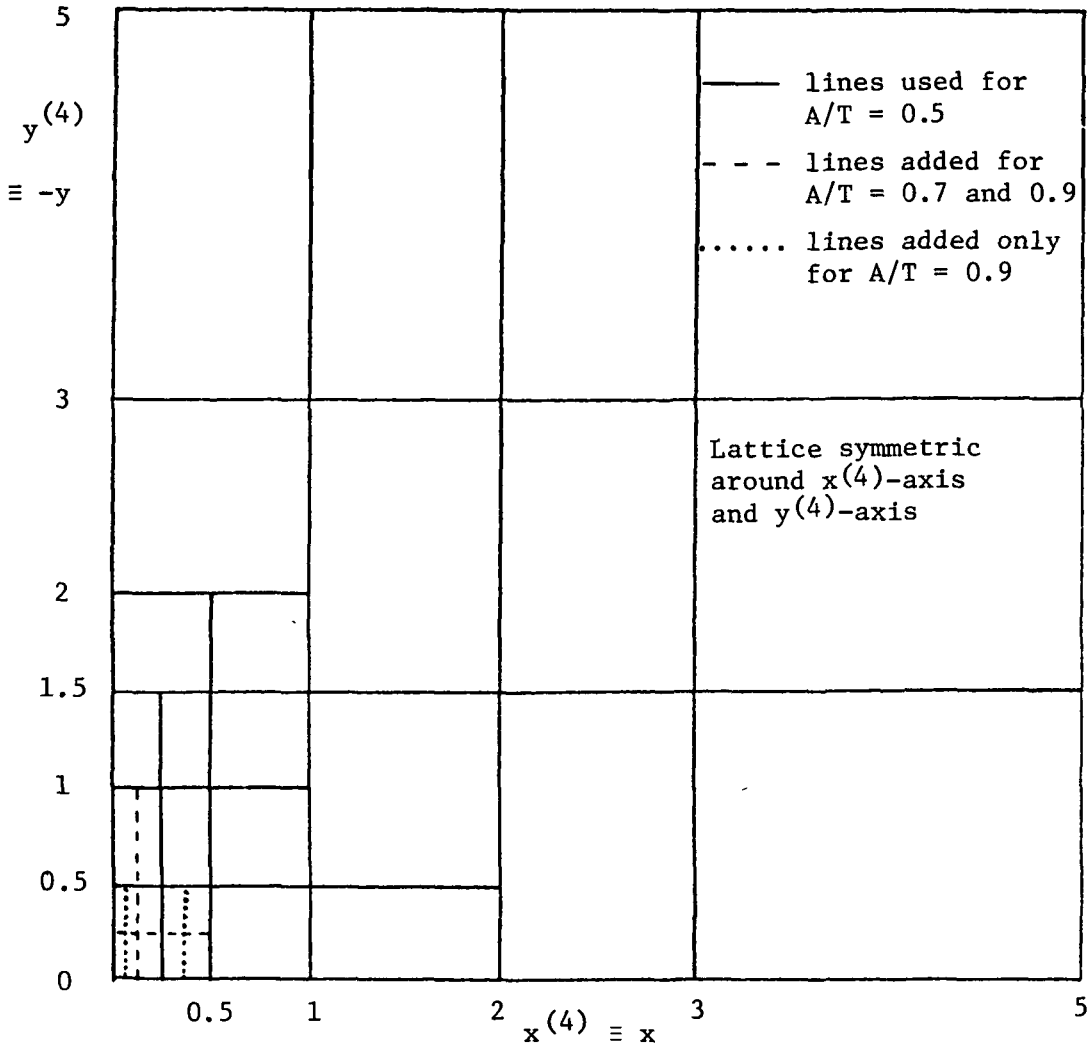

FIGURE B2. BACK LATTICE BEHIND SURFACE CRACK IN PLATE WITH A/2C = 0.50, A/T = 0.5 TO 0.9

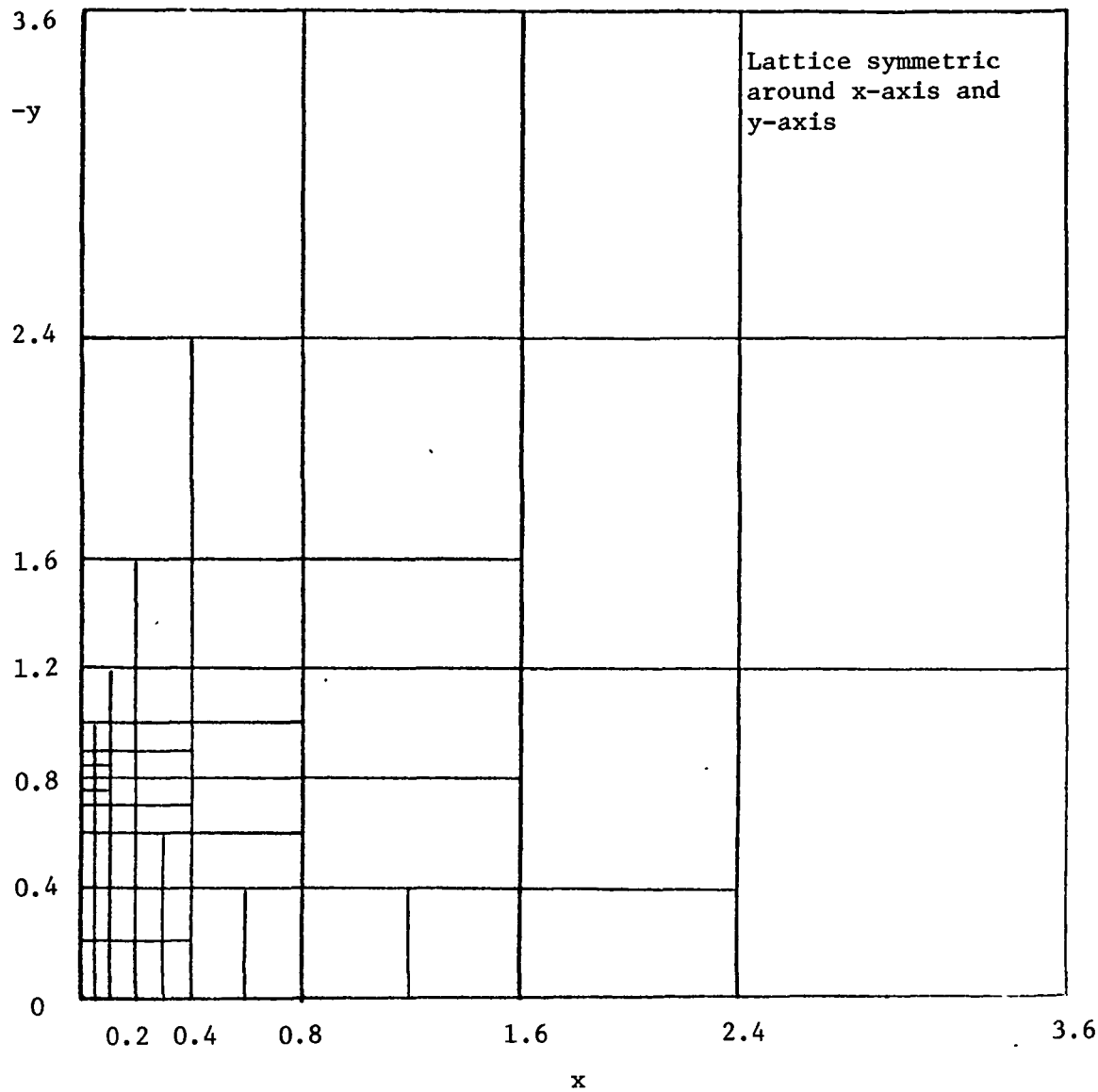

FIGURE B3. FRONT LATTICE FOR SURFACE CRACK IN PLATE WITH A/2C = 0.25, A/T = 0.0 to 0.7

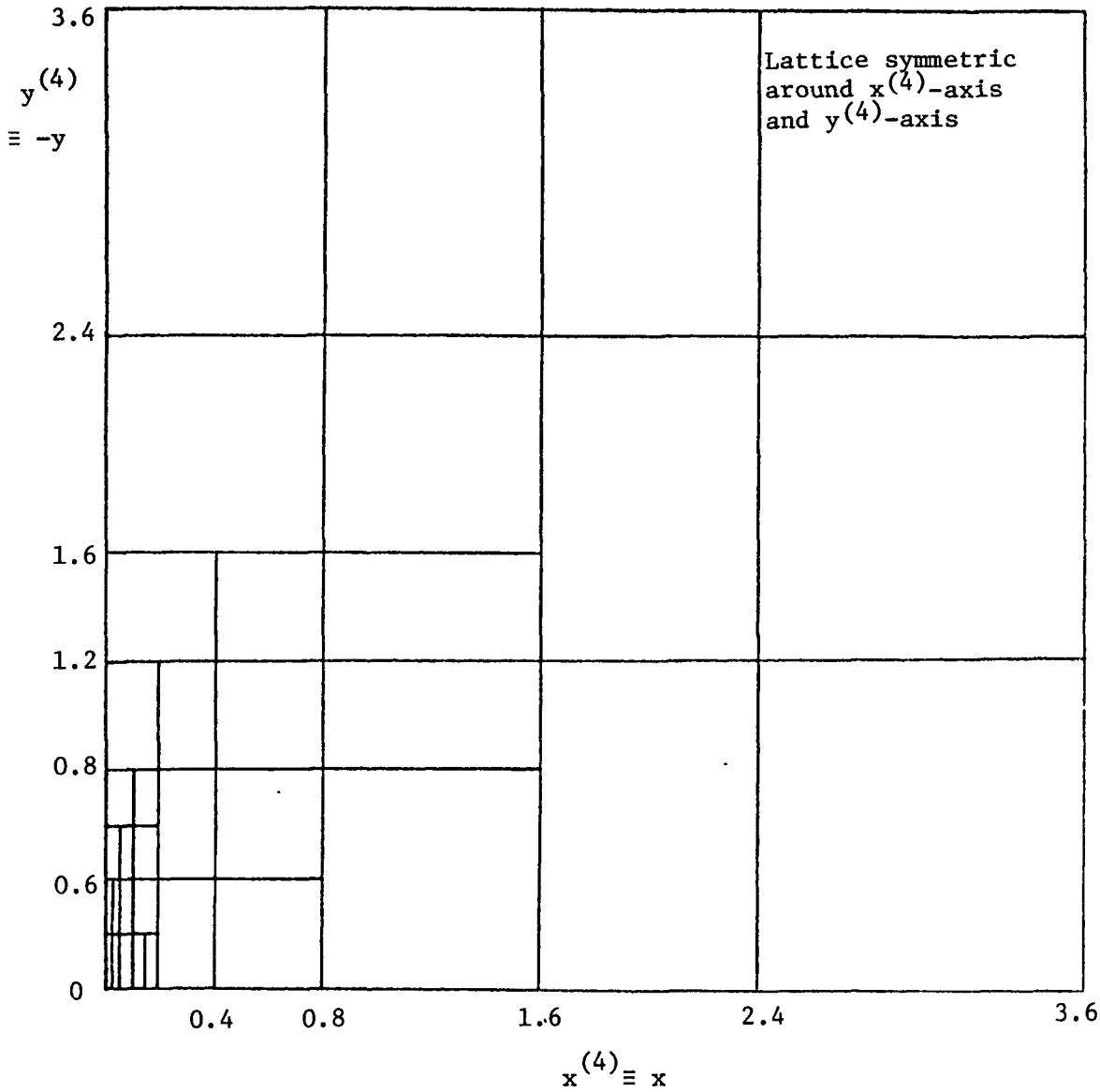

FIGURE B4. BACK LATTICE BEHIND SURFACE CRACK IN PLATE WITH A/2C = 0.25
A/T = 0.5 or 0.7

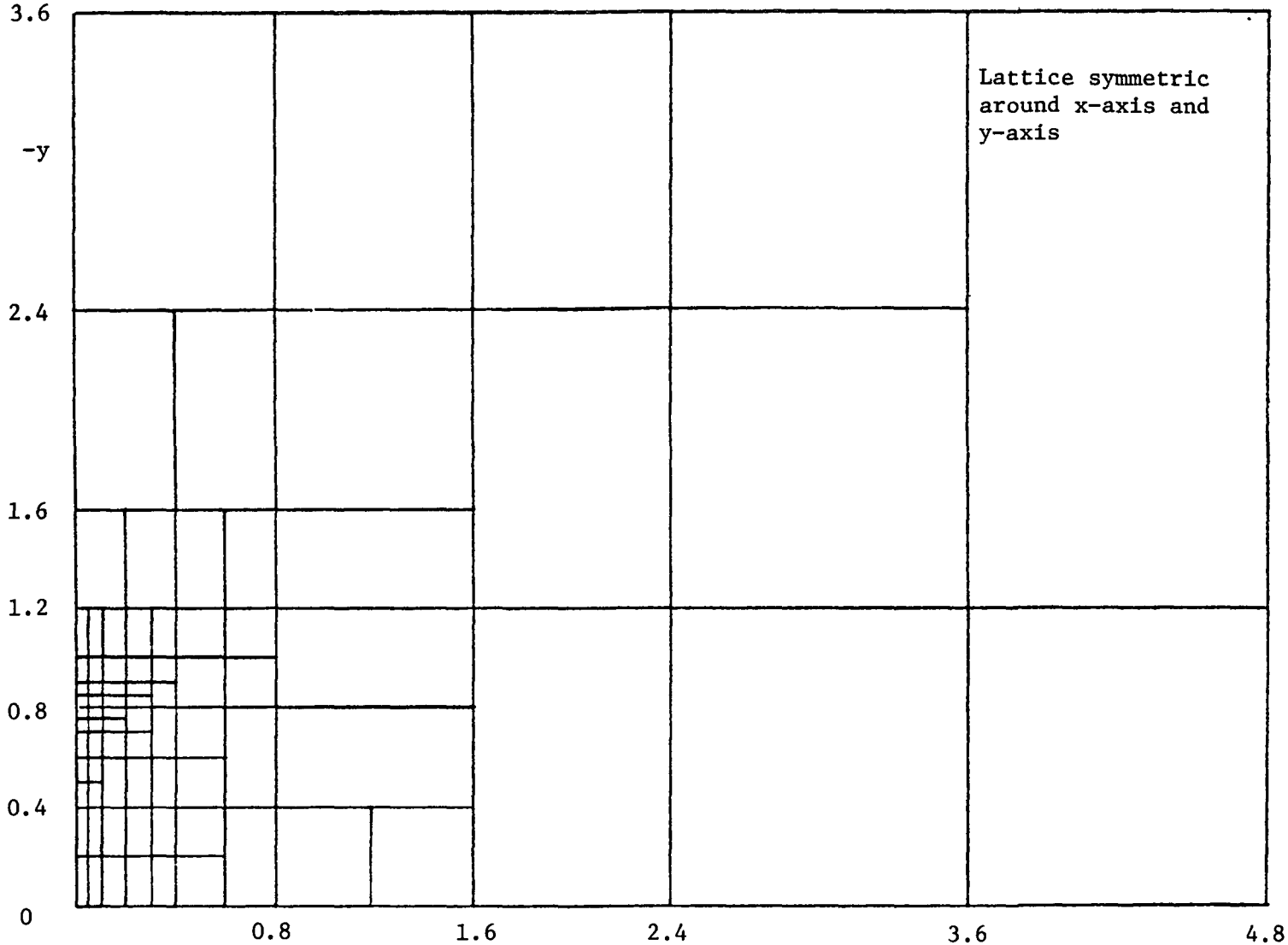

FIGURE B5. FRONT LATTICE FOR SURFACE CRACK IN PLATE WITH A/2C = 0.25, A/T = 0.9

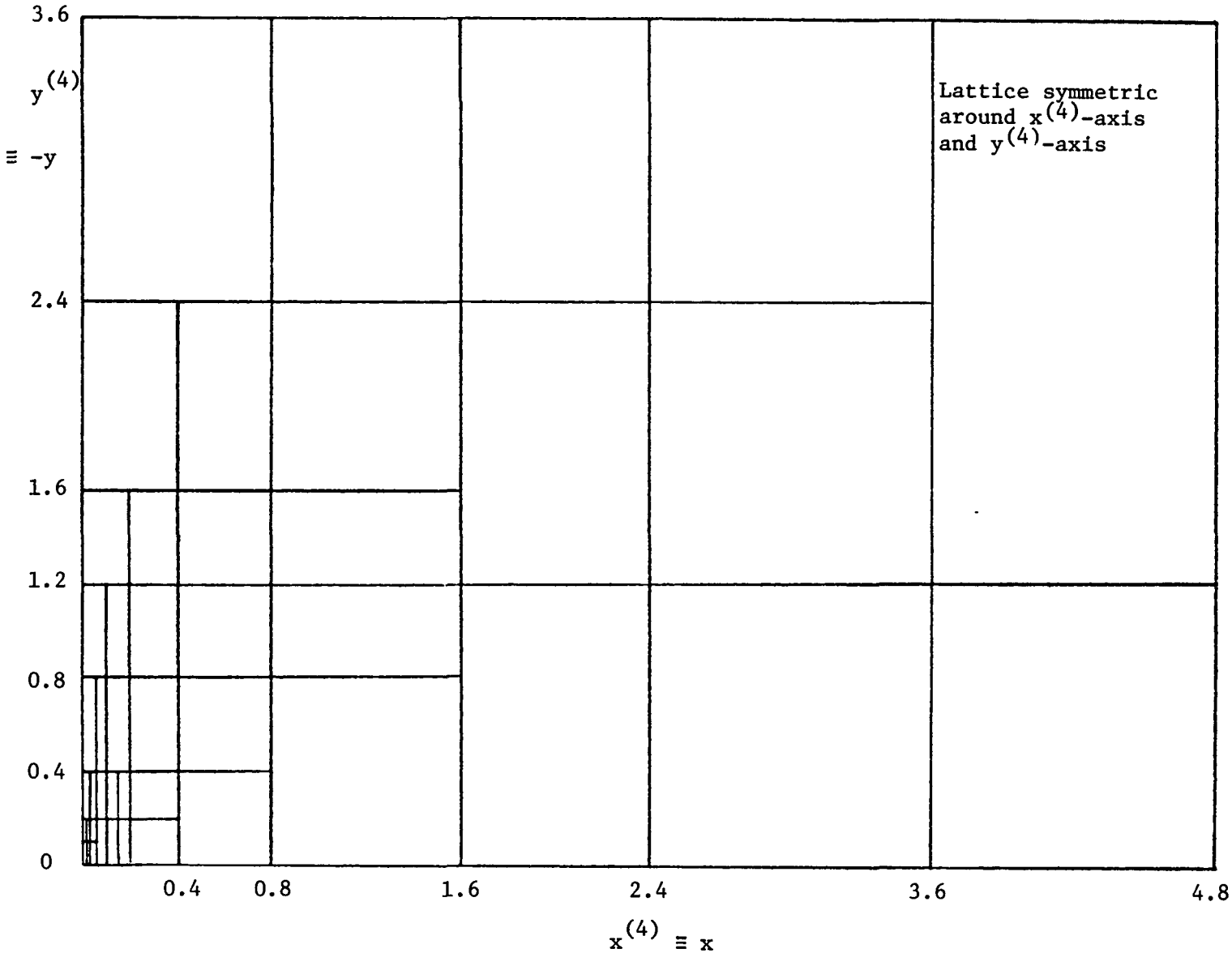

FIGURE B6. BACK LATTICE BEHIND SURFACE CRACK IN PLATE WITH A/2C = 0.25, A/T = 0.9

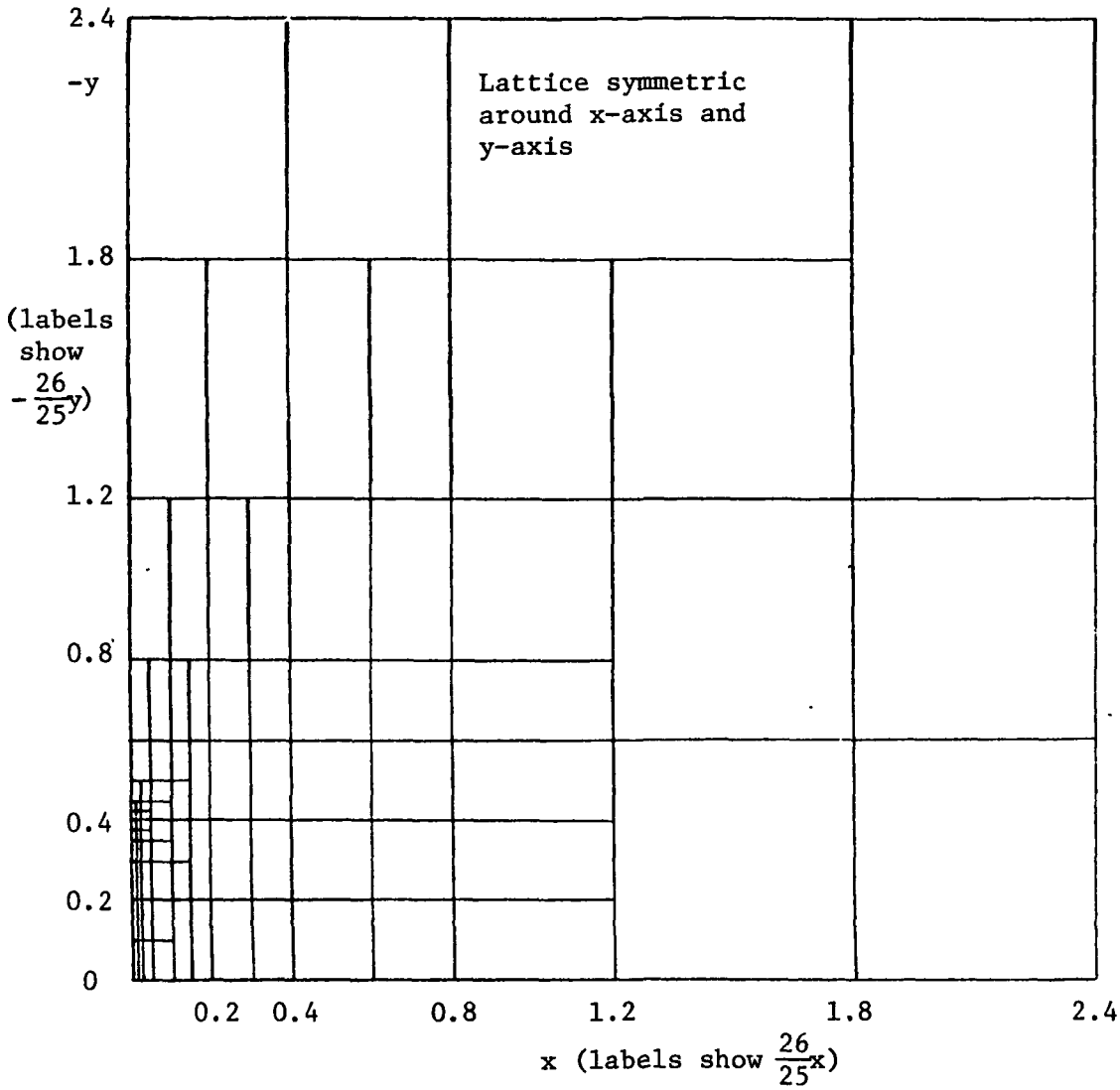

FIGURE B7. FRONT LATTICE FOR SURFACE CRACK IN PLATE WITH A/2C = 0.10, A/T = 0.0 or 0.5

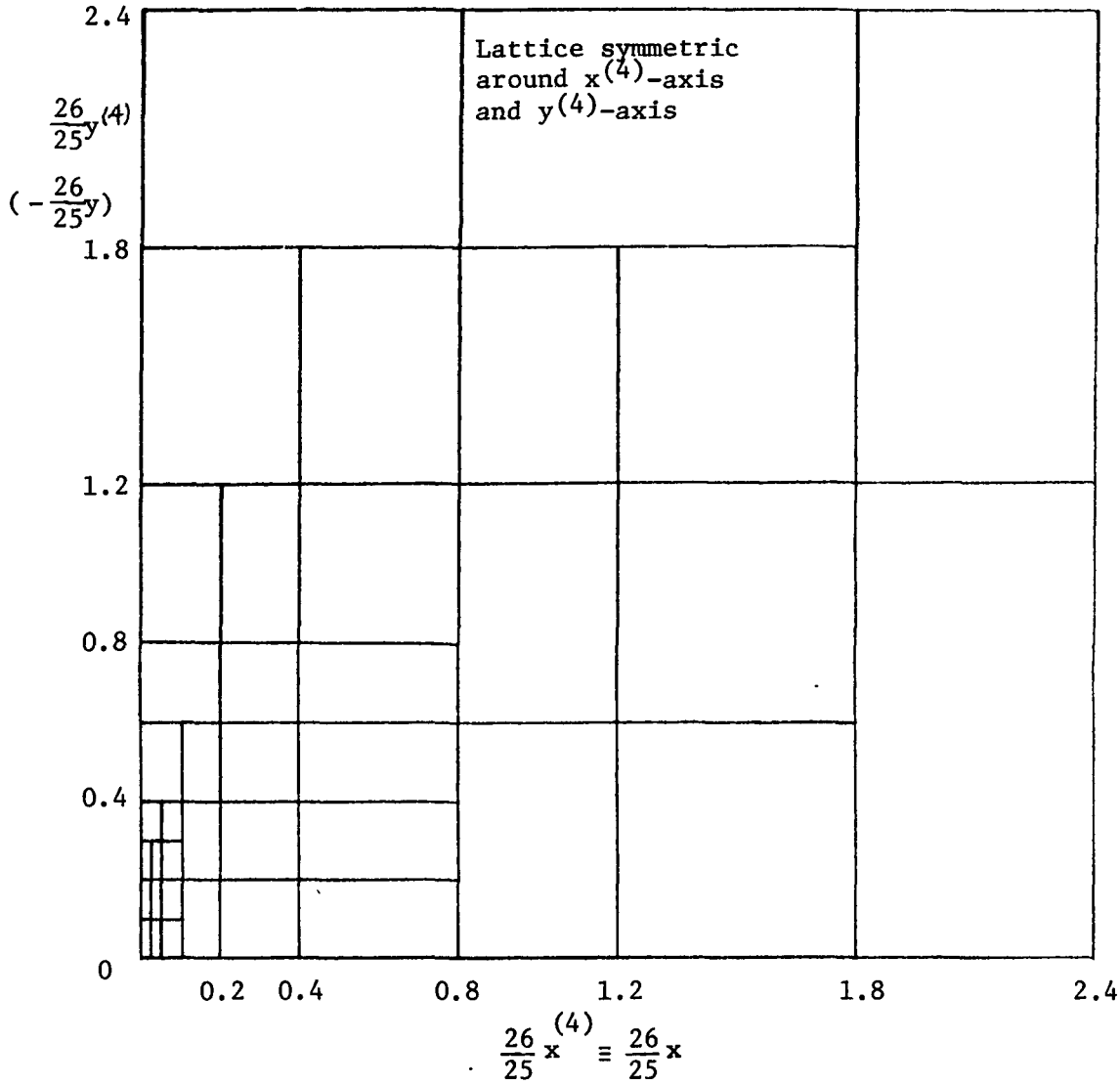

FIGURE B8. BACK LATTICE BEHIND SURFACE CRACK IN PLATE WITH A/2C = 0.10, A/T = 0.5

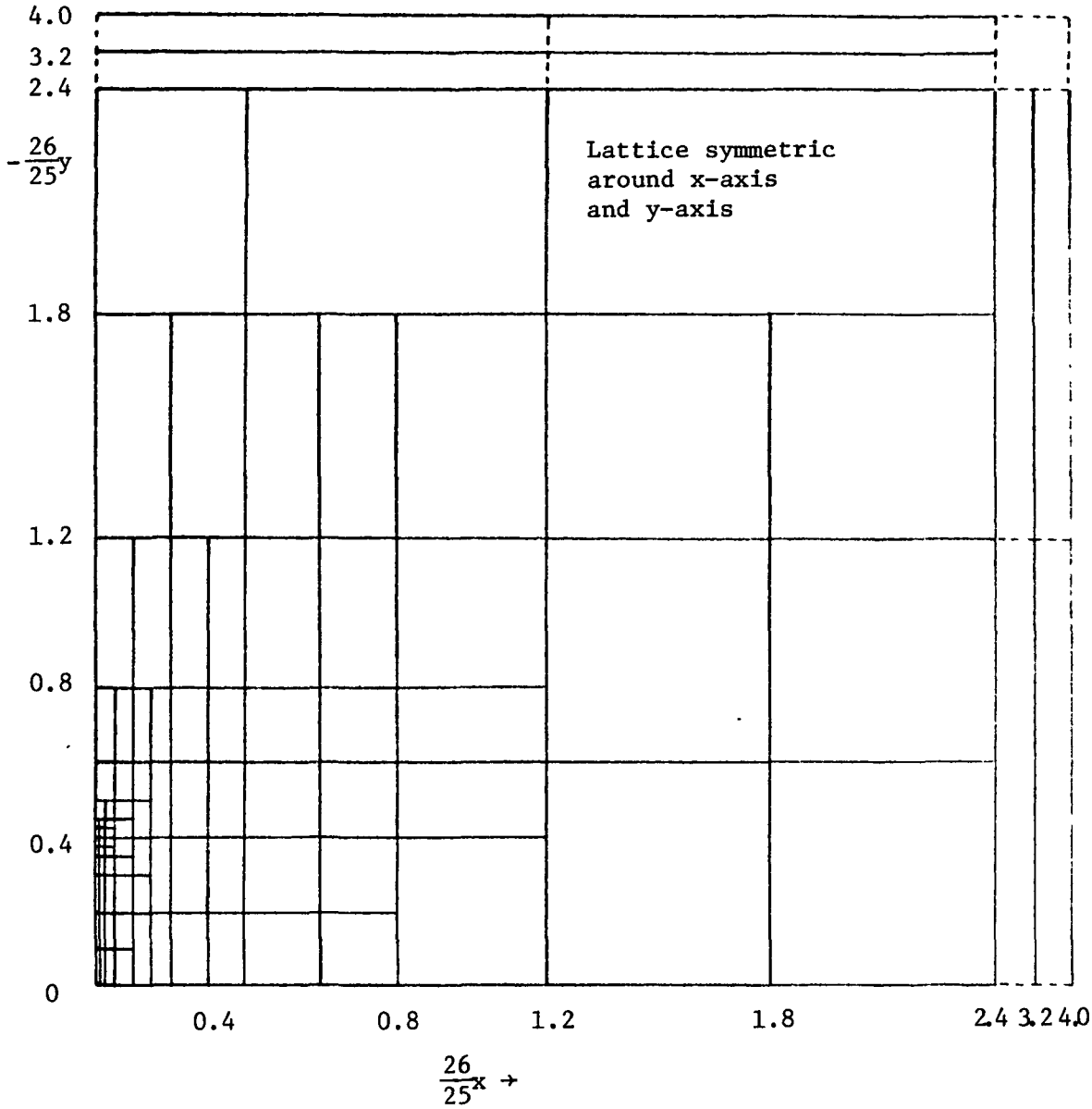

FIGURE B9. FRONT LATTICE FOR SURFACE CRACK IN PLATE WITH A/2C = 0.10, A/T = 0.7

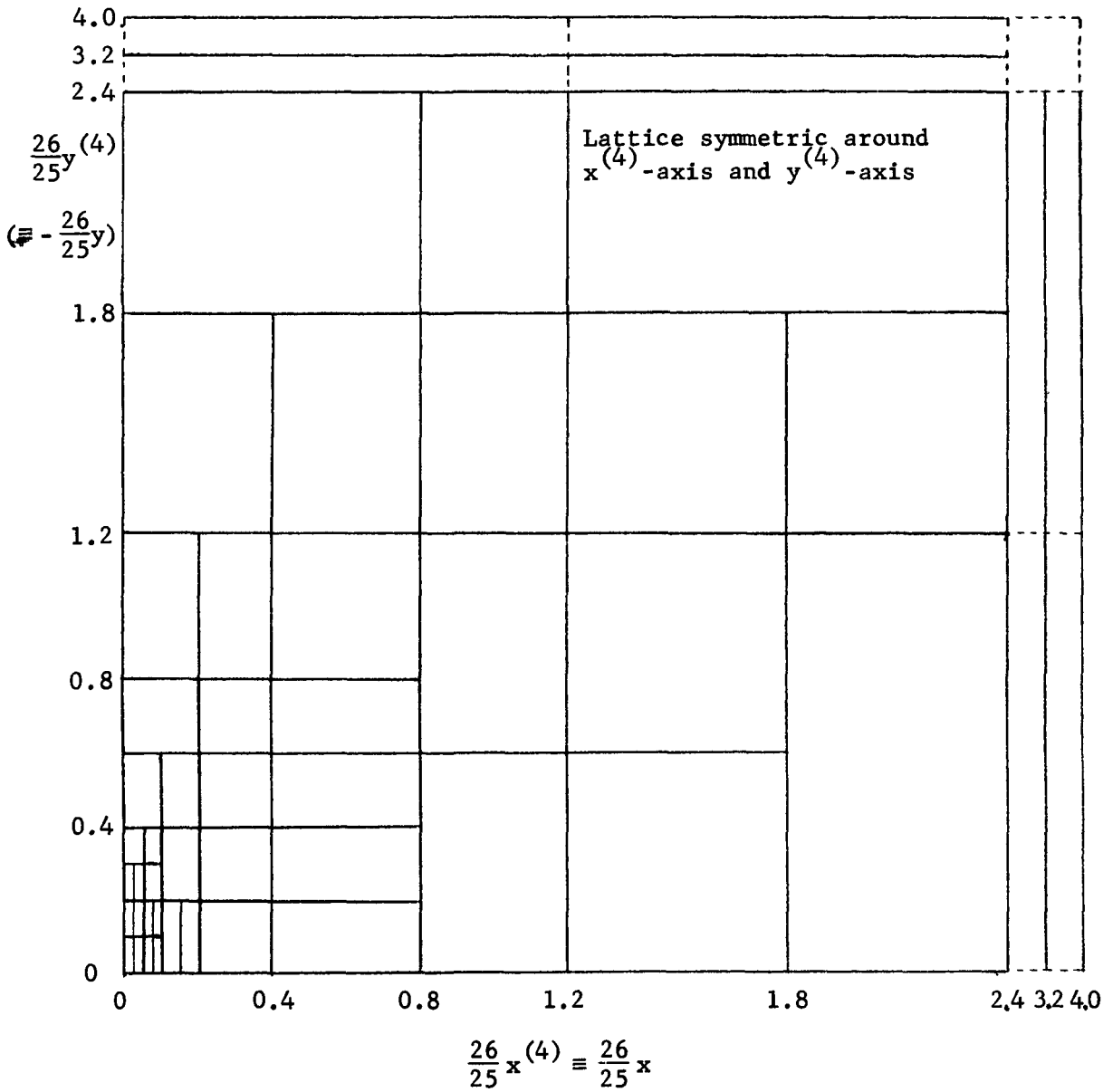

FIGURE B10. BACK LATTICE BEHIND SURFACE CRACK IN PLATE WITH A/2C = 0.10, A/T = 0.7

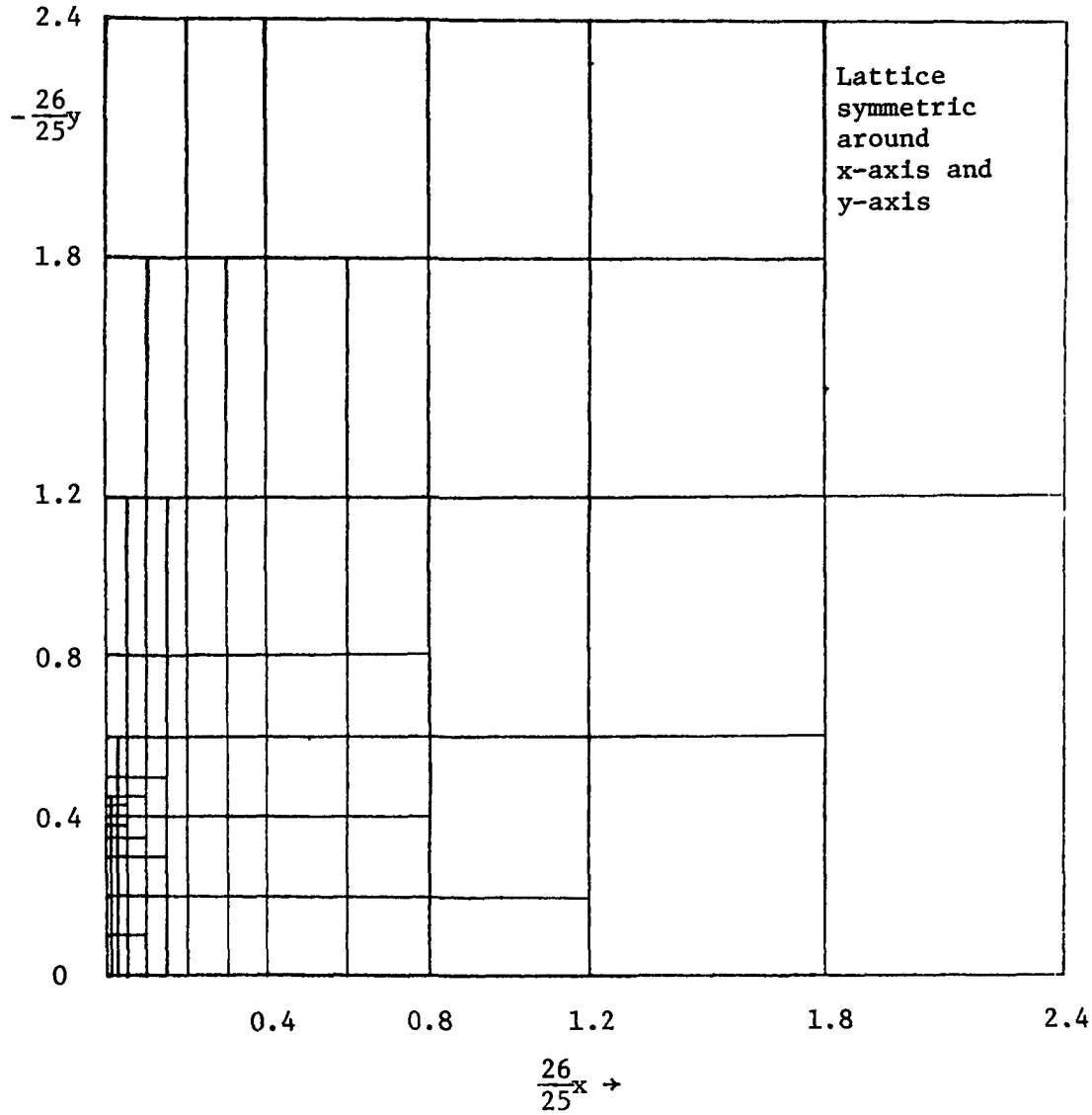

FIGURE B11. FRONT LATTICE FOR SURFACE CRACK IN PLATE WITH A/2C = 0.10, A/T = 0.9

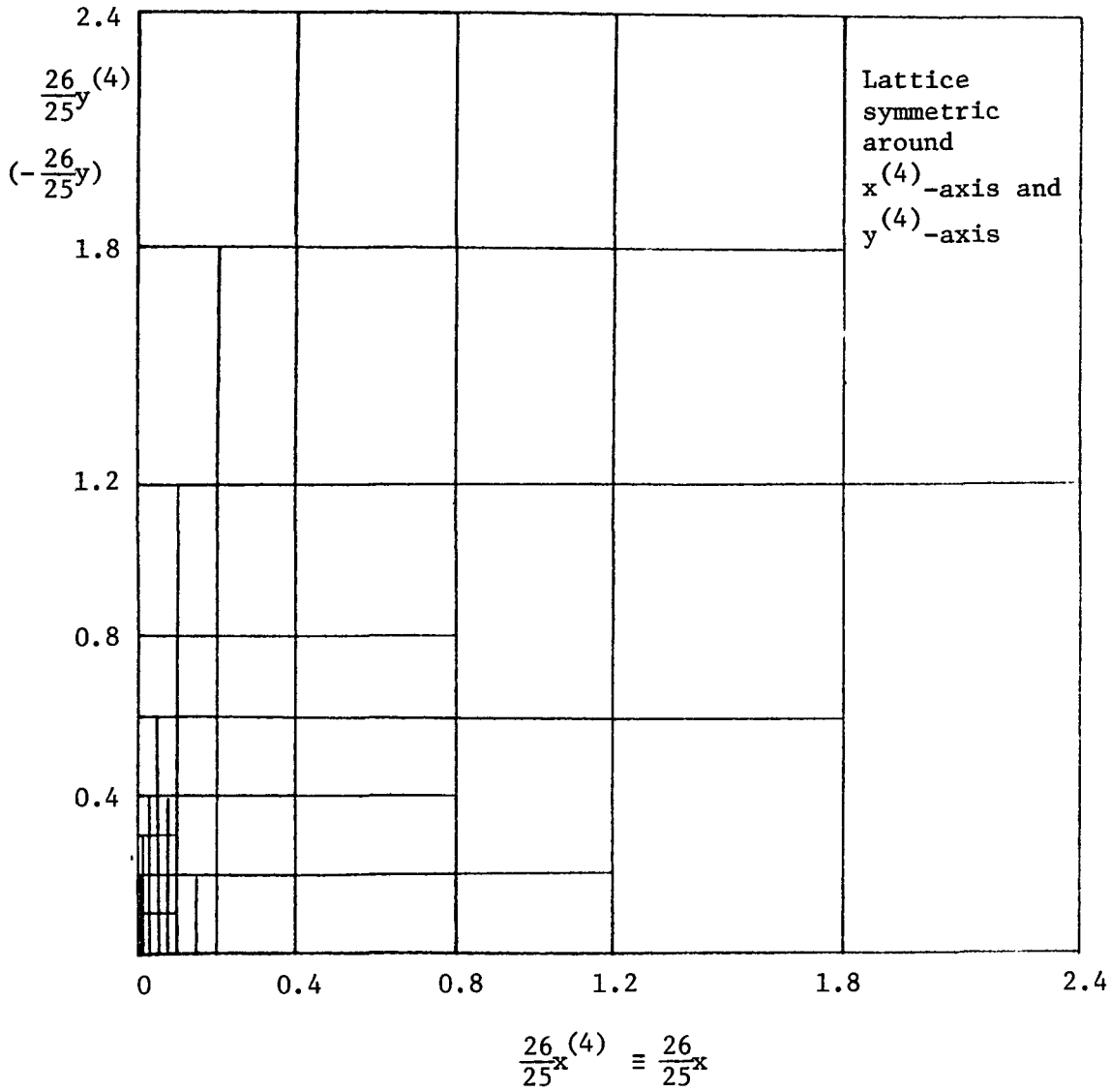

FIGURE B12. BACK LATTICE BEHIND SURFACE CRACK IN PLATE WITH A/2C = 0.10, A/T = 0.9

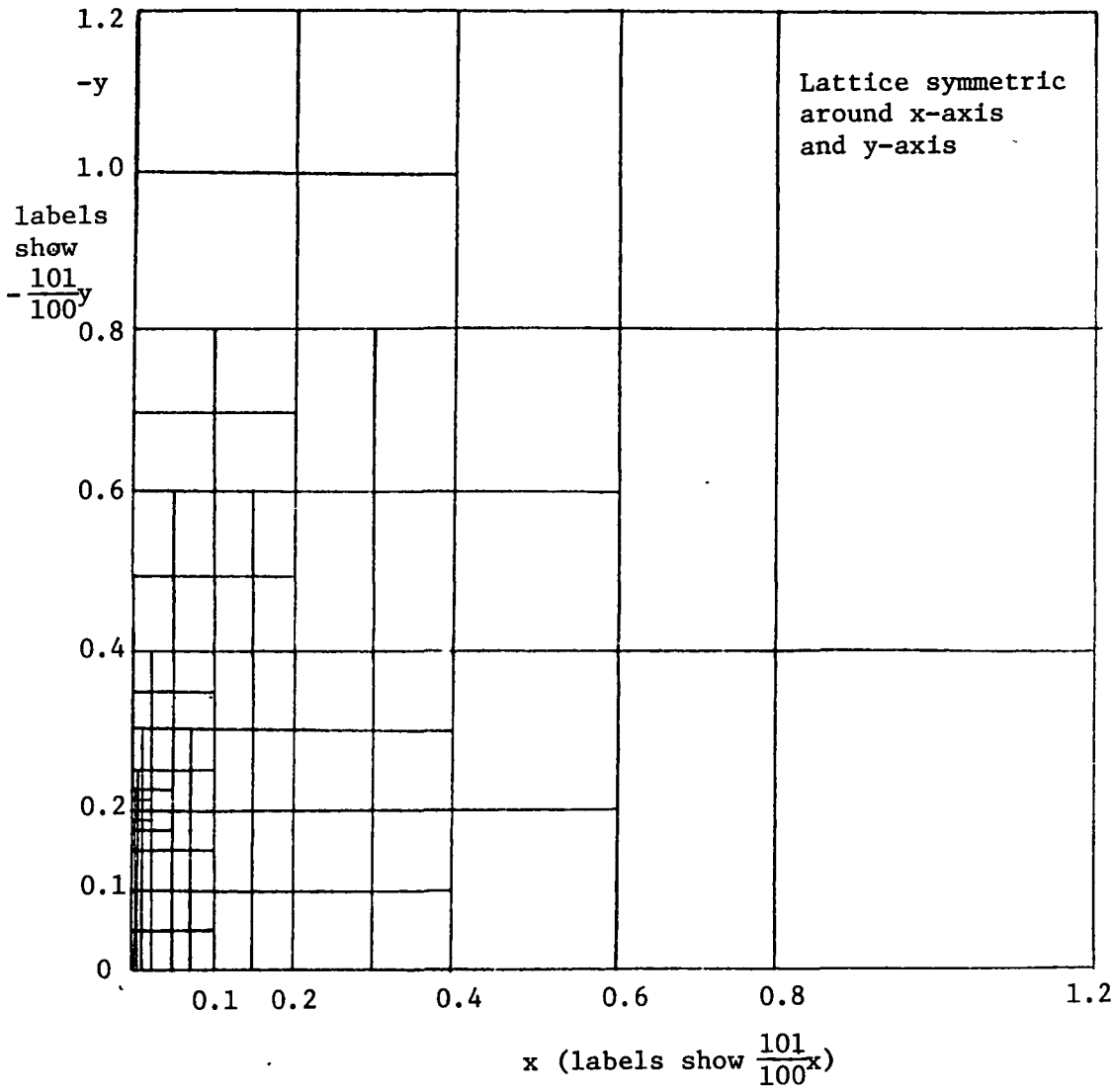

FIGURE B13. FRONT LATTICE USED WITH SURFACE CRACK HAVING A/2C = 0.05

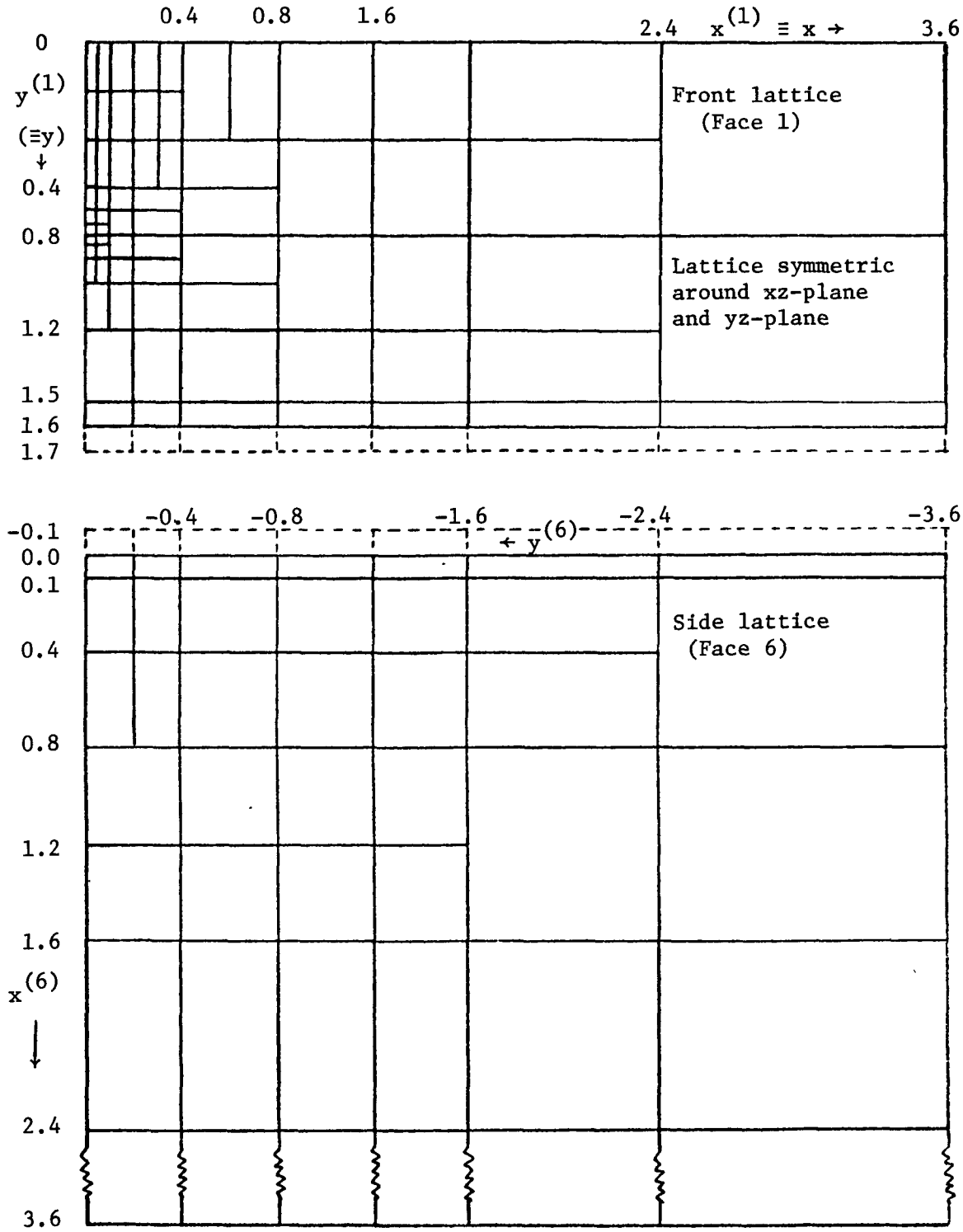

FIGURE B14. LATTICES FOR SURFACE CRACK IN A BAR WITH A/2C = 0.25, A/T = 0.0, W/2C = 2.0

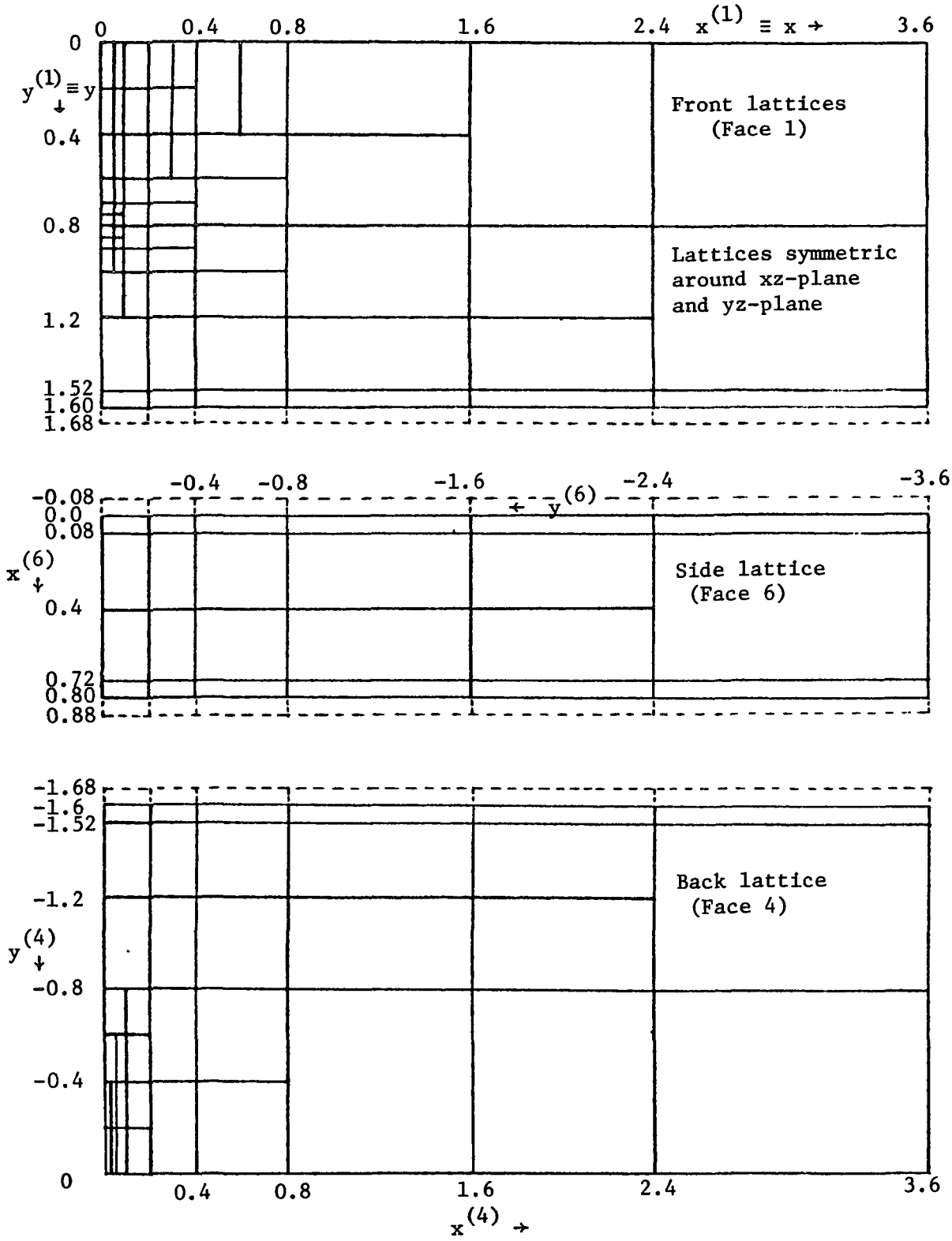

FIGURE B15. LATTICES FOR SURFACE CRACK IN BAR WITH A/2C = 0.25, A/T = 0.5, W/2C = 2.0

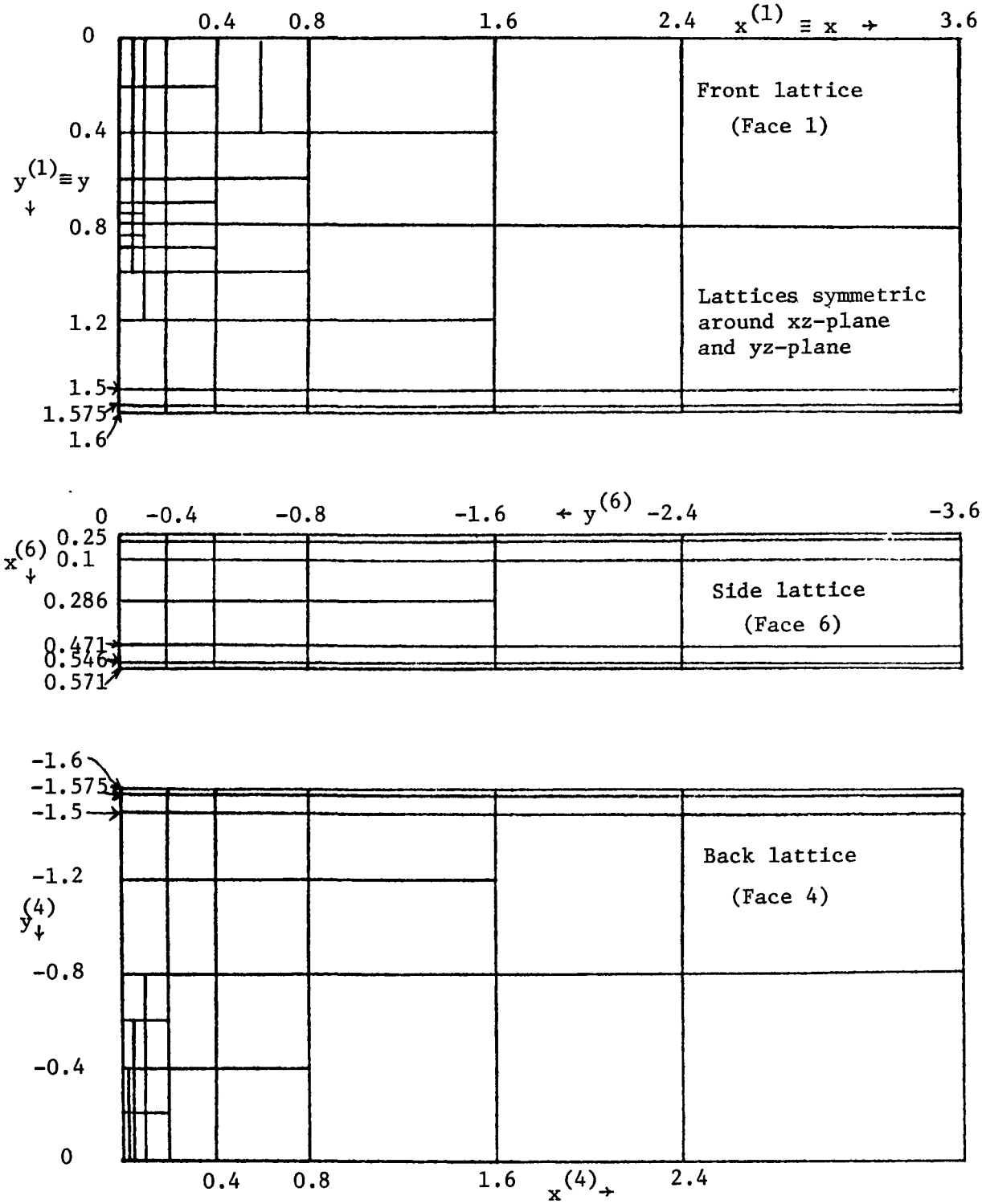

FIGURE B16. LATTICES FOR SURFACE CRACK IN BAR WITH A/2C = 0.25, A/T = 0.7, W/2C = 2.0

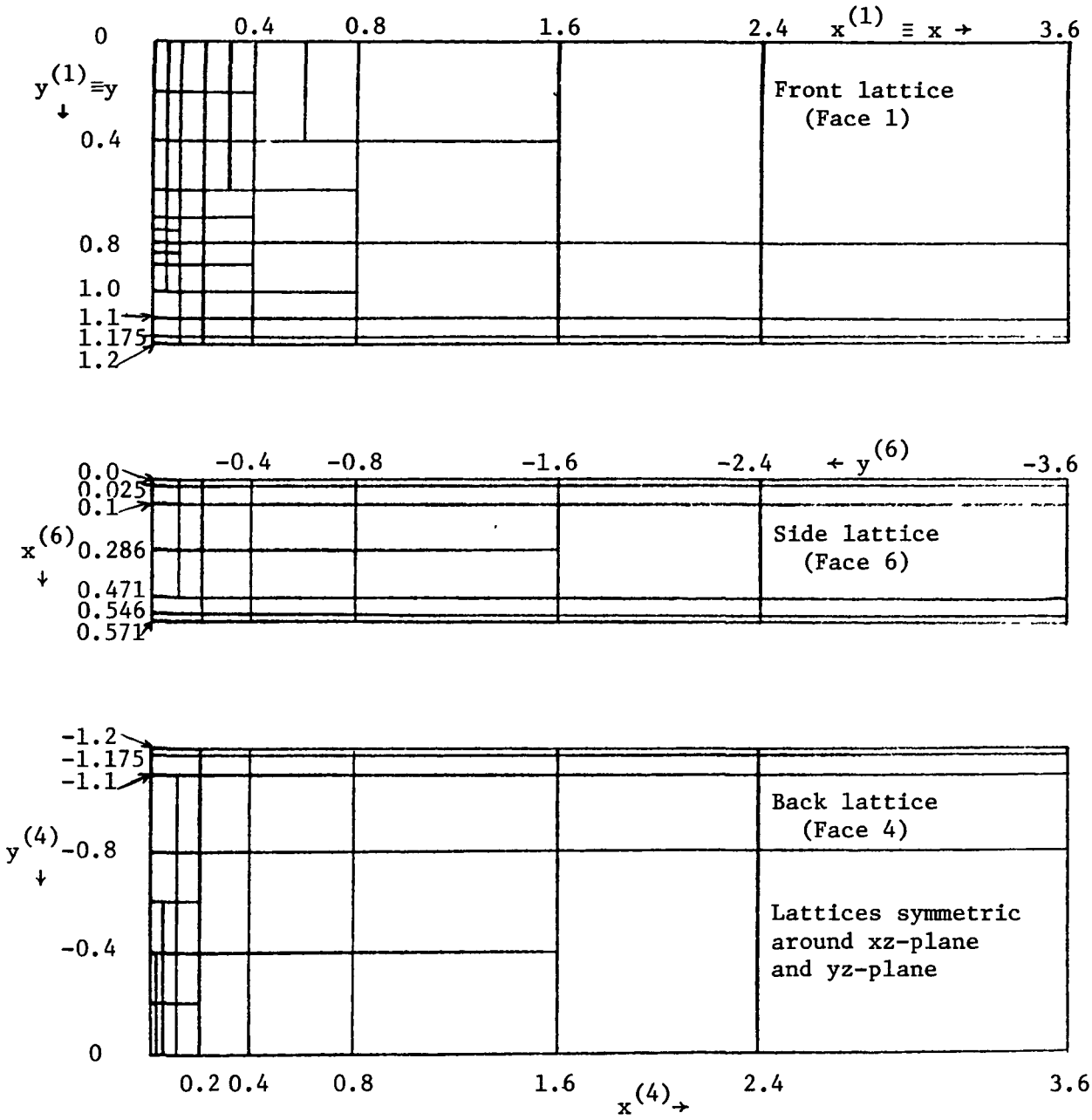

FIGURE B17. LATTICES FOR SURFACE CRACK IN BAR WITH A/2C = 0.25, A/T = 0.7, W/2C = 1.5

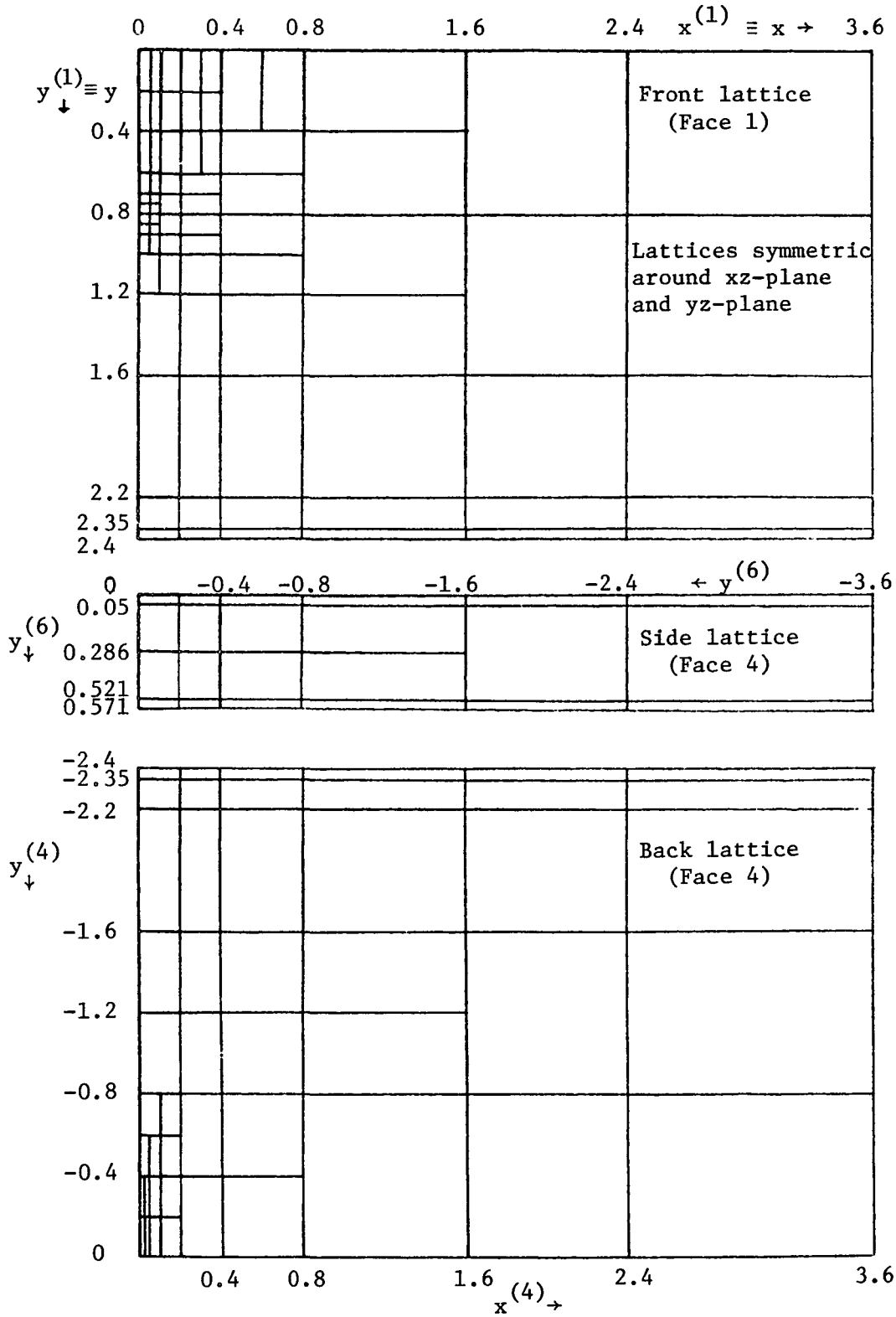

FIGURE B18. LATTICES FOR SURFACE CRACK IN BAR WITH A/2C = 0.25, A/T = 0.7, W/2C = 3.0

APPENDIX C

STRESS COMPONENTS NEAR SURFACE CRACKS UNDER NORMAL LOAD

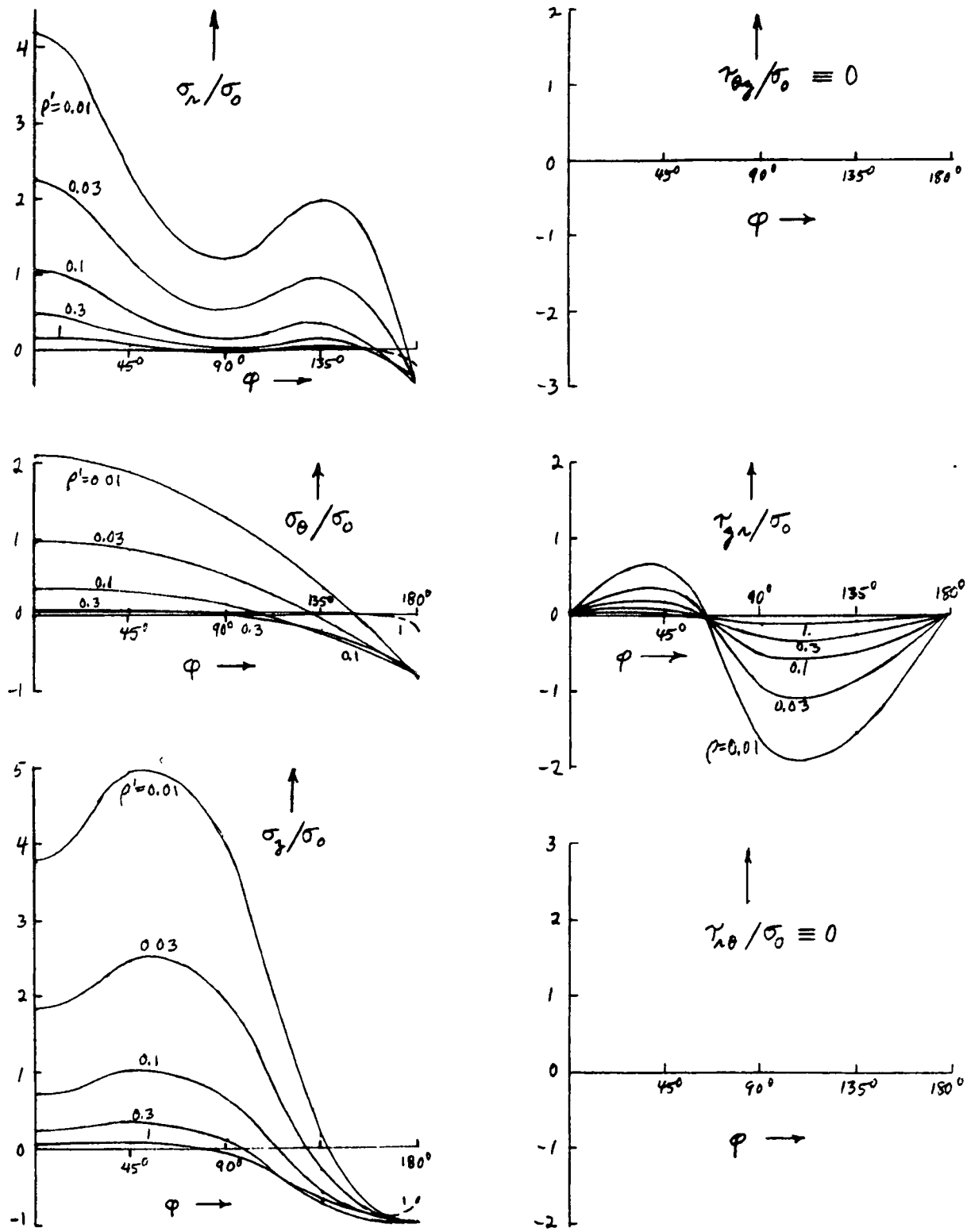

FIGURE C1. STRESSES WHERE θ = 0° NEAR CRACK WITH A/2C = 0.50, A/T = 0.0

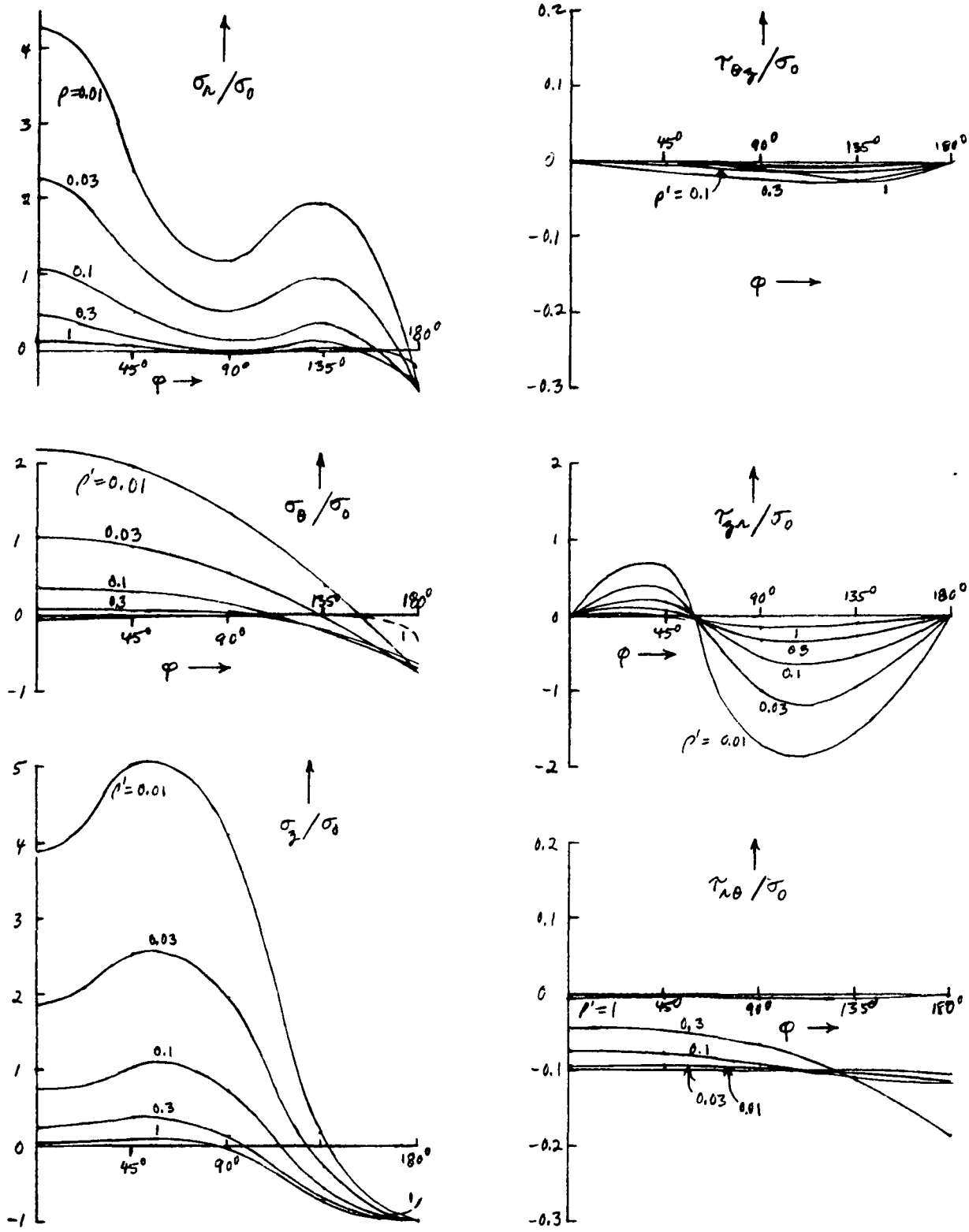

FIGURE C2. STRESSES WHERE θ = 45° NEAR CRACK WITH A/2C = 0.50, A/T = 0.0

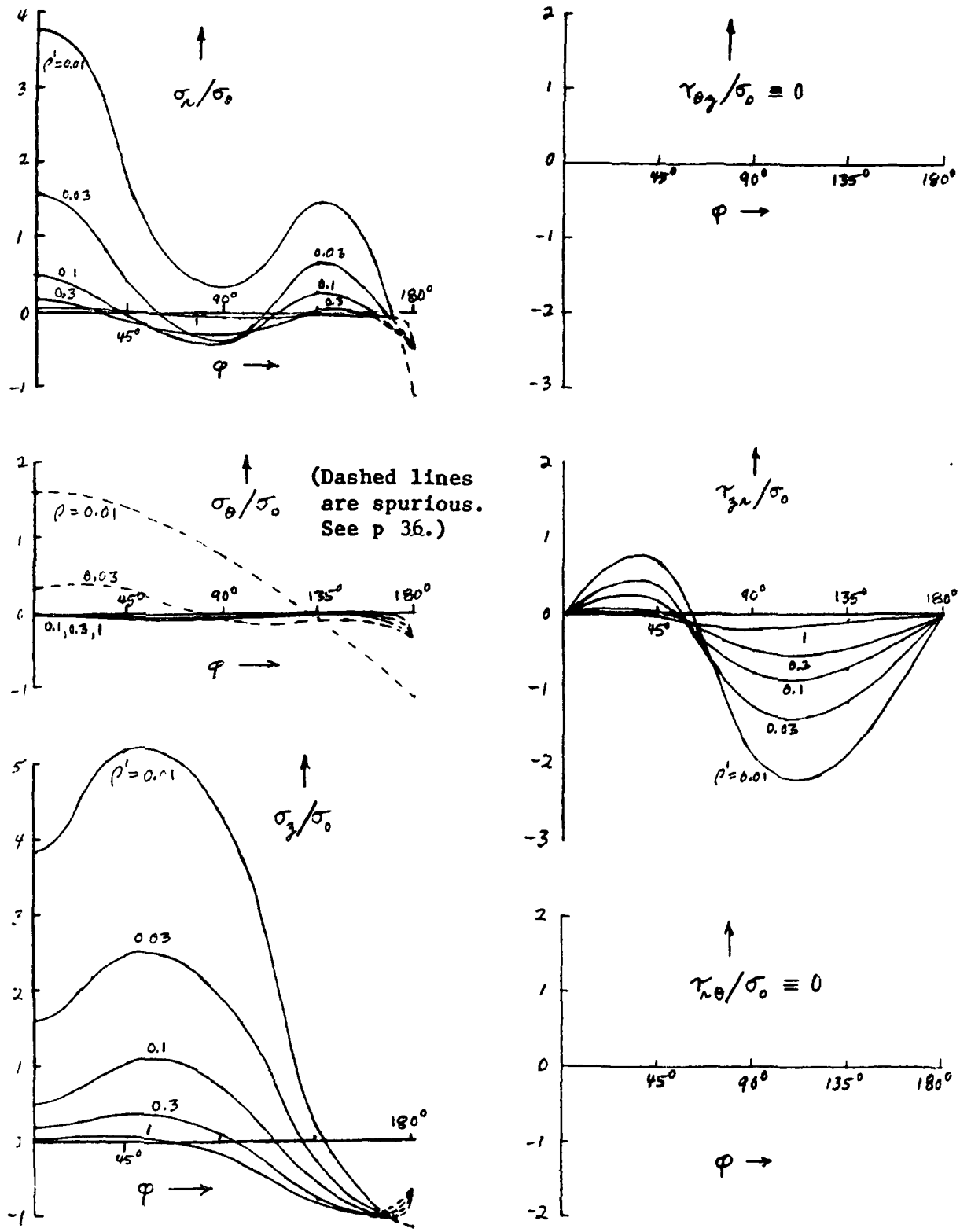

FIGURE C3. STRESSES WHERE θ = 90° NEAR CRACK WITH A/2C = 0.50, A/T = 0.0

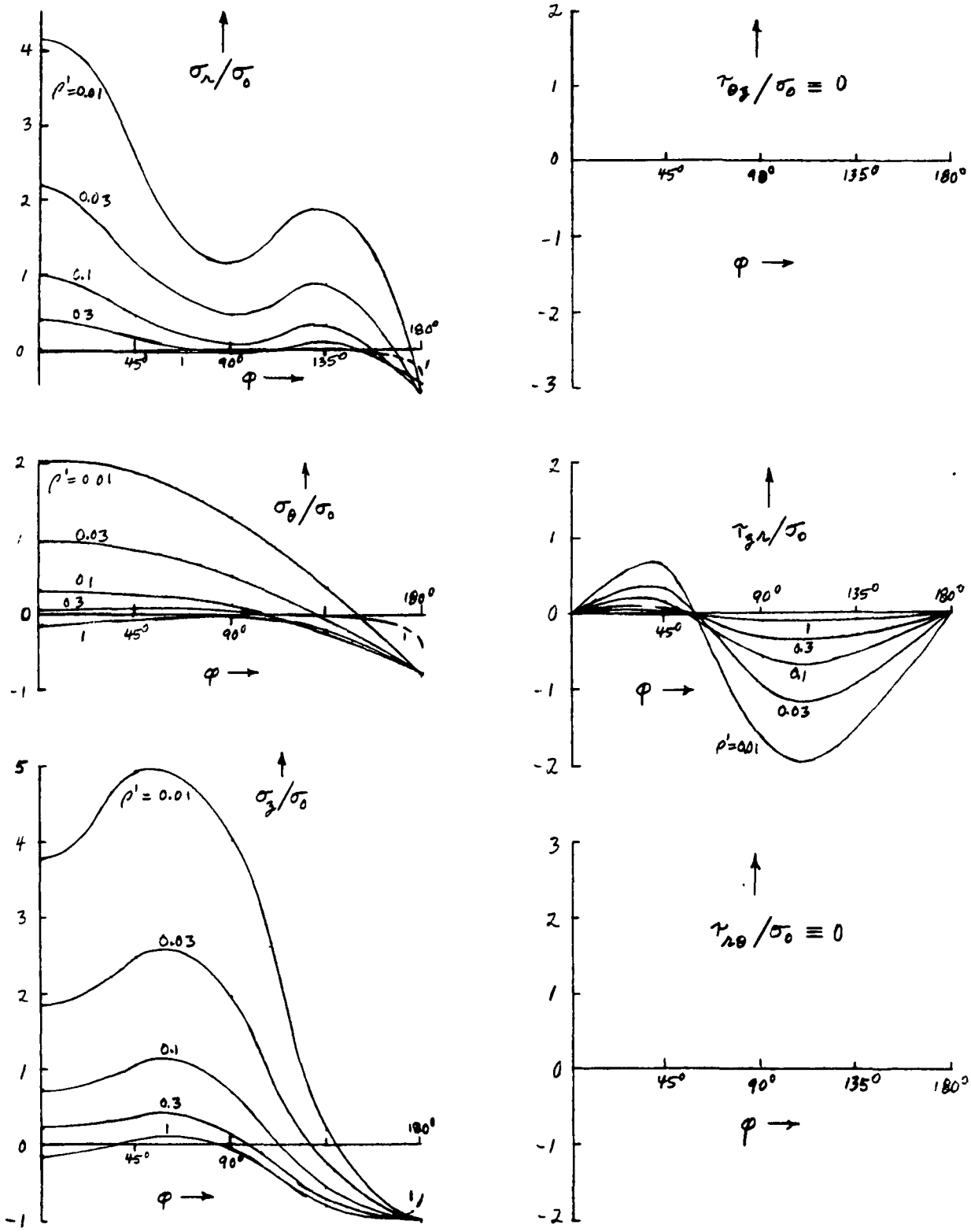

FIGURE C4. STRESSES WHERE θ = 0° NEAR CRACK WITH A/2C = 0.50, A/T = 0.5

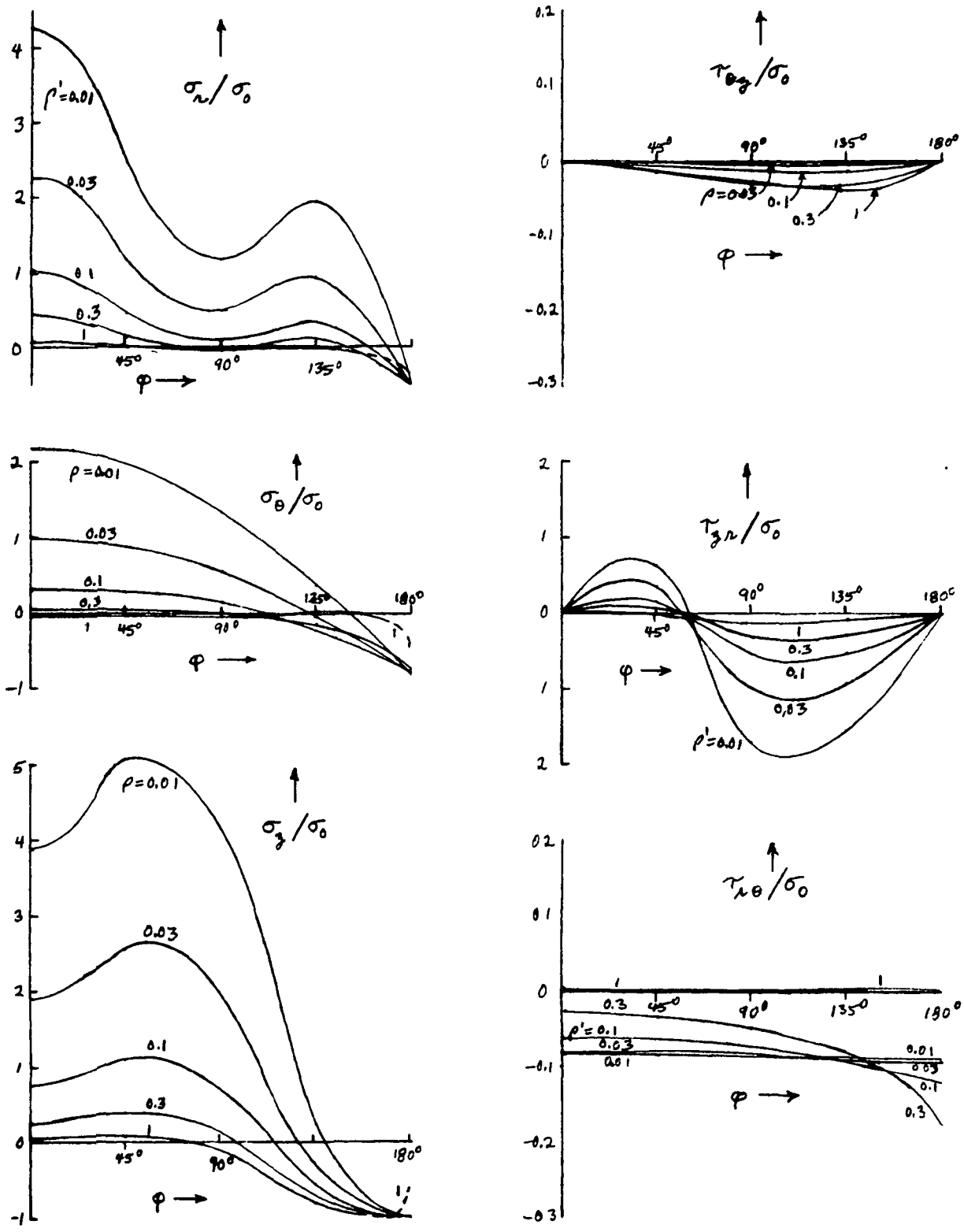

FIGURE C5. STRESSES WHERE θ = 45° NEAR CRACK WITH A/2C = 0.50, A/T = 0.5

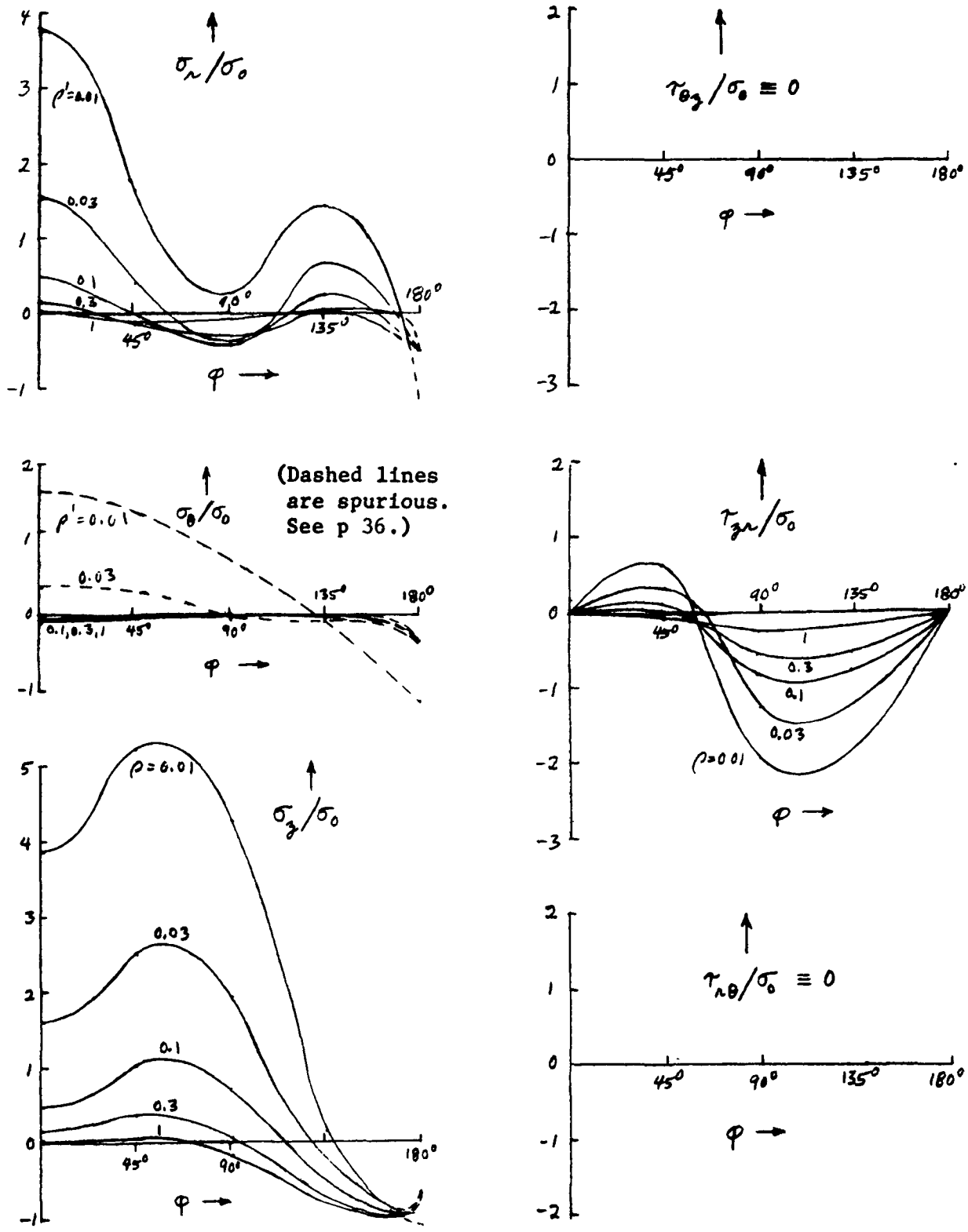

FIGURE C6. STRESSES WHERE θ = 90° NEAR CRACK WITH A/2C = 0.50, A/T = 0.5

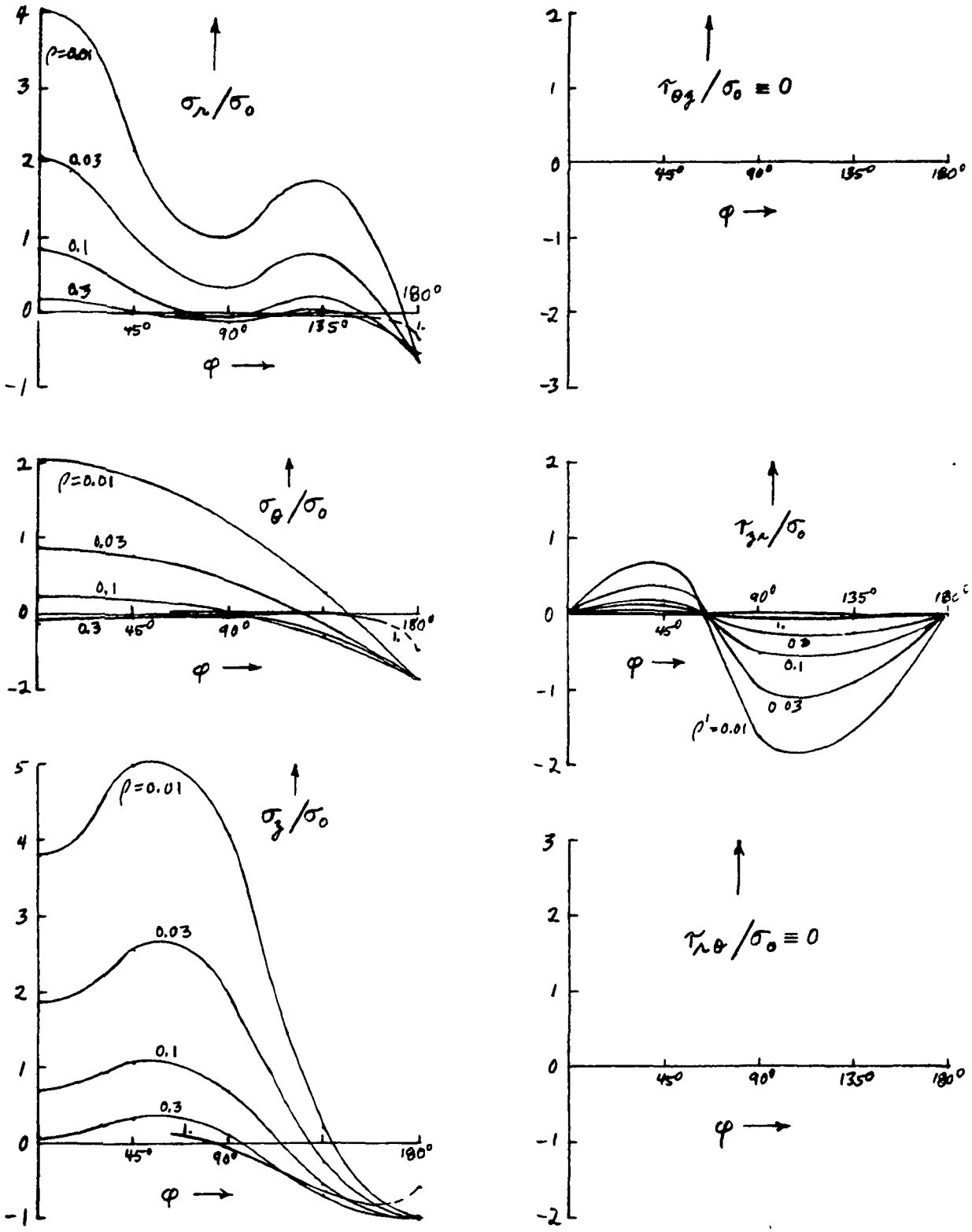

FIGURE C7. STRESSES WHERE θ = 0° NEAR CRACK WITH A/2C = 0.50, A/T = 0.7

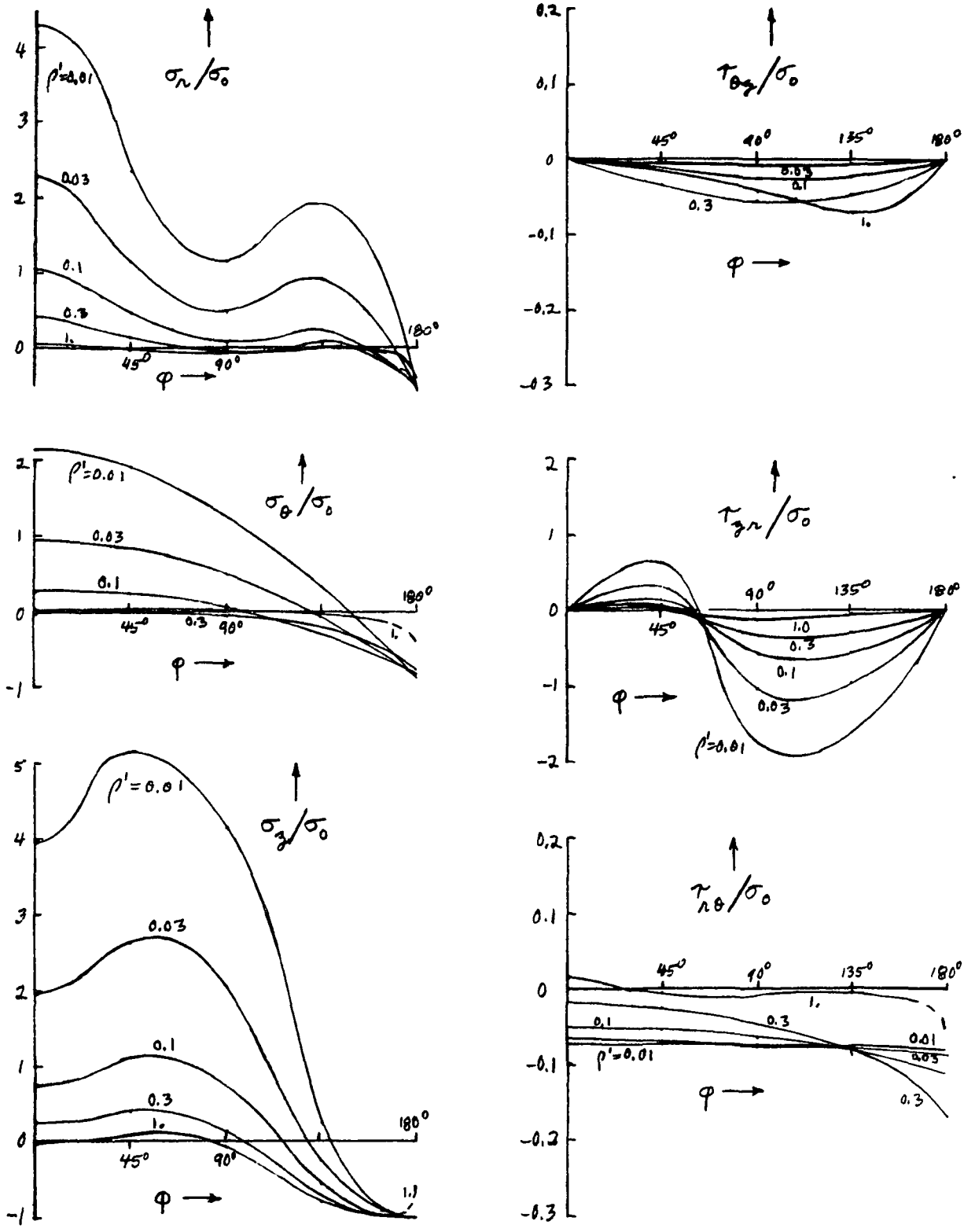

FIGURE C8. STRESSES WHERE θ = 45° NEAR CRACK WITH A/2C = 0.50, A/T = 0.7

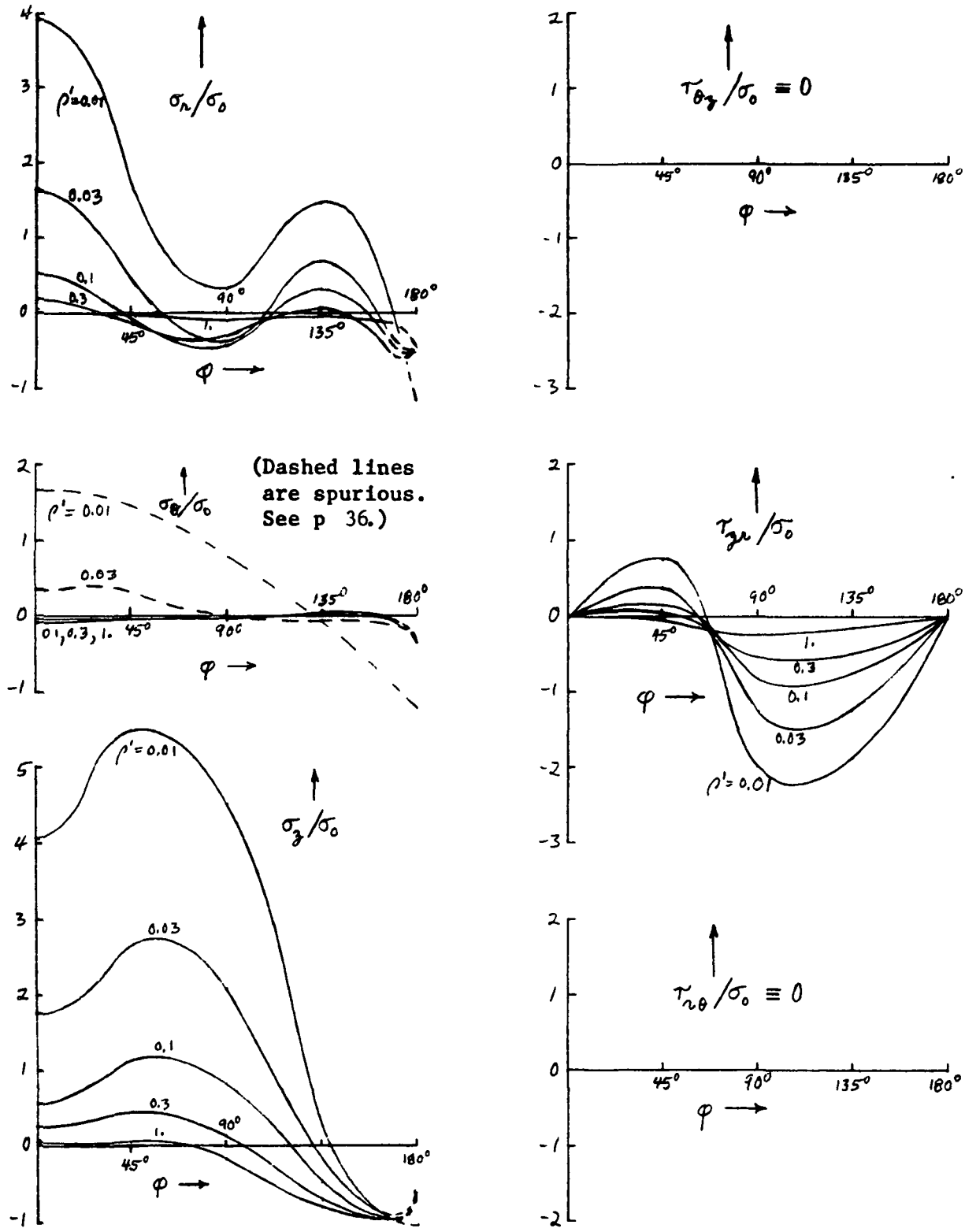

FIGURE C9. STRESSES WHERE θ = 90° NEAR CRACK WITH A/2C = 0.50, A/T = 0.7

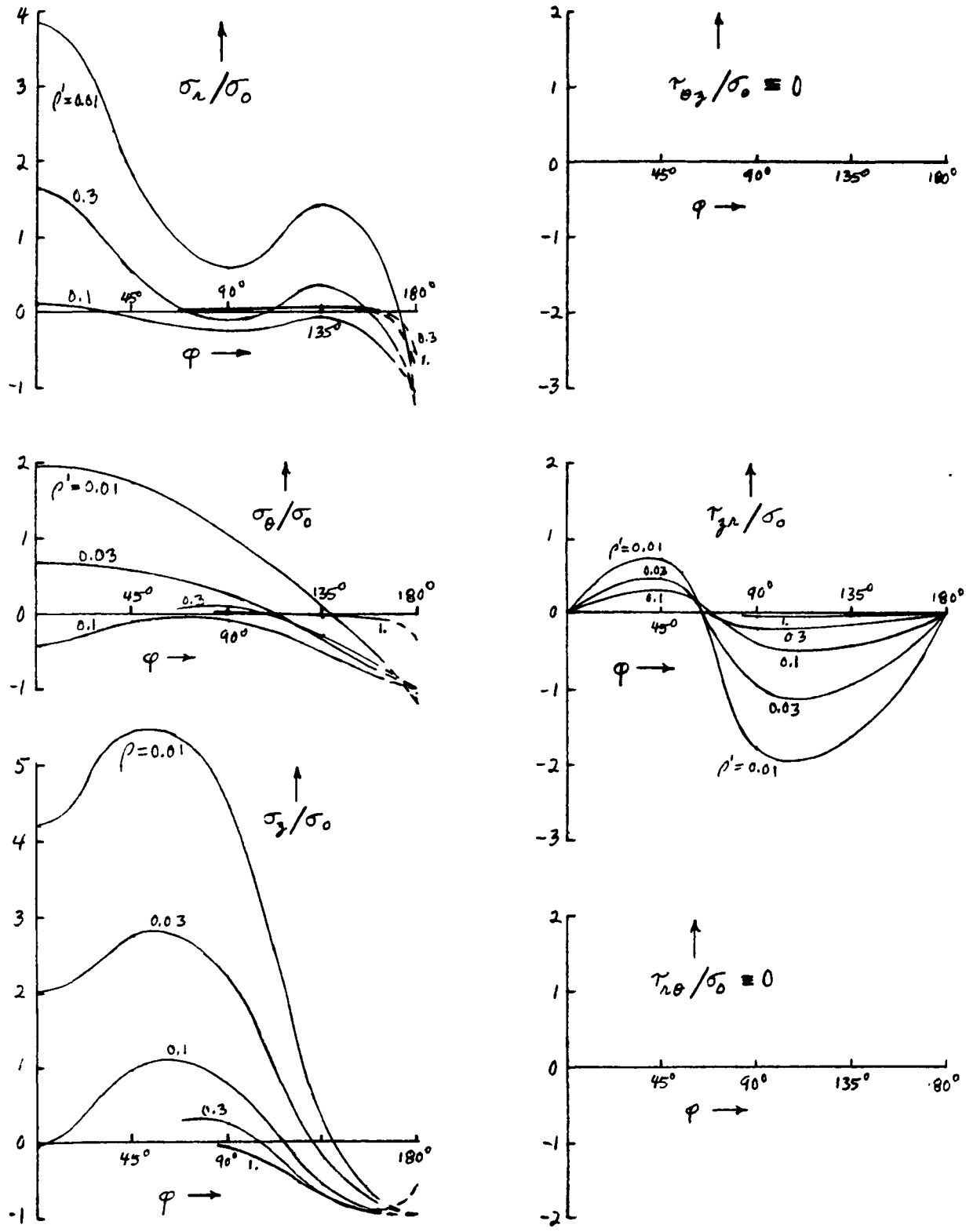

FIGURE C10. STRESSES WHERE θ = 0° NEAR CRACK WITH A/2C = 0.50, A/T = 0.9

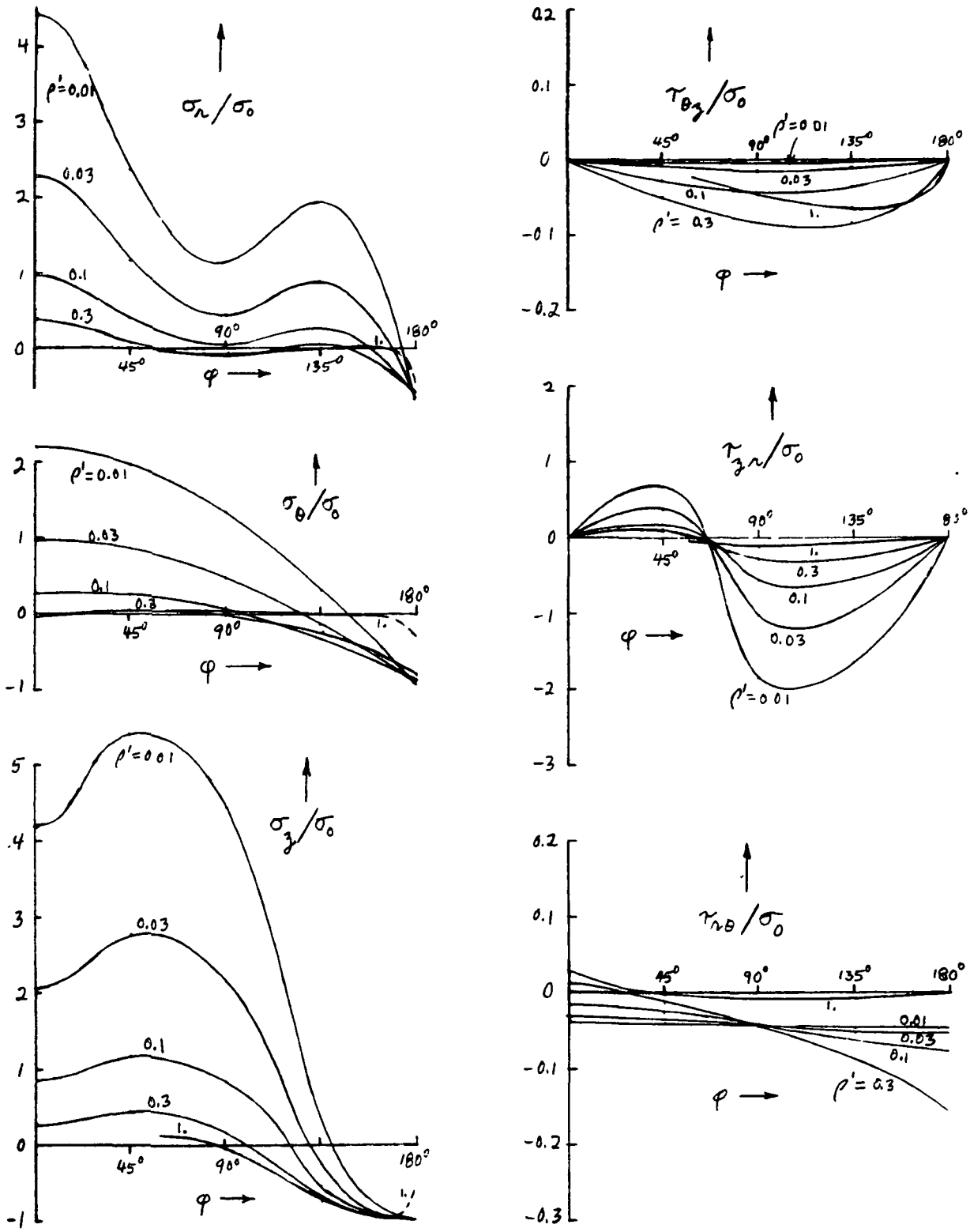

FIGURE C11. STRESSES WHERE θ = 45° NEAR CRACK WITH A/2C = 0.50, A/T = 0.9

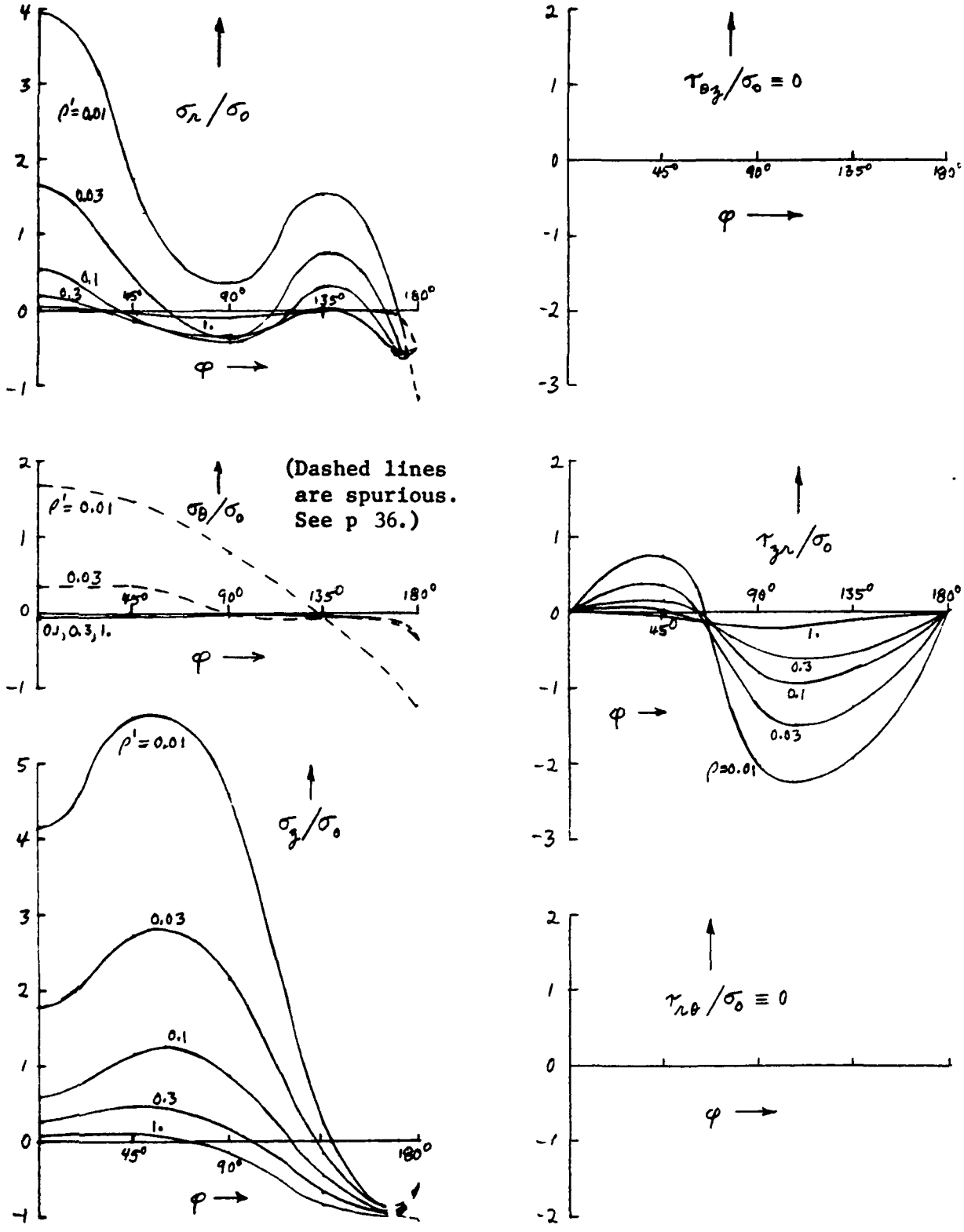

FIGURE C12. STRESSES WHERE θ = 90° NEAR CRACK WITH A/2C = 0.50, A/T = 0.9

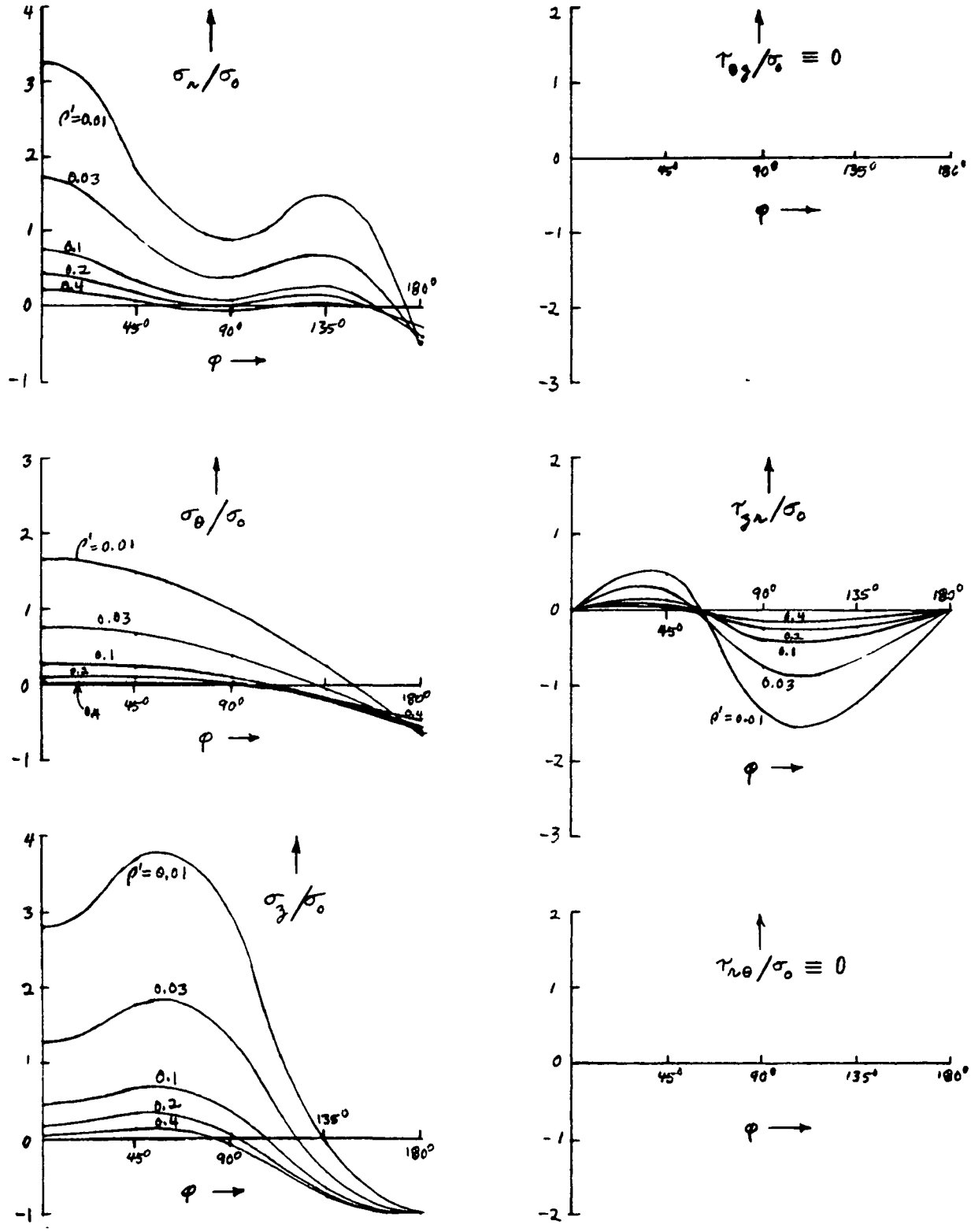

FIGURE C13. STRESSES WHERE θ = 0° NEAR CRACK WITH A/2C = 0.25, A/T = 0.0

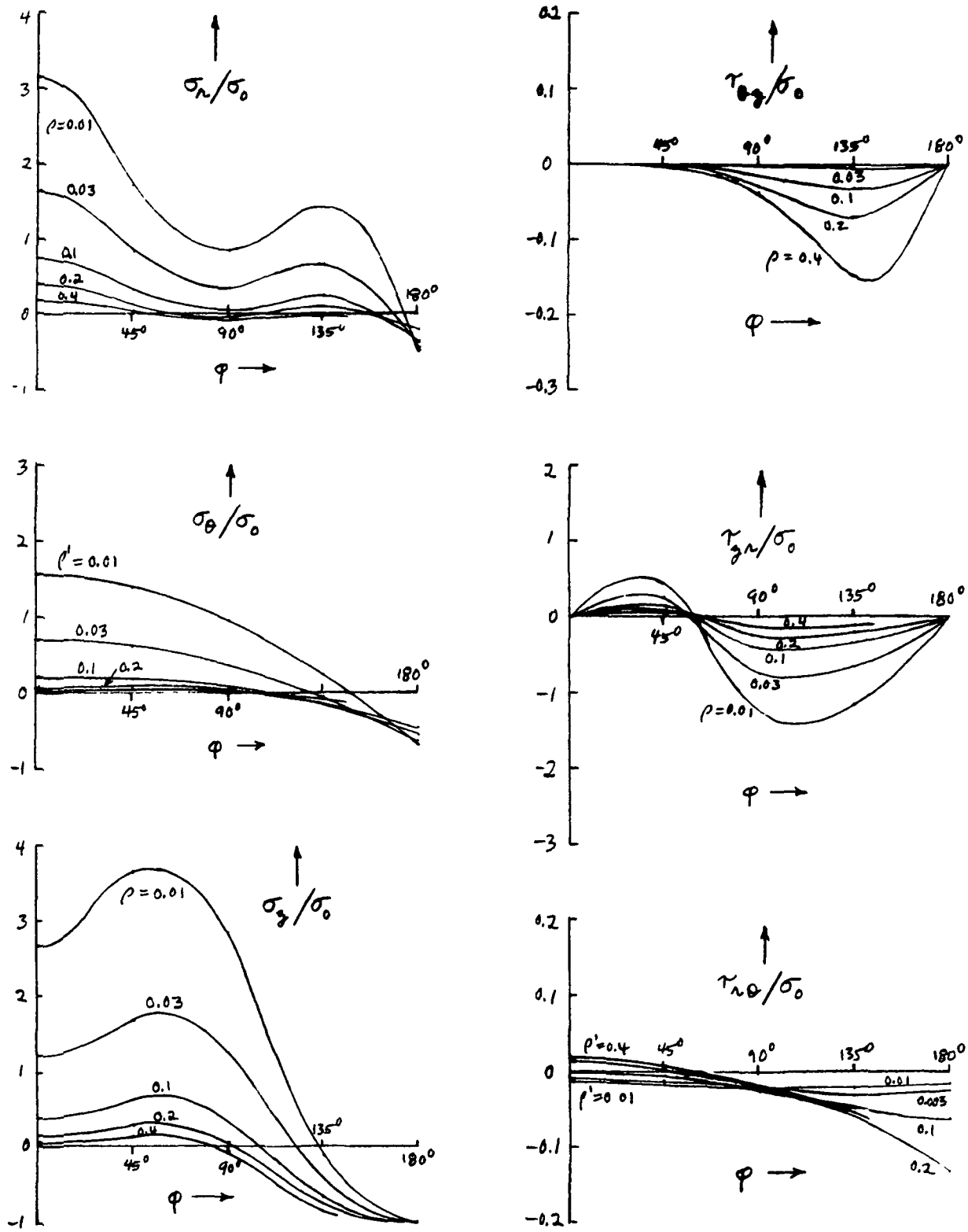

FIGURE C14. STRESSES WHERE θ = 30° NEAR CRACK WITH A/2C = 0.25, A/T = 0.0

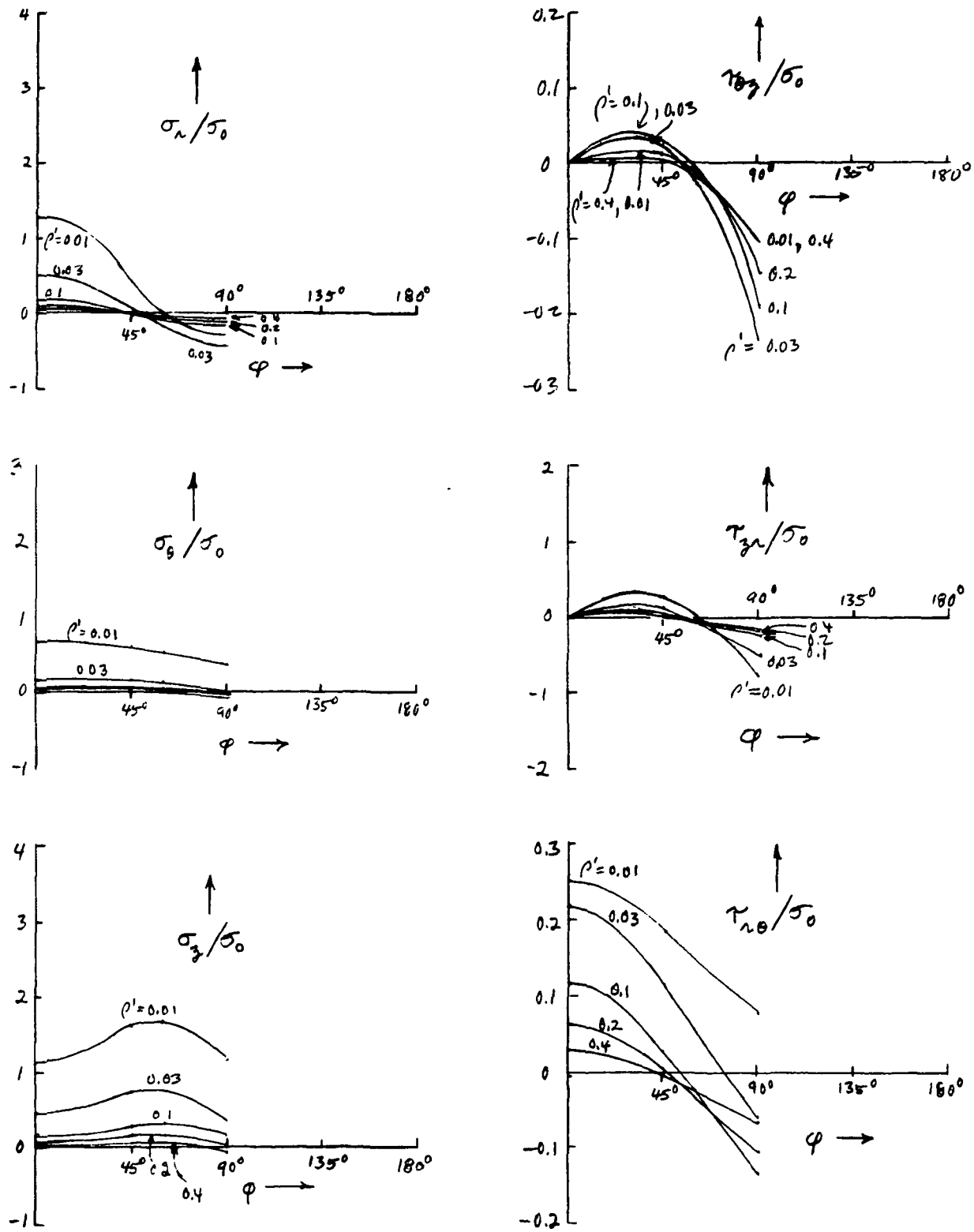

FIGURE C15. STRESSES WHERE $\theta = \theta_{tip}$ NEAR CRACK WITH A/2C = 0.25, A/T = 0.0

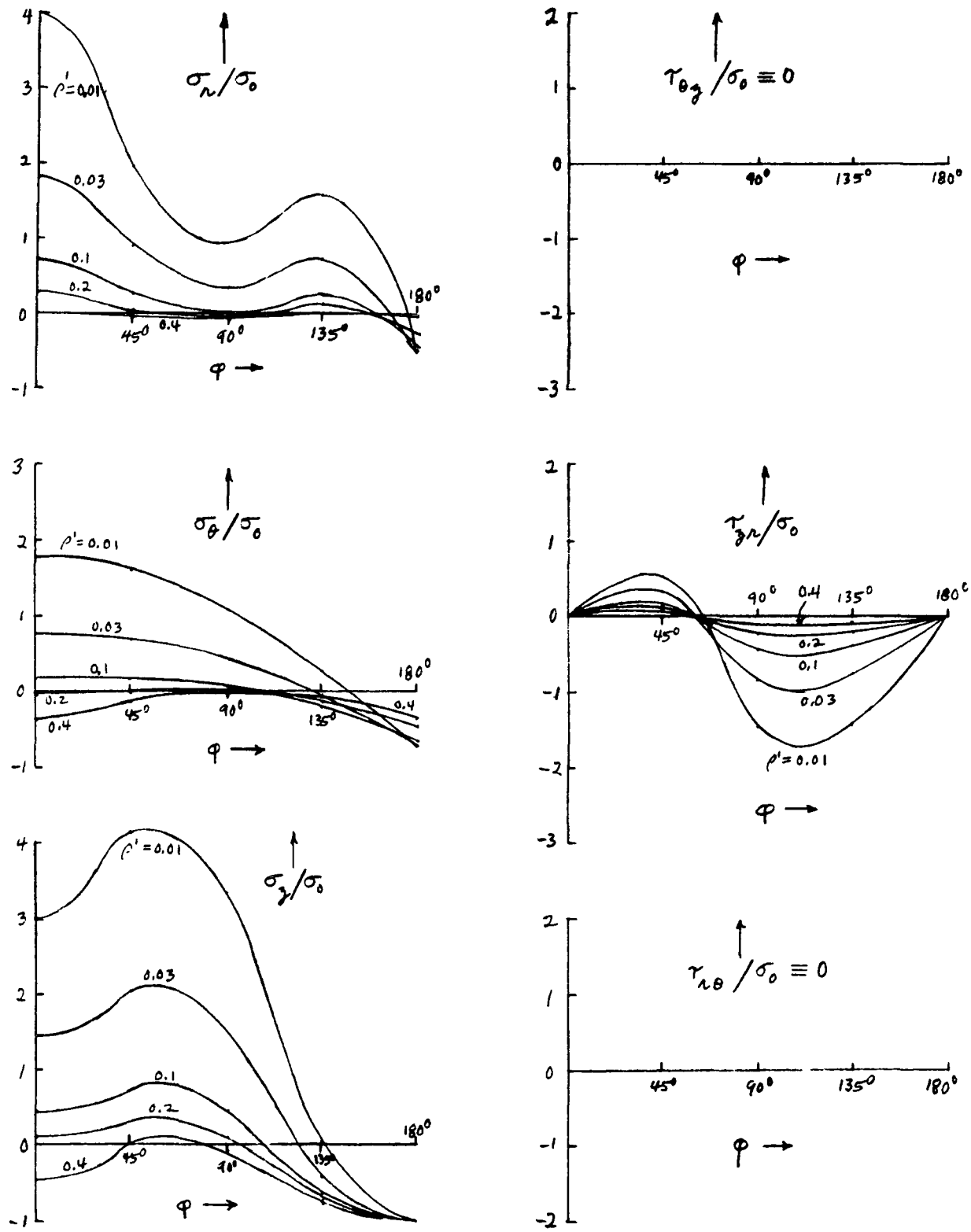

FIGURE C16. STRESSES WHERE θ = 0° NEAR CRACK WITH A/2C = 0.25, A/T = 0.5

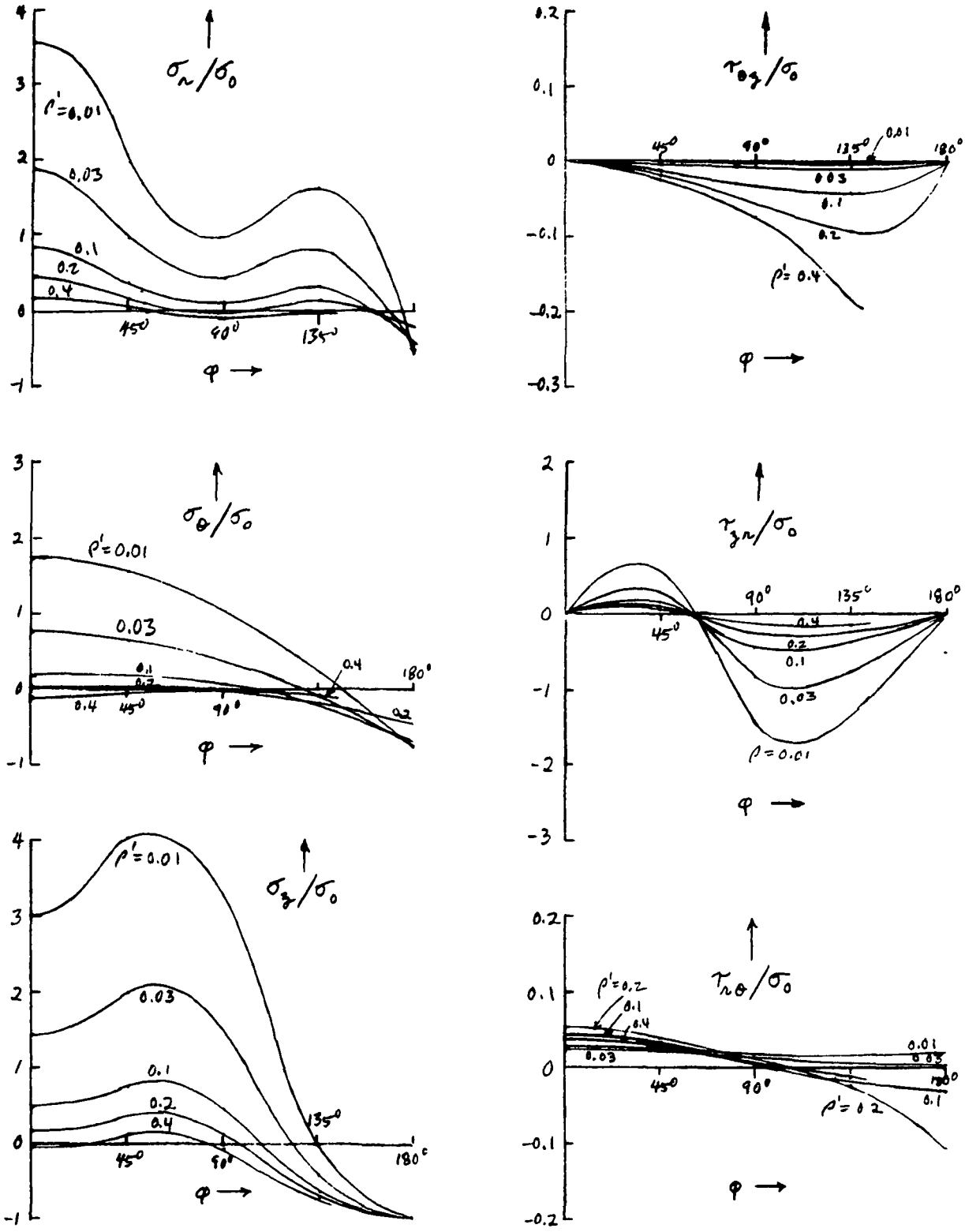

FIGURE C17. STRESSES WHERE θ = 30° NEAR CRACK WITH A/2C = 0.25, A/T = 0.5

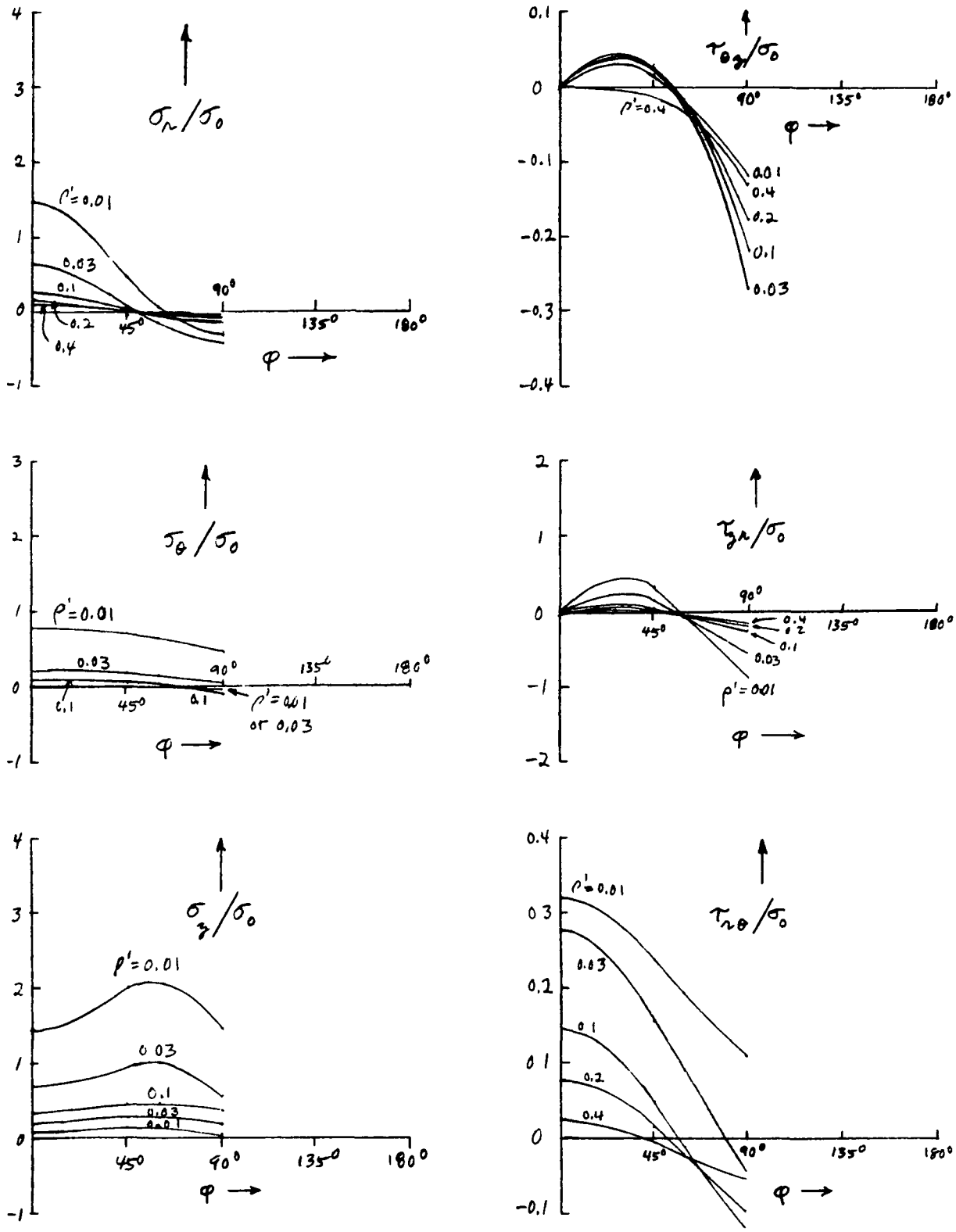

FIGURE C18. STRESSES WHERE $\theta = \theta_{tip}$ NEAR CRACK WITH A/2C = 0.25, A/T = 0.5

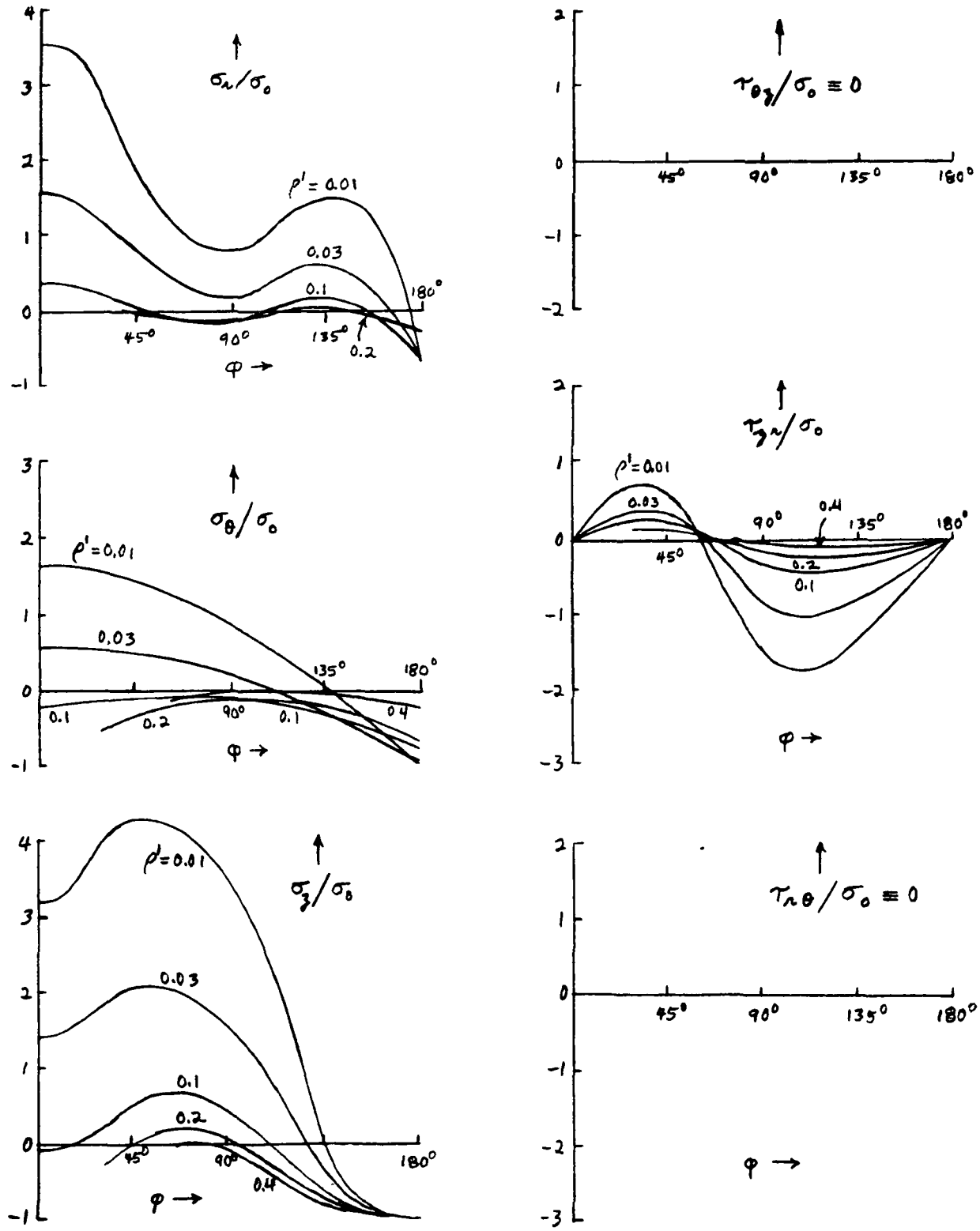

FIGURE C19. STRESSES WHERE θ = 0° NEAR CRACK WITH A/2C = 0.25, A/T = 0.7

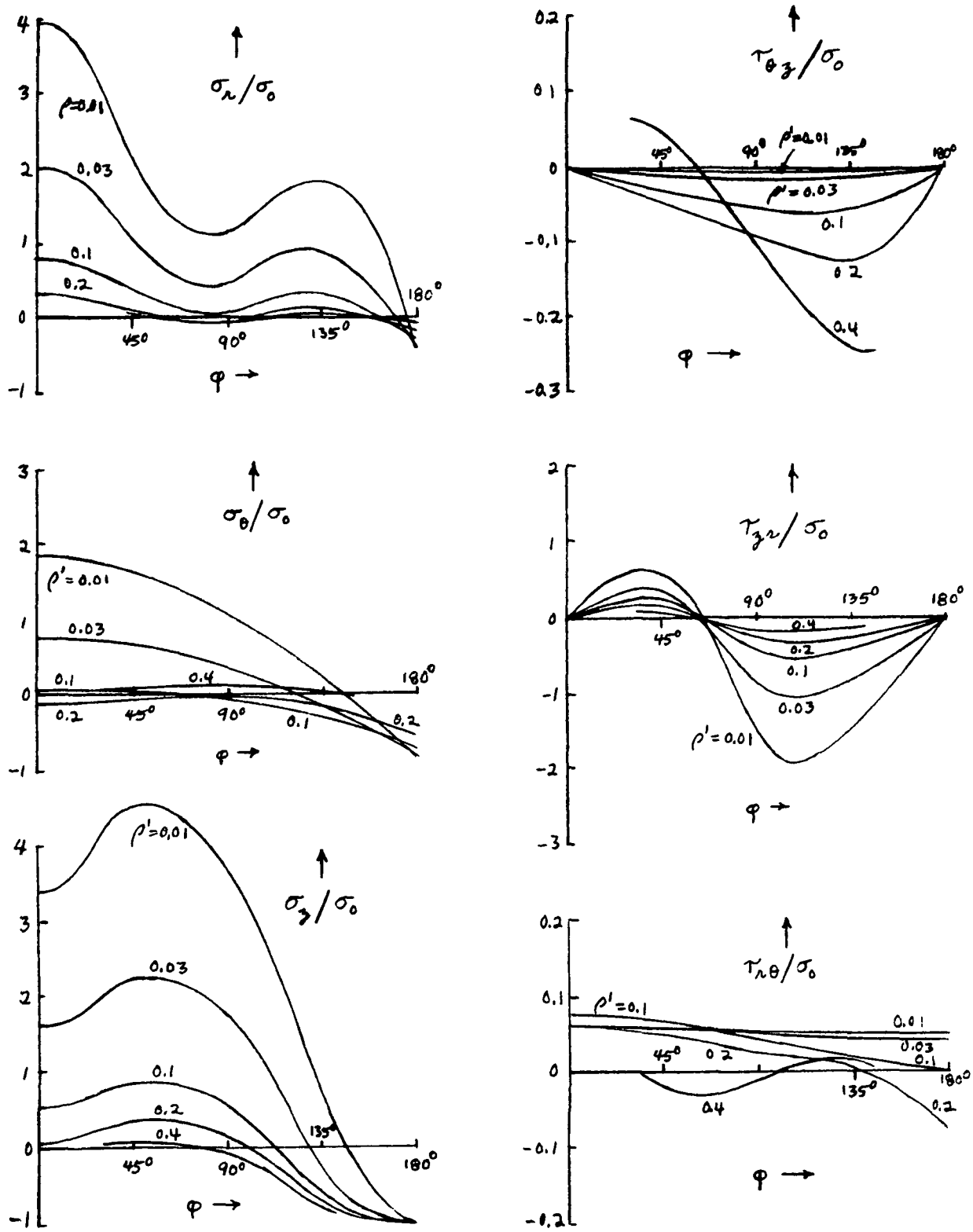

FIGURE C20. STRESSES WHERE θ = 30° NEAR CRACK WITH A/2C = 0.25, A/T = 0.7

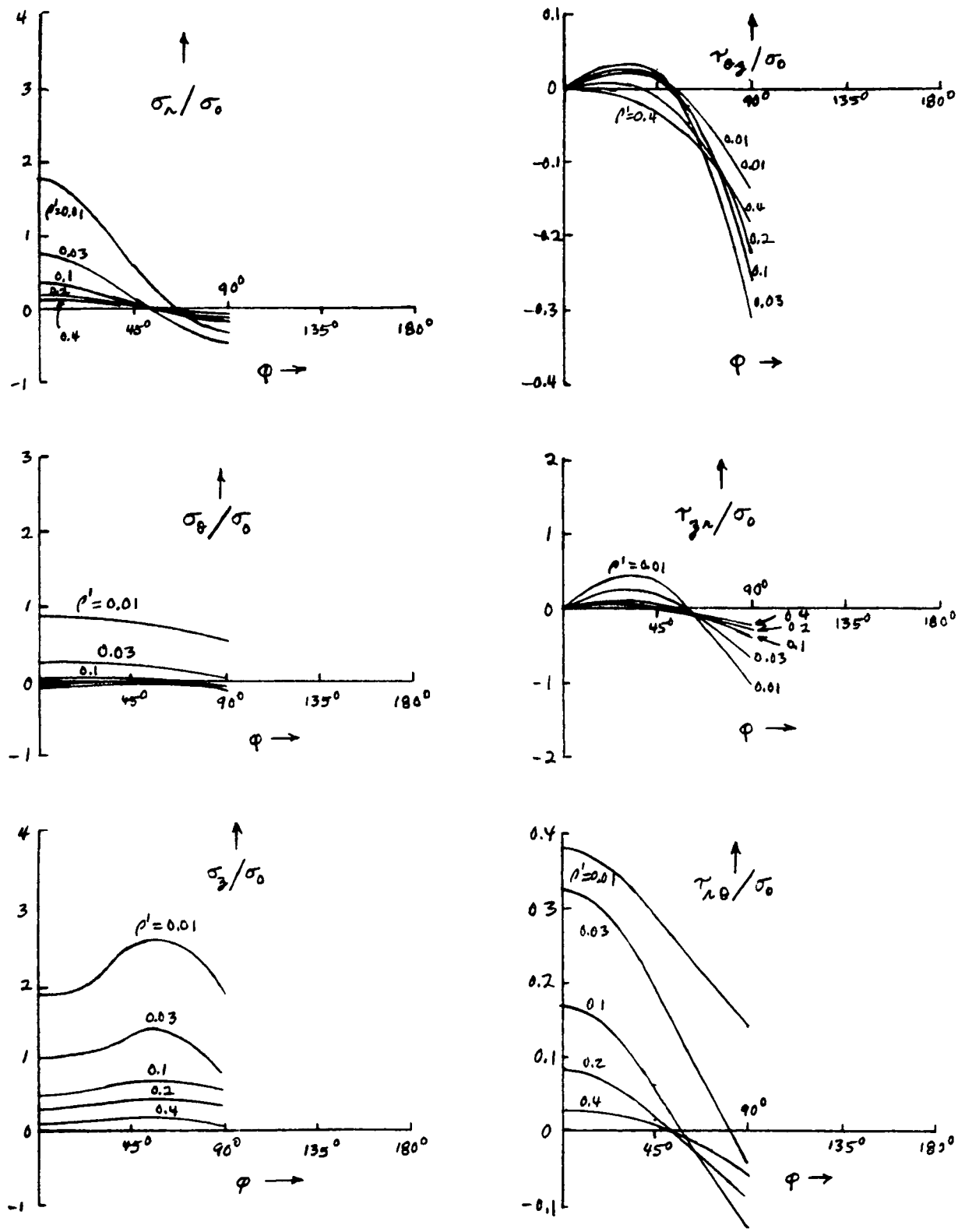

FIGURE C21. STRESSES WHERE $\theta = \theta_{tip}$ NEAR CRACK WITH A/2C = 0.25, A/T = 0.7

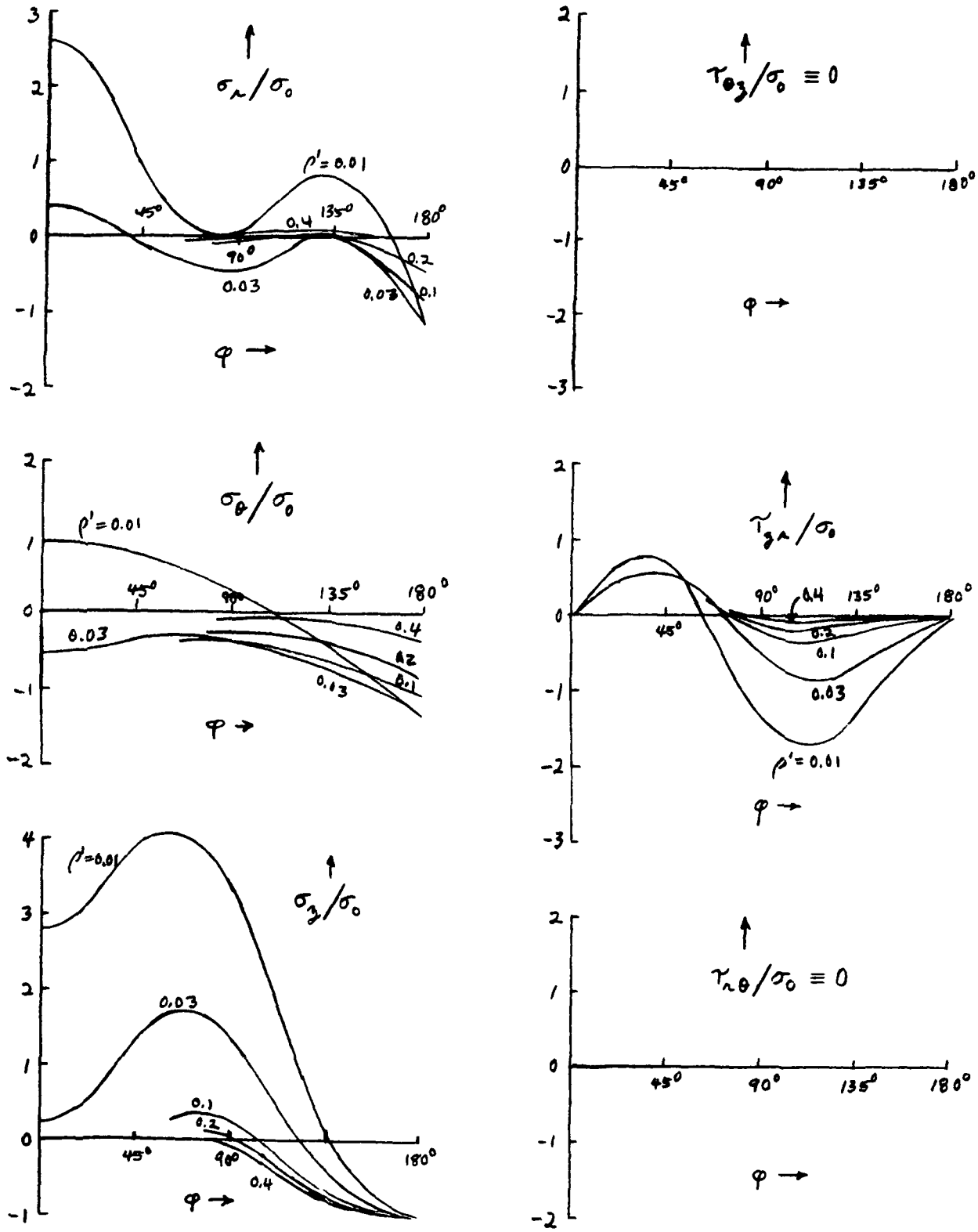

FIGURE C22. STRESSES WHERE θ = 0° NEAR CRACK WITH A/2C = 0.25, A/T = 0.9

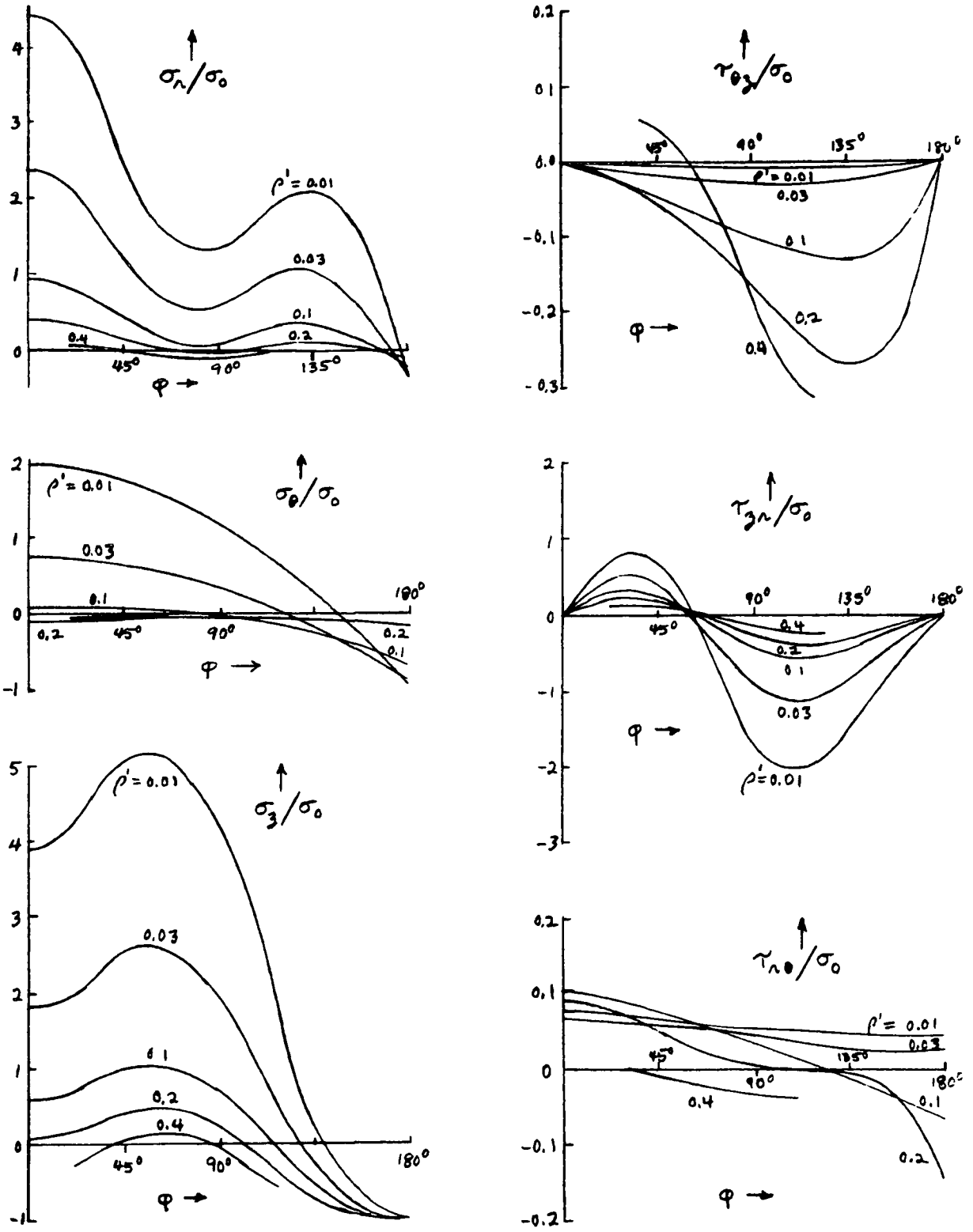

FIGURE C23. STRESSES WHERE θ = 40° NEAR CRACK WITH A/2C = 0.25, A/T = 0.9

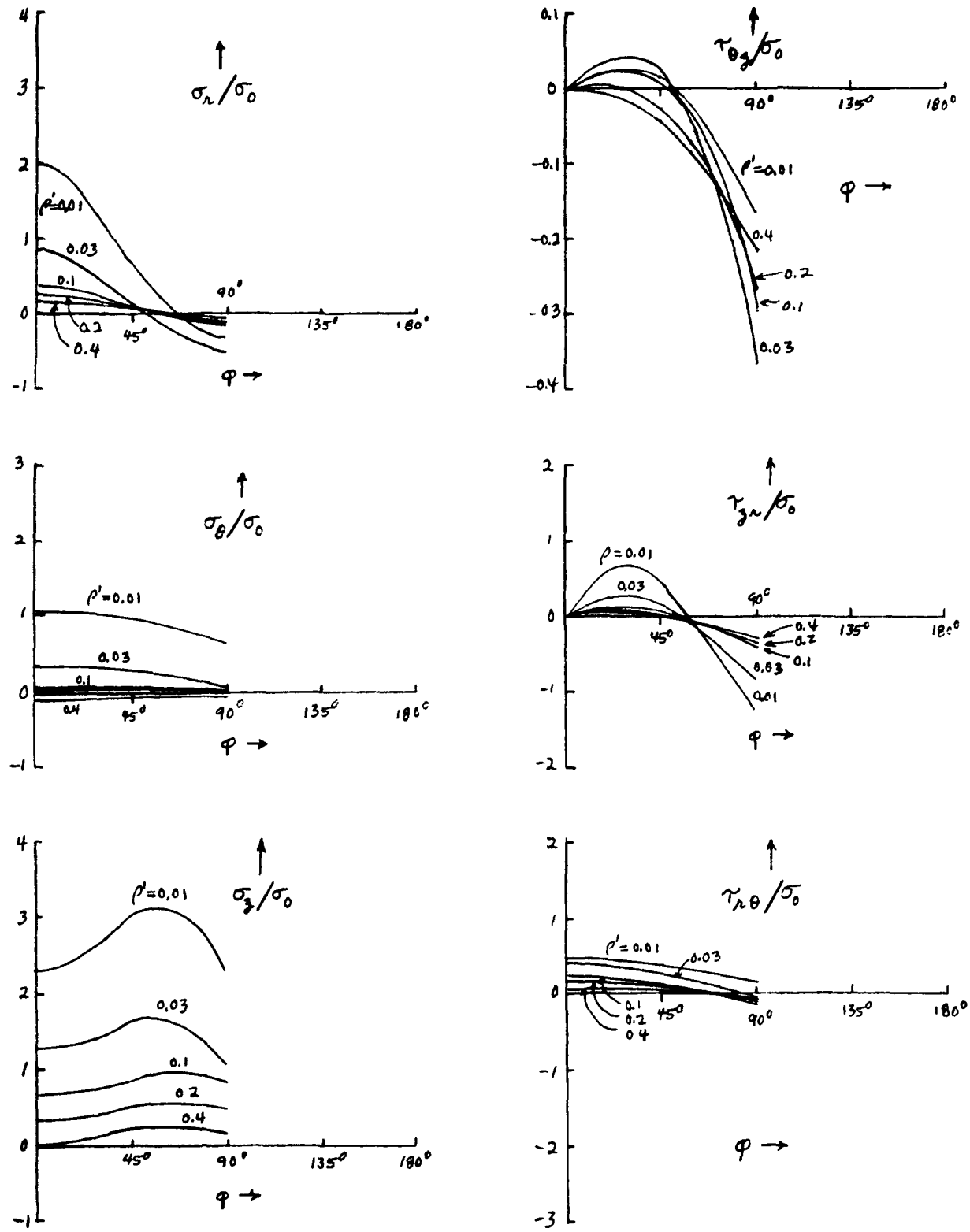

FIGURE C24. STRESSES WHERE $\theta = \theta_{tip}$ NEAR CRACK WITH A/2C = 0.25, A/T = 0.9

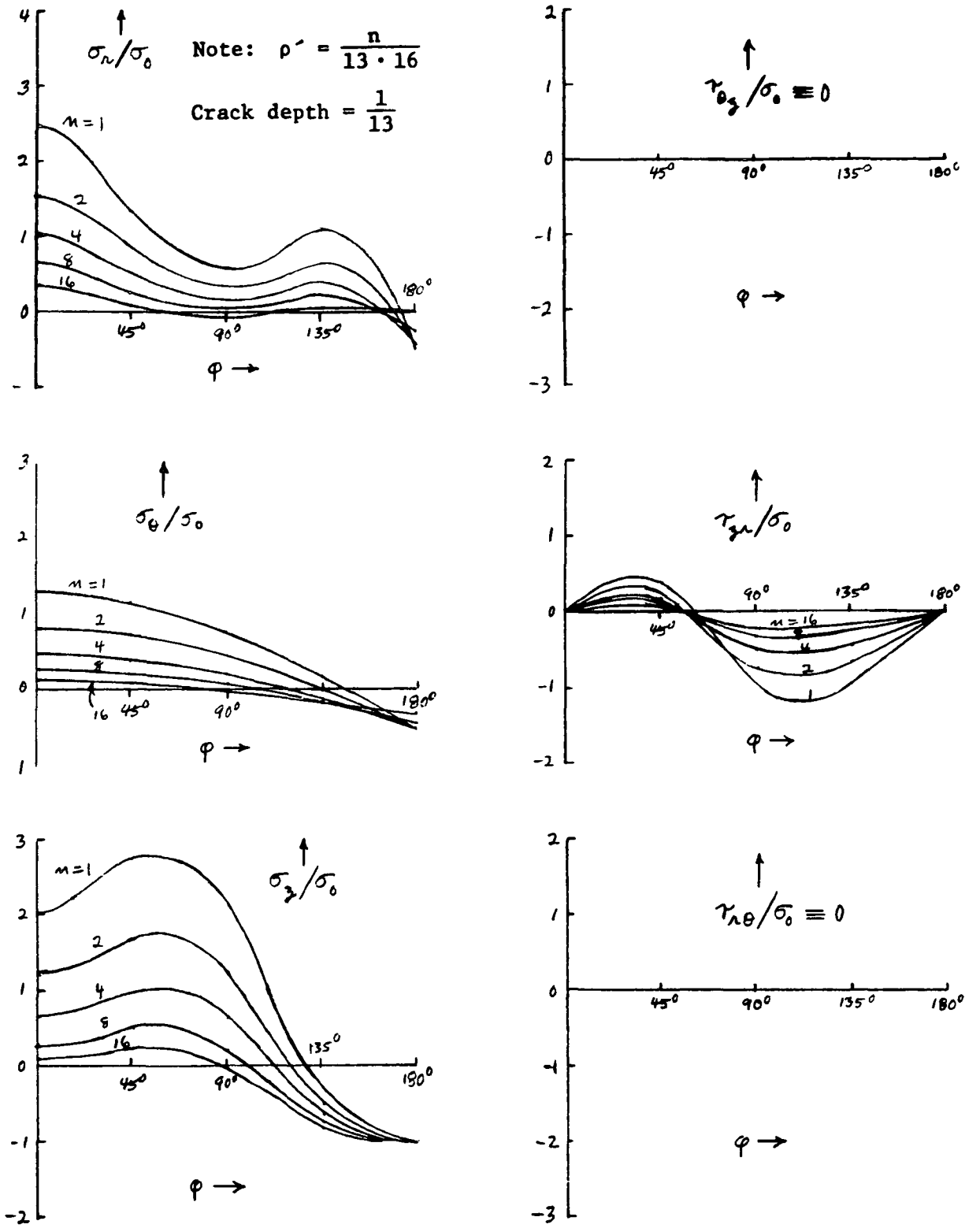

FIGURE C25. STRESSES WHERE θ = 0° NEAR CRACK WITH A/2C = 0.10, A/T = 0.0

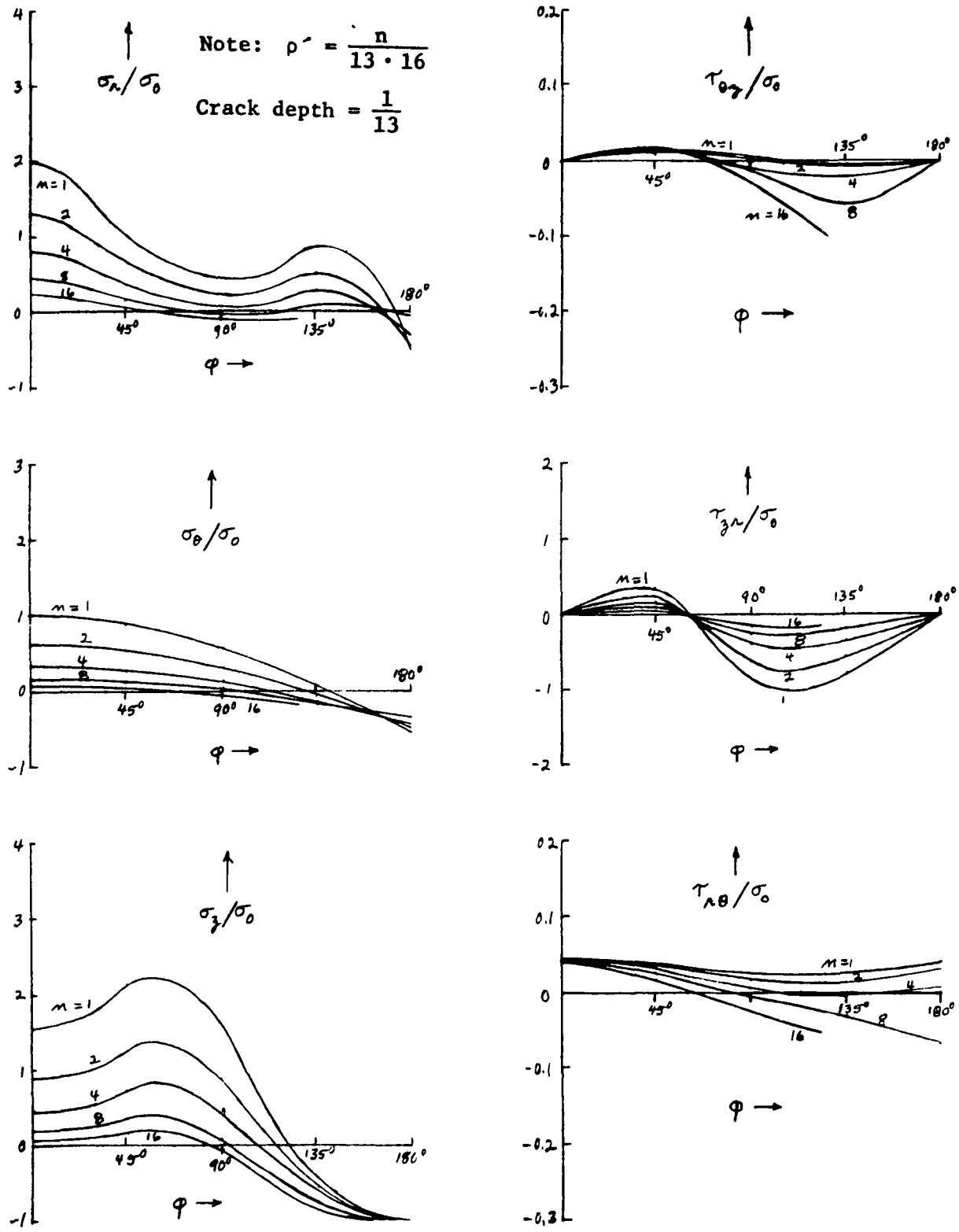

FIGURE C26. STRESSES WHERE θ = 15° NEAR CRACK WITH A/2C = 0.10, A/T = 0.0

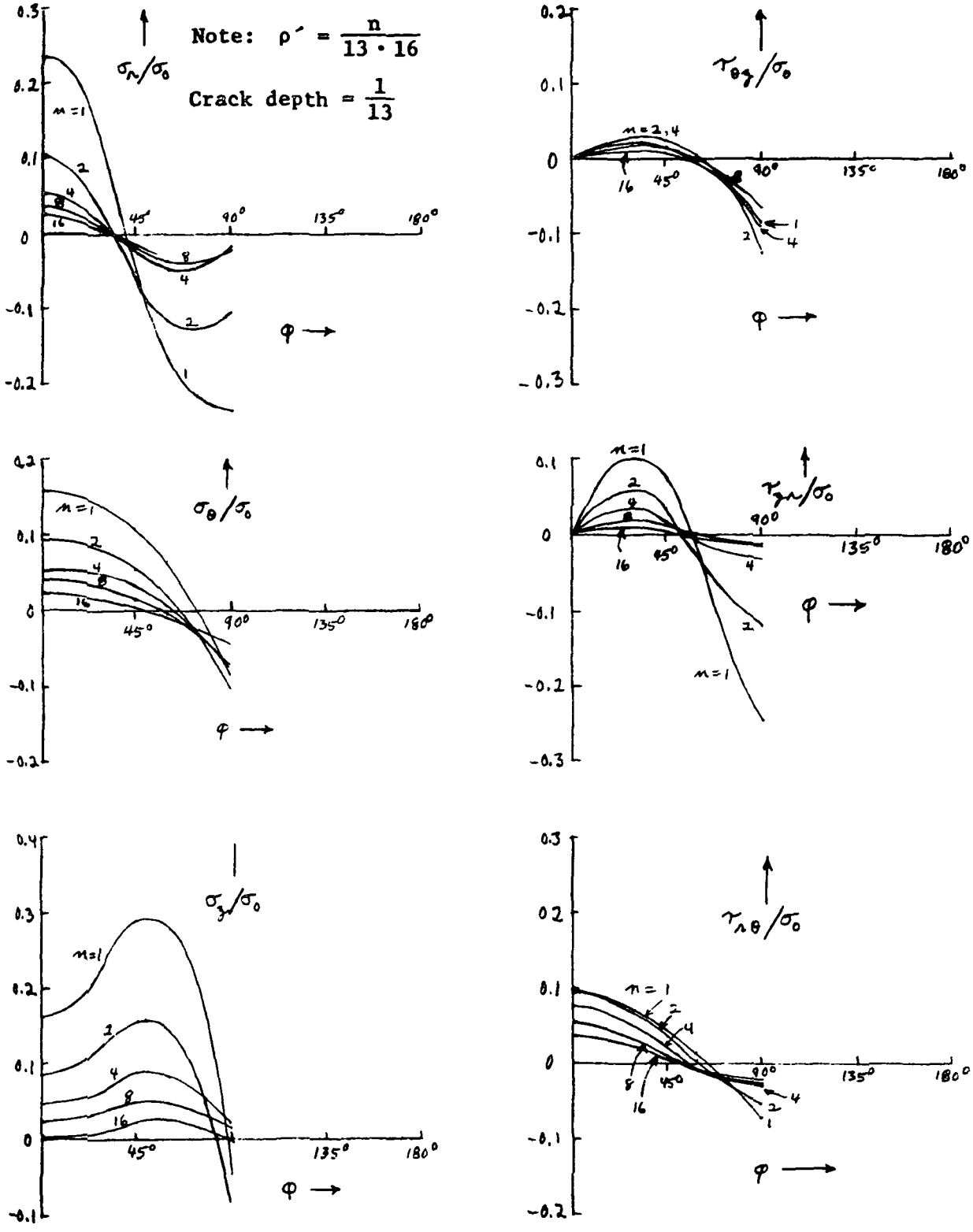

FIGURE C27. STRESSES WHERE $\theta = \theta_{tip}$ NEAR CRACK WITH A/2C = 0.10, A/T = 0.0

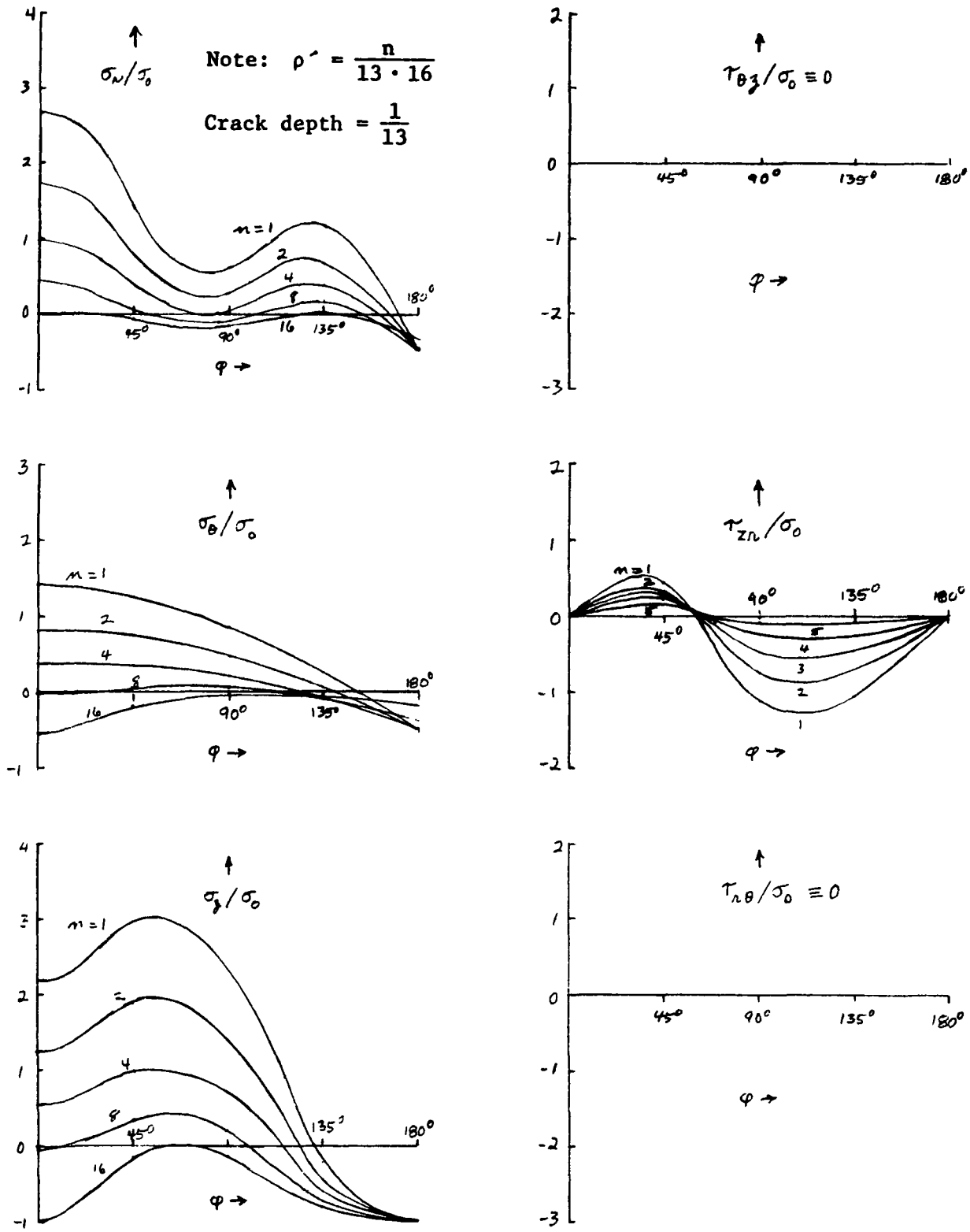

FIGURE C28. STRESSES WHERE θ = 0° NEAR CRACK WITH A/2C = 0.10, A/T = 0.5

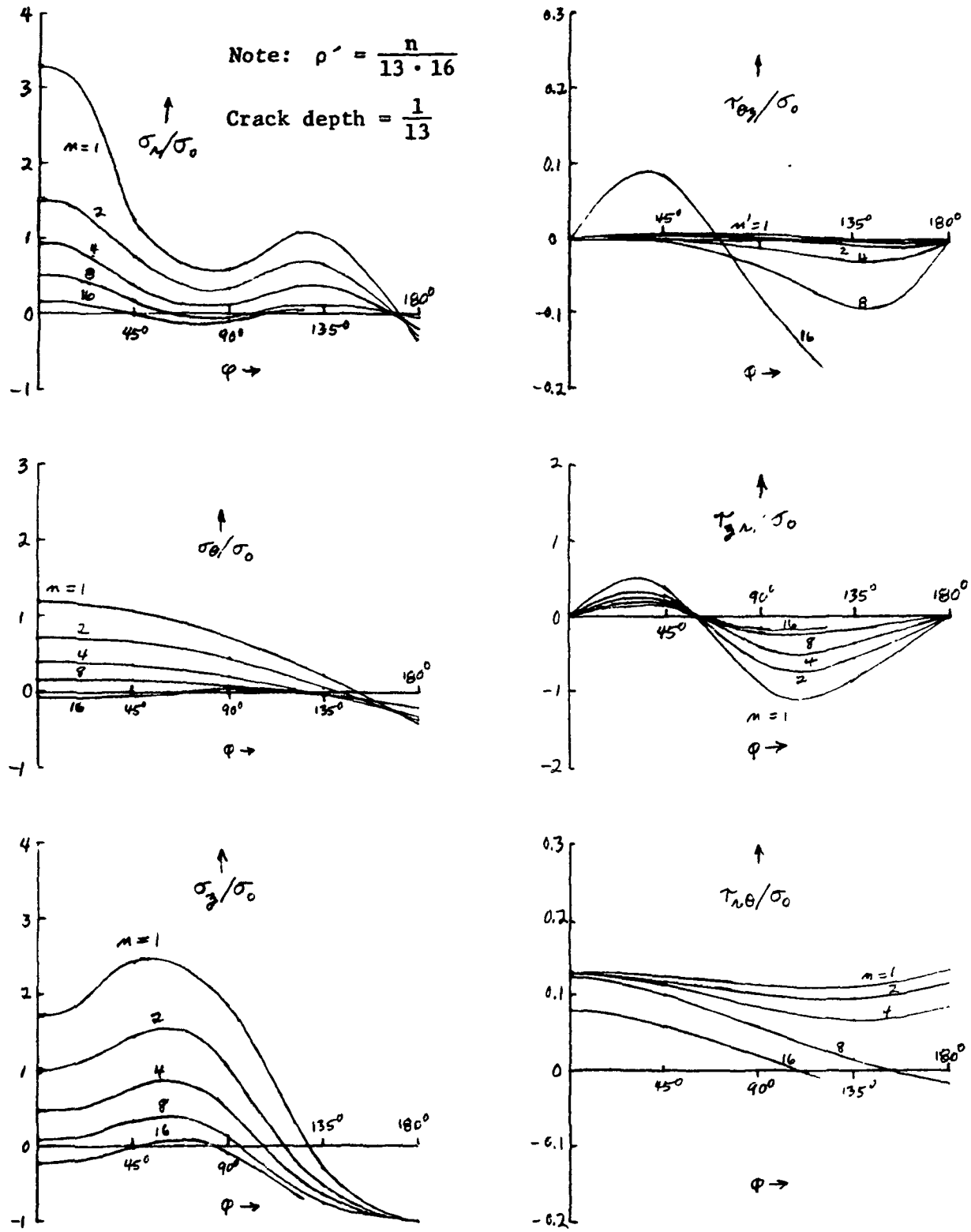

FIGURE C29. STRESSES WHERE θ = 15° NEAR CRACK WITH A/2C = 0.10, A/T = 0.5

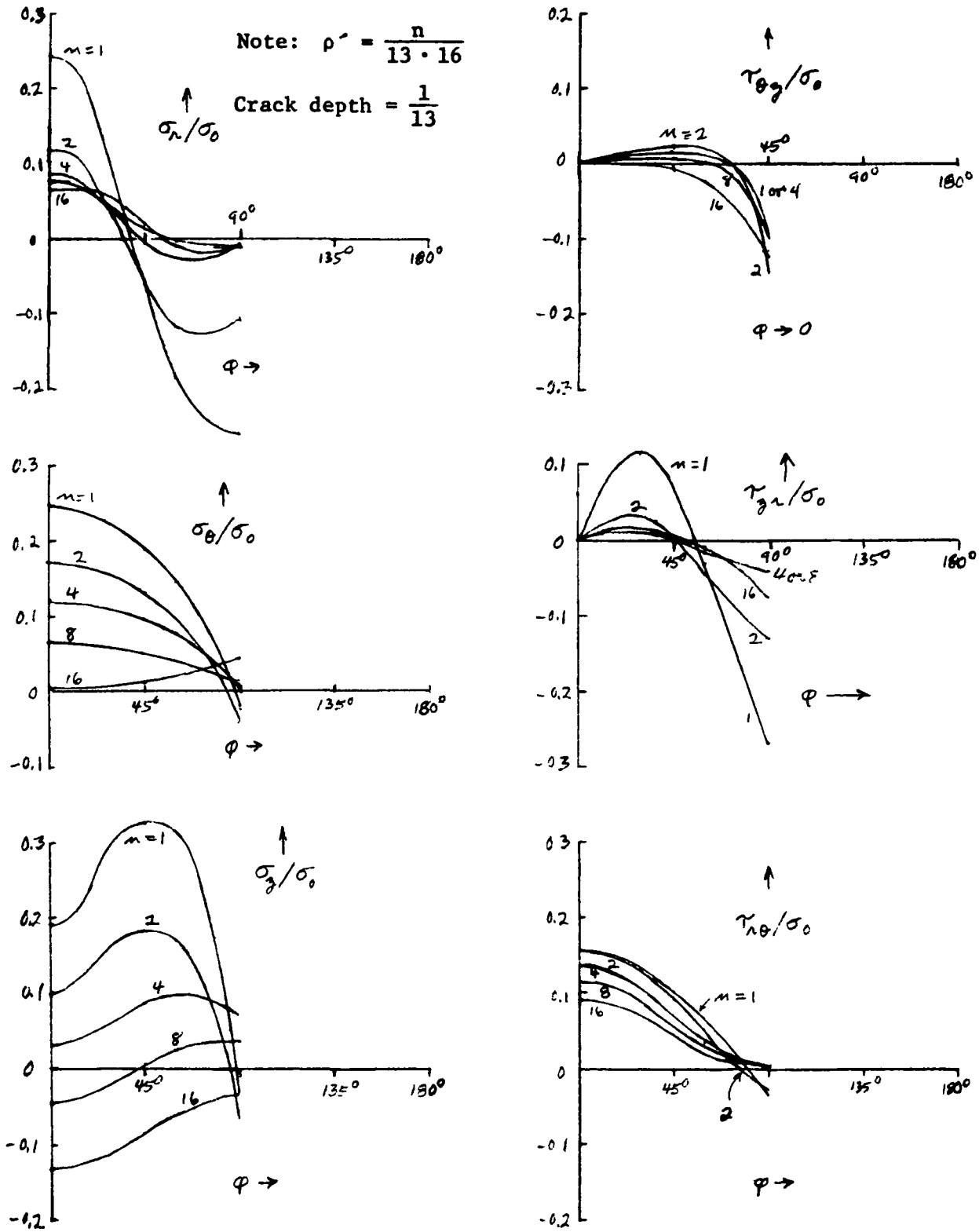

FIGURE C30. STRESSES WHERE $\theta = \theta_{tip}$ NEAR CRACK WITH A/2C = 0.10, A/T = 0.5

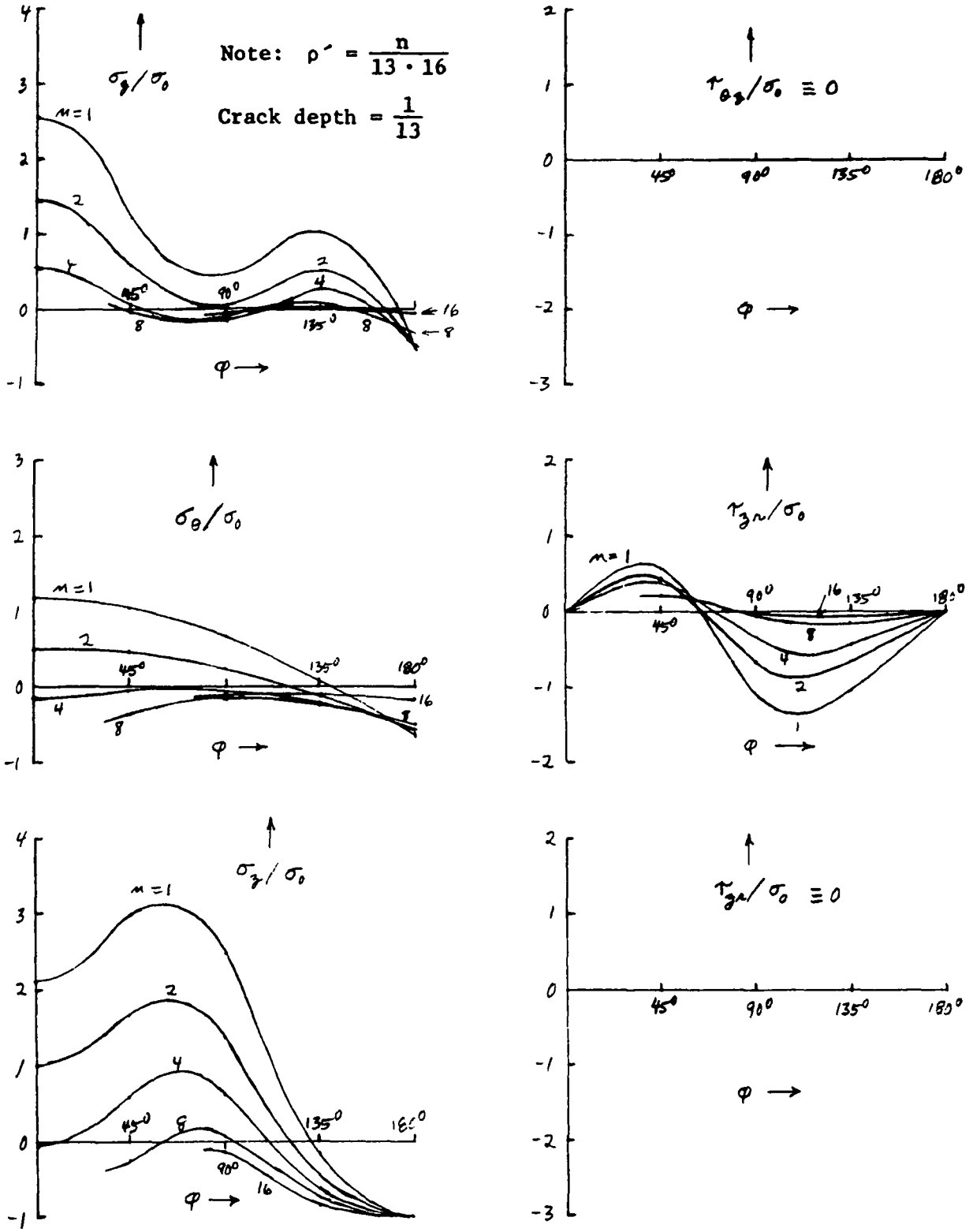

FIGURE C31. STRESSES WHERE θ = 0° NEAR CRACK WITH A/2C = 0.10, A/T = 0.7

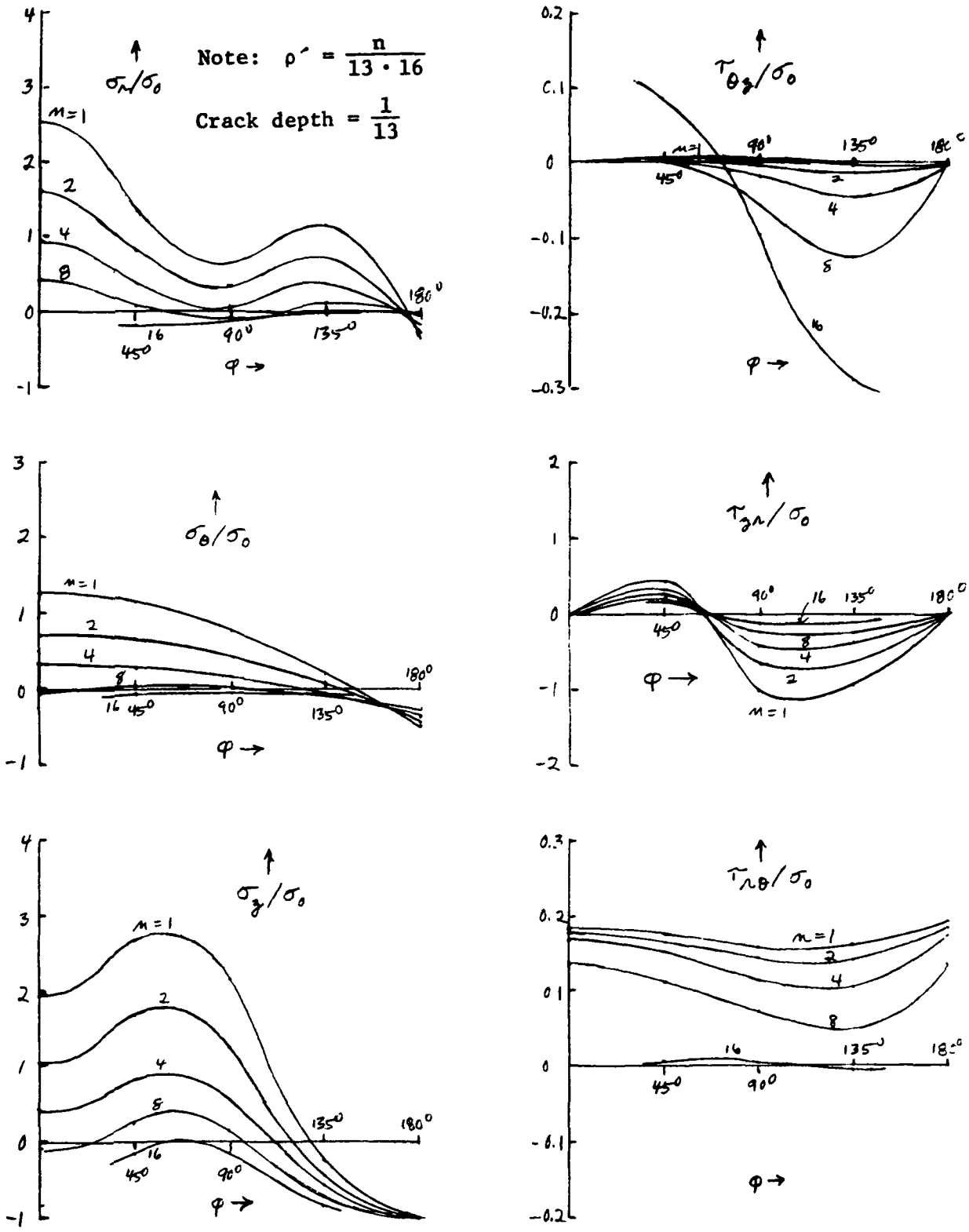

FIGURE C32. STRESSES WHERE θ = 15° NEAR CRACK WITH A/2C = 0.10, A/T = 0.7

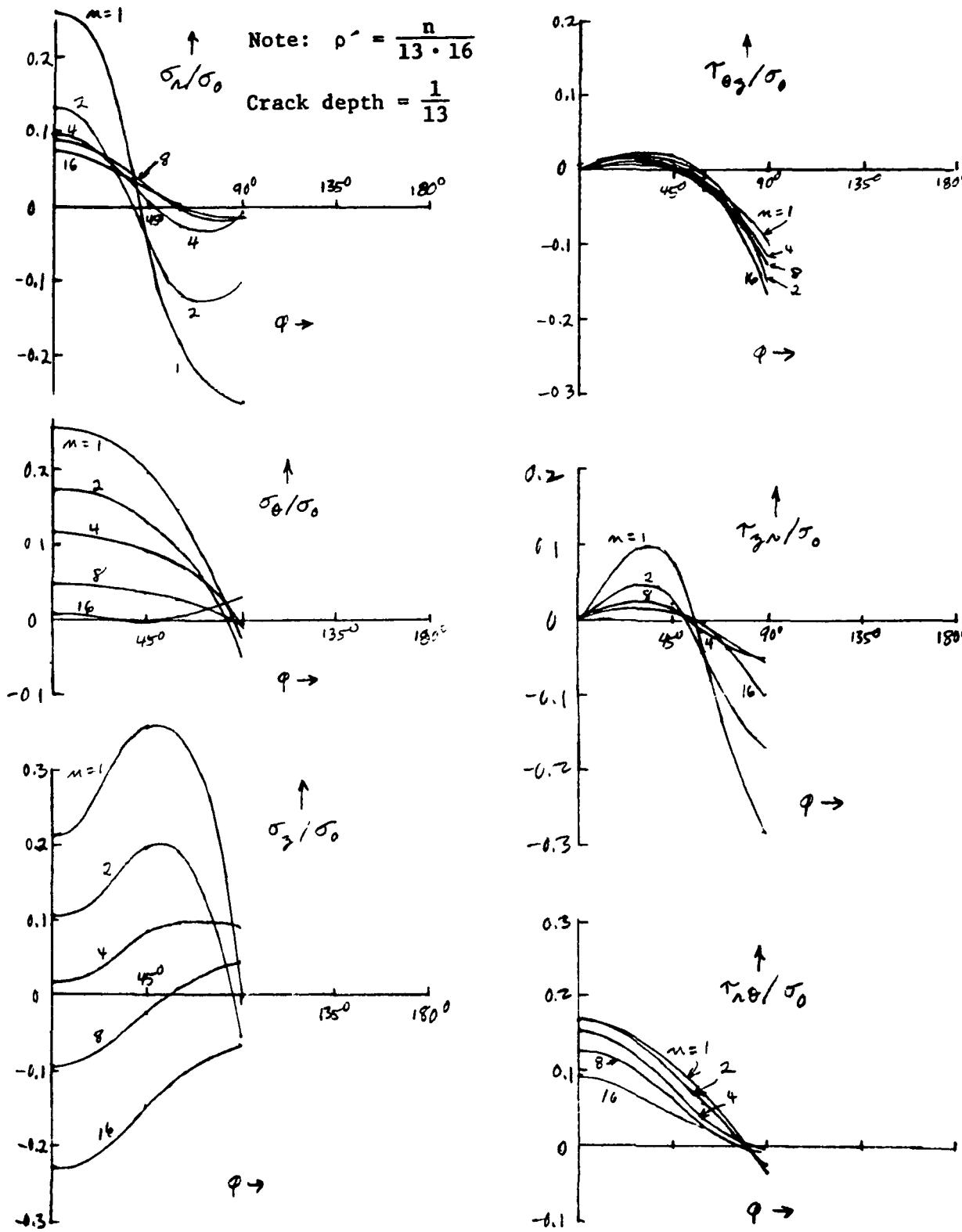

FIGURE C33. STRESSES WHERE $\theta = \theta_{tip}$ NEAR CRACK WITH A/2C = 0.10, A/T = 0.7

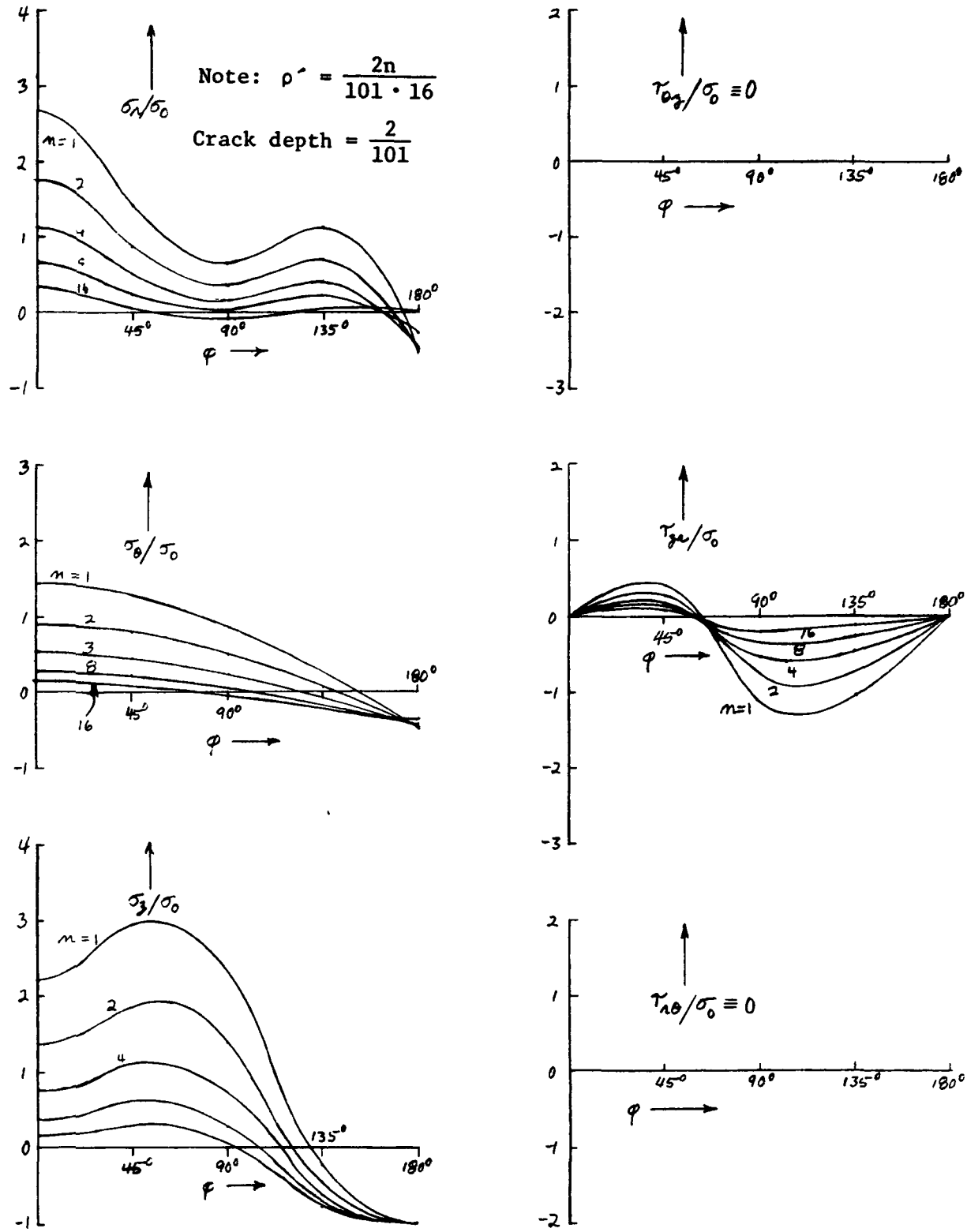

FIGURE C34. STRESSES WHERE θ = 0° NEAR CRACK WITH A/2C = 0.05, A/T = 0.0

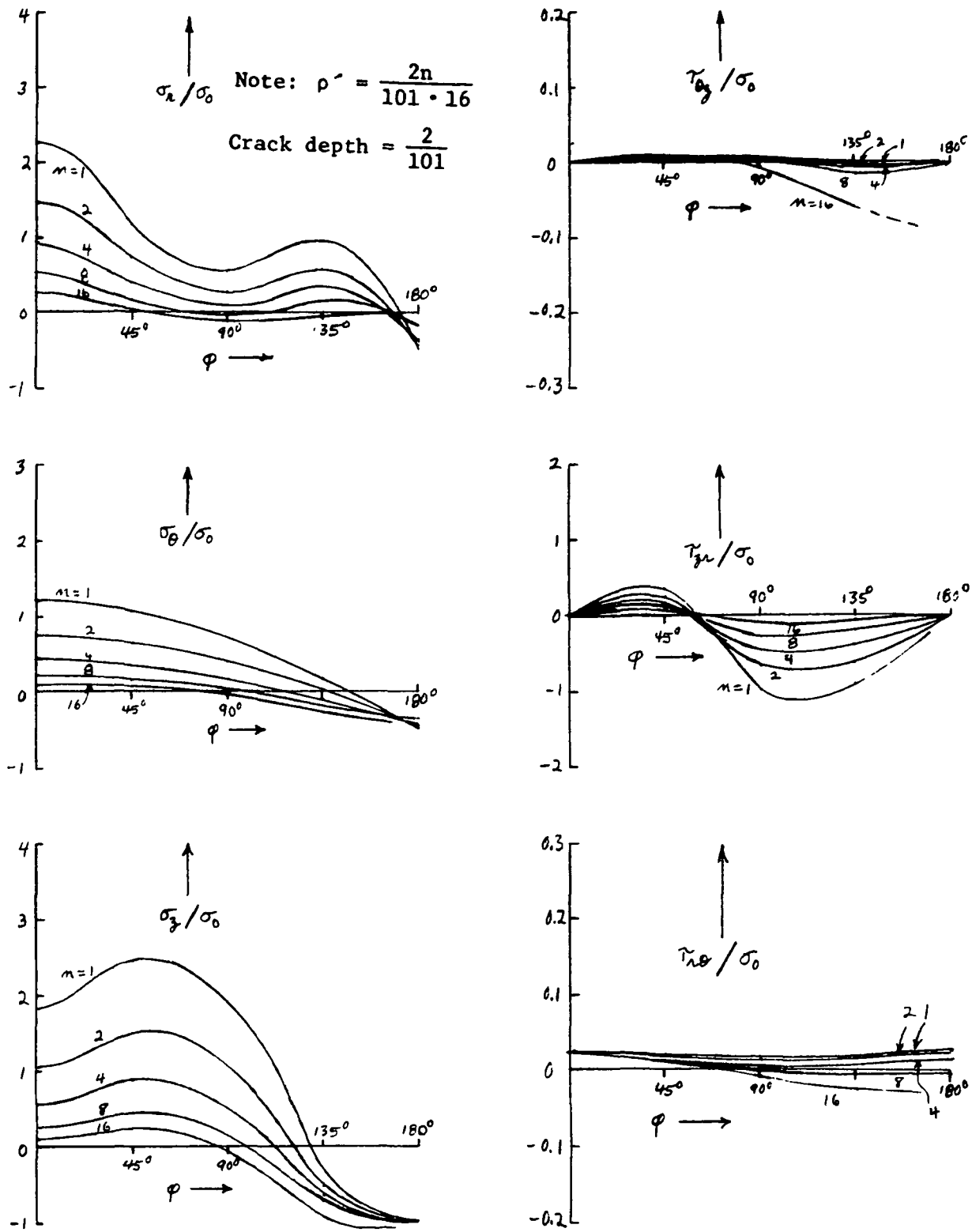

FIGURE C35. STRESSES WHERE θ = 6° NEAR CRACK WITH A/2C = 0.05, A/T = 0.0

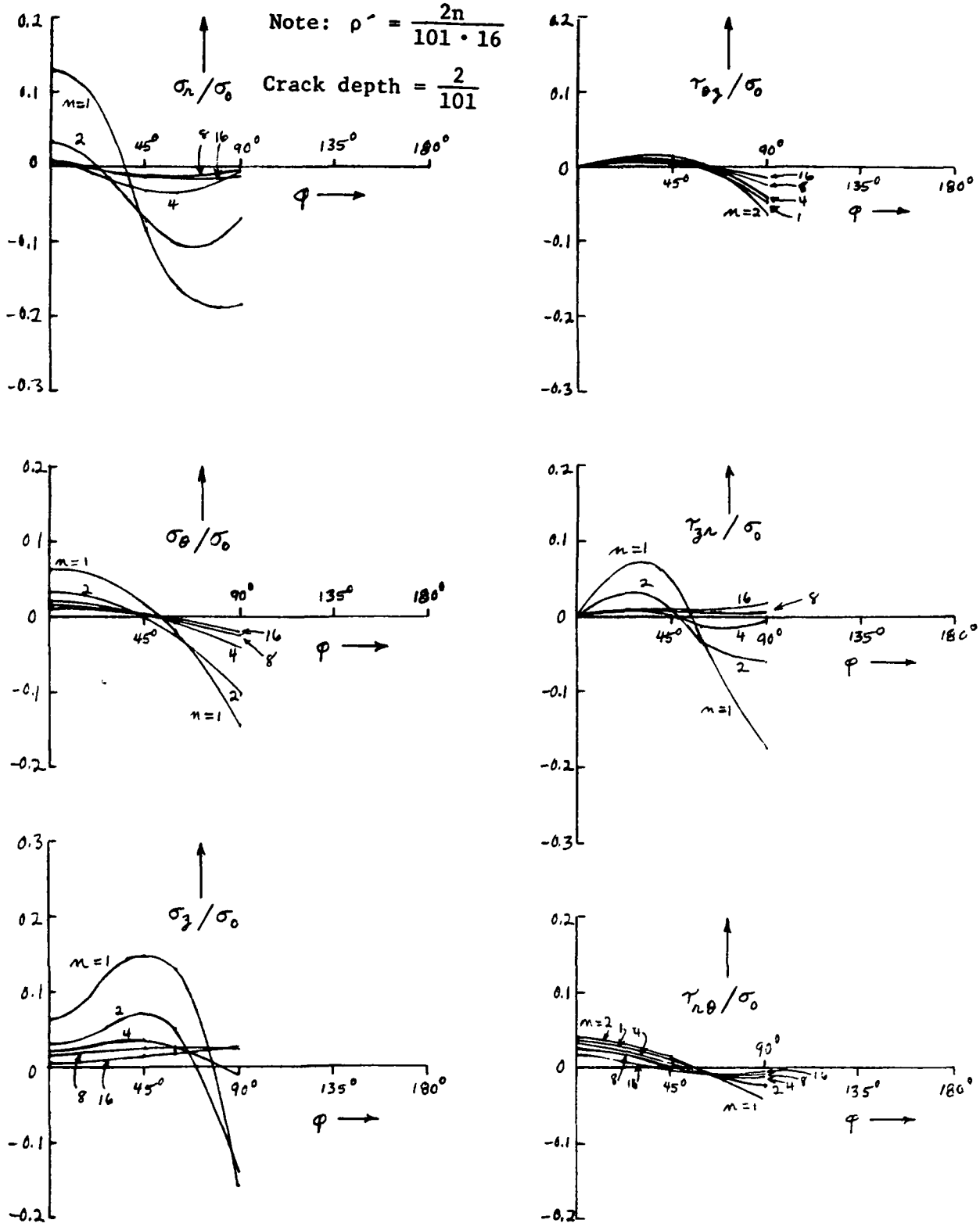

FIGURE C36. STRESSES WHERE $\theta = \theta_{tip}$ NEAR CRACK WITH A/2C = 0.05, A/T = 0.0

APPENDIX D

CRACK OPENING DISPLACEMENTS FOR CRACKS UNDER NORMAL AND OBLIQUE LOADS

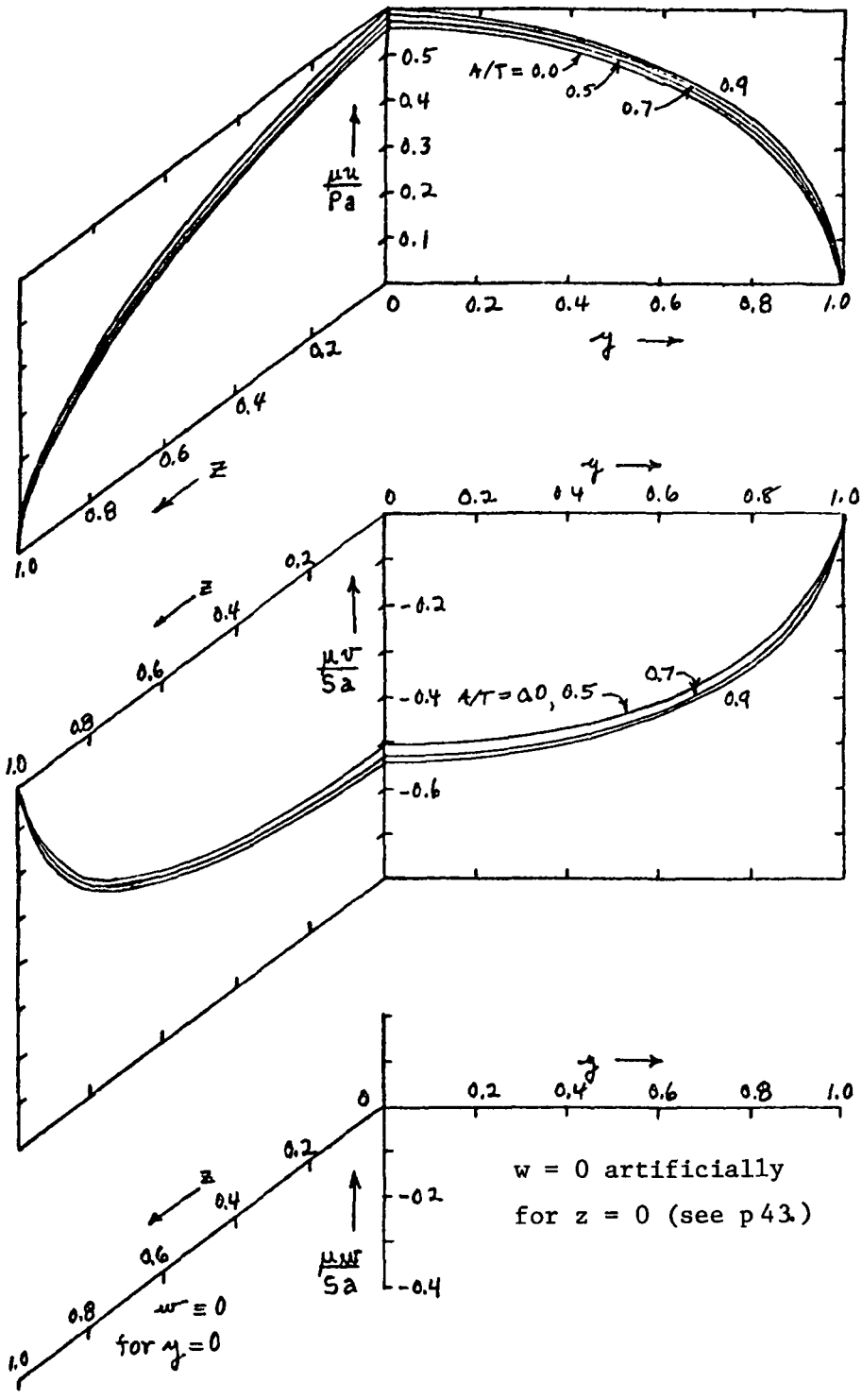

FIGURE D1. CRACK OPENING DISPLACEMENTS FOR SURFACE CRACKS WITH A/2C = 0.50 UNDER NORMAL OR LATERAL SHEAR LOADS

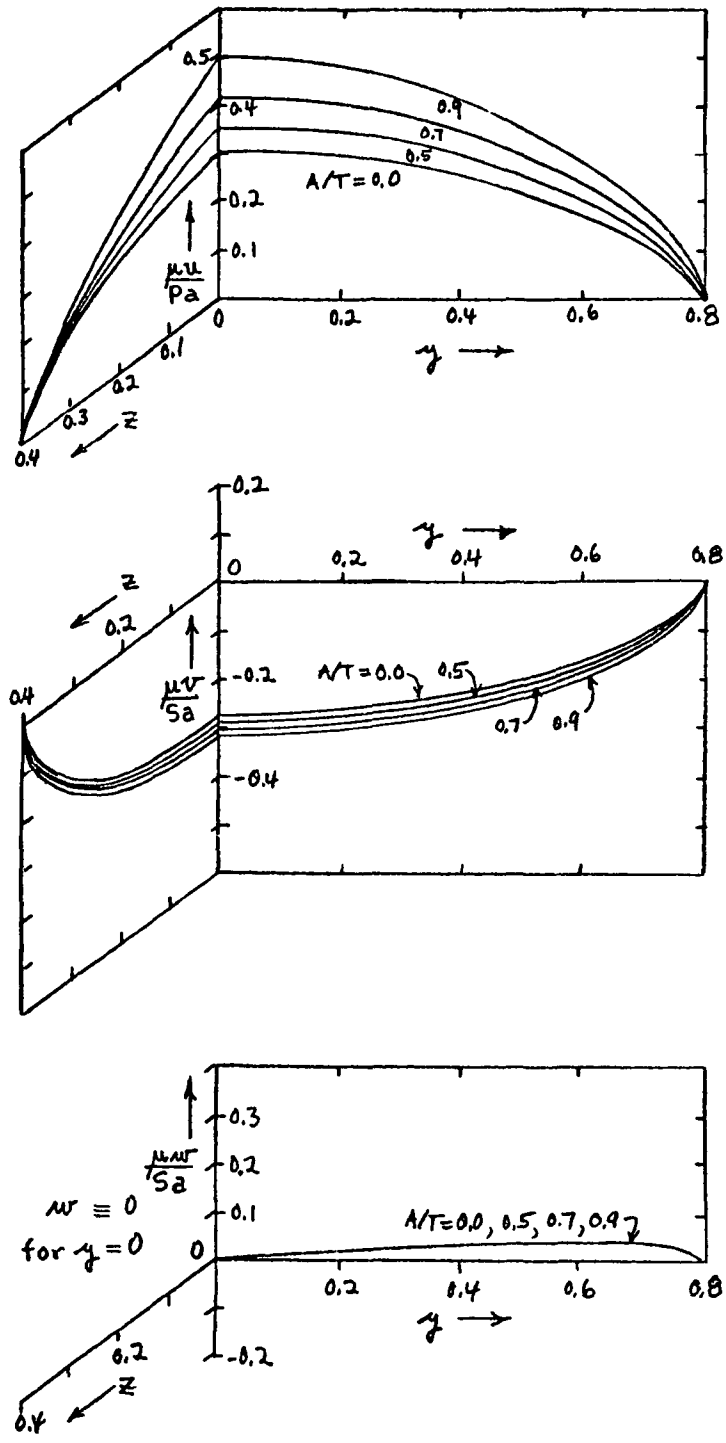

FIGURE D2. CRACK OPENING DISPLACEMENTS FOR SURFACE CRACKS WITH A/2C = 0.25 UNDER NORMAL OR LATERAL SHEAR LOADS

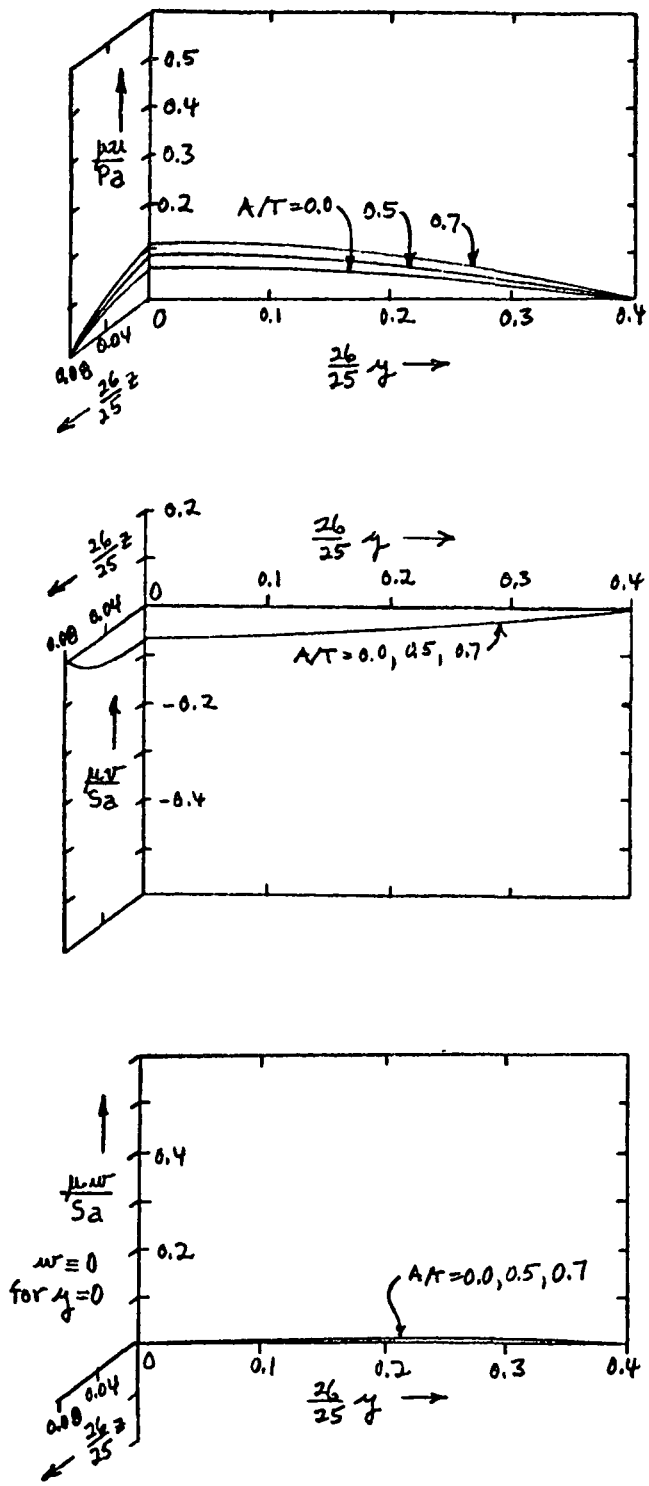

FIGURE D3. CRACK OPENING DISPLACEMENTS FOR SURFACE CRACKS WITH A/2C = 0.10 UNDER NORMAL OR LATERAL SHEAR LOAD

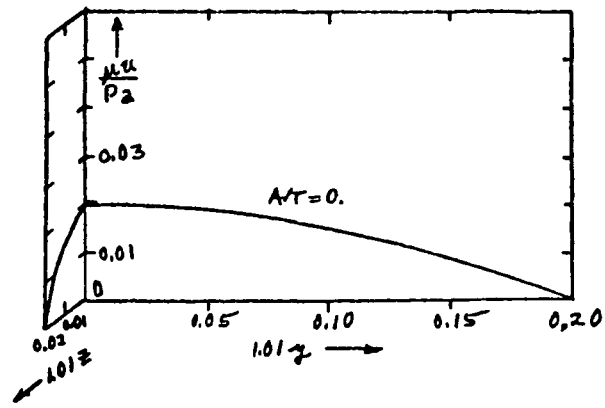

FIGURE D4. CRACK OPENING DISPLACEMENTS FOR A SURFACE CRACK WITH A/2C = 0.10, A/T = 0.0 UNDER NORMAL LOAD

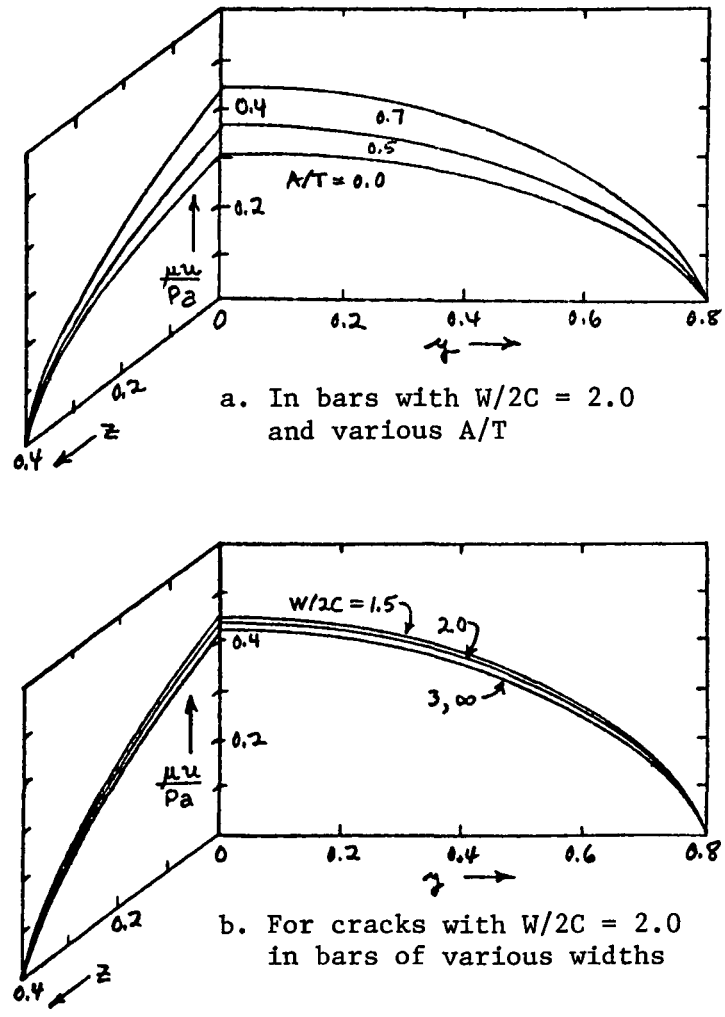

a. In bars with W/2C = 2.0 and various A/T

b. For cracks with W/2C = 2.0 in bars of various widths

FIGURE D5. CRACK OPENING DISPLACEMENTS IN BARS WITH PART-CIRCULAR SURFACE CRACKS (A/2C = 0.25) UNDER NORMAL LOAD

APPENDIX E

STRESS INTENSITY FACTORS FOR SURFACE CRACKS UNDER OBLIQUE LOADS

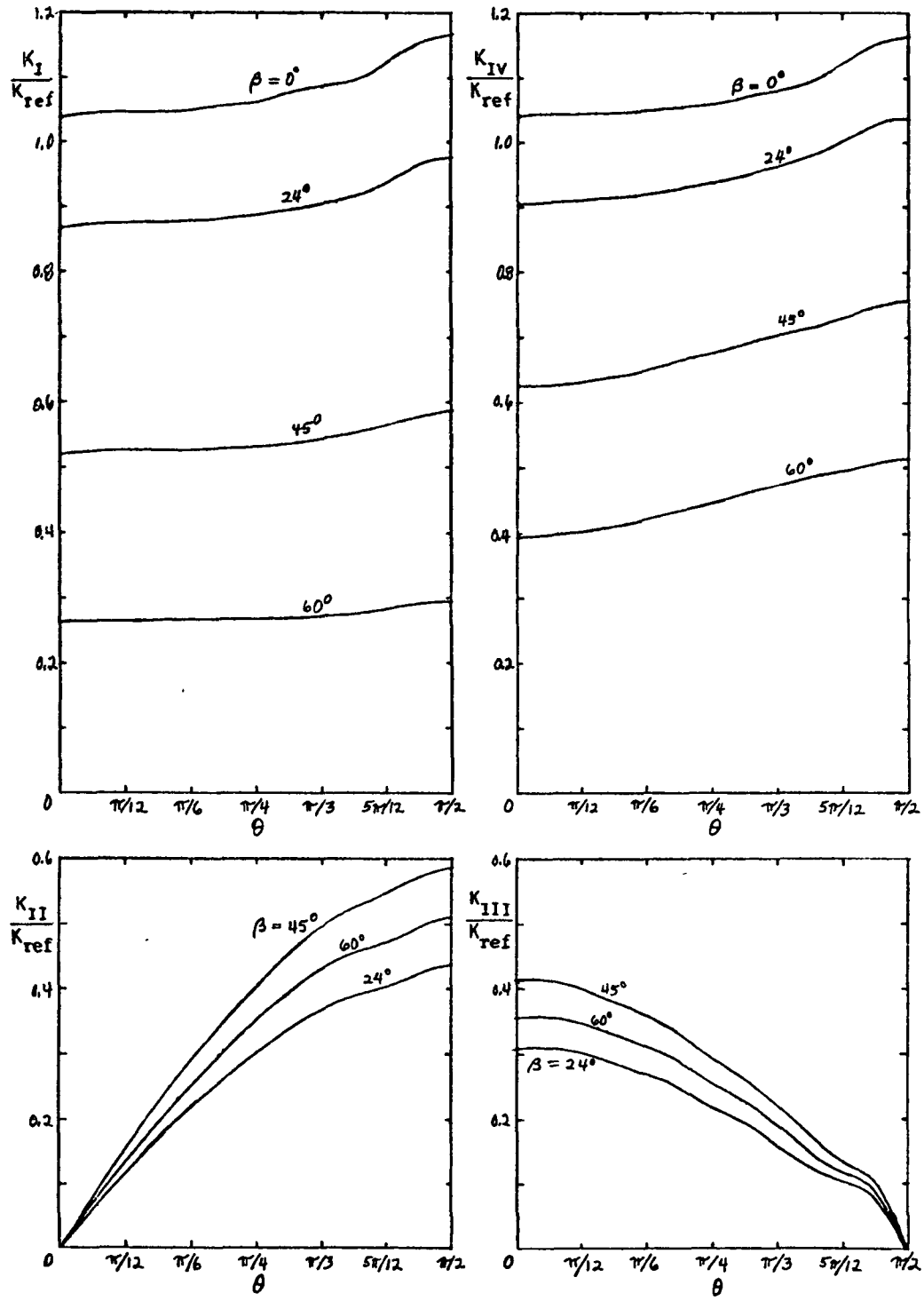

FIGURE E1. STRESS INTENSITY FACTORS ALONG A CRACK WITH A/2C = 0.50, A/T = 0.0 UNDER OBLIQUE LOADS

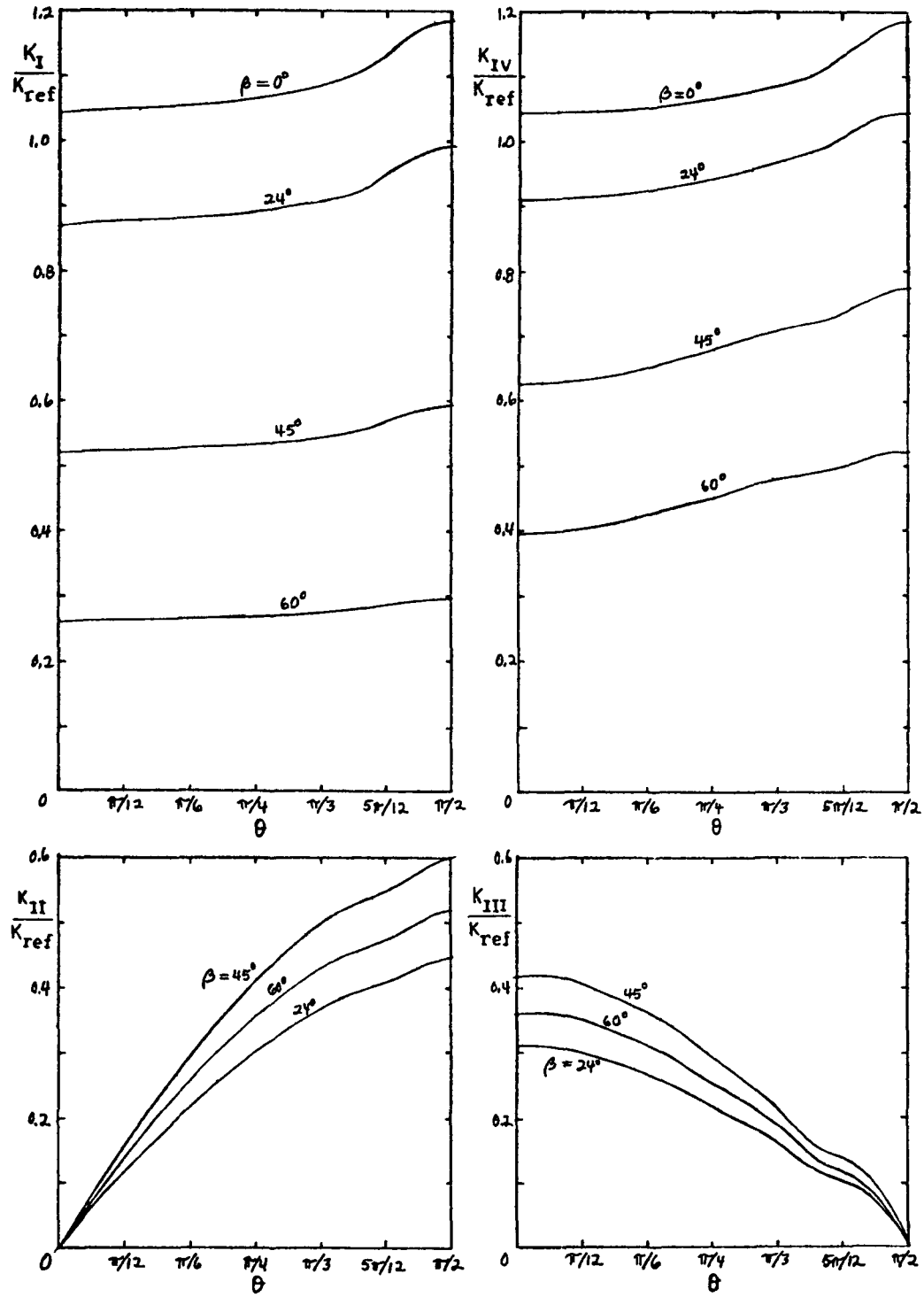

FIGURE E2. STRESS INTENSITY FACTORS ALONG A CRACK WITH A/2C = 0.50, A/T = 0.5 UNDER OBLIQUE LOADS

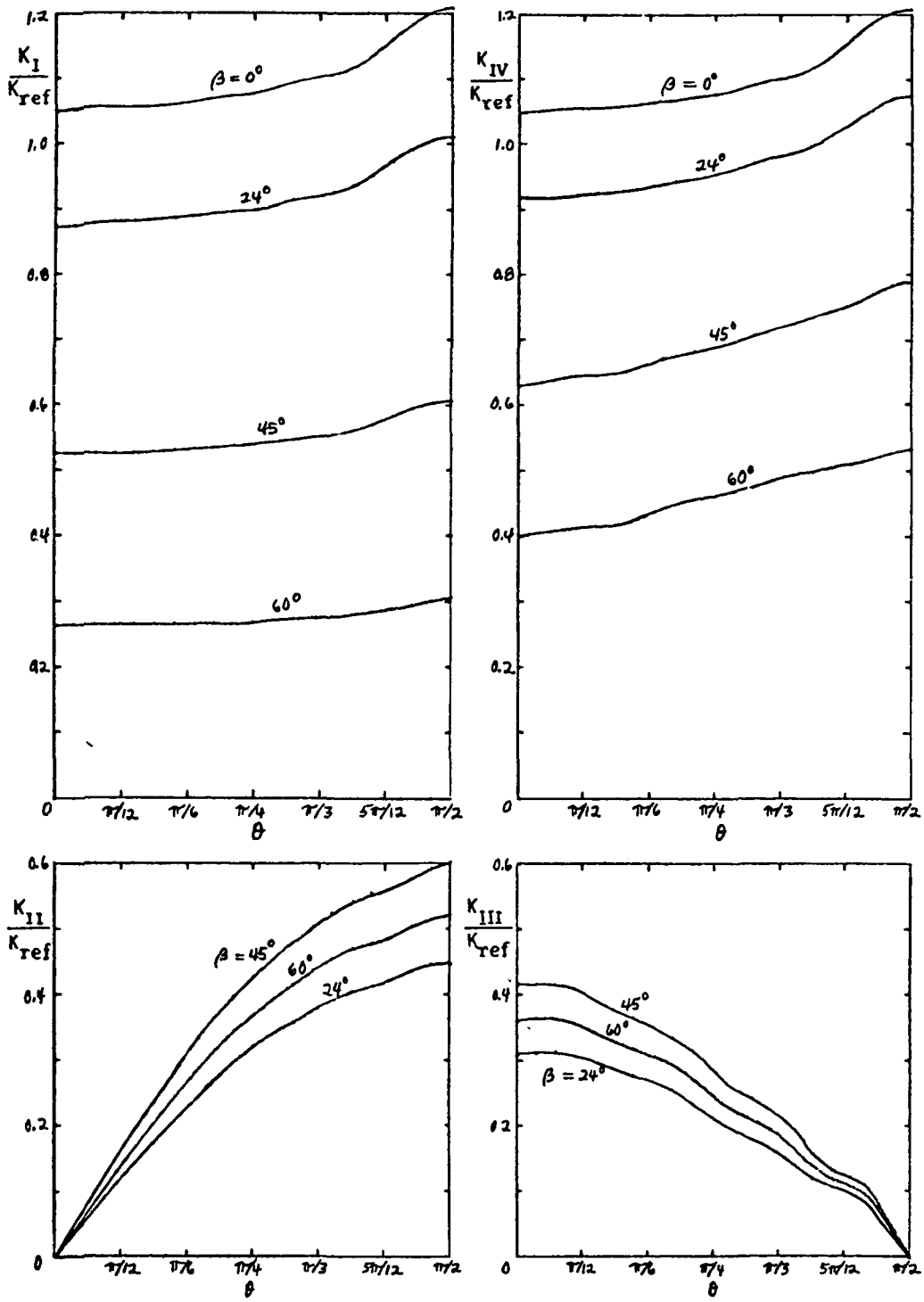

FIGURE E3. STRESS INTENSITY FACTORS ALONG A CRACK WITH A/2C = 0.50, A/T = 0.7 UNDER OBLIQUE LOADS

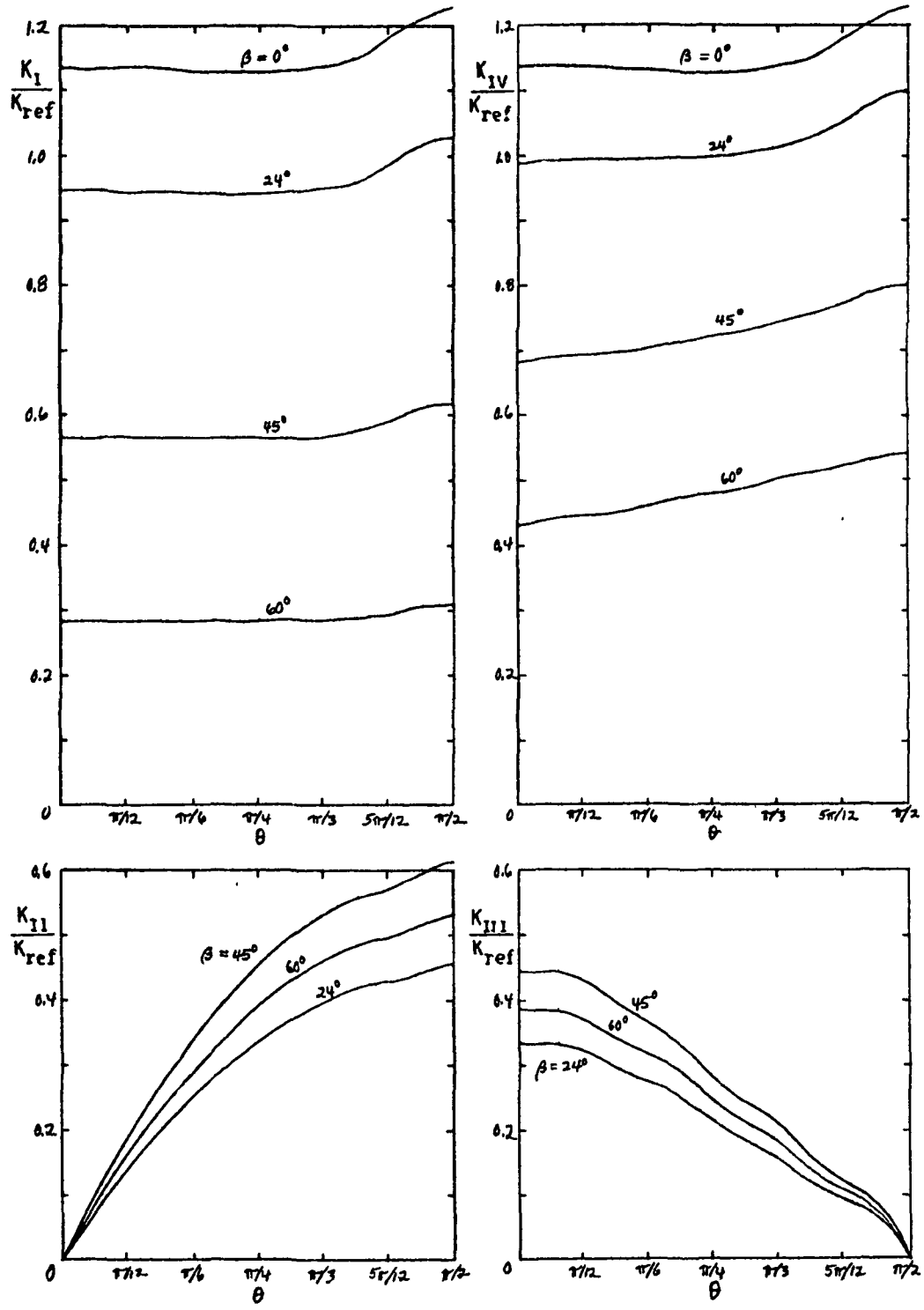

FIGURE E4. STRESS INTENSITY FACTORS ALONG A CRACK WITH A/2C = 0.50, A/T = 0.9 UNDER OBLIQUE LOADS

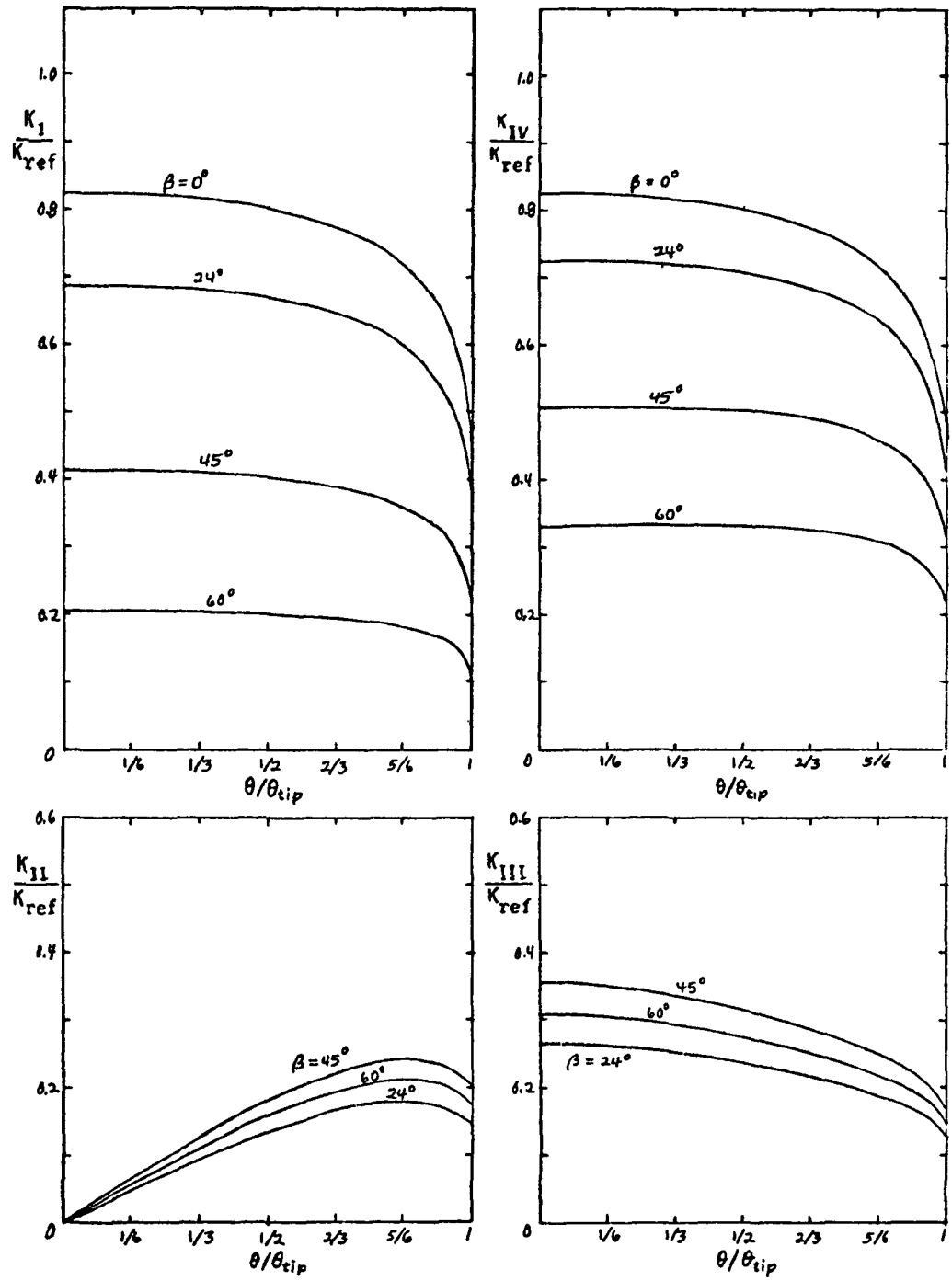

FIGURE E5. STRESS INTENSITY FACTORS ALONG A CRACK WITH A/2C = 0.25, A/T = 0.0 UNDER OBLIQUE LOADS

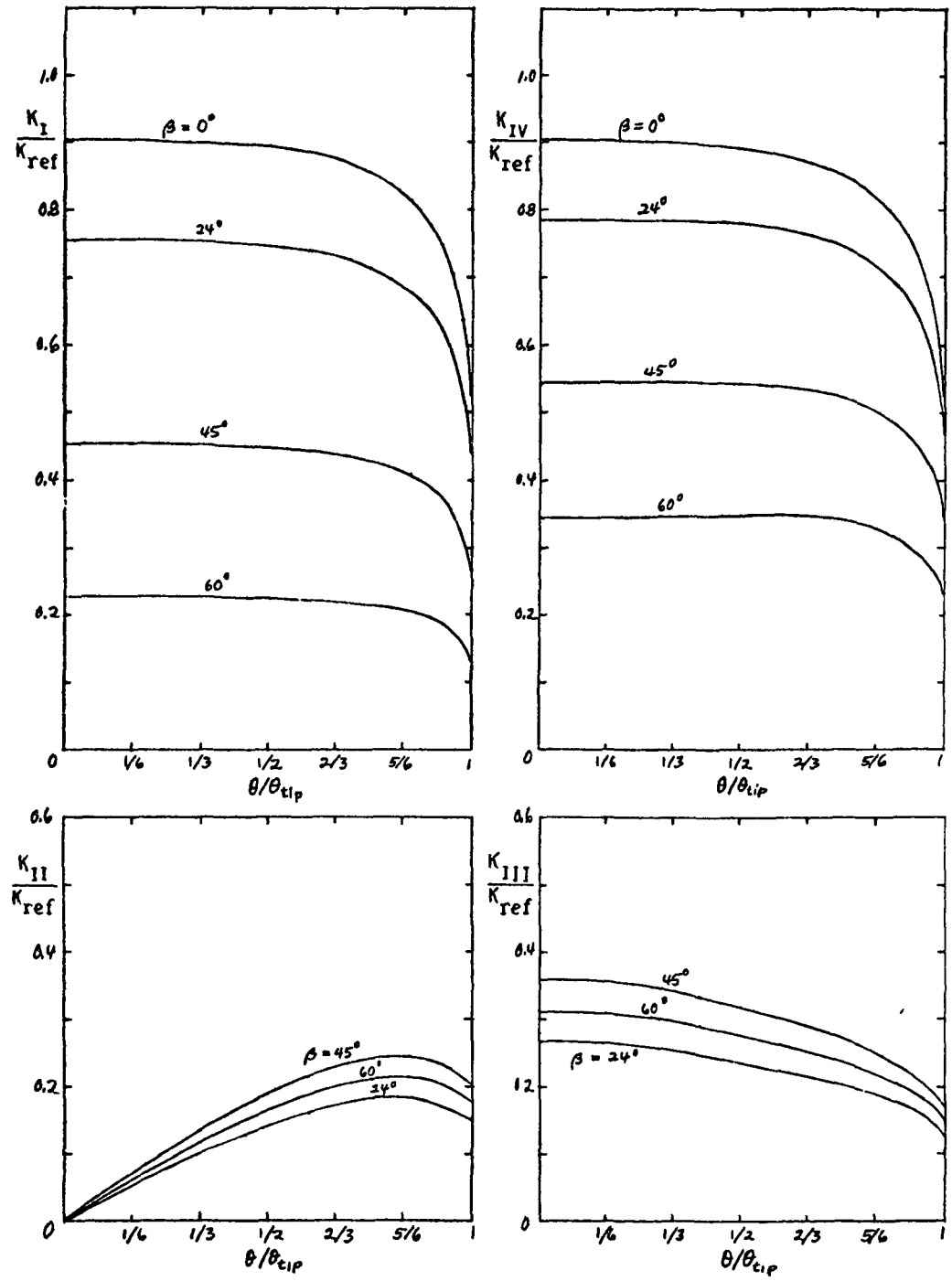

FIGURE C6. STRESS INTENSITY FACTORS ALONG A CRACK WITH A/2C = 0.25, A/T = 0.5 UNDER OBLIQUE LOADS

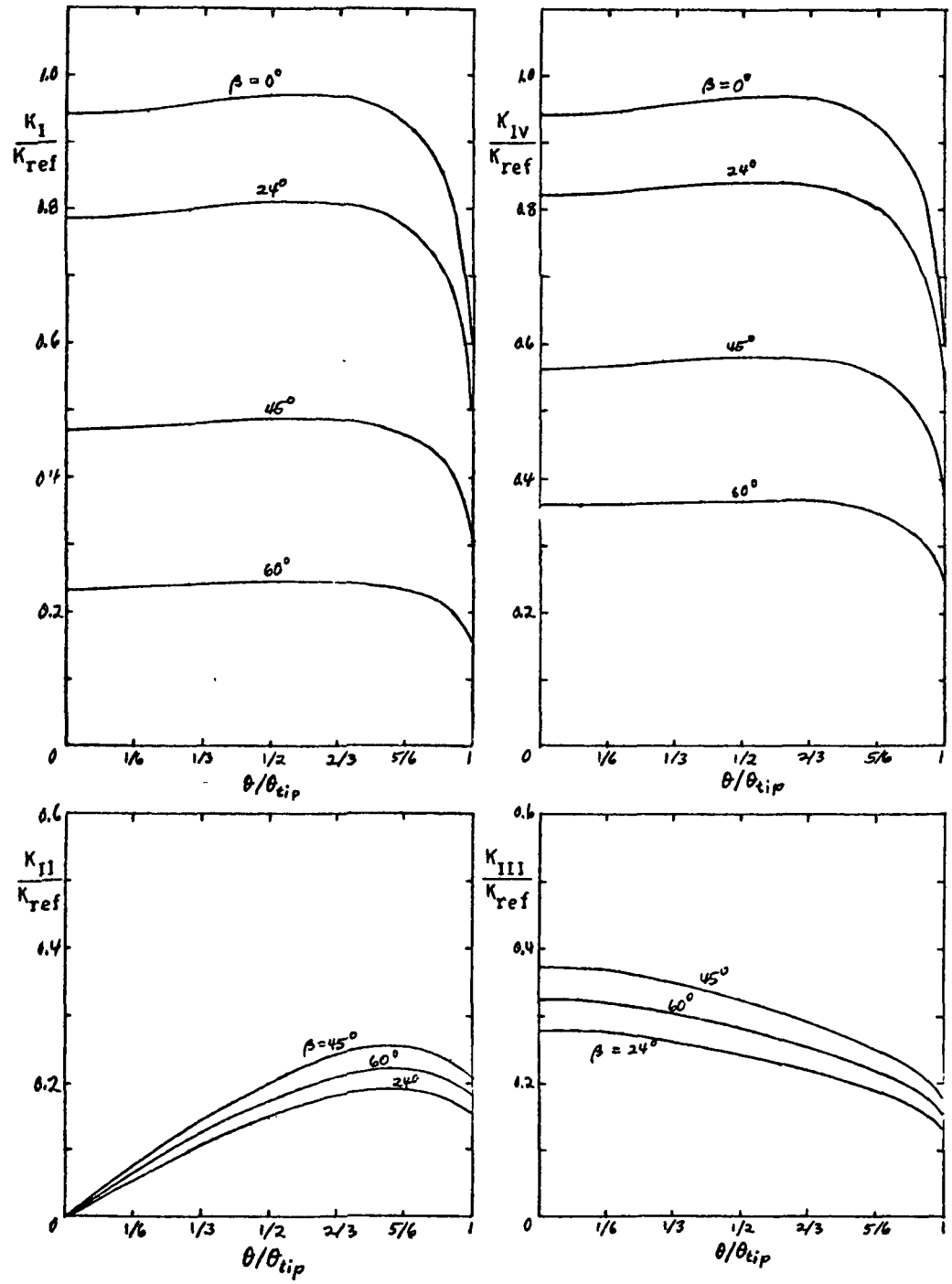

FIGURE E7. STRESS INTENSITY FACTORS ALONG A CRACK WITH A/2C = 0.25 A/T = 0.7 UNDER OBLIQUE LOADS

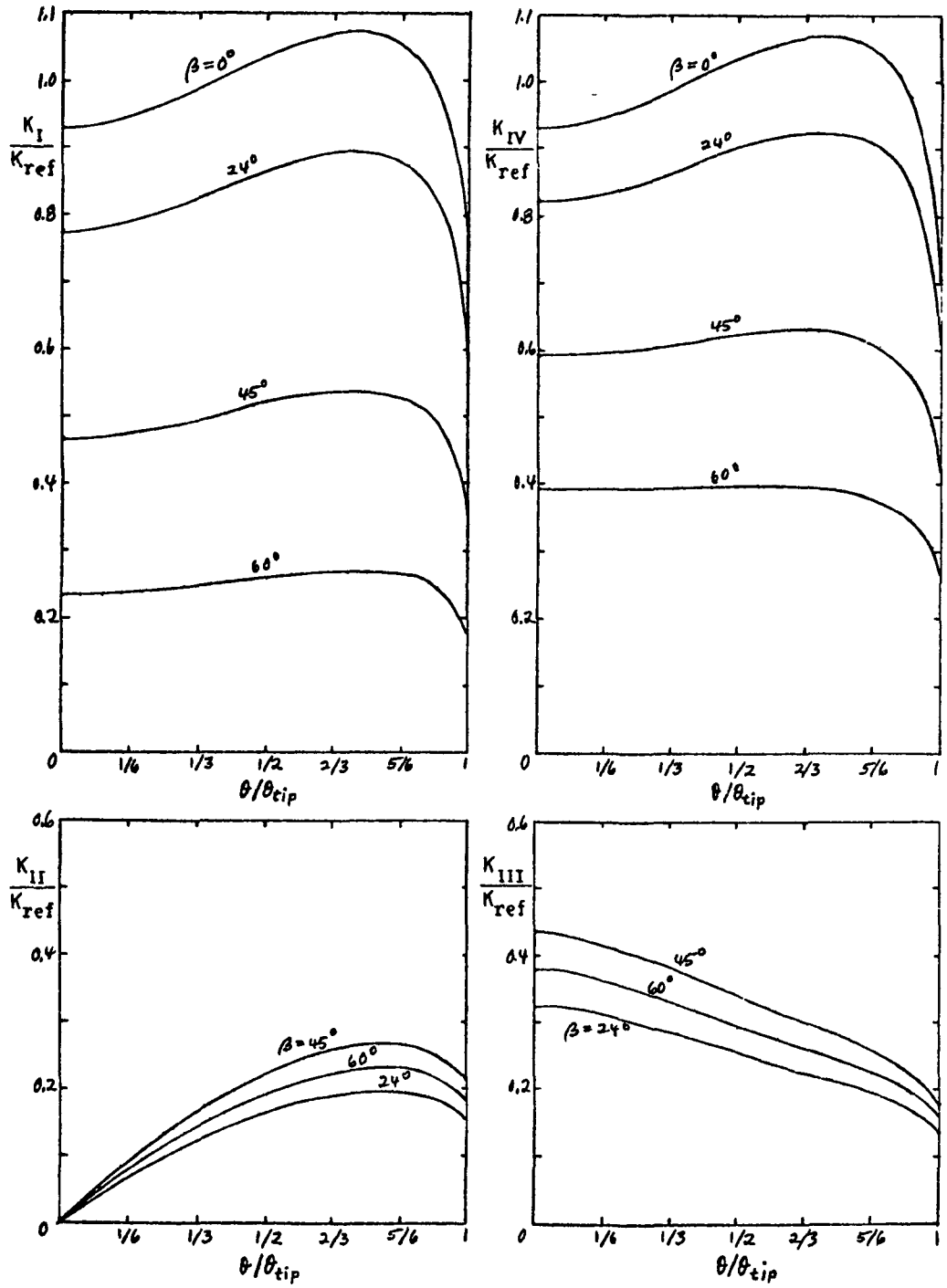

FIGURE E8. STRESS INTENSITY FACTORS ALONG A CRACK WITH A/2C = 0.25, A/T = 0.9 UNDER OBLIQUE LOADS

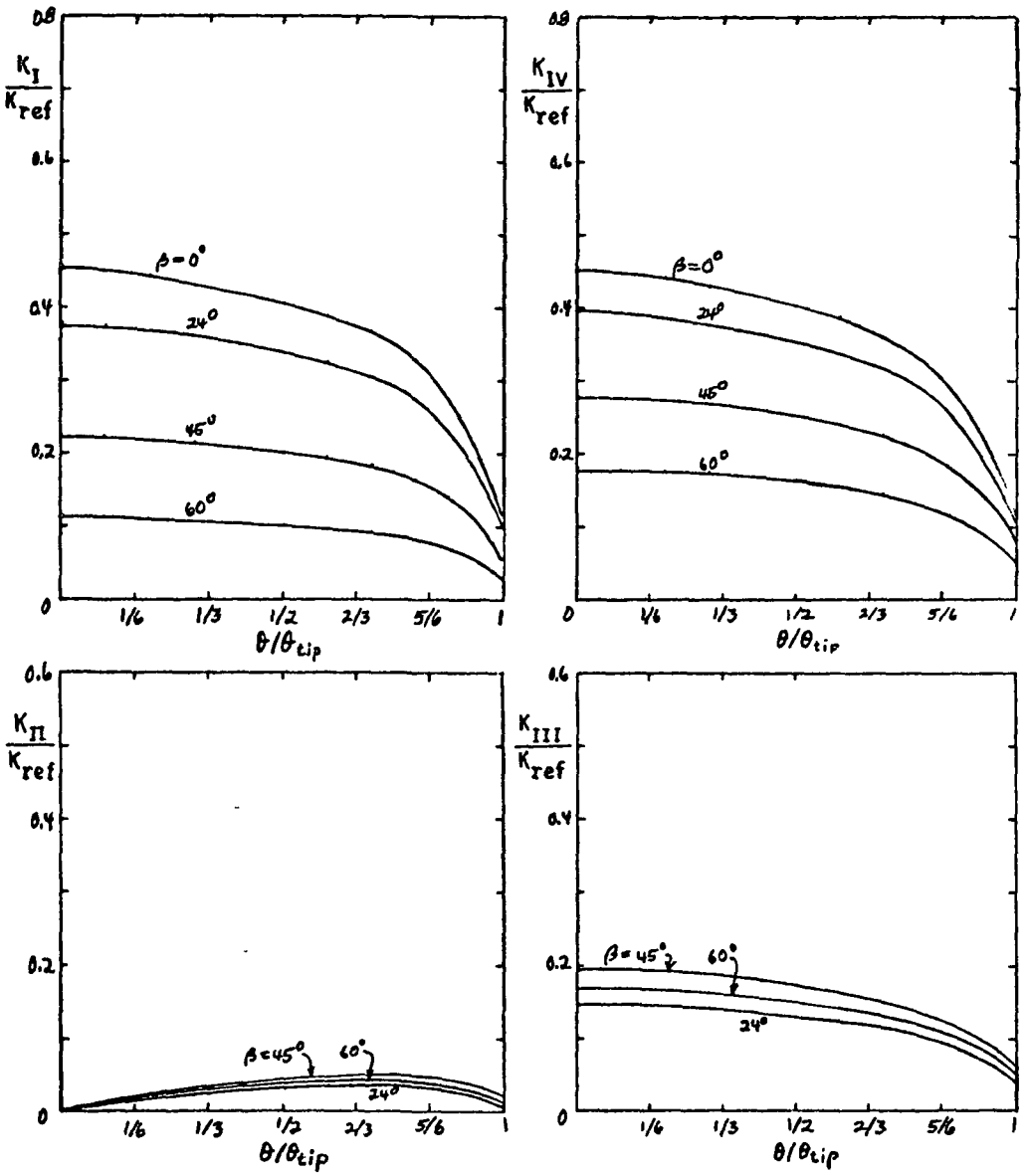

FIGURE E9. STRESS INTENSITY FACTORS ALONG A CRACK WITH A/2C = 0.10, A/T = 0.0 UNDER OBLIQUE LOADS

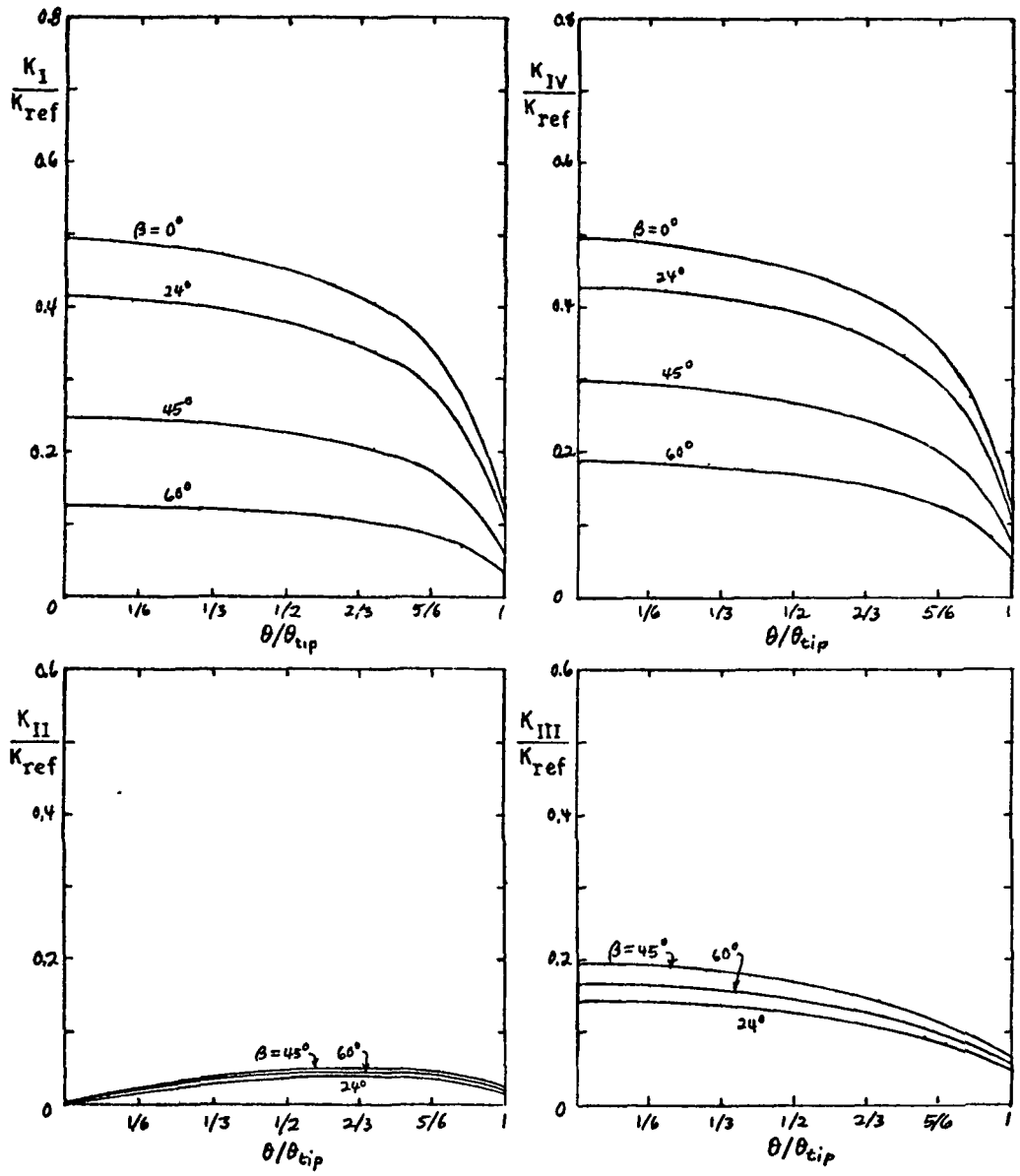

FIGURE E10. STRESS INTENSITY FACTORS ALONG A CRACK WITH A/2C = 0.10, A/T = 0.5 UNDER OBLIQUE LOADS

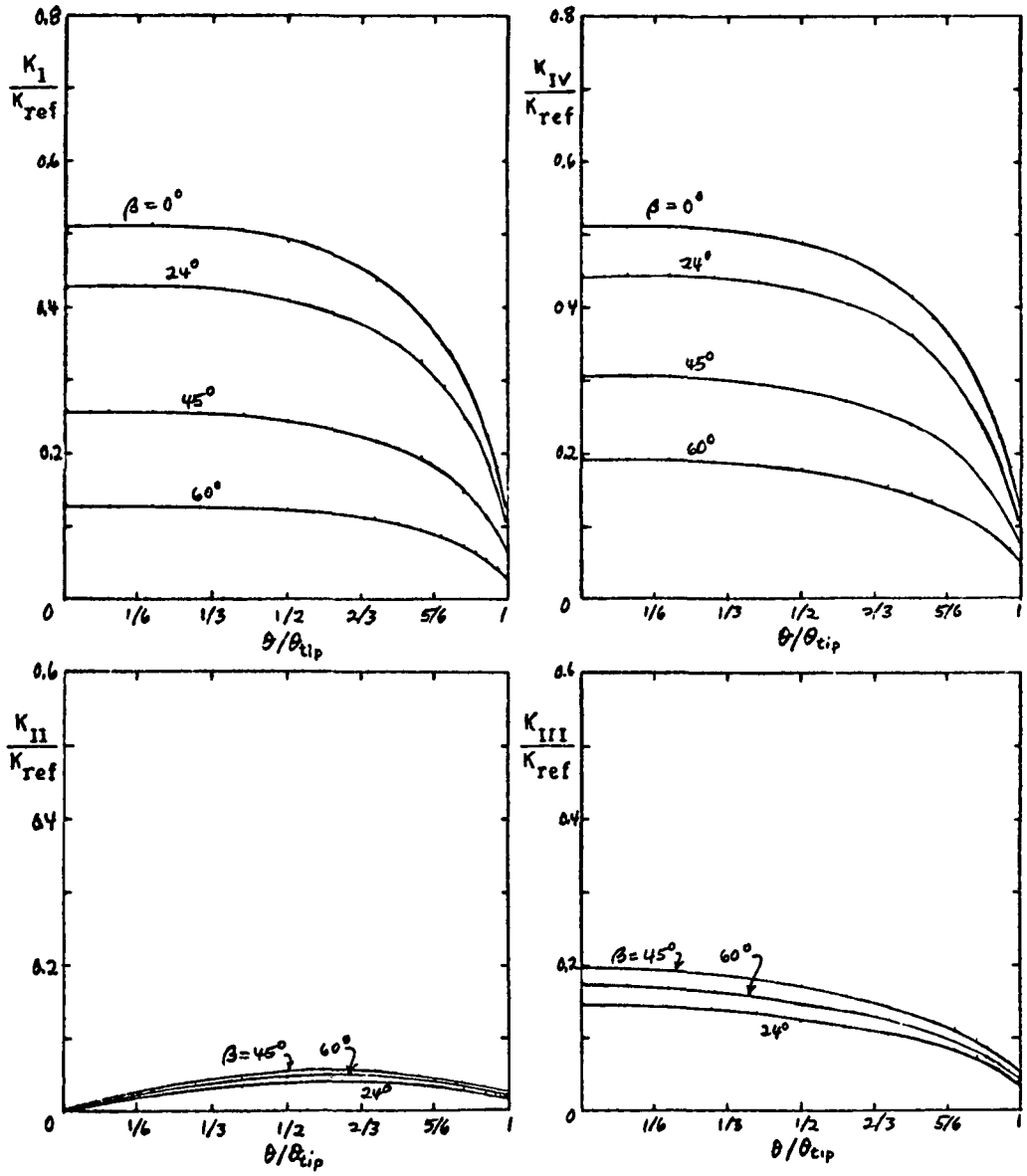

FIGURE E11. STRESS INTENSITY FACTORS ALONG A CRACK WITH A/2C = 0.10, A/T = 0.7 UNDER OBLIQUE LOADS

APPENDIX F

REMARKS ON FORMULAS FOR STRESSES AROUND AN EMBEDDED CRACK

If the faces of a deeply embedded circular crack are subjected to arbitrarily distributed normal and tangential loads, acting oppositely on the two faces, then the stresses and displacements in the surrounding body can all be expressed in terms of known functions of position multiplied by constants determined by the loads [1,2,3]. Using the cylindrical coordinates (r,θ,z) based on the crack circle, it having radius a, and letting $\rho = r/a$ and $\zeta = z/a$, those functions of position are functions of (ρ,ζ) multiplied by $\sin m\theta$ or $\cos m\theta$ (where $m = 0,1,2,\ldots$). The non-trigonometric factors depend on m and on a second index k (where $k = 0,1,2,\ldots$) and are simple combinations of integrals of the form

$$I^{n'}_{M,N}(\rho,\zeta) = \int_0^\infty e^{-\xi|\zeta|}\,\xi^{n'-\frac{1}{2}}\,J_M(\rho,\xi)\,J_{N+\frac{1}{2}}(\xi)\,d\zeta \quad ,$$

but with the combination of integrals varying according to the stress or displacement component involved. The load constants to be used do not change from one stress or displacement component to another, but they do vary with the indices m and k and also with the type of load applied to the crack face. Thus for cases having symmetry around $\theta = 0$, normal loads on the crack involve constants here denoted as $\alpha'_{m,k}$ while shearing loads involve constants $\beta'_{m,k}$ and $\gamma'_{m,k}$. For cases with antisymmetry around $\theta = 0$, the corresponding loads constants are denoted as $\hat{\alpha}'_{m,k}$, $\hat{\beta}'_{m,k}$ and $\hat{\gamma}'_{m,k}$. Since all load systems can be resolved into sums of parts symmetric or antisymmetric around $\theta = 0$, these load constants cover all possible loadings.

More explicitly, letting μ be the shear modulus*, the stress and displacement components can be represented as

---

* Note that $\mu = E/[2(1 + \nu)]$, where E is Young's modulus and ν is Poisson's ratio.

$$
\left.
\begin{aligned}
u &= a\sum_{m=0}^{\infty}\sum_{k=0}^{\infty}\Big\{\Big[\alpha'_{m,k}F^{u}_{m,k,1}+\beta'_{m,k}F^{u}_{m,k,2}+\gamma'_{m,k}F^{u}_{m,k,3}\Big]\cos m\theta \\
&\quad -\Big[\hat{\alpha}'_{m,k}F^{u}_{m,k,1}+\hat{\beta}'_{m,k}F^{u}_{m,k,2}+\hat{\gamma}'_{m,k}F^{u}_{m,k,3}\Big]\sin m\theta\Big\} \quad , \\
v &= a\sum_{m=0}^{\infty}\sum_{k=0}^{\infty}\Big\{\Big[\alpha'_{m,k}F^{v}_{m,k,1}+\beta'_{m,k}F^{v}_{m,k,2}+\gamma'_{m,k}F^{v}_{m,k,3}\Big]\sin m\theta \\
&\quad +\Big[\hat{\alpha}'_{m,k}F^{v}_{m,k,1}+\hat{\beta}'_{m,k}F^{v}_{m,k,2}+\hat{\gamma}'_{m,k}F^{v}_{m,k,3}\Big]\cos m\theta\Big\} \quad , \\
w &= a\sum_{m=0}^{\infty}\sum_{k=0}^{\infty}\Big\{\Big[\alpha'_{m,k}F^{w}_{m,k,1}+\beta'_{m,k}F^{w}_{m,k,2}+\gamma'_{m,k}F^{w}_{m,k,3}\Big]\cos m\theta \\
&\quad -\Big[\hat{\alpha}'_{m,k}F^{w}_{m,k,1}+\hat{\beta}'_{m,k}F^{w}_{m,k,2}+\hat{\gamma}'_{m,k}F^{w}_{m,k,3}\Big]\sin m\theta\Big\} \quad ; \\
\sigma_r &= \mu\sum_{m=0}^{\infty}\sum_{k=0}^{\infty}\Big\{\Big[\alpha'_{m,k}F^{rr}_{m,k,1}+\beta'_{m,k}F^{rr}_{m,k,2}+\gamma'_{m,k}F^{rr}_{m,k,3}\Big]\cos m\theta \\
&\quad -\Big[\hat{\alpha}'_{m,k}F^{rr}_{m,k,1}+\hat{\beta}'_{m,k}F^{rr}_{m,k,2}+\hat{\gamma}'_{m,k}F^{rr}_{m,k,3}\Big]\sin m\theta\Big\} \quad , \\
\sigma_\theta &= \mu\sum_{m=0}^{\infty}\sum_{k=0}^{\infty}\Big\{\Big[\alpha'_{m,k}F^{\theta\theta}_{m,k,1}+\beta'_{m,k}F^{\theta\theta}_{m,k,2}+\gamma'_{m,k}F^{\theta\theta}_{m,k,3}\Big]\cos m\theta \\
&\quad -\Big[\hat{\alpha}'_{m,k}F^{\theta\theta}_{m,k,1}+\hat{\beta}'_{m,k}F^{\theta\theta}_{m,k,2}+\hat{\gamma}'_{m,k}F^{\theta\theta}_{m,k,3}\Big]\sin m\theta\Big\} \quad , \\
\sigma_z &= \mu\sum_{m=0}^{\infty}\sum_{k=0}^{\infty}\Big\{\Big[\alpha'_{m,k}F^{zz}_{m,k,1}+\beta'_{m,k}F^{zz}_{m,k,2}+\gamma'_{m,k}F^{zz}_{m,k,3}\Big]\cos m\theta \\
&\quad -\Big[\hat{\alpha}'_{m,k}F^{zz}_{m,k,1}+\hat{\beta}'_{m,k}F^{zz}_{m,k,2}+\hat{\gamma}'_{m,k}F^{zz}_{m,k,3}\Big]\sin m\theta\Big\} \quad , \\
\tau_{\theta z} &= \mu\sum_{m=0}^{\infty}\sum_{k=0}^{\infty}\Big\{\Big[\alpha'_{m,k}F^{\theta z}_{m,k,1}+\beta'_{m,k}F^{\theta z}_{m,k,2}+\gamma'_{m,k}F^{\theta z}_{m,k,3}\Big]\sin m\theta \\
&\quad +\Big[\hat{\alpha}'_{m,k}F^{\theta z}_{m,k,1}+\hat{\beta}'_{m,k}F^{\theta z}_{m,k,2}+\hat{\gamma}'_{m,k}F^{\theta z}_{m,k,3}\Big]\cos m\theta\Big\} \quad , \\
\tau_{zr} &= \mu\sum_{m=0}^{\infty}\sum_{k=0}^{\infty}\Big\{\Big[\alpha'_{m,k}F^{zr}_{m,k,1}+\beta'_{m,k}F^{zr}_{m,k,2}+\gamma'_{m,k}F^{zr}_{m,k,3}\Big]\cos m\theta \\
&\quad -\Big[\hat{\alpha}'_{m,k}F^{zr}_{m,k,1}+\hat{\beta}'_{m,k}F^{zr}_{m,k,2}+\hat{\gamma}'_{m,k}F^{zr}_{m,k,3}\Big]\sin m\theta\Big\} \quad , \\
\tau_{r\theta} &= \mu\sum_{m=0}^{\infty}\sum_{k=0}^{\infty}\Big\{\Big[\alpha'_{m,k}F^{r\theta}_{m,k,1}+\beta'_{m,k}F^{r\theta}_{m,k,2}+\gamma'_{m,k}F^{r\theta}_{m,k,3}\Big]\sin m\theta \\
&\quad +\Big[\alpha'_{m,k}F^{r\theta}_{m,k,1}+\beta'_{m,k}F^{r\theta}_{m,k,2}+\gamma'_{m,k}F^{r\theta}_{m,k,3}\Big]\cos m\theta\Big\} \quad .
\end{aligned}
\right\}
$$

Here the functions $F^{u}_{m,k,1}$ to $F^{r\theta}_{m,k,3}$ depend only on ρ and ζ. As examples, one may cite those related to σ_z, which are

$$F^{zz}_{m,k,1}(\rho,\zeta) = -\left[I^{1}_{m,m+2k+1} + |\zeta|\, I^{2}_{m,m+2k+1}\right],$$

$$F^{zz}_{m,k,2}(\rho,\zeta) = \frac{\zeta}{2}\, I^{2}_{m,m+2k+2},$$

$$F^{zz}_{m,k,3}(\rho,\zeta) = \left\{\begin{array}{ll} \dfrac{\zeta}{2-\nu}\, I^{2}_{m,m} & \text{for } k = 0 \\[2ex] \dfrac{\zeta}{2}\, I^{2}_{m,m+2k} & \text{for } k \geq 1 \end{array}\right\}.$$

Complete lists of the functions $F^{u}_{m,k,1}$ to $F^{r\theta}_{m,k,3}$ are given in References 1,2, 3, and 14. Since they involve so many integrals $I^{n'}_{M,N}(\rho,\zeta)$ it can be seen why the highly efficient means that have been designed to evaluate those integrals are important. Those means are described in a forthcoming paper (J. C. Bell, "Evaluation of Integrals Involving Products of Bessel Functions Having Application to Crack Stress Analyses").

These formulas were derived for deeply embedded cracks, but they are useful also for surface cracks when they are coordinated with formulas for stresses from appropriate freeing loads applied on the cracked surface, or on other surfaces if the body is finite. Even brief examination of these formulas shows important features of some analyses for surface crack. Thus for semicircular cracks under normal loads symmetric around $\theta = 0$, so that the only non-vanishing load constants are the $\alpha'_{m,k}$ and the face with the crack is at $\theta = \pm\frac{\pi}{2}$, the loads to be freed on that face are

$$\sigma_\theta = \mu \sum_m \sum_k \alpha'_{m,k}\, F^{\theta\theta}_{m,k,1}(\rho,\zeta) \cos\frac{m\pi}{2} \quad (= \sigma_z \text{ in face system})$$

$$\tau_{\theta z} = \mu \sum_m \sum_k \alpha'_{m,k}\, F^{\theta}_{m,k,1}(\rho,\zeta) \sin\frac{\pm m\pi}{2} \quad (= \mp\, \tau_{zx} \text{ in face system})$$

$$\tau_{r\theta} = \mu \sum_m \sum_k \alpha'_{m,k}\, F^{r\theta}_{m,k,1}(\rho,\zeta) \sin\frac{\pm m\pi}{2} \quad (= \tau_{yz} \text{ in face system})$$

If only even values of m are used (as is proper for the semicircular crack), the crack loads do not induce any shear stress as the face, since $\sin\frac{\pm m\pi}{2} = 0$. This situation is convenient if the body is a half space, but it interferes with reciprocity between crack and surface loads in analyses for plates of finite thickness.

Knowledge of the coefficients $\alpha'_{m,k}$, $\beta'_{m,k}$, ---, $\hat{\gamma}'_{m,k}$ provides input for evaluation of the stress intensity factors of all three modes. In particular, if the stress intensity factor of the first mode is defined as

$$k_1 = \lim_{r\to a} \sqrt{2(r-a)}\ \sigma_z(r,\theta,0) \quad ,$$

then (as was shown in [1] and [2])

$$k_1 = \mu\sqrt{a} \sum_{m=0}^{\infty} (\alpha''_m \cos m\theta - \hat{\alpha}''_m \sin m\theta) \quad ,$$

where

$$\alpha''_m = \sqrt{\frac{2}{\pi}} \sum_{k=0}^{\infty} (-1)^k \alpha'_{m,k} \quad , \qquad \hat{\alpha}''_m = \sqrt{\frac{2}{\pi}} \sum_{k=0}^{\infty} (-1)^k \hat{\alpha}'_{m,k} \quad .$$

The stress intensity factors of the second and third modes are defined to be

$$k_2 = \lim_{r\to a+} \sqrt{2(r-a)}\ \tau_{zr}(r,\theta,0) \quad ,$$

$$k_3 = \lim_{r\to a+} \sqrt{2(r-a)}\ \tau_{\theta z}(r,\theta,0) \quad ,$$

and for them it was found that

$$k_2 = \mu\sqrt{a} \sum_{m=0}^{\infty} \left[\left(\beta''_m - \gamma''_m\right) \cos m\theta - \left(\hat{\beta}''_m - \hat{\gamma}''_m\right) \sin m\theta \right] \quad ,$$

$$k_3 = \mu\sqrt{a} \sum_{m=0}^{\infty} \left[\left(\beta''_m + \gamma''_m\right) \sin m\theta + \left(\hat{\beta}''_m + \hat{\gamma}''_m\right) \cos m\theta \right] \quad ,$$

where

$$\beta''_m = \frac{1}{\sqrt{2\pi}} \sum_{k=0}^{\infty} (-1)^k \beta'_{m,k} - \frac{\nu\gamma'_{m,0}}{\sqrt{2\pi}(2-\nu)} \quad , \qquad \gamma''_m = \frac{1}{\sqrt{2\pi}} \sum_{k=0}^{\infty} (-1)^k \gamma'_{m,k} \quad ,$$

Stress intensity factors defined with an extra factor $\sqrt{\pi}$, as is often included, are denoted here as K_I, K_{II} and K_{III} respectively instead of k_1, k_2 and k_3.